

**Spectral fluorescence of chlorophyll and
phycobilins as an *in-situ* tool of phytoplankton analysis
– models, algorithms and instruments**

Dissertation
zur Erlangung des Doktorgrades
der Mathematisch-Naturwissenschaftlichen Fakultät
der Christian-Albrechts-Universität
zu Kiel

vorgelegt von
Martin Beutler
Kiel, März 2003

Referent: Prof. Dr. U.-P. Hansen.....

Korreferent:

Tag der mündlichen Prüfung:.....

Zum Druck genehmigt: Kiel, den.....

.....

Der Dekan

Vorbemerkung

Teilergebnisse dieser Dissertation sind bereits wie folgt vorab veröffentlicht bzw. eingereicht worden:

Veröffentlicht:

Beutler, M., K. H. Wiltshire, B. Meyer, C. Moldaenke & H. Dau (1998): Rapid depth-profiling of the distribution of spectral groups of microalgae in lakes, rivers and the sea. In: *Photosynthesis: Mechanisms and effects V* (ed. G. Garab). pp. 4301-4304. Kluwer Academic Publishers, Dordrecht.

Beutler, M., Wiltshire, K. H., Meyer, B., Moldaenke, C. & Dau, H. (2001). In situ profiles of phytoplankton: algal composition and biomass determined fluorometrically. In *Proceedings of the Ninth International Conference on Harmful Algal Blooms, Hobart, Australia, 7-11 February 2000* (ed. G. M. Hallegraeff, S. I. Blackburn, C. J. Bolch and R. J. Lewis), pp. 202-205. Intergovernmental Oceanographic Commission of UNESCO, Paris.

Beutler, M., Wiltshire, K. H., Lüring, C., Moldaenke, C. & Lohse, D. (2002). Fluorometric depth-profiling of chlorophyll corrected for yellow substances. In *Aquaculture environment and marine phytoplankton*, vol. 34 (ed. G. Arzul), ISSN 0761-3962. pp. 231-238. Ifremer, Brest.

Beutler, M., Wiltshire, K. H., Meyer, B., Moldaenke, C., Lüring, C., Meyerhöfer, M., Hansen, U.-P. & Dau, H. (2002). A fluorometric method for the differentiation of algal populations in vivo and in situ. *Photosynthesis Research* 72, 39-53.

Beutler, M., Wiltshire, K. H., Arp, M., Kruse, J., Reineke, C., Moldaenke, C. & Hansen, U.-P.. A reduced model of the fluorescence from the cyanobacterial photosynthetic apparatus designed for the in situ detection of cyanobacteria. (In Druck) *Biochimica et Biophysica Acta-Bioenergetics*.

Eingereicht:

Schimanski, J., Moldaenke, C., Hansen U.-P. & Beutler, M. A model for correcting the fluorescence signal from a free-falling depth profiler. (Eingereicht) *Photosynthesis Research*.

Beutler, M., Wiltshire, K. H., Reineke, C. & Hansen U.-P. An algorithm and practical fluorescence models from red cyanobacteria and cryptophyta designed for the *in situ* detection of phytoplankton. (Eingereicht) *Biochimica et Biophysica Acta-Bioenergetics*.

In Vorbereitung:

Beutler, M., Wiltshire, K. H., Reineke, C., Ruser, A. and Hansen, U.-P. *In situ* analysis of phytoplankton by deconvolution of fluorescence excitation and emission matrices. (Manuskript fertig zum Einreichen).

Diese Arbeit wurde finanziert vom BMBF (Projektnummer 03F0287A).

Content

Chapter	Page
Abbreviations	5
Introduction	7
Chapter 1. Biophysical background	9
1.1 Photosynthesis	9
1.1.1 Photosystems and spectral algal groups	11
1.1.2 Light harvesting in cyanobacteria	12
1.1.3 Electron transport chain and linear electron transport	12
1.1.4 Photosystem II chlorophyll fluorescence	13
1.1.5 Origins of chlorophyll fluorescence	14
1.1.6 Quenching mechanisms	14
1.1.7 Photosystem II chlorophyll fluorescence transients	15
Chapter 2. A fluorometric method for the differentiation of algal populations <i>in vivo</i> and <i>in situ</i> .	18
2.1 Abstract	18
2.2 Introduction	19
2.3 Materials and methods	21
2.3.1 Fluorescence measurements	21
2.3.2 Algal cultures	23
2.3.3 Growth of cultures and sampling	24
2.3.4 Determination of chlorophyll concentrations	24
2.3.5 Determination of biovolume	26
2.3.6 Mathematical evaluation	26
2.3.7 Norm spectra	28
2.4 Results	29
2.4.1 Measurement of norm spectra	29
2.4.2 Linear independence of the norm spectra	30
2.4.3 Laboratory tests: common dilution factor for all classes	30
2.4.4 Influence of pre-illumination on the norm curves	32
2.4.5 Influence of scattering on the norm curves	33
2.4.6 <i>In situ</i> test: comparison with HPLC determinations	34
2.4.7 <i>In situ</i> test: depth profiles	35
2.4.8 <i>In situ</i> tests: depth profiles and biovolume	36
2.5 Discussion	38
2.5.1 Reliability	38
2.5.2 Detection limit	39
2.5.3 Relation of fluorescence to chlorophyll content and productivity	39
2.5.4 Relation of fluorescence to biovolume concentrations	39
2.5.5 Future developments to overcome present limitations	39

Chapter 3. Fluorometric depth-profiling of chlorophyll corrected for yellow substances.....	41
3.1 Abstract.....	41
3.2 Introduction	42
3.3 Materials and methods.....	43
3.3.1 Set-up of the submersible instrument	43
3.3.2 Determination of chlorophyll concentrations and algal cultures	43
3.3.3 Mathematical evaluation.....	43
3.3.4 Fluorescence-offsets of natural water-samples.....	43
3.4 Results and discussion.....	44
3.4.1 Norm spectra of phytoplankton compared with spectra of yellow substances.....	44
3.4.2 Variability of natural fluorescence offsets.....	44
3.4.3 Dilution experiment and <i>in situ</i> profile.....	45
Chapter 4. A model for correcting the fluorescence signal from a free-falling depth profiler.....	47
4.1 Abstract.....	47
4.2 Introduction	48
4.3 Materials and methods.....	49
4.3.1 Algal growth	49
4.3.2 Chlorophyll determination.....	49
4.3.3 Fluorometer set-up.....	49
4.3.4 Mathematical evaluation.....	50
4.3.5 Model for the depth profiler	53
4.4 Results	58
4.4.1 Fluorometer tests	58
4.4.2 Fluorescence induction curves.....	59
4.4.3 Tests with flowing suspensions	60
4.5 Discussion.....	63
Chapter 5. A reduced model of the fluorescence from the cyanobacterial photosynthetic apparatus designed for the <i>in situ</i> detection of cyanobacteria	65
5.1 Abstract.....	65
5.2 Introduction	66
5.3 Materials and methods.....	69
5.3.1 Growth experiments.....	69
5.3.2 Fluorescence measurements	70
5.3.3 Determination of chlorophyll concentrations	72
5.3.4 Phycobilin determination.....	72
5.3.5 Number of photosystem II reaction centres.....	72
5.4 Results	74
5.4.1 Effect of pigment variability on two different evaluation problems	74
5.4.2 Cyanobacteria with different pigmentation for the investigation for variability of spectra and for testing the model.....	74

5.4.3	A simplified model of energy transfer in the antennae of cyanobacteria	75
5.4.4	Test of the first assumption with cyanobacteria of different pigmentation types (Equation (B8) in the <i>Appendix A</i>)	76
5.4.5	Estimation of chlorophyll and photosystem II by fluorescence in cyanobacteria	77
5.4.6	Variation of cyanobacterial fluorescence excitation spectra.....	79
5.4.7	Norm spectra of other spectral algal groups	81
5.4.8	Tests using dilution experiments.....	82
5.4.9	Aging cultures	83
5.4.10	Sensitivity to changed light intensity	84
5.5	Discussion.....	86
5.5.1	Variation of cyanobacterial pigments	86
5.5.2	Applicability of the model in Figure 5.5 for the estimation of cyanobacterial pigments.....	86
5.5.3	Variation of cyanobacterial pigments	87
Chapter 6. An algorithm and practical fluorescence models from red cyanobacteria and cryptophyta designed for the <i>in situ</i> detection of phytoplankton		
6.1	Summary.....	90
6.2	Introduction.....	91
6.3	Materials and methods	93
6.3.1	Growth experiments.....	93
6.3.2	Fluorescence measurements.....	94
6.3.3	Pigment determination	95
6.4	Results.....	96
6.4.1	Red cyanobacteria grown with different pigmentation.....	96
6.4.2	Growth of cryptophyta under different light intensities and growth of different species	97
6.4.3	Simplified models of energy transfer in the antennae of red cyanobacteria and cryptophyta.....	98
6.4.4	Validation of fluorescence model of the red cyanobacterial apparatus	100
6.4.5	Comparison of the calculated and measured phycoerythrin, chlorophyll and photosystem II centre concentrations in cryptophyta.....	101
6.4.6	Identification in the presence of other phytoplankton.....	104
6.4.7	Aging of red cyanobacterial cultures	105
6.4.8	Sensitivity to state transitions (coupling of phycobilisome to photosystem II) ...	106
6.5	Discussion.....	108
6.5.1	Variation of cyanobacterial pigments and cryptophytal pigments.....	108
6.5.2	Reliability of prediction of pigment contents in red cyanobacteria by the model in <i>Appendix D</i>	108
6.5.3	Prediction of pigment contents in cryptophyta by the model in <i>Appendix E</i>	109
Chapter 7. In situ analysis of phytoplankton by deconvolution of fluorescence excitation and emission matrices.....		
7.1	Abstract.....	111

7.2	Introduction	112
7.3	Materials and methods.....	114
7.3.1	Fluorescence measurements	114
7.3.2	Fluorescence profiler	115
7.3.3	Pigment determination.....	116
7.4	Results	117
7.5	Discussion.....	126
	Conclusion	128
	Abstract	131
	Zusammenfassung.....	134
	Appendix	137
	Appendix A. Fitting by norm spectra.....	137
	Appendix B. Energy distribution model (blue cyanobacteria).....	139
	Appendix C. Mathematical fit for several excitations wavelengths and detection wavelengths with variable cyanobacterial norm spectra	143
	Appendix D. Fluorescence model of phycoerythrin-containing cyanobacteria	145
	Appendix E. Energy distribution model of cryptophytes.....	151
	Appendix F. Mathematical fit for cyanobacterial spectra with several excitations wavelengths and detection wavelengths using variable cyanobacterial norm spectra	154
	References.....	158
	Danksagung.....	168
	Curriculum vitae	169

Abbreviations

ADP:	adenosine-di-phosphate
AOA:	algae online analyser
APC:	allophycocyanin
ATP:	adenosine-tri-phosphate
Chl:	chlorophyll
DCM:	deep chlorophyll maximum
DOM:	dissolved organic matter
ETC	electron transport chain
F:	fluorescence intensity
F _m :	maximal fluorescence
F _o :	dark fluorescence
F _v :	variable fluorescence
GFH:	gelatine filter
HAB:	harmful algal blooms
HPLC:	high performance liquid chromatography
IF:	interference filter
NADP:	nicotinamide-adenine-dinucleotide-phosphate
Q _A :	primary electron acceptor
q _N :	non-photochemical quenching
q _P :	photochemical quenching
L _{cm} :	core linker protein
LED:	light-emitting diode
PAM:	pulse amplitude modulation
PBS:	phycobilisome
PB:	phycobiliprotein
PC:	phycocyanin
PE:	phycoerythrin
PhAR	photosynthetic actinic radiation
PS:	photosystem
REE	rapid electron transfer
UV:	ultra violet
YS	yellow substances

Introduction

Although aquatic biomass is equivalent to only 0.3 % of the terrestrial biomass, its high turnover rate is responsible for about 40-50 % of net global primary production (Falkowski & Raven (1997); Häder (1999)). Algae and cyanobacteria contribute substantially to O₂ production in lakes and rivers.

Over the last two decades the frequency and intensity of toxic phytoplankton blooms have increased in coastal areas (Hallegraeff (1993); Anderson (1997); Millie *et al.* (1999)). Human activity and rise in human population is generally quoted as the main causative for this. With the associated growing problems to human health and fisheries loss costs caused by harmful algal blooms (HABs), there is a need for a better understanding of the origins and evolution of HABs. The estimation of primary production and such problems as HABs calls for methods for quantitative and qualitative analyses of phytoplankton in natural waters. However, as far back as 1890, Haeckel (1890) already considered phytoplankton counting a task which could not be accomplished without 'ruin of mind and body', and even now, the determination of algal biomass is still problematic and laborious.

The group-specific assessment of microalgal populations with a high temporal and spatial resolution should be a prerequisite for the estimation of photosynthetic productivity or water quality. However, currently available methods for determination of the microalgal population distribution in waters are typically lacking in these areas and thus instrumental measurements do not allow a thorough understanding of the role of phytoplankton in aquatic ecosystems. The only ecologically differentiating methods involve *post hoc* enumeration of algae. The delay between sampling a water body and obtaining the final results mostly excludes the use of these methods for supervision or monitoring tasks. Furthermore, traditional methods are often very time consuming. Here, an approach is presented based on the measurement of the fluorescence emission of chlorophyll (Chl) and phycobiliproteins (PBs) excited with several wavelengths. It yields the differentiated assessment of microalgae population distributions within a few minutes.

Fluorescence emission of the photosystem (PS II) is widely used as a measure of Chl contents of algae in aquatic systems (Yentsch & Menzel (1963); Holm-Hansen (1965)). Depth profiling of Chl fluorescence has been carried out since the early seventies (Kiefer (1973)). Since then some attempts have been made to distinguish different groups of phytoplankton using their fluorescence properties *in vivo* (Yentsch & Yentsch (1979); Yentsch & Phinney (1985)). Kolbowski & Schreiber (1995) used light-emitting diodes. This approach did not only differentiate between three major algal groups by correct assessment of dark fluorescence yield, F₀, but also provided the determination of the effective quantum yield at a given actinic light intensity with the help of the saturation pulse method. This led to a measure of the relative photosynthetic electron transport rate for each of the algal groups. The feasibility of this approach was confirmed by the work of Gilbert *et al.* (2000). They compared oxygen evolution with the photosynthetic flux obtained from *in vivo* fluorescence of different algal taxa. Gerhardt & Bodemer (1998) used delayed fluorescence excitation spectroscopy to distinguish between algal groups. Cowles *et al.* (1993) presented vertical profiles of phycoerythrin (PE) containing

algae, and Desiderio *et al.* (1997) determined profiles of fluorescence emission spectra without relation to the biomass or diversity of algal groups. Beutler (1998) extended the approach of Kolbowski & Schreiber (1995) by another spectral algal group, the cryptophyta. This was done by means of deconvolution of a five-point excitation spectrum. One field of applying the approaches of Beutler (1998) and Kolbowski & Schreiber (1995) are the Blue Box and the Ferry Box projects in which ferries and freighters will be equipped with sensors for low cost screening of coastal systems. Sea water is monitored along their normally fixed route over several years and by letting it flow through a recording system including a sensor, thus providing data regarding water quality, algal species, algal concentration and photosynthetic activity (Colijn *et al.* (2002); Ruser, (2001)).

The concept of algal differentiation by Beutler (1998) is based on differences in the composition of peripheral antennae of PS II of five different spectral algal groups (green, blue, brown, mixed and red) and stable norm spectra. In the work of Beutler (1998) it was only possible to differentiate between four algal groups. The distinction between only four spectral groups is not high enough in some ecological important situations, and furthermore the applicability in submersible instruments for *in situ* applications was not tested yet. Problems with this method also result from the naturally occurring yellow substances (YS) which emit fluorescence that interferes with phytoplankton fluorescence. Another problem arises from norm spectra of phytoplankton that contain phycobilins, like cyanobacteria. Those organisms show variable norm spectra (Beutler (1998)). This is due to adaptation processes in these organisms to different environmental conditions (Demarsac & Houmard (1993); Müller *et al.* (1993); Reuter & Müller (1993); Bryant (1995)).

In this work the concept of Beutler (1998) was first tested (*Chapter 2*) for its reliability for *in situ* measurements in submersible instruments. Test of the linear independence of norm spectra (required for the fit procedure), pre-illumination effects and effects of light scattering by particles were investigated and discussed. Fluorometric results were compared to biovolume concentrations obtained from microscope counts (*Chapter 2*). The concept of algal differentiation was refined by addition of a YS correction (see *Chapter 3*). This was achieved by using a sixth ultra violet (UV) - emitting excitation light-emitting diode (LED). With the new set-up a mean norm spectrum for YS was determined and tested. In *Chapter 4* a mathematical model for the estimation of algal fluorescence parameters in flowing samples, essential for fluorometric depth profiling, was evolved and verified.

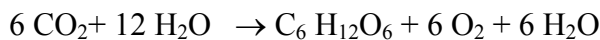
The variability of the cryptophyta and cyanobacterial photosynthetic apparatus which cause problems in phytoplankton detection and discrimination were approached in *Chapter 5*. In this chapter it is described how this problem was solved for blue cyanobacteria by the use of a simplified numerical fluorescence model, new fit procedure and the additional detection channel detecting at the emission wavelength of PC (650 nm). The aim of the work described in *Chapter 6* was to evolve a practical model for the red cyanobacterial photosynthetic apparatus and a fit algorithm that can cope with the adaptation mechanisms in cyanobacteria and with interference of cryptophyta carrying PE₅₆₆. Finally, all the findings were tested with natural samples using an improved submersible profiler (*Chapter 7*).

Chapter 1. Biophysical background

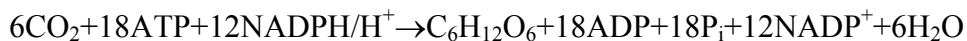
The experiments and models calculations carried out in this thesis are based on the fundamental theory of photosynthesis with a strong emphasis on energy conversion and light harvesting processes. In this chapter a brief overview is given of the overall photosynthetic process, the photosynthetic organelles, proteins and the energy transfer interactions. Details are given on the algal antennae systems. The basic theory on Chl fluorescence and nomenclature, which is essential in Chl fluorescence analysis, is presented.

1.1 Photosynthesis

Oxygenic photosynthesis is a complex endogenous process. Absorption of light utilizes energy for the synthesis of carbohydrates from carbon dioxide and water (Falkowski & Raven (1997); Häder (1999)). Solar radiation energy is therefore stored by primary production of biomass. The overall equation for photosynthesis is:



This reaction comprises many single steps. These steps can be assigned to light (electron transport chain (ETC)) and dark (Calvin Cycle) reactions. During the light reactions ATP (adenosine-tri-phosphate) and nicotinamide-adenine-dinucleotide-phosphate (NADP)H/H⁺ are produced from adenosine-di-phosphate (ADP) and NADP⁺, respectively. Both ATP and NADP⁺ provide energy for the dark reactions. Carbon dioxide is reduced in the dark reactions and carbohydrates are synthesized. The total reaction of the Calvin cycle can be summarised as:



P_i: inorganic phosphate

Photosynthesis takes place on and in the thylakoid membranes (Figure 1.1). This is a closed membrane system with an aqueous inner volume (lumen). The cytosolic outer side of the thylakoids is called stroma. The proteins and organelles involved in the light reactions are located in and on the thylakoid membrane (distributed on PS II, PS I and the ETC). The places of the dark reactions can be found in the stroma. In higher plants and most algae the thylakoid membranes are located in chloroplasts, Figure 1.2. These are closed cell compartments within the plant or algal cell. Prokaryotic cells like cyanobacteria lack chloroplasts. Here the thylakoid membranes can be found free within the cytoplasm.

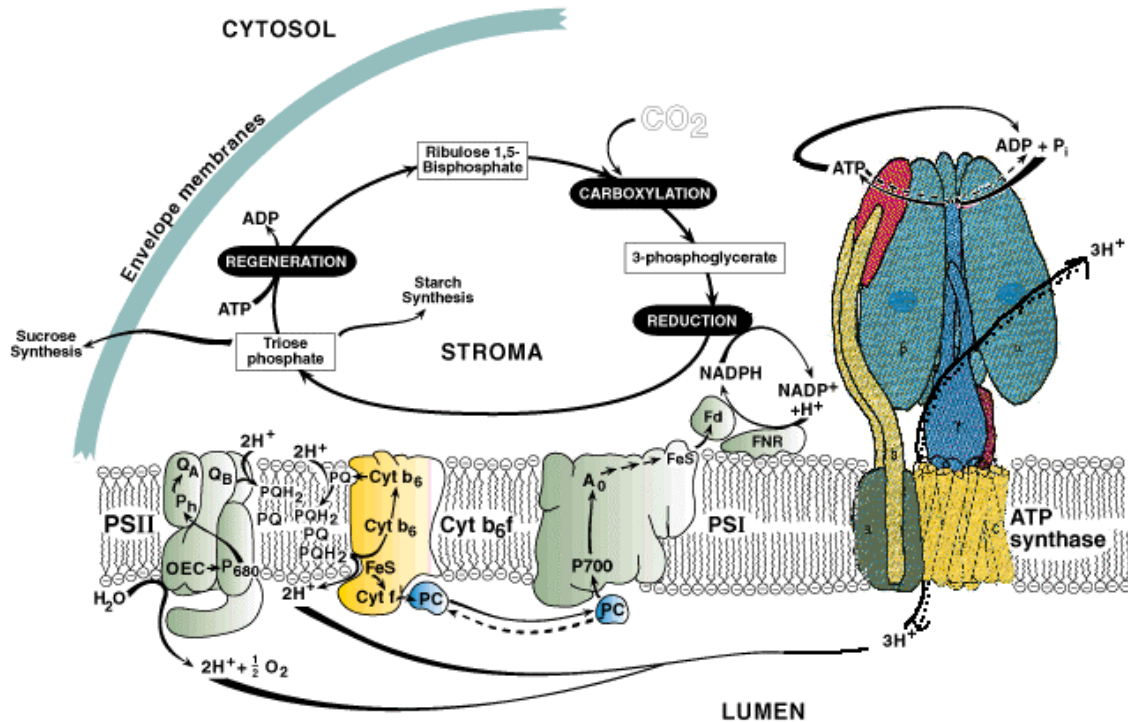


Figure 1.1. Thylakoid membrane with the 4 membrane intrinsic polypeptide complexes: PS I, PS II, cytochrome b_6/f and the ATP synthase connected to the Calvin Cycle in the stroma. Abbreviations: OEC: oxygen evolving complex, P680: reaction centre Chl of PS II, Ph: phaeophytin acceptor of PS II, Q_A and Q_B : quinone acceptors of PS II, PQ and PQH_2 : plastoquinone and reduced plastoquinone, Cyt: cytochrome, PC: plastocyanin (note that PC does not mean phycocyanin in this figure) FeS: bound iron sulfur acceptor of PS I, P700: reaction centre Chl of PS I, A_0 : primary acceptor of PS I, Fd: soluble ferredoxin, FNR: ferredoxin-NADP reductase (adapted from Ort & Whitmarsh (1996) and Junge *et al.* (1997))

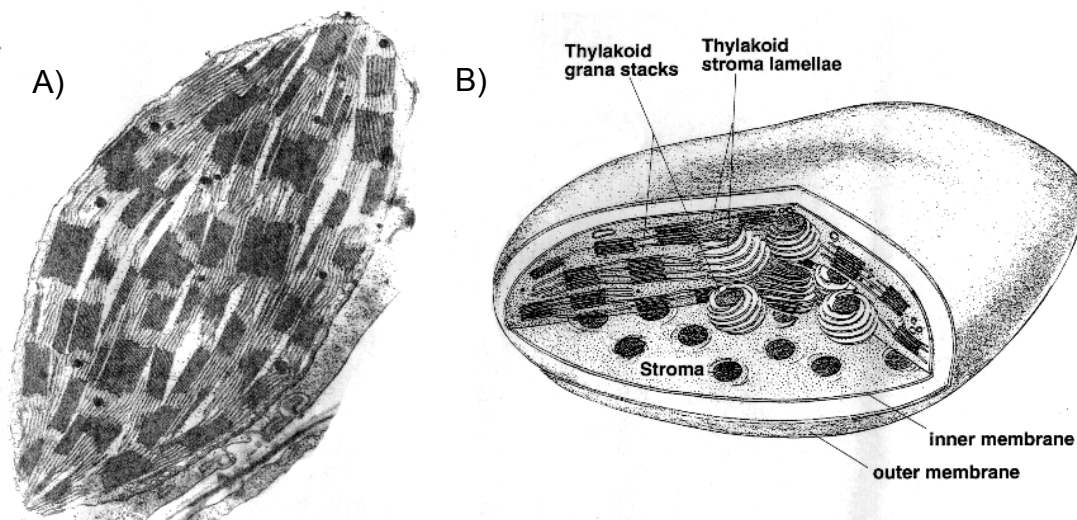


Figure 1.2. A) An electron micrograph of a plant chloroplast (Micrograph by A.D. Greenwood, reprinted from Whitmarsh & Govindjee (1995)). The chloroplast is about 6 μ m long. Inside the chloroplast is the photosynthetic membrane, which is organized into stacked and unstacked regions. It is not known why the photosynthetic membrane has such a complicated architecture. The stacked regions are linked by unstacked membranes. B) A model of the chloroplast (Ort (1994)) showing the photosynthetic membrane.

1.1.1 Photosystems and spectral algal groups

Light energy, which is necessary to drive photosynthesis, is absorbed by the antennae systems of PS I and PS II. A PS consists of a peripheral antenna or light-harvesting complex, an inner antenna and the reaction centre. Most light energy is absorbed by the peripheral antenna. In higher plants this antenna consists of Chl *a*, Chl *b* and carotenoids. In algae and cyanobacteria the composition of the peripheral antennae has a bigger variety. Algal classes can be assigned to spectral algal groups (e.g. van den Hoek *et al.* (1995), see Table 1.1). Each of the five spectral algal groups is characterised by similar fluorescence excitation spectra resulting from the pigment composition and structure of their peripheral antennae (Beutler, (1998), see Table 1.1). In the green group, the peripheral antennae contains Chl *a*, Chl *b* and xanthophyll. In the blue group, phycobilisomes (PBSs) function as peripheral antennae (mainly phycocyanin (PC)). The members of the brown group contain Chl *a*, Chl *c* and xanthophyll (often fucoxanthin or peridinin). Whereby it should be noted that the colour names are not meant to label specific divisions (e.g. brown does not mean phaeophyta). The peripheral antennae of the red group are composed of PBSs, as in the blue group. PE dominates in the red group instead of the PC. The mixed group has a combination of Chl *a* and Chl *c*₂ with one PB that can be either PE or PC. Seven different phycobilins are known (Lichtle *et al.* (1992); McKay *et al.* (1992)). Here, only the PE₅₆₆-containing members of the mixed group are considered as they are mainly important in freshwater. PE₅₆₆ has a maximum absorbance at a wavelength of 566 nm.

Spectral Group	Peripheral Antenna	Division
Green	Chlorophyll-a/b, Carotenoids	Chlorophyta
Blue	Phycobilisomes (Phycocyanin)	Blue cyanobacteria
		Glaucophyta
Brown	Chlorophyll-a/c, Carotenoids	Heterokontophyta (e.g. diatoms)
		Haptophyta
		Dinophyta
Red	Phycobilisomes (Phycoerythrin)	Rhodophyta Red cyanobacteria
Mixed	Chlorophyll-a/c ₂ , Phycobiliprotein	Cryptophyta

Table 1.1. Spectral groups of microalgae (Beutler (1998)).

1.1.2 Light harvesting in cyanobacteria

A central role in this thesis, primarily because of their specialized photosynthetic light harvesting mechanisms, play cyanobacteria. In these organisms light absorption processes of photosynthesis take place in PBSs, PS II and PS I (Glazer (1989); Bryant (1995); van Thor *et al.* (1998)). Figure 1.3 shows the typical structures of phycobilisomes. Unlike eukaryotic algae, the light-harvesting antennae of cyanobacteria contain no Chl. In species containing PE (called red cyanobacteria in here), the PBSs consist of PBs, PE, PC and in the core regions of PBS allophycocyanin (APC). Linker polypeptides are present in the PBSs. These are non-pigmented, with the exception of the large core linker (L_{CM}). PC and APC contain the ether-linked chromophore phycocyanobilin and can occur in PBSs as trimers or hexamers. Cyanobacterial species without PE (here named blue cyanobacteria) have a structure analogous to the red cyanobacteria but lacking PE.

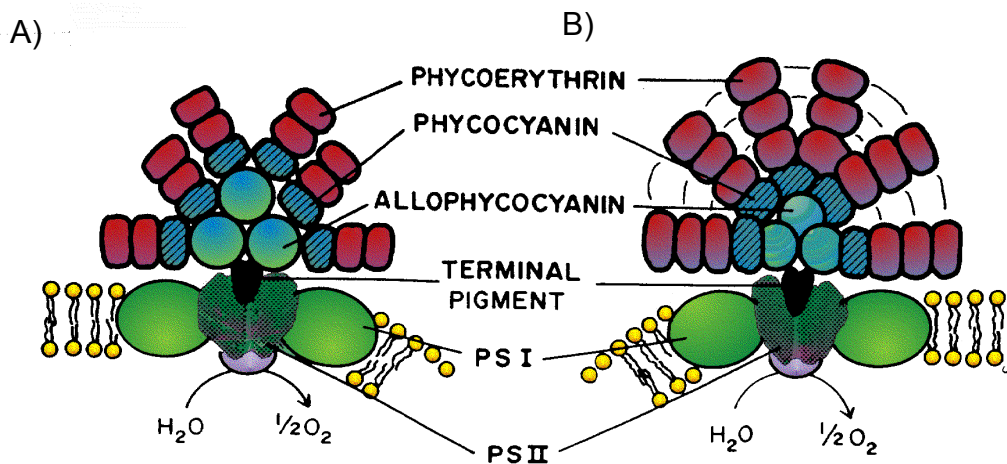


Figure 1.3. Schematic of a (A) hemidiscoidal phycobilisome, (B) and a more complex hemispherical phycobilisome (Gantt (1986))

1.1.3 Electron transport chain and linear electron transport

Electron transfer through the ETC starts after absorption of a photon followed by excitation of the reaction centre of PS II (Figure 1.4). In the reaction centre charge separation takes place and the electron acceptor is reduced. In four steps a manganese complex splits two water molecules from the lumen in one oxygen molecule, four protons and four electrons. The ETC consists of many components. In a series of redox reactions electrons are transferred from one reaction partner to another. The reduced phaeophytin is reoxidised due to the transfer of electrons to the primary electron acceptor (Q_A). Ferredoxin is reduced via further electron acceptors (*inter alia* plastoquinone pool and PS I (see Figure 1.4 for details)).

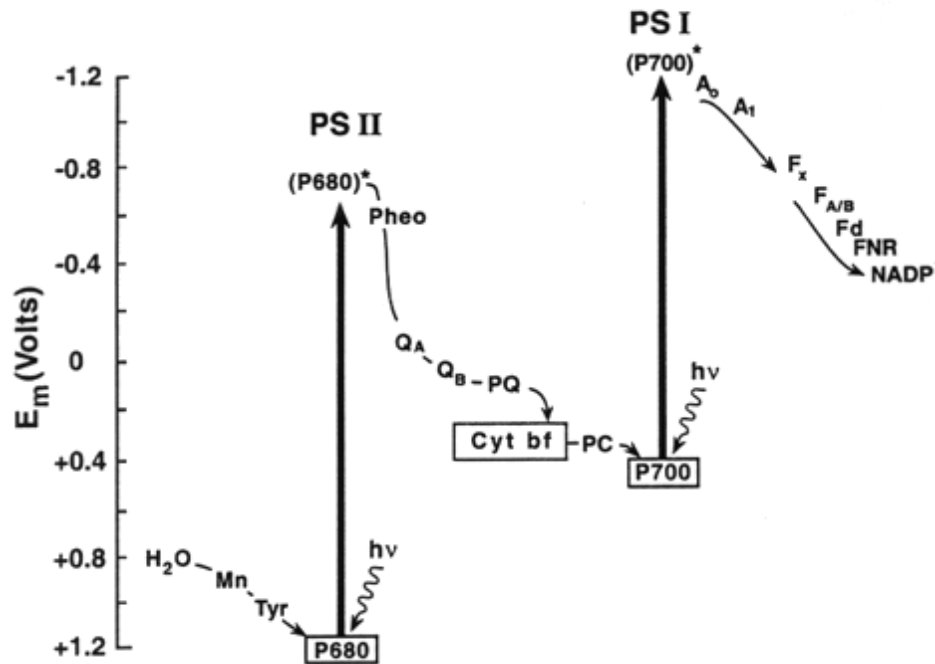


Figure 1.4. Linear photosynthetic ETC reprinted and adapted from Blankenship (1992): Abbreviations: Mn - manganese complex, Tyr - tyrosine; P680 – PS II reaction centre Chl (ground state); P680* - PS II reaction centre Chl (excited state), Pheo - phaeophytin; Q_A and Q_B - primary electron acceptors of PS II, PQ plastoquinone pool, Cyt bf, b-type cytochrome PC plastocyanin (note that PC does not mean phycocyanin in this Figure), P700 – PS I reaction centre Chl (ground state); P700* - PS II reaction centre Chl (excited state), A_0 and A_1 - primary electron acceptors of PS I, F_x $F_{A/B}$, iron sulfur centres; F_d - ferredoxin FNR/ ferredoxin/NADP+ oxidoreductase NADP - nicotinamide adenine dinucleotide phosphate

The transport of four electrons via the thylakoid membrane causes the transport of protons on the membrane. This leads to formation of a pH gradient. The gradient provides the driving force for the ATPase to synthesise ATP from ADP and phosphate (Mitchell (1977); Witt (1979)).

In the case of the linear electron transport, ferredoxin gives its charge to the enzyme ferredoxin-NADP-reductase. This facilitates the synthesis of NADPH/ H^+ from NADP $^+$. NADPH/ H^+ is used within the Calvin Cycle as a reductant for carbon dioxide under consumption of ATP. Apart from the linear electron transport there are other possibilities for the electrons to exit PS I. The two most important ones are cyclic electron transport (Heber *et al.* (1978); Katona *et al.* (1992)) and pseudocyclic electron transport (Mehler reaction Hormann *et al.* (1993)). In the cyclic electron transport electrons from PS I enter the ETC again via the plastoquinone pool. During the pseudocyclic electron transport one electron is transferred to an oxygen molecule from the water splitting process.

The overall process of the ETC is involved in fluorescence quenching as it competes PS II Chl fluorescence emission. Thus the state of the ETC influences the Chl fluorescence yield. Details on this are explained below.

1.1.4 Photosystem II chlorophyll fluorescence

In this study Chl fluorescence provides the experimental access. Chl fluorescence of the antennae of PS II has become very important in photosynthesis research (Schreiber *et al.*

(1986); Schreiber & Bilger (1993)) but also has its place in ecological research (see *Chapter 2*). Chl fluorescence can be measured after illumination of photosynthetic organisms. From an analysis of the Chl fluorescence conclusion can be drawn on the physiological of a photosynthetic system.

1.1.5 Origins of chlorophyll fluorescence

As described above Chl is present in the two PSs. The absorption spectrum of Chl has two maxima: in the blue (450 nm) and red (680 nm) wavelength regions. These originate from the transition from the ground state S_0 to higher singlet states S_x . Higher excitation states can de-excite radiationless or via energy transfer to neighbour molecules to the S_1 state. The emission of Chl fluorescence is only possible from the transition from S_1 state to the S_0 state. All together there are four different pathways for Chl to de-excite from the S_1 state to the ground state S_0 :

- emission of a single light quantum (fluorescence)
- thermal de-excitation via heat emission (thermal deactivation)
- transfer of energy to a neighbour molecule or to the reaction centre of the PS
- indirectly by phosphorescence via a triplet state

The occurrence of phosphorescence is rare and hardly detectable under physiological condition. Both PSs differ in their absorption and fluorescence characteristics. The wavelength of maximal absorbance of PS I in eukaryotic algae and higher plants (for details on cyanobacterial PS I see Myers *et al.* (1980); Gill & Wittmershaus (1999); Gobets *et al.* (2001) and *Chapter 5*) is 700 nm and that of PS II 680 nm. The maximum of fluorescence intensity can be found for PS I at 735 nm and PS II at 683 nm. At room temperature it can be assumed that all variable fluorescence originates from PS II (Baker & Webber (1987)). The quotient of the number of photons emitted as fluorescence and the total number of absorbed photons is called fluorescence quantum yield.

1.1.6 Quenching mechanisms

All mechanisms that cause de-excitation of the S_1 state of Chl and lower fluorescence intensity, proportional to the number of de-excitations, are called quenching mechanisms. Two different quenching mechanisms can be distinguished: non-photochemical quenching and photochemical quenching. Photochemical quenching mechanisms lower the fluorescence by transfer excitons to the ETC. Non-photochemical quenching comprises all mechanisms that do not pass energy to the ETC without a photochemical use.

A ‘pot’ model provides a simple overview of these mechanisms (Figure 1.5). A ‘pot of excitons’ is filled by flow from the antennae. The volume pool comprises all PS II of the sample. De-excitation of exciton-energy has three different pathways: thermal de-excitation, photochemical de-excitation and emission of fluorescence. These pathways are represented by rate constants k_t , k_p and k_f . The exchange of energy can be described by the rate constant p . Two special cases for the energy exchange exist: the first is described by the separate unit model ($p = 0$). In this case no energy exchange takes place between the PSs. The second case is

expressed by the matrix model ($p \rightarrow \infty$), whereby rapid excitation transfer takes place (REE) (Karukstis (1992); Dau (1994b)).

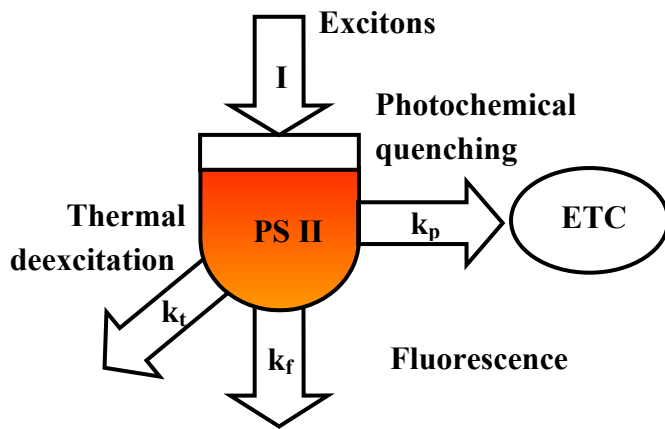


Figure 1.5. Pot model: exciton flow with intensity I induced by absorbed light energy fills PS II like a pool. De-excitation can take place by three different mechanisms: thermal (k_t), emission of fluorescence (k_f) and photochemical quenching.

1.1.7 Photosystem II chlorophyll fluorescence transients

A dark adapted photosynthetic system exposed to sudden illumination shows a characteristic fluorescence (Kautsky & Hirsch (1931)). These transients originate from different steps in ETC and non-photochemical quenching processes with different time constants. A multiphase increase of the fluorescence intensity (i.e. fluorescence quantum yield) at the beginning of the transient is then followed by a multiphase decrease (Figure 1.6).

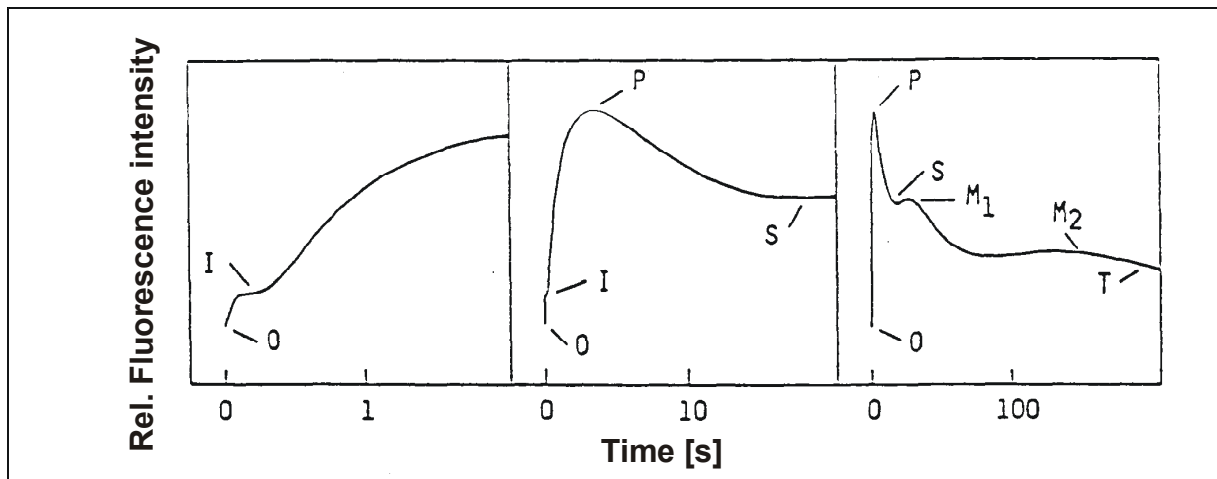


Figure 1.6. Fluorescence transient of dark adapted leaves in different time scales: O - fluorescence of the ground state I - intermediate level, P - maximal fluorescence, S - quasi stationary level, Mx - slow maxima, T - steady state (Briantais *et al.* (1986)).

The transients of Chl fluorescence can be divided into different phases. Prior to the illumination the fluorescence quantum yield is not zero. It is possible to measure the ground fluorescence F_0 with a weak (non-actinic) measuring light. After the start of the illumination with actinic light the fluorescence quantum yield rises with a plateau between the maximum P. In the case that the measuring light has a saturating effect on the photosynthetic apparatus all primary acceptors, Q_A , would be reduced and the fluorescence yield would reach its maximum. The Calvin Cycle reduces Q_A and leads to a decrease in fluorescence quantum yield. The last phase

T is the so-called steady state phase. In the steady state all quenching mechanisms and exciton flow of absorbed light quanta are in balance. The assignment of different phases of the transient is named O-I-D-P-T nomenclature (the letter D marks a ‘dip’ between phases I and P, Briantais *et al.* (1986); Hansen *et al.* (1991)). Another nomenclature that defines fluorescence parameters and the calculation of the photosynthetic parameters used as a standard in fluorescence quenching analysis was given by (van Kooten & Snel (1990) (Table 1.2)). This nomenclature was also employed in this thesis where applicable. The principles of Chl fluorescence quenching analysis is explained by Figure 1.7.

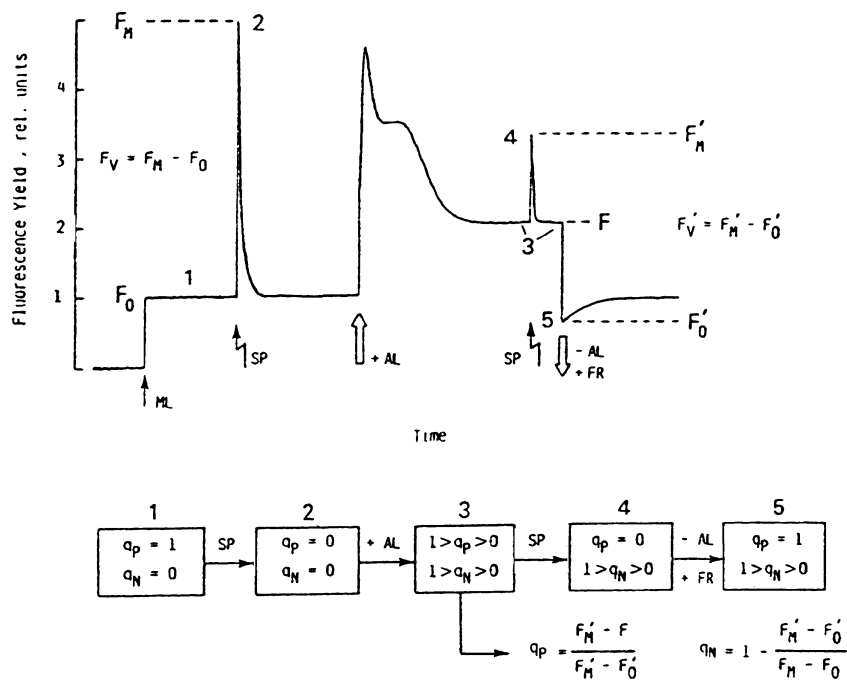


Figure 1.7. Principles of quenching analysis by the saturation pulse method (van Kooten & Snel (1990)). Fluorescence yield is measured with a modulation fluorometer. Depending on the light conditions 5 different states are distinguished and the corresponding points in the induction curve characterised by fluorescence yield notations (e.g. F_m , F_0) and quenching coefficients (q_p and q_N). Fluorescence quenching at a given time following the onset of actinic illumination (at point 3) is evaluated by comparisons with the dark adapted reference state (1), which is characterised by $q_p = 1$ and $q_N = 0$. In both cases a pulse of saturating light is applied to close all PS II reaction centres, thus eliminating photochemical quenching ($q_p = 0$) (points 2 and 4). It is assumed that non-photochemical quenching is not affected during a saturation pulse. q_p and q_N are quenching coefficients designating the relative decrease in variable fluorescence yield. The fluorescence yield F'_0 i.e., in the energised state with all reaction centres open, is determined briefly after switching off actinic light in the presence of weak far-red illumination (point 5). ML, weak modulated measuring light (approx. $6 \text{ nE}^{-2} \text{ s}^{-1}$ at 660 nm); SP, saturating light pulse (approx. $10000 \text{ } \mu\text{E m}^{-2} \text{ s}^{-1}$, $400 \text{ nm} < \lambda < 700 \text{ nm}$, applied for 0.5 – 2 s); AL continuous actinic light; FR, far red light (approx. $6 \text{ } \mu\text{E m}^{-2} \text{ s}^{-1}$, $\lambda > 700 \text{ nm}$).

a: fluorescence intensity indicators

F	fluorescence intensity	actual fluorescence intensity at any time
F₀	minimal fluorescence (dark)	fluorescence intensity with PS II reaction centres open while the photosynthetic membrane is in a non-energised state i.e. dark or low light adapted $q_P = 1$ and $q_N = 1$. It can also be used for the O level in the O-I-D-P-T nomenclature but it should be clearly described how it is determined.
F_I	fluorescence at I level	fluorescence intensity at I level (O-I-D-P-T nomenclature)
F_P	fluorescence at P level	fluorescence intensity at P level (O-I-D-P-T nomenclature)
F_S	fluorescence in steady state	fluorescence intensity at the steady state. i.e., T-level in O-I-D-P-T nomenclature. Steady state is defined as a period within which the fluorescence intensity does not change while the external parameters remain constant
F_m	maximal fluorescence (dark)	fluorescence intensity with all PS II reaction centres closed (i.e. $q_P = 0$) all non-photochemical quenching processes are at a minimum (i.e. $q_N = 0$) (this is the classical maximum fluorescence level in the dark or low light adapted state)
F'_m	maximal fluorescence (light)	fluorescence intensity with all PS II reaction centres closed in any light adapted state i.e. $q_P = 0$ and $q_N \geq 0$
F'₀	minimal fluorescence (light)	fluorescence intensity with PS II reaction centres open in any light adapted state i.e.. $q_P = 1$ and $q_N \geq 0$
F_V	variable fluorescence (dark)	maximum variable fluorescence in the state when all non-photochemical processes are at a minimum, i.e. $(F_m - F_0)$
F'_V	variable fluorescence (light)	maximum variable fluorescence in any light adapted state i.e. $(F'_m - F'_0)$

b: quenching parameter and photochemical yield

q_P	photochemical quenching	$(F'_m - F) / (F'_m - F'_0)$
q_N	non-photochemical quenching	$(F'_m - F'_0) / (F'_m - F'_0)$
Φ_P	photochemical yield	$(F_m - F_0) / (F_m)$

Table 1.2. Definition of Chl fluorescence nomenclature according to van Kooten & Snel (1990), see Figure 1.7 for its application.

Chapter 2. A fluorometric method for the differentiation of algal populations *in vivo* and *in situ*.

2.1 Abstract

Fingerprints of excitation spectra of chlorophyll fluorescence can be used to differentiate 'spectral groups' of microalgae *in vivo* and *in situ* in, e. g., vertical profiles within a few minutes. The investigated spectral groups of algae (green group - chlorophyta; blue - cyanobacteria; brown - heterokontophyta, haptophyta, dinophyta; mixed - cryptophyta) are each characterised by a specific composition of photosynthetic antennae pigments and, consequently, by a specific excitation spectrum of the chlorophyll fluorescence. Particularly relevant are chlorophyll *a*, chlorophyll *c*, phycocyanin, phycoerythrin, fucoxanthin and peridinin. A laboratory based instrument and a submersible instrument were constructed containing light-emitting diodes to excite chlorophyll fluorescence in five distinct wavelength ranges. Norm spectra were determined for the four spectral algal groups (several species per group). Using these norm spectra and the actual five-point excitation spectrum of a water sample, a separate estimate of the respective chlorophyll concentration is rapidly obtained for each algal group. The results of dilution experiments are presented. *In vivo* and *in situ* measurements are compared with results obtained by high performance liquid chromatography. Depth profiles of the distribution of spectral algal groups taken over a time period of few seconds are shown. The described method for algal differentiation opens up new research areas and monitoring, supervision potential related to photosynthetic primary production in aquatic environments.

Introduction

The greatest problem of existing plankton determination methods is that these methods are usually retrospective and not suited to instant assays *in situ*. Aspects such as patchiness, vertical algal migration and nanoplankton can hardly be detected because of time-consuming enumeration problems that is the analysis of a low number of samples (Edgar & Laird (1993); Carrick & Schelske (1997)). The method most employed for phytoplankton determination is cell counting under a reversed microscope (Utermöhl (1958)). Another important method beside the microscopical counting for the determination of phytoplankton abundance is the measurement of pigments by high performance liquid chromatography (HPLC). Using marker carotenoids this method enables the determination of taxons (Jeffrey & Hallegraeff (1980); Gieskes & Kraay (1984); Mackey *et al.* (1996); Wiltshire *et al.* (1998)). This method is also retrospect.

In this work five spectral excitation ranges are used to differentiate groups of microalgae *in situ* within a few seconds. Numerous laboratory tests are presented leading to a new submersible instrument for *in situ* applications. Measurement examples are presented which where derived from the analysis of different waterbodies, including seawater. These include the vertical distribution of algae in a eutrophic lake as determined with the submersible instrument in comparison with standard microscopical biomass determinations, which proves the feasibility of monitoring algal assemblage composition and biovolume *in situ* using a sensor.

Chl fluorescence emission measured around 685 nm is accepted as a measure of Chl contents of algae in aquatic systems. Depth profiling of Chl fluorescence has been carried out since the early seventies (Kiefer (1973)). Since then attempts have been made to distinguish different groups of phytoplankton using their fluorescence properties *in vivo* (Yentsch & Yentsch (1979); Yentsch & Phinney (1985)). Kolbowski & Schreiber (1995) used light-emitting diodes and were able to distinguish fluorescence kinetics caused by different groups of algae. Cowles *et al.* (1993) show vertical profiles of PE containing algae and Desiderio *et al.* (1997) of fluorescence emission spectra without relation to the biomass or diverse algal groups. Seppala & Balode (1998) employed spectral fluorescence in the Baltic Sea. Millie *et al.* (2002) used fluorescence and absorbance spectra to discriminate microalgae. The rapid *in situ* estimation of the Chl concentrations related to individual algal groups has as yet not been approached.

The concept for fluorometric differentiation of algal populations is based on insights on energy transfer and fluorescence emission of photosynthetic organisms obtained over the last two decades. It was found that Chl fluorescence is mainly emitted by Chl *a* of the PS II antenna system, which consists of an evolutionary conserved Chl *a*-containing core and species-dependent peripheral antennae. In Figure 2.1, $A_{\text{peri}}(\lambda_{\text{ML}})$ and $A_{\text{core}}(\lambda_{\text{ML}})$ represent the absorption of the peripheral and core antennae, respectively. The species-dependent $A_{\text{peri}}(\lambda_{\text{ML}})$ affects both

the Chl-fluorescence excitation spectrum (see *Results* below) and the colour of the respective photosynthetic organism. Algal colour is a useful taxonomic criterion, and algal taxonomic groups differ significantly in their fluorescence excitation spectrum (see Table 1.1 for different spectral algal groups).

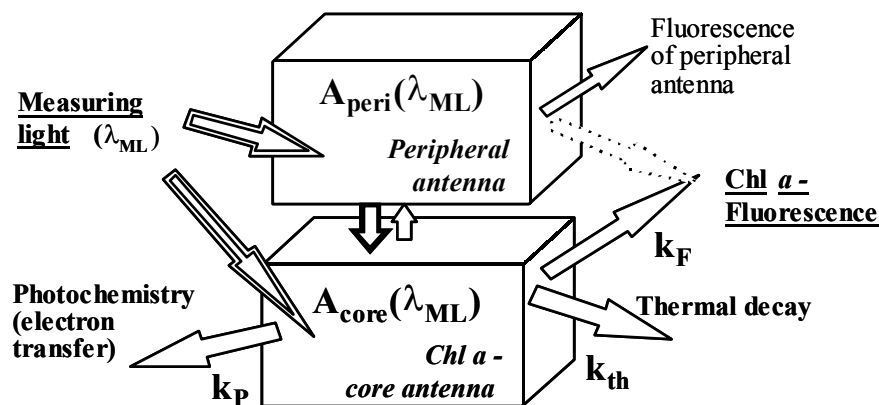


Figure 2.1. General model for PS II antenna systems. $A_{\text{peri}}(\lambda_{\text{ML}})$ and $A_{\text{core}}(\lambda_{\text{ML}})$ denote the absorption cross-section of the peripheral and core antenna, respectively. The exciton dynamics in the PS II core antenna are characterised by REE (Dau (1994b)); the details of the excited state dynamics in the peripheral antenna (e.g., the phycobilisome system of cyanobacteria) are, in the present context, of minor importance and therefore not explicitly considered.

Here the four spectral groups: green group, blue, brown and mixed (cryptophyta) are considered. Those algal groups occur in many aquatic systems.

Experiments were carried out with a laboratory-based and a submersible fluorometer, which enable rapid measurement of the Chl *a* fluorescence intensities excited at five distinct wavelengths. The evaluation of the Chl concentration associated with individual algal groups is based on a fit of the measured spectra by so-called norm curves. In contrast to the instrument of Kolbowski & Schreiber (1995), Beutler (1998) added one additional diode that enables the determination of an additional algal group (PE-containing algae). However, in order to increase sensitivity the mean intensity of the measuring light was higher ($4.5 \mu\text{Em}^{-2}\text{s}^{-1}$). The approach of Beutler (1998) was tested for its reliability and the feasibility of use in submersible instruments. The reliability of this approach was tested by several experiments in the laboratory. *In situ* experiments are presented which show its benefits. It is also shown that the fluorometric estimates provide a reliable measure of algal biovolume.

2.2 Materials and methods

2.2.1 Fluorescence measurements

In order to measure the norm spectra and to carry out laboratory and *in vivo* experiments a bench-top fluorometer was developed. Figure 2.2 illustrates the function of the fluorometer. The following light-emitting diodes were employed for excitation of pigment complexes (centre wavelengths and light intensity are given in parenthesis): Oshino OL-ESB 41510 (450 nm, $3 \mu \text{E m}^{-2}\text{s}^{-1}$, Oshino-Lamps, Tokio, Japan), 525 nm Kingbright 40-L-2543MGC (525 nm, $7 \mu \text{E m}^{-2}\text{s}^{-1}$, Kingbright, City of Industries, USA), 2 x 570 nm Oshino OL SUG 14180 (570 nm, $3 \mu \text{E m}^{-2}\text{s}^{-1}$, Oshino-Lamps, Tokio, Japan), Hewlett Packard HLMP-DL08 (590 nm, $6 \mu \text{E m}^{-2}\text{s}^{-1}$), Oshino OL-SUA 14180 (610 nm, $3 \mu \text{E m}^{-2}\text{s}^{-1}$, Oshino-Lamps, Tokio, Japan). Light intensities were determined at the position of the algae suspension using the photosynthetic actinic radiation (PhAR) sensor Hansatech QRT 1 (Hansatech, U.K.).

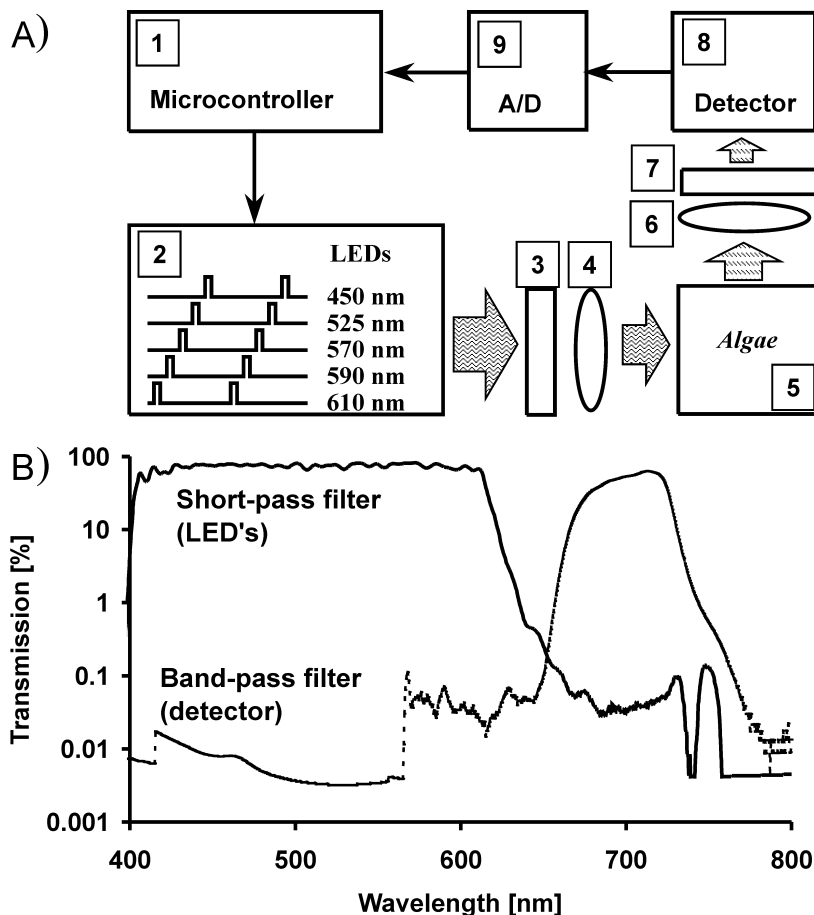


Figure 2.2. Fluorometer (Beutler (1998)): (A) components, (1) microcontroller, (2) five light-emitting diodes (see text), (3) short-pass filter to block red and IR emission (see B), (4) focussing lens ($f = 25 \text{ mm}$), (5) sample volume containing algal suspension (see also Figure 2.3), (6) focussing lens, (7) band-pass filter (see B), (8) integrated photomultiplier, (9) 12-bit AD-converter (conversion rate of 100 kHz). (B) transmission spectra of the short-pass filter (DT cyan special, Balzers, Liechtenstein, (3) in A) and the band-pass filter (bbe-fk1, bbe Moldaenke GmbH, Kiel, Germany, (7) in A).

In the instrument, five LEDs are switched on sequentially at a frequency of 5 kHz. The duration of the measuring pulse is 0.1 ms. The LED light passes through a short-pass filter (50% transmission at 615 nm DT cyan special, Balzers, Liechtenstein) and a focussing lens. The spectra are shown in Figure 2.2 B. Chl fluorescence emitted by the algal suspension was detected using a photomultiplier (H6779-01, Hamamatsu, Hamamatsu-City, Japan) behind a band pass filter (bbe-fk1, bbe Moldaenke GmbH, Kiel, Germany). The photomultiplier signal was digitised by an AD-converter (12-bit AD-converter, conversion rate of 100 kHz) and processed by the same microcontroller (MM-103-5CAQ 18, Phytec, Mainz, Germany) used for controlling the LEDs.

A cuvette (25 x 25 x 70 mm) filled with 25 ml of algal suspension was placed in the measuring chamber of the instrument.

Depth profiles obtained from *in situ* experiments were recorded with the submersible probe sketched in Figure 2.3 A. The set-up can be briefly described as follows: the instrument set-up of Figure 2.2 was mounted inside a steel tube (photograph in Figure 2.3B). A light shield in the form of an outer tube prevents the incidence of direct sunlight. The measurement of water pressure enables calculation of the submersion depth. Data can be stored in the probe or is transferred on-line to a computer. In the latter case, the probe sends a set of data (water depth and fluorescence data) every second to a computer or laptop during measurement. Sample water flows across the measuring cavity when the instrument is lowered into the water. In this study, the average vertical velocity of the probe during depth profiling was 30 cm s⁻¹.

In the dilution experiments (Figures 2.6 and 2.7), norm spectra had been obtained by measurement of the fluorescence excitation spectra of cultures of the four algal species (see algal cultures) actually used in this experiment. The standard deviations of the norm spectra were determined in order to account for different accuracy at different wavelengths in the subsequent mathematical analysis. Prior to the spectral analysis, the samples were exposed to the measuring light for 90 s. Each measurement (duration of 9 s) was repeated 10 times using the same sample. Standard deviations were calculated on basis of these 10 measurements.

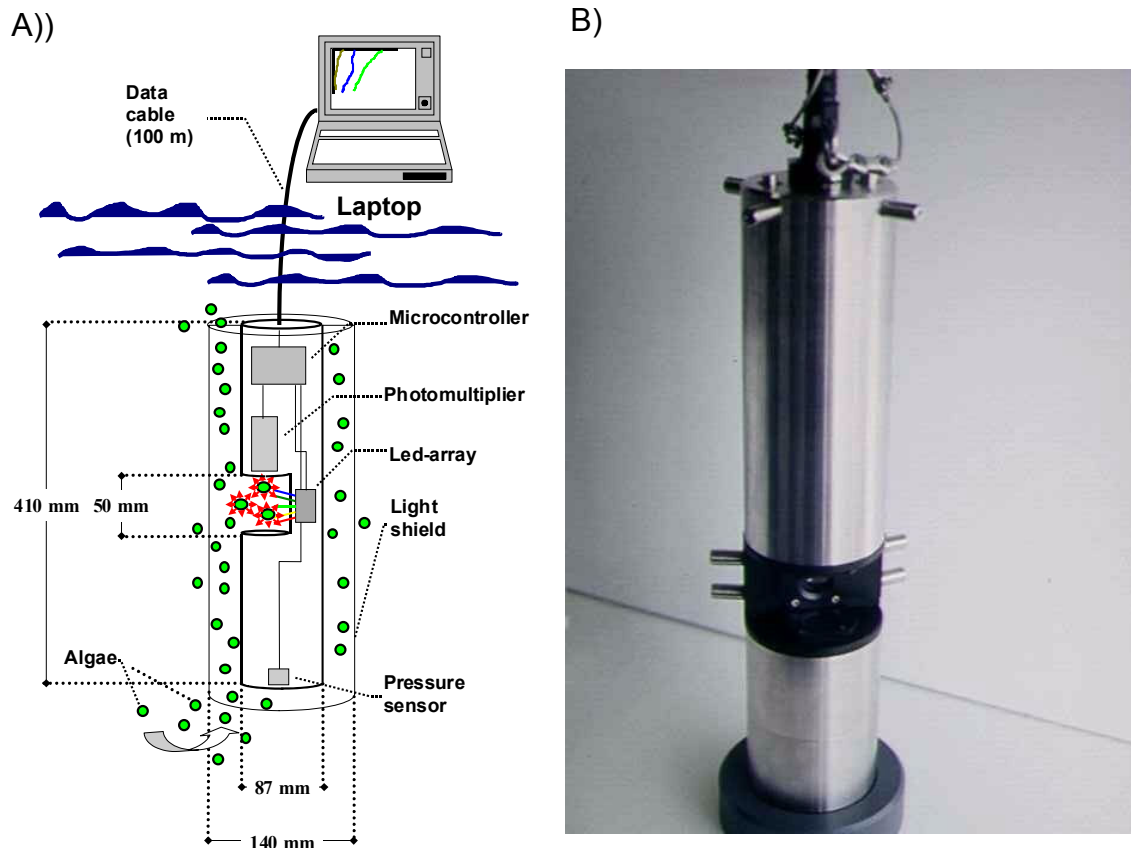


Figure 2.3. A) The submersible probe. All electronic and optical components depicted in Figure 2.2 are enclosed in a stainless steel housing with an open measuring cavity (50 mm height) as indicated. The stainless steel housing is encased in a black polyethylene cylinder (diameter of 140 mm), open at the bottom and top, serving as a light shield. Data is transferred on-line via a RS 485 interface and cable to a personal computer, on board a research vessel. The measured water pressure (piezo-sensor) is used to calculate the actual water depth. Deconvolution of the data is done by the connected computer. B) Photograph of the submersible probe. The optics are installed in the black measuring chamber. The covering (black polyethylene cylinder) is not shown.

2.2.2 Algal cultures

In order to obtain norm spectra the following cultures of the four differentiated spectral algal groups (Table 1.1: green, blue, brown, mixed) were grown. The cyanobacteria were new isolates. The others were taken from culture collections.

The green group (chlorophyta): *Chlamydomonas* sp., *Chlorella* sp., *Micractinium* sp., *Monoraphidium* sp., *Scenedesmus falcatus*, *Scenedesmus obliquus*, *Scenedesmus quadricauda*, *Scenedesmus subspicatus*, *Scenedesmus acutus*.

The blue group (cyanobacteria): *Microcystis aeruginosa* (6 strains), *Microcystis wesenbergii* (8 strains), *Microcystis viridis*, *Anabaena* sp., *Aphanizomenon* sp., *Synechococcus leopoliensis*.

The brown group (diatoms and dinophyta): *Cyclotella meneghiniana*, *Nitzschia* sp., *Synedra* sp., *Ceratium furcoides*.

The mixed group (cryptophyta): *Cryptomonas* sp. (3 strains), *Cryptomonas erosa*.

In the dilution experiments of Figures 2.6 and 2.7, the following algal cultures were employed: green group: *Chlorella vulgaris*, blue group: *Microcystis aeruginosa*, brown spectral group: *Cyclotella meneghiniana*, mixed spectral group: *Cryptomonas* sp.

2.2.3 Growth of cultures and sampling

All cultures used in the experiments (*norm spectra* and *laboratory experiments*) were grown for 14 days in white light (light intensity $20 \mu\text{E m}^{-2}\text{s}^{-1}$) in WC medium (Guillard & Lorenzen (1972)) at a temperature of 20 °C. Subsamples of the cultures were diluted with WC medium for fluorescence measurement within the linear range of the fluorometer. Measurements of fluorescence were made at a temperature of 20 °C.

For determination of the norm spectra, samples were diluted to linear range of the fluorometer with WC medium for fluorescence measurements. Three samples of each culture were measured in a 25 ml cuvette (optical path-length 25 mm). Cultures were filtered with a sieve (mesh size 50 μm). Samples were adapted to the measuring light for 90 s before starting the measurement (measurement duration of 9 s) to exclude pre-illumination effects.

For an illustration of the operation under *in-situ* conditions, samples were taken on a cruise in March '98 at five stations at the Schlei (Figure 2.10), a brackish 50-km fjord of the Baltic Sea (Germany) at the sites (a) Schleimünde, (b) Bienebek, (c) Ulsnis, (d) Große Breite and (e) Fahrdorf. Samples were collected with a 5 l Ruttner water sampler at a water depth of 1 m. Samples were adapted to the measuring light for 90 s prior to the start of the measurement. Three measurements of 9 s duration were averaged.

To test the *in situ* fluorescence determination profiles were recorded with the submersible instrument. The integration per data point was 1 s.

2.2.4 Determination of chlorophyll concentrations

HPLC is a special mode of chromatography and a widely used analytical technique (e.g. Shoaf (1978); Stransky (1978); Kazakevich & McNair (2002)). Chromatographic processes can be defined as separation techniques involving interactions between stationary and mobile phases. HPLC utilizes a liquid mobile phase to separate the components of a mixture. These components (or analytes) are first dissolved in a solvent, and then forced to flow through a chromatographic column under high pressure. In the column, the mixture is separated into its components. The stationary phase is defined by the immobile packing material in the column. The interaction of the solute with mobile and stationary phases can be manipulated through different choices of both solvents and stationary phases.

HPLC instrumentation typically includes a pump, injector, column, detector and recorder or data system. The heart of the system is the column where the separation occurs. Since the stationary phase is composed of micrometer size porous particles, a high pressure pump is required to move the mobile phase through the column. The chromatographic process begins by injecting the solute onto the top of the column. Separation of components occurs as the analytes and mobile phase are pumped through the column. Eventually, each component elutes from the column as a narrow band (or peak) on the recorder. Detection of the eluting components is important, and this can be either selective or universal, depending upon the detector used. The response of the detector to each component is displayed on a chart recorder

or computer screen and is known as a chromatogram. To collect, store and analyse the chromatographic data, computers, integrators, and other data processing equipment are frequently used.

In ion-exchange chromatography the stationary bed has an ionically charged surface of opposite charge to the sample ions. This technique is used almost exclusively with ionic or ionisable samples. The stronger the charge on the sample, the stronger it will be attracted to the ionic surface and thus, the longer it will take to elute. In normal phase chromatography, the stationary bed is strongly polar in nature (e.g., silica gel), and the mobile phase is nonpolar (such as n-hexane or tetrahydrofuran). Polar samples are thus retained on the polar surface of the column packing longer than less polar materials. Reversed-phase chromatography as employed in this thesis is the inverse of this principle. The stationary bed is nonpolar (hydrophobic, e.g. nucleosil) in nature, while the mobile phase is a polar liquid, such as mixtures of water and methanol or acetonitrile. The less polar the substance is, the longer it will be retained.

Time (min)	%A	%B	%C
0	100	0	0
5	50	50	0
10	50	50	0
15	0	100	0
25	0	100	0
27	100	0	0
29	0	0	100
32	0	0	100
35	100	0	0

Table 2.1. Gradient of solvents used in the first HPLC analysis of the pigments. Time is measured after injection of the sample in the HPLC system. Solvent mixture 'A' consisted of an 80:10:10 methanol: water: ammonium acetate solution and solvent 'B' was a 90:10 methanol: acetone mix. Solvent 'C' was a methanol: propanol mix in a ratio of 10:7.7. The numbers give the relative amounts of solvent ABC at the time in the first column.

Here, concentrations of Chl were determined according to Wiltshire *et al.* (1998) using HPLC (for calibrating the fluorometer, see norm spectra). The method was a shortened version of the Mantoura & Llewellyn (1983) method. It was a binary gradient method where solvent 'A' consisted of a 80:10:10 methanol:water:ammonium acetate solution and solvent 'B' was a 90:10 methanol:acetone mixture. A third solvent 'C' was a methanol: propanol mixture in a ratio of 10:7.7. This provided a better separation of the carotenes. All solvents were degassed nanograde HPLC solvents. The flow rate was 1 ml·min⁻¹. The column was a reversed phase 5C18, 25 cm long column packed with Nucleosil. The gradient used is given in Table 2.1. The

algae were extracted according to the method of Wiltshire *et al.* (1998) involving ultrasonification with quartz sand on ice.

In dilution experiments, Chl concentrations were determined according to Nusch (1980) (in the following denoted as 'spectrochemical' determination of the Chl content) and for *in vivo* experiment according to Barlow *et al.* (1997) via HPLC.

2.2.5 Determination of biovolume

Biovolume concentrations were calculated from phytoplankton cell counts of water samples taken at the same time in ten 1 m depth intervals (Figure 2.12 and 2.13). Samples were taken with a 2-liter-Ruttner water sampler and preserved with Lugol's solution. Total cell numbers were counted in 1 ml sedimentation chambers and average specific biovolumes were calculated with a geometrical formula using linear measurements of dimensions of 50 cells of each species.

2.2.6 Mathematical evaluation

The investigations are based on the analysis of Chl fluorescence from PS II measured around 685 nm at physiological temperatures. For Chl *a* containing photoautotrophs, the mathematical evaluation was based on the following assumptions:

1. constant PS II:PS I ratio,
2. constant fluorescence excitation spectra (independent of physiological status of the cells and the individual strain within the group) and
3. linear independence of the norm spectra.

The validity of these assumptions is discussed below. Here, they are used to derive the required mathematical equations.

For green algae, the response of Chl fluorescence to modulated measuring light can be described by

$$F(\lambda_{ML}) = N_{PS II} c_{instr} I_{ML}(\lambda_{ML}) A_{PS II}(\lambda_{ML}) \Phi_F \quad (2.1)$$

with: $N_{PS II}$, number of PS II in the sample volume; $A_{PS II}(\lambda_{ML})$, PS II absorption cross-section (in m^2); I_{ML} , intensity of the measuring light (in $\mu E m^{-2} s^{-1}$); Φ_F , fluorescence yield (Φ_F and its variability are discussed in, e.g., Dau (1994b, a); Govindjee *et al.* (1996); c_{instr} , a fluorometer-dependent constant.

Equation (2.1) is only valid for algal suspensions which are optically sufficiently thin. Additional terms which correct for mutual shading of algae and for fluorescence reabsorption would otherwise be required.

Equation (2.1) holds for green algae (green group, see Introduction) and, presumably, also holds for the organisms of the brown group. It has quite a simple form as one global

absorption coefficient $A_{\text{PS II}}$ is assumed. This is legitimate because REE within the Chl *a/b* type peripheral antennae (Dau (1994b); Dau & Sauer (1996); Dau (1996)) keeps the deviation from the Boltzmann distribution of excited states (which involves all PS II Chls) below 10% (Appendix in Dau & Sauer (1996)). Consequently the fluorescence yield Φ^{F} per PS II exciton is independent of the wavelength λ_{ML} of the measuring light, even though the absorption spectra may be different. However, this needs to be reformulated for phycobilisome-containing organisms (blue and mixed group) because the assumption of REE that involves all antenna pigments is not valid for these organisms. For PBS-containing organisms, the excited state equilibration within the PS II core antenna is still under scrutiny, but it is highly likely that the assumption of REE for the PS II core antenna is sufficiently good. The REE domain, however, is unlikely to include the peripheral PS II antenna (meaning the PBS). Any absorption event occurring in the PBS system is followed by rapid transfer of excited state energy to the core antenna which competes with decay processes (fluorescence and non-radiative decays). The effective yield for transfer of excited-state energy from the peripheral antenna to the PS II core antenna is denoted as $\Phi_{\text{T}}(\lambda_{\text{ML}})$. It depends on the excitation wavelength. Using $\Phi_{\text{T}}(\lambda_{\text{ML}})$ the detectable fluorescence intensity can be calculated as follows:

$$F_{\text{k}}(\lambda_{\text{ML}}) = N_{\text{PS II,k}} c_{\text{instr}} I_{\text{ML}}(\lambda_{\text{ML}}) A_{\text{eff,k}}(\lambda_{\text{ML}}) \Phi_{\text{F,k}} \quad (2.2)$$

with
$$A_{\text{eff,k}}(\lambda_{\text{ML}}) = \Phi_{\text{T,k}}(\lambda_{\text{ML}}) A_{\text{peri,k}}(\lambda_{\text{ML}}) + A_{\text{core}}(\lambda_{\text{ML}}) \quad (2.3)$$

where $A_{\text{peri,k}}(\lambda_{\text{ML}})$ and $A_{\text{core}}(\lambda_{\text{ML}})$ are the individual absorption cross-sections of the peripheral and the core antenna, respectively. The parameter $A_{\text{eff,k}}(\lambda_{\text{ML}})$ represents an effective absorption cross-section of the PS II (core complex + peripheral antenna); $\Phi_{\text{F,k}}$ denotes the wavelength-independent fluorescence yield measurable for direct (absorption by a pigment of the core antenna) or indirect excitation (energy transfer from the peripheral antenna to the core antenna) of the PS II-core antenna. The superscript 'k' labels species-dependent parameters which refer to properties of the peripheral antenna of the *i*'th species or species group. (Whether the properties of the core antenna are fully species-independent is still unclear, although this is of minor importance here).

Equation (2.2) is equivalent to Equation (2.1) but of more general validity. For a sufficiently thin optical suspension containing a mixture of various species, the fluorescence intensity is obtained by summarising over the $F_{\text{k}}(\lambda_{\text{ML}})$ of the contributing species or algae groups.

According to assumption 3, the determination of the distribution of the spectral algal groups is based on the premise that the measured excitation spectrum is a superposition of the signals from the individual cells.

$$F(\lambda_{ML}) = \sum_{k=1 \text{ to } n} C_{CHLa,k} f_k(\lambda_{ML}) I_{ML}(\lambda_{ML}) \quad (2.4)$$

$$\text{with } f_k(\lambda_{ML}) = c_{instr} (N_{PS II,k} / C_{CHLa,k}) A_{eff,k}(\lambda_{ML}) \Phi_{F,k} \quad (2.5)$$

where $C_{Chl,k}$ is the concentration of Chl *a* which is contained in cells of the *k*'th species (or algal group). Equation (2.4) indicates that, provided the value of f_k is known for a sufficient number of excitation wavelengths (see Figure 2.4 below), an estimate of the Chl concentration per individual algal group can be obtained (see *Appendix A*).

Again, this only holds for an optically thin sample. Furthermore, it is assumed that for each algal group the number of PS II ($N_{PS II}$) is proportional to the corresponding Chl *a* concentration, C_{Chla} . This assumption is not obvious, as strong variations in PS II/PS I stoichiometry can change the ratio between $N_{PS II}$ and C_{Chla} . For example, pronounced variations in the PS II – PS I stoichiometry might change the ratio between $N_{PS II}$ and C_{Chla} (see also *Discussion* below)

2.2.7 Norm spectra

The norm spectra $f_k(\lambda_{ML})$ are of crucial importance for the evaluation by means of Equations (2.4) and (2.5). They have to fulfil the following requirements:

- They have to be linearly independent, i.e., it must be impossible to present one of them by an adequately weighted sum of the other ones.
- The shape of each norm spectrum has to be constant for the algal group represented, e.g., it has to be independent of the number of cells and of the difference between the environmental parameters prevailing during the determination of the norm spectra and those in the actual experiment.
- The norm spectra have to be determined with sufficient accuracy.

2.3 Results

2.3.1 Measurement of norm spectra

The f_k -values were obtained for various species of four spectral algal groups at five distinct excitation wavelengths (Figure 2.4). In the following, the set of five mean values of f_k obtained for each individual species group are called 'norm spectra'. Figure 2.4 demonstrates that each spectral group is characterised by a specific norm spectrum. The maximum for the green group is at 450 nm due to the Chl *a/b* antennae. A high signal is found at the 610 nm LED in the blue group. This is caused by PC. In this group, the largest standard deviation for all groups occurs at an excitation wavelength of 610 nm corresponding to interspecies differences within this group. In addition, the brown group (diatoms and dinoflagellates) has a high signal in the green wavelength region (525 nm) because of the pigments fucoxanthin (diatoms) and peridinin (dinoflagellates). High fluorescence intensity caused by PE was found for the cryptophyta (*Cryptomonas*) at 570 nm.

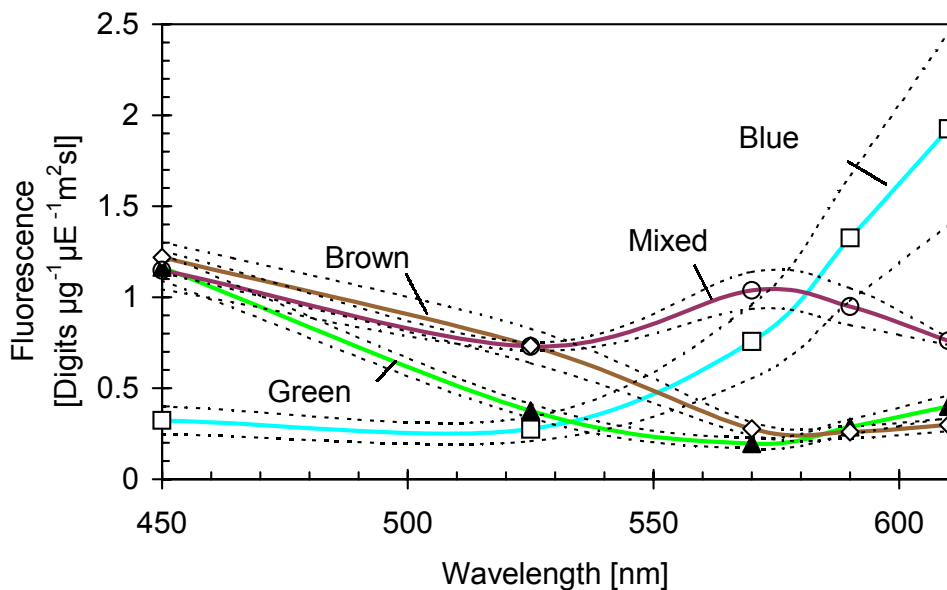


Figure 2.4. Mean fluorescence-excitation probabilities for four spectral algal groups (norm spectra, Beutler (1998)). Excitation probabilities were determined for several species per spectral algal group (see text). Data points shown are mean values (green, closed triangles; blue, open squares; brown, open circles; mixed, open diamonds). The measured fluorescence intensities were normalised to the Chl content and the light intensity of the respective LED. The spectra from members of each spectral algal group were averaged. The error line (dotted) represents the species-dependent differences in the excitation spectrum of an individual spectral group. These curves were calculated by adding/subtracting the standard deviation ($\sigma(n-1)$) of the spectra taken from the diluted cultures to/from the average spectra of the spectral algal group. Units on the Y-axis: Digitised photomultiplier voltage in [Digits] per measuring light intensity [$\mu\text{E m}^{-2} \text{s}^{-1}$] and Chl concentration of the algal sample [$\mu\text{g l}^{-1}$].

2.3.2 Linear independence of the norm spectra

The first requirement of norm spectra is linear independence. All four norm spectra were fitted by a sum of the other three curves. Figure 2.5 shows that the best fits for each curve failed to approximate the norm spectra. This verifies that the premise of independence holds.

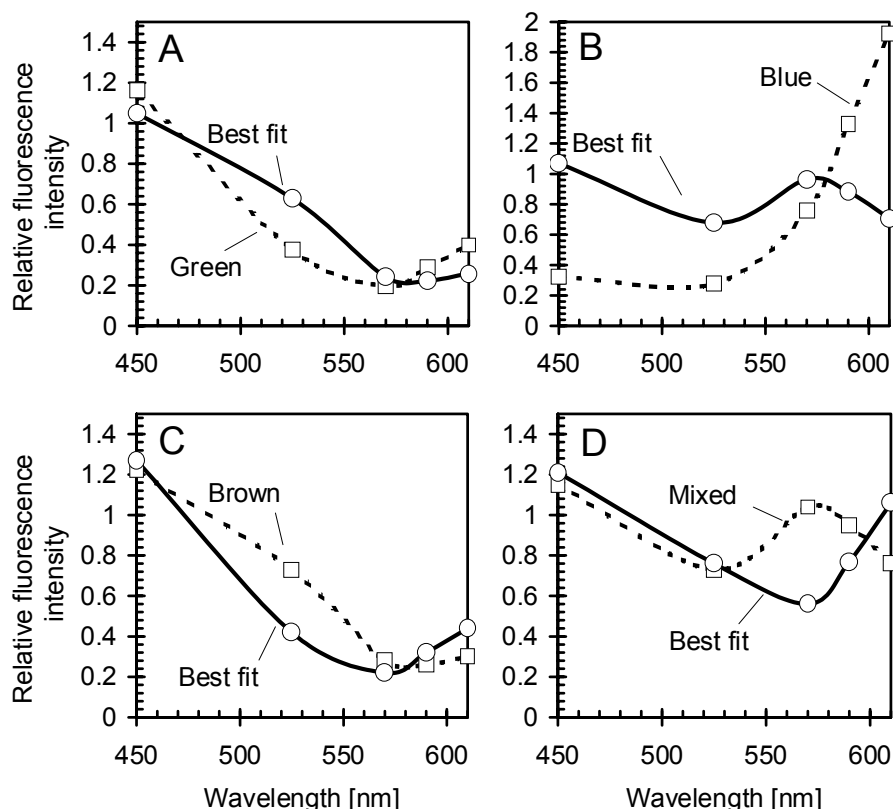


Figure 2.5. Attempt to fit one norm spectra by the weighted sum of the other. The experiment was carried out for four norm spectra of four spectral groups. (A) Green spectral group, (B) Blue spectral group, (C) Brown spectral group and (D) Mixed spectral group (dotted lines and circles: norm spectrum of a single spectral algal group, solid lines and squares: best fit of the spectrum). The failure of these fits is a crucial premise for the evaluation using Equations (2.4) and (2.5).

2.3.3 Laboratory tests: common dilution factor for all classes

In the dilution experiments of Figure 2.6, C_{Chla} of three algal group was kept constant while C_{Chla} of the blue spectral group increased. For Chl *a* concentrations below 30 ng l^{-1} (or 30 pg ml^{-1}), the fluorometrically determined Chl *a* (of the single spectral algal groups) concentrations deviate significantly from the anticipated value (solid line). However, for Chl *a* concentrations ranging from $\sim 80 \text{ ng l}^{-1}$ to $80 \text{ } \mu\text{g l}^{-1}$ the fluorometric method is reasonably precise (deviations below 25 %).

For Chl concentrations equal or greater than $4 \times 100 \text{ } \mu\text{g l}^{-1}$, the suspension is no longer optically sufficiently thin. Deviations occur due to a light intensity gradient in the sample

volume and, in particular, due to fluorescence re-absorption. A correction for these factors is possible, but has not been applied to the data shown in Figure 2.6.

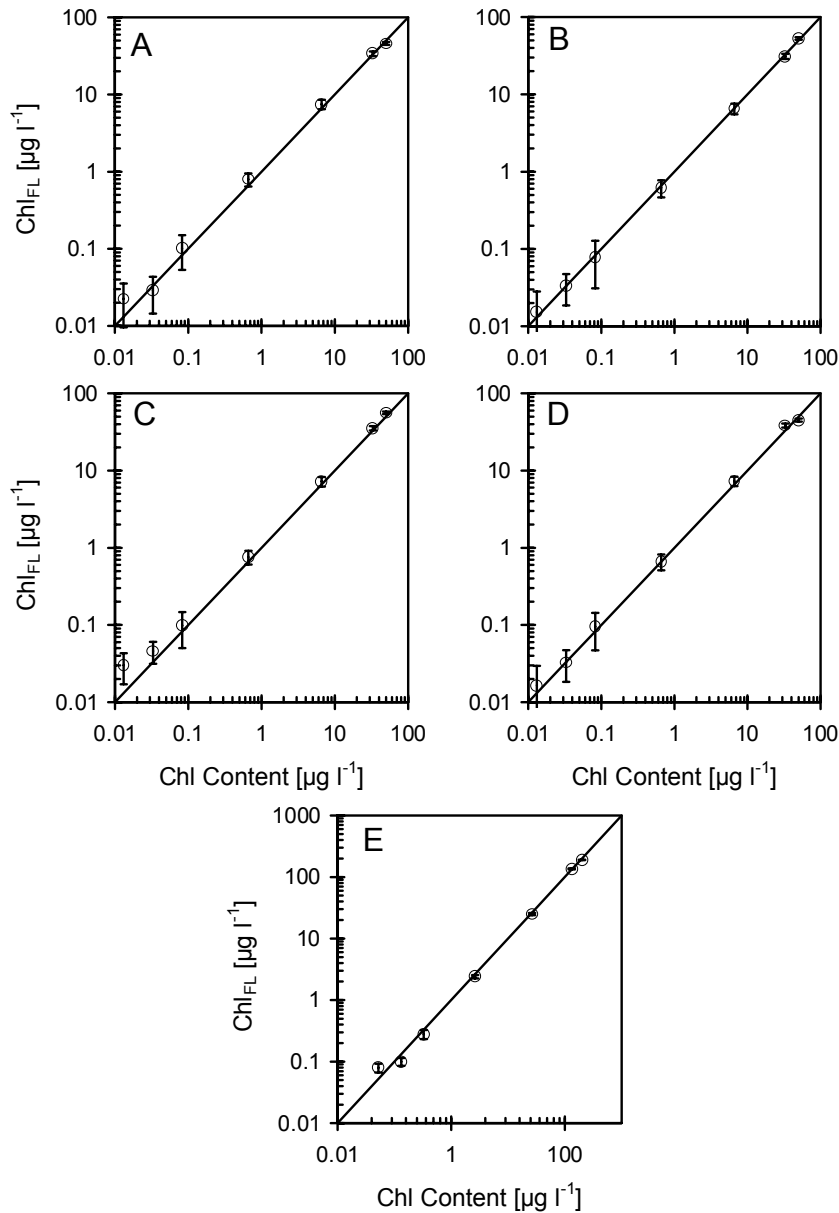


Figure 2.6. Fluorometrically determined Chl concentrations for samples obtained by dilution of a single algal suspension Beutler (1998). The suspensions contained algae of four spectral groups; one quarter of the total Chl was associated with each algal group. The fluorometrically determined Chl content is shown versus the spectrochemically determined concentration for each individual algal group (A, green; B, blue; C, brown; D, mixed) and for the total Chl content (E). The error bars indicate the standard deviation.

In another series of experiments, C_{Chla} of three algal groups was kept constant whereas the C_{Chla} of the fourth group was varied. In Figure 2.7, the result is shown for variation of the concentration of cyanobacteria (blue group). For C_{Chla} below 400 ng l^{-1} (cyanos) and above $20 \mu\text{g l}^{-1}$ (green and mixed) significant errors in the fluorometrically determined Chl *a* concentrations of the least-concentrated algal group are observed. By analysis of various similar

experiments it was found that whenever the ratio between the greatest and the smallest C_{CHLa} reaches a value of about $20 \mu\text{g l}^{-1}$ the Chl *a* concentration of the least-concentrated algal group is not correctly determined; typically, it is overestimated.

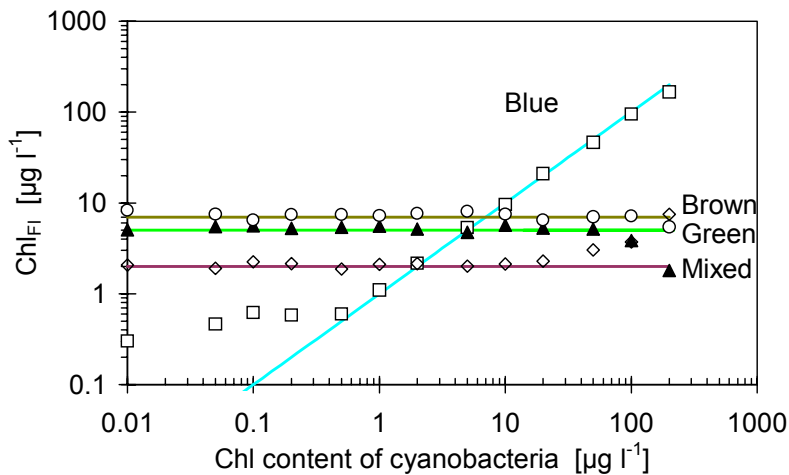


Figure 2.7. Variation of contribution of a single algal group (Beutler (1998)). Algal suspensions with a constant Chl content of the green, brown and mixed group (green $5 \mu\text{g l}^{-1}$, brown $7 \mu\text{g l}^{-1}$, mixed $2 \mu\text{g l}^{-1}$) and a varying Chl content of the blue group were used. The fluorometrical estimate of the Chl content (green, closed triangles; blue, open squares; brown, open circles; mixed, open diamonds) is shown versus the spectrochemically determined Chl content of the blue group.

2.3.4 Influence of pre-illumination on the norm curves

In *in situ* experiments, the algae were naturally exposed to sunlight of different intensities, in particular when depth profiles were determined. Thus, the algae were adapted to different light intensities. To test the submersible probe, the algae are kept in the dark for 2 s. Figure 2.8 shows norm spectra measured upon illumination with different light intensities and measured after a dark period of 2 s.

The constant distance between the dotted lines and smooth lines in the logarithmic plots of Figure 2.8 verifies that the shape of the norm curves is constant. The finding that the curve shapes are hardly dependent on the pre-illumination is not surprising. However, the amplitude was also found to be constant (deviation lower than 25%). This independence of pre-illumination is an important support for the analysis presented here, especially as it shows that the omission of the pre-illumination period of the measurements shown in Figure 2.4 is legitimate in the submersible probe. Its origin is probably in the ability of the algae to adjust their photosynthetic apparatus to the prevailing illumination.

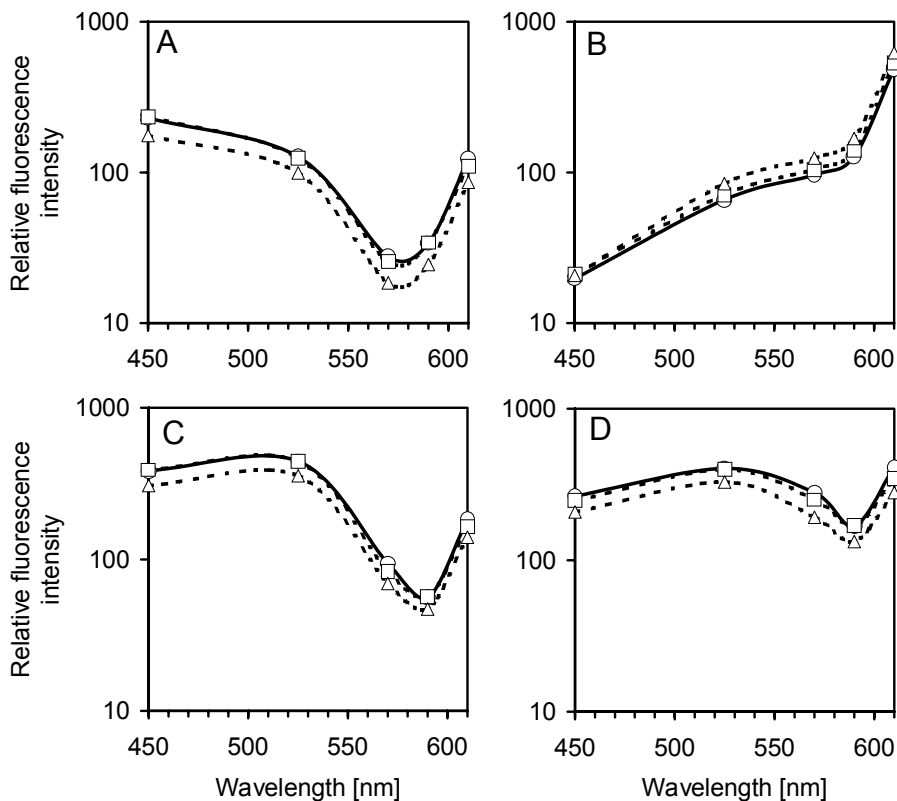


Figure 2.8. Influence of pre-illumination on the norm curves. Norm spectra of algal cultures of a single spectral algal group illuminated for 1 hour with different light intensities and measured after a dark period of 2 s for 1 s. (A) Green spectral group: *Chlorella vulgaris*, (B) Blue spectral group: *Synechococcus leopoliensis*, (C) Brown spectral group: *Cyclotella* sp., (D) Mixed spectral group: *Cryptomonas* sp.. Circles and solid lines: cells dark adapted, squares and dotted lines: cells adapted with $100 \mu\text{E m}^{-2} \text{s}^{-1}$, triangles and dotted lines: cells adapted with $1200 \mu\text{E m}^{-2} \text{s}^{-1}$).

2.3.5 Influence of scattering on the norm curves

Light scattering particles are present in all 'natural samples'. Light is scattered out of the excitation beam resulting in a decrease of the effective excitation intensity, and thus part of the fluorescence light is scattered and does not reach the detector. An experiment using Betonite as a light scatterer is shown in Figure 2.9. Even at a reduction of transmission by 50% (path length of 25 mm), the detected Chl content is decreased by only 5%. Thus, it can be assumed that the light scattering problem will affect the accuracy of the method by less than 10%, unless extremely turbid water samples are investigated. Possible improvements at higher absorption are discussed below.

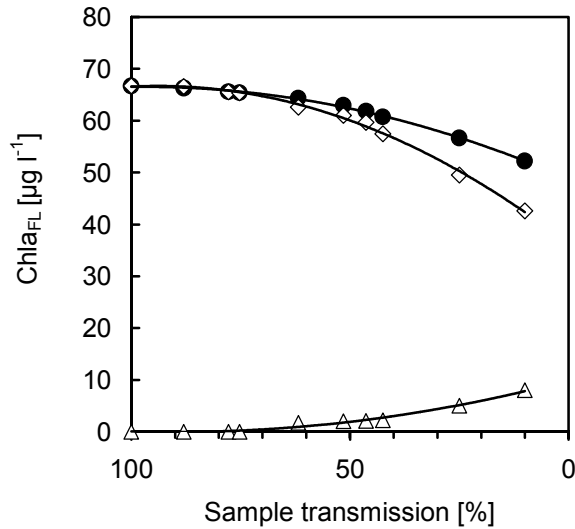


Figure 2.9. Influence of scattering on the norm curves. Suspension of *Chlorella vulgaris* with constant Chl amounts and changing amounts of scattering particles (Bentonite). Circles: Total fluorometrically determined Chl amount. Diamonds: Fluorometrically determined Chl amount of green spectral group. Triangles: Fluorometrically determined Chl amount of brown spectral group.

2.3.6 *In situ* test: comparison with HPLC determinations

In the *in situ* experiments, the reliability of the analysis by means of Equations (2.4) and (2.5) was checked by comparing the results with those of HPLC determinations. The instrument set-up was checked for reliability in the Schlei fjord, a narrow bay with a length of 40 km and connected to the Baltic Sea. The site was chosen because of the natural Chl concentration gradient. This is quite low in the Baltic Sea and quite high in the eutrophic end of the Schlei fjord. Consequently, this aquatic system is ideal for testing a wide Chl range. In Figure 2.10, the results of the determination of total Chl content by fluorometrical analyses HPLC-analyses are compared. The fluorescence measurements are in good agreement with the HPLC-analyses.

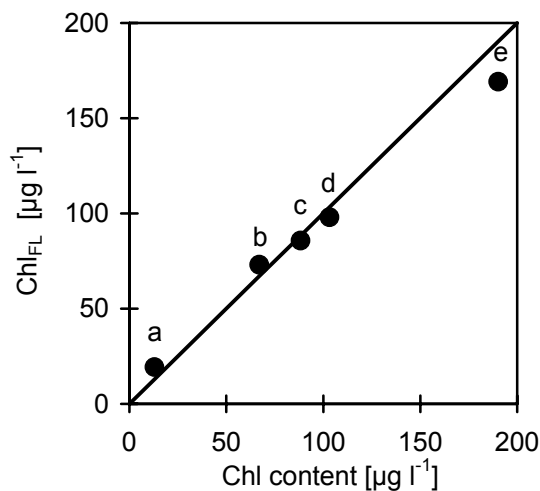


Figure 2.10. Determination of total Chl content in the Schlei fjord. The fluorometrically detected Chl content (Chl_{FL}) and the Chl content found by HPLC-analyses are compared.

2.3.7 *In situ* test: depth profiles

Having established the reliability of the method under *in situ* conditions, the benefits of high velocity data acquisition are now demonstrated: measuring depth profiles with the submersible probe (Figure 2.3). In Figure 2.11, profiles measured in the morning and around noon provide examples for the application of the probe in the study of algal migration. Clearly visible is the vertical migration of dinoflagellates. The phytoplankton (identified in the light-microscope) consisted of dinophyta (*Ceratium* spp.), chlorophyta (*Phacotus* sp.), cyanobacteria (*Microcystis* spp., *Anabaena* spp.) and cryptophyta (*Cryptomonas* spp.). Dinophyta were dominating. At 9:30 *am* most of the dinophyta were found at the surface (0 m - 2 m); a maximum for cryptophyta was found at approx. 5 m. At 2:00 *pm* the dinophyta migrated downwards into water layers with higher nutrient concentrations. Their maximum concentration was found at a depth of 3 m. The other algal groups did not migrate. It is noteworthy that the sum of the Chl *a* concentrations measured during a depth profile results - for each individual algal group - in approximately the same value at 9:30 *am* and 2:00 *pm* (difference below 10 % for each algal group). The observed constancy of biomass renders it unlikely that artefactual Chl estimates potentially due to photoinhibition (at 2:00 *pm*) affect the results significantly.

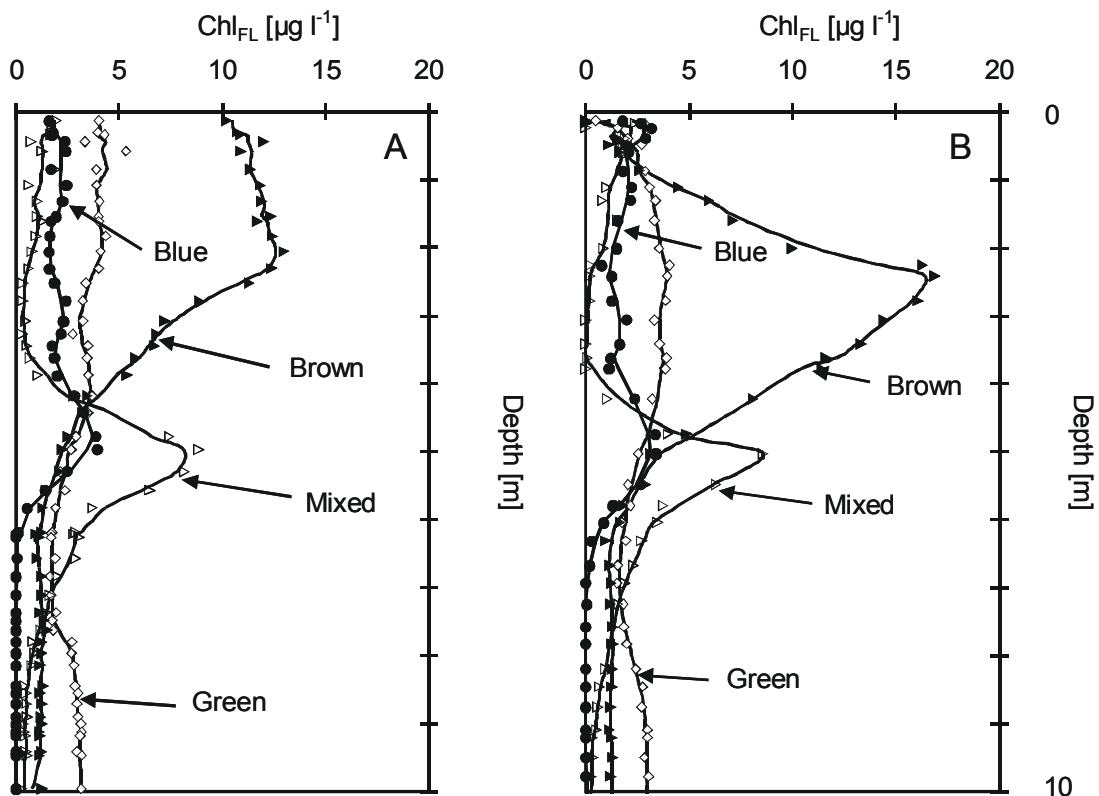


Figure 2.11. Depth profiles and algal population distributions. The two profiles were recorded at the same spot of a lake (Plußsee, Northern Germany, August 4th) at 9:30 *pm* (A) and 2:00 *am* (B). The integration-time per data point was 1 s.

2.3.8 *In situ* tests: depth profiles and biovolume

To test the relation of biovolume to fluorometric Chl estimates two depth profiles of a five point fluorescence excitation spectrum were recorded with the submersible probe in the Plußsee in August 1998 at two hour intervals. One example of the deconvoluted depth profile is presented in Figure 2.12 A.

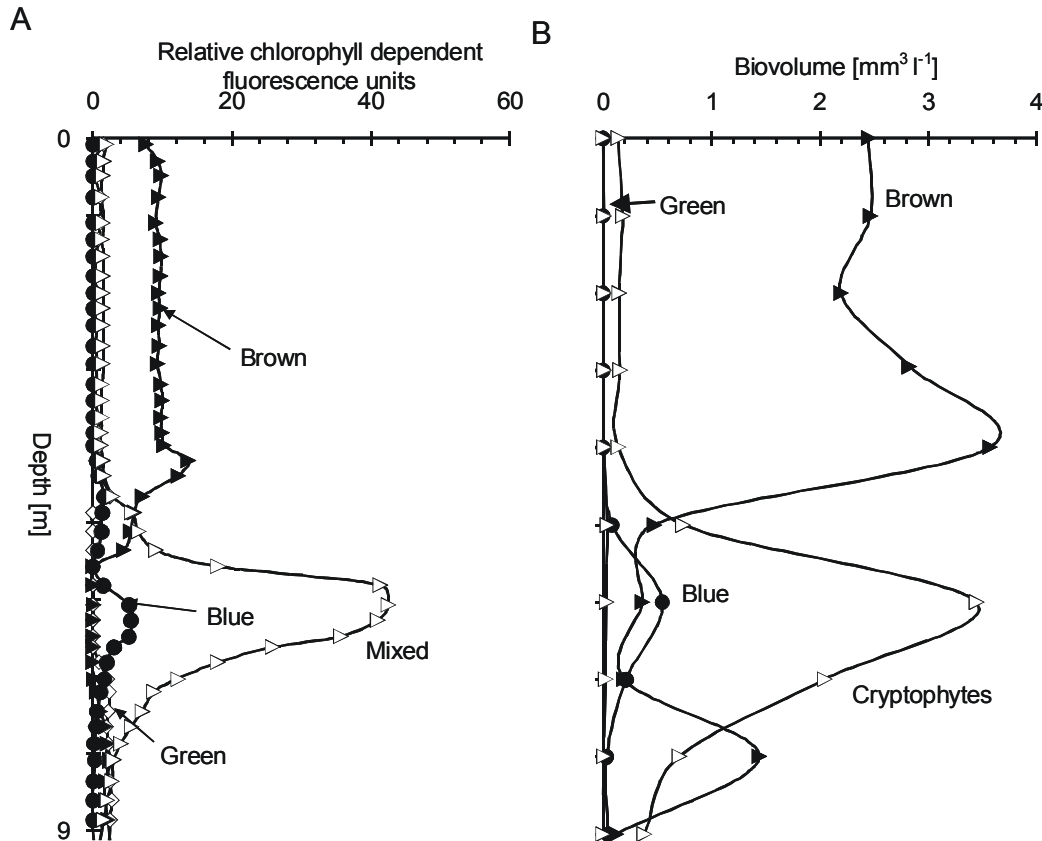


Figure 2.12. (A) Depth-profiles recorded with the submersible probe and deconvoluted to Chl-dependent fluorescence units in August 1998, 8:00 *am* at the stratified Plußsee of four spectral algal groups (green, blue, brown and mixed) and (B) the corresponding calculated phytoplankton biovolume concentrations for species of the four spectral groups: green (*Closterium acutum*), blue (*Limnothrix rosea*), brown (*Ceratium furcoides*, *C. hirundinella*, *Mallomonas caudata*), mixed (cryptophyta).

This profile is representative of the typical summer phytoplankton community in this lake. Both fluorescence profiles were compared to the corresponding biovolume concentrations (Figure 2.12 B).

The algal taxonomic groups found by microscopic examination of different depth-samples were cyanobacteria, dinoflagellates, chrysophyta, cryptophyta and chlorophyta. The measured fluorescence intensity for each spectral group was significantly correlated with the biovolume of associated algae found at different depths for these groups. In August (Figure 2.12) the blue spectral group (y) was represented by cyanobacteria (x) where $r = 0.96$, $y = 5.57x$. The brown spectral group was due to dinoflagellates (y) and chrysophyta (x) $r = 0.94$, $y = 3.42x$. The mixed spectral group (y) was attributed to cryptophyta (x), $r = 0.94$, $y = 11.5x$. The green spectral group (chlorophyta) was in the range of the limit of detection (below $0.077 \text{ mm}^3 \text{ liter}^{-1}$ biovolume in this case) for both methods.

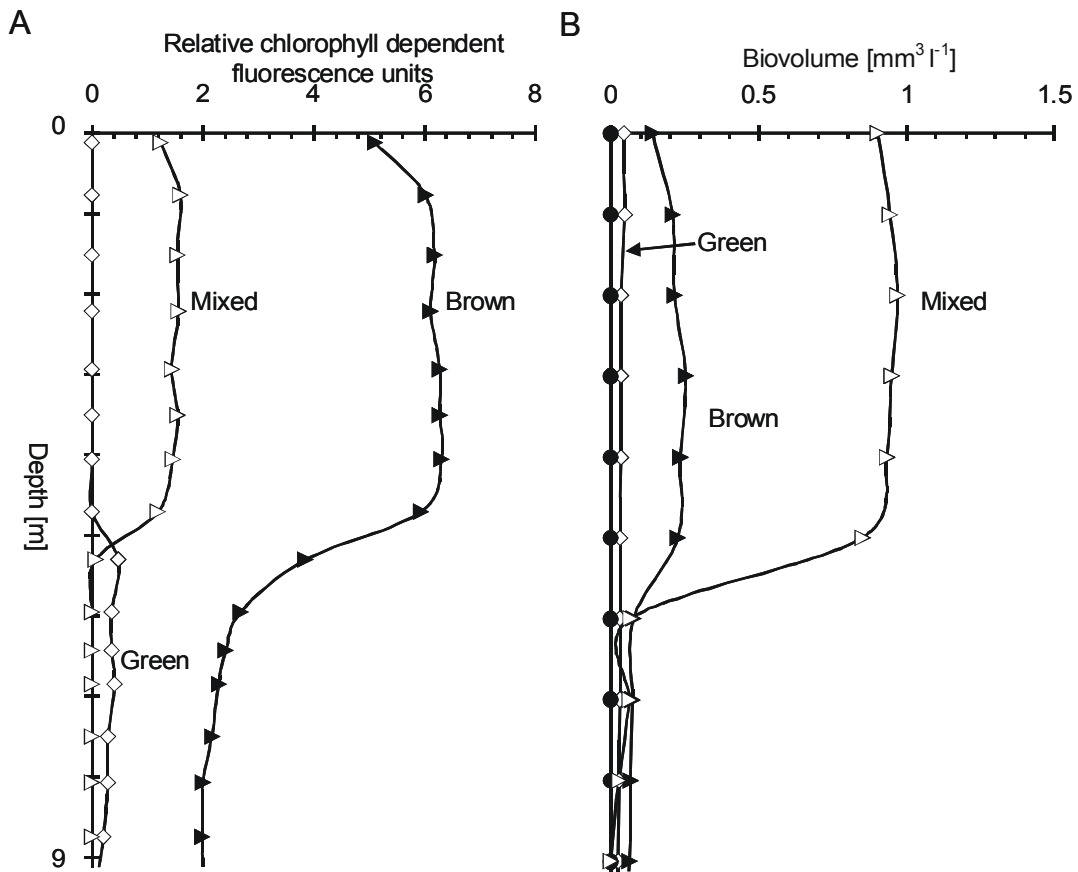


Figure 2.13. (A) Depth-profiles recorded with the submersible probe and deconvoluted to Chl-dependent fluorescence units in March 1999, 10:00 *am* at the eutrophic lake Plußsee of four spectral algal groups (green, blue, brown and mixed) and (B) the corresponding calculated phytoplankton biovolume concentrations for species of three spectral groups: green (*Closterium acutum*), brown (*Asterionella formosa*, *Mallomonas akrokomos*, *Stephanodiscus hantzschii*, *Stephanodiscus parvus*), mixed (cryptophyta).

Another profile (Figure 2.13A) was recorded at lake Plußsee in March 1999 with the submersible instrument. The phytoplankton community consisted of species typical for spring in this lake. The profile was again compared to biovolume concentrations (Figure 2.13 B) calculated from phytoplankton cell counts of water samples taken simultaneously in ten 1 m depth intervals. The algal groups found at different depths in this profile were diatoms, chrysophyta, cryptophyta and chlorophyta. The fluorescence intensities found for each spectral group were also significantly correlated with the biovolume of associated algae found at different depths for these groups.

The ratio of fluorescence intensity to biovolume in spring (Figure 2.13) was different from the summer results (Figure 2.12). The brown spectral group (y) was correlated with the biovolume of diatoms and chrysophyta (x) as: $r = 0.97$, $y = 1.48 x$. The mixed spectral group (y) was attributed to cryptophytes (x), $r = 0.94$, $y = 27.25 x$. The green spectral group (chlorophyta) were in the range of the limit of detection for both methods (below $0.045 \text{ mm}^3 \text{ liter}^{-1}$ biovolume in this case). The change of fluorescence to biovolume ratio is probably caused by changes in the Chl to biovolume ratio.

2.4 Discussion

2.4.1 Reliability

Fitting measured excitation spectra by norm curves seems to be a promising approach as indicated by the experiments shown in Figures 2.10 – 2.13. The as yet unsurpassed temporal and spatial resolution is expected to open up new applications as indicated by Figures 2.10 – 2.13. This multi-wavelength approach accounts for different fluorescence characteristics of different species and also offers the possibility of correcting for dissolved organic matter (DOM) (by an additional 370-nm LED, see *Chapter 3*).

This kind of analysis depends entirely on the reliability of the norm spectra. However, the investigations in Figures 2.5 to 2.9 provide good evidence that the problem of adequate norm spectra is less serious than initially expected. The most important result is the linear independence of the norm curves (Figure 2.5) as verified by the fact that one norm spectrum cannot be fitted by an adequately weighted sum of the others. This implies that in a noise-free record, the Chl content related to one group cannot falsely be transferred to the readings of the other groups. This finding is supported by other results. The determination of algal groups is not corrupted by dilution over 3.5 orders of magnitude (Figure 2.6). This also holds (in a smaller range) even when one group is diluted with constant background of the others (Figure 2.7).

The results of Figures 2.5 to 2.7 ensure that the mathematical deconvolution procedure yields reliable results when the norm curves are obtained under the same conditions as the investigated samples. However, a crucial premise is also the constancy of the norm curves. Two problems may arise leading to different caveats: A change in the scaling factor with different environmental conditions may lead to erroneous estimations of the Chl content of the related group, but would not lead to transfer of the Chl content to the readings of other groups. Or, a change in actual curve shape may cause more serious problems and this may result in such a transfer of the Chl content to the readings of other groups.

With respect to the above mentioned considerations, it is very important that pre-illumination did not cause a significant change of the shape of the norm spectra (Figure 2.8). There is an effect on the scaling factor. Basically, such an effect is expected as light changes the redox states of the intermediates of the photosynthetic chain, the thermal de-activation in the antennae and phosphorylation state of LHC controlling the distribution of light to PS II and PS I (Dau (1994b)). However, the effect found in Figure 2.9 is surprisingly small. Probably the constancy of the scaling factor is caused by the ability of the algae to adjust their photosynthetic efficiency to the prevailing light conditions. The last test deals with light scattering. Figure 2.9 shows that even at an absorption of up to 50% the influence on the reliability of the method is small.

In spite of the results of Figure 2.8. the following caveat holds. For measurements close to the water surface, sunlight may directly illuminate the shielded volume of the submersible probe (in particular around noon) thus eliminating the dark-adaptation period of 2 s. In such a scenario, algal discrimination may be corrupted at water depths less of than 50 cm.

2.4.2 Detection limit

The minimal Chl concentration which is reliably detectable is about 20 ng /l (Figure 2.6). However, this very low value is only obtained under very favourable conditions. The lower limit depends on the noise of the measured spectrum including the electronic noise of the spectrometer (negligible), the noise caused by the water and scattering particles (Figure 2.9), cell size and morphology and also on the variation of the norm curves with different composition of its members (as indicated by the error lines in the norm spectra of Figure 2.4 which present species-dependent variations of the fluorescence excitation spectra within one spectral algal group). It is obvious that the noise of the spectra of the groups at high concentration corrupts the determination of a group with low concentration. An investigation of the norm spectra and its dependence on the composition of the group and on the environmental conditions should be used for measurements in the field with due care. Even though the results of Figures 2.5 to 2.8 are very encouraging, a determination of norm curves with algae obtained from the actual place of interest is required for high-precision determinations. This is usual for fluorescence devices and should always be carried out (see Wiltshire *et al.* (1998)).

2.4.3 Relation of fluorescence to chlorophyll content and productivity

In natural waters the amount of PS II is a major determinant of the rate of light-driven photosynthetic electron transport (per volume) and, thus, of the rate of primary biomass production. However, the efficiency of PS II reaction centres depends on the adaptation of photochemical and non-photochemical quenching factors. The above investigation of the influence of pre-illumination (Figure 2.8) seems to indicate that algae adapt in such a manner that the role of light intensity on operation conditions becomes less severe. Such an effect increases the reliability of estimating productivity from the measurements of Chl fluorescence.

2.4.4 Relation of fluorescence to biovolume concentrations

The successful correlation with biovolume in Figures 2.12 and 2.13 clearly demonstrates that correct and rapid assessment of the phytoplankton community structure *in situ* with unsurpassed spatial and temporal resolution now is really possible. However, as is to be expected, the ratio of fluorescence to biovolume changes over time and with different algal species, the correlation needs to be calibrated for the specific algal association being examined. The constancy of the norm curves described above may also not hold for the cyanobacteria. In this group, some members are known (Reuter & Müller (1993); van Thor *et al.* (1998)) that can produce different amounts of PE and PC depending on nutrition conditions and light environment. This might already be a problem in Figure 2.12 where it is not clear if the *Limnothrix rosea* present belongs to the red or the blue group and if it thus falsifies the results. The problem of the red spectral group, i.e. red cyanobacteria, is discussed and solved in *Chapter 6*.

2.4.5 Future developments to overcome present limitations

Assumption 2 of the mathematical evaluation was independence of Chl-fluorescence on the physiological state. In cases where this assumption does not hold, corrections can be obtained from wave-length dependent F_0 and F_m determination (Kolbowski & Schreiber (1995)). For a

submersible instrument the protocol of Kolber *et al.* (1998) should be used with single-turnover flashes of 0.1 ms. The multiple-turn over protocol (Schreiber's Fm) with at least 200 ms (Kolbowski & Schreiber (1995)) is too slow for appropriate *in vivo* measurements with a rapidly falling probe. The probe's movement and its relation to the fluorescence parameters is discussed in detail in *Chapter 4*.

To enable measurements in waters with large amounts of scattering particles (transmission below 50 %), it is intended to correct for turbidity by combining transmission and fluorescence measurement. Another potential problem are high concentrations of DOM in the investigated water sample. This is approached in the next chapter.

Chapter 3. Fluorometric depth-profiling of chlorophyll corrected for yellow substances

3.1 Abstract

As described above, the 'spectral groups' of algae (green, blue, brown, mixed) are each characterised by a specific composition of photosynthetic pigments. This results in a specific Chl fluorescence excitation spectrum and was used in *Chapter 2* to determine the amount of chlorophyll and the algal group composition of phytoplankton. Yellow substances (coloured dissolved organic matter) may interfere with the measurement because of overlap in the excitation spectra with phytoplankton. In a new approach chlorophyll fluorescence was corrected for the influence of yellow substances.

The newly developed probe is a submersible fluorometer which measures emission intensity over six characteristic wavelength ranges employing pulsed light-emitting diodes. The submersible probe transfers all data on-line to a computer or stores them in the probe (fluorescence data plus the simultaneously measured water pressure for depth determination). The six-point excitation spectra are deconvoluted on the basis of norm spectra, which have been obtained by analysis of several species in each spectral group. The use of an UV-excitation source (370 nm light-emitting diode) enables differentiation between algal fluorescence and fluorescence by yellow substances.

3.2 Introduction

In the previous chapter it was shown to be possible to distinguish between four algal groups (green, blue brown, mixed) *in situ* fluorescence profiles and to correlate the biomass concentrations of different spectral groups of algae. In natural waters, new components come into play and these are large amounts of organic compounds found in natural waters. The related emission fluorescence from yellow substances (YS) can corrupt the determination of Chl fluorescence as a measure of Chl-concentration and as an indicator of phytoplankton (Gower & Borstad (1983); Doerffer (1988)). Their fluorescence characteristics have been used to estimate amounts of YS in natural waters. (Matthews *et al.* (1996); Mittenzwey *et al.* (1997)). YS are part of the DOM and are defined as DOM which absorbs in the UV and blue spectral wavelength range. YS can be split up into two major groups - humic substances and non-humic substances. The lignins are prominent representatives of the non-humic substances. Most organic material and YS originate from land plants and soil. This means that eutrophic freshwater lakes and marine coastal zones generally contain much more organic matter and YS than oligotrophic ocean and lake systems (e.g. Kalle (1961)).

The emission spectra of YS are not in a narrow band, but rather the emission extends over a wide range of the blue-green wavelength region. The determination of the distribution of the spectral algal groups and YS is based on the premise that the measured excitation spectrum at a fixed emission wavelength is a superposition of the signals from the individual cells as given in the following equation:

$$F(\lambda_{ML}, \lambda_{em}) = \{ \sum_{k=1 \text{ to } n} C_k f_k(\lambda_{ML}, \lambda_{em}) I_{ML}(\lambda_{ML}) \} + C_{YS} f_{YS}(\lambda_{ML}, \lambda_{em}) I_{ML}(\lambda_{ML}) \quad (3.1)$$

with: C_k being an instrument dependent constant depending on algal group (k'th group), $f_k(\lambda_{ML}, \lambda_{em})$ the fluorescence intensity of the k'th spectral algal group, I_{ML} the intensity of the measuring light (in $\mu E m^{-2} s^{-1}$), $\lambda_{ML}, \lambda_{em}$ excitation and emission wavelengths, respectively, C_{YS} instrument dependent constant of YS, and $f_{YS}(\lambda_{ML}, \lambda_{em})$ fluorescence intensity of YS.

Here, the fluorescence characteristics of YS are utilized to correct for the influence on Chl fluorescence by installing in a sixth excitation LED with an emission wavelength of 370 nm for enhanced excitation of YS in the two fluorometers of *Chapter 2*.

3.3 Materials and methods

3.3.1 Set-up of the submersible instrument

The set-up is identical to that of the submersible instrument in Figure 2.3 of *Chapter 2* but extended by a sixth excitation LED with an emission wavelength of 370 nm (with Balzers B-42-filter blocking light that is more red than 430 nm).

3.3.2 Determination of chlorophyll concentrations and algal cultures

Concentrations of Chl (see also *Chapter 2*) were determined according to Wiltshire *et al.* (1998) using HPLC. For calibrating the fluorometer, the following species were chosen as representatives for the spectral algal groups: green spectral group: *Chlorella vulgaris*; blue spectral group: *Microcystis aeruginosa*; brown spectral group: *Cyclotella meneghiniana*; mixed spectral group; *Cryptomonas* sp.

3.3.3 Mathematical evaluation

The fit procedure of *Chapter 2, Appendix A* was employed. The mean of the spectra shown in Figure 3.1 was employed as a fifth norm spectrum.

3.3.4 Fluorescence-offsets of natural water-samples

Fluorescence excitation spectra of different natural water samples filtered through glass fibre filters (Whatman G/F pore size 0.7 μm) were recorded using the set-up as described above. Samples were collected from the surface (except tap water, Kiel) of the sampling location from different sites in Northern Germany.

3.4 Results and discussion

3.4.1 Norm spectra of phytoplankton compared with spectra of yellow substances

To differentiate between YS and phytoplankton significant differences in their fluorescence excitation spectra are of crucial importance. In Figure 3.1 a spectrum of YS is compared with norm spectra of spectral groups of phytoplankton. In this case the displayed spectrum of YS is a sample of the Plußsee in Northern Germany from a depth of 1m filtered through a glass fibre filter. The characteristic fluorescence in the UV region is obvious. A high signal is found at the 610 nm LED in the blue group. This is caused by PC. In addition, the ‘brown group’ (here diatoms and dinoflagellates) has a high signal in the green wavelength region (525 nm) because of fucoxanthin (diatoms) and peridinin (dinoflagellates). High fluorescence intensity caused by PE was found for the cryptophyta (*Cryptomonas*) at 570 nm. The differences in spectra are large enough to differentiate between phytoplankton fluorescence and fluorescence caused by YS.

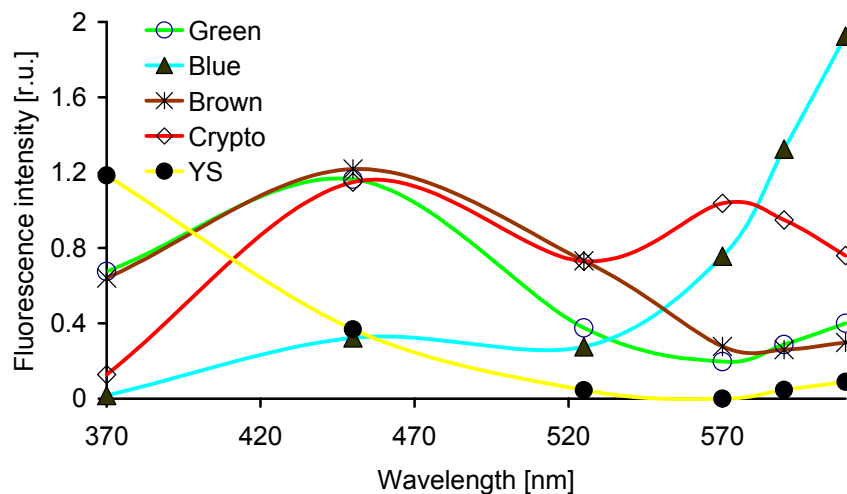


Figure 3.1. Norm spectra of spectral algal groups and YS. Mean fluorescence intensity of four spectral algal groups and YS at six excitation wavelengths in digits (photovoltage at the photomultiplier) normalised to Chl *a* concentration ($\mu\text{g l}^{-1}$) for spectral algal groups.

3.4.2 Variability of natural fluorescence offsets

To ensure reliable correction of phytoplankton fluorescence spectra, all naturally occurring YS must show the same characteristics in their spectra. For this reason the variation in the fluorescence spectra of YS in filtrates of natural waters was investigated. All spectra show similar patterns. A high fluorescence intensity is characteristic if excited with light at 370 nm in the UV region. The variation of the spectra is low (Figure 3.2).

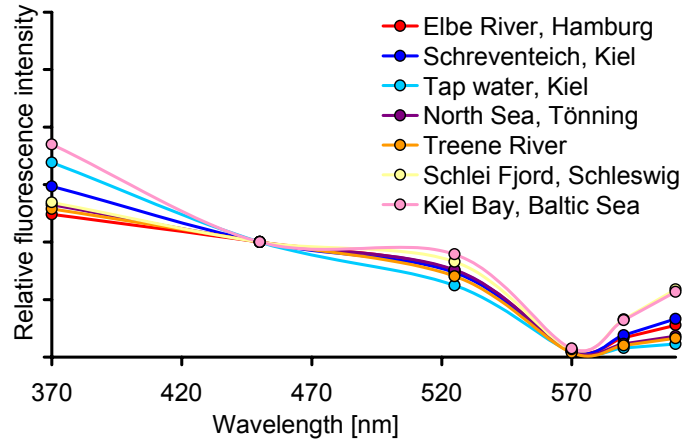


Figure 3.2. Fluorescence-offsets of natural water samples from different sites in Northern Germany. Spectra are normalised to fluorescence intensity at 450 nm. All spectra have similar characteristics and show high fluorescence intensity if excited by 370 nm light.

3.4.3 Dilution experiment and *in situ* profile

To test the set-up and to test if the calculation of YS is correct, a dilution experiment was carried out as shown in Figure 3.3. Algae were added to the filtered water of the river Elbe. A fluorescence excitation spectrum of this sample was determined and the amount of Chl and relative amount of YS was calculated. This sample represented 100% concentration. The sample was then diluted with filtered water to lower Chl concentrations. Fluorescence measurements of the diluted samples show that the share of YS was detected properly. The instrument was tested in an *in situ* profile taken with the profiler (Figure 3.4) in the eutrophic Plußsee. The lake and consequently also the algal distribution were stratified in this example. Fluorescence of YS is distributed constantly with depth.

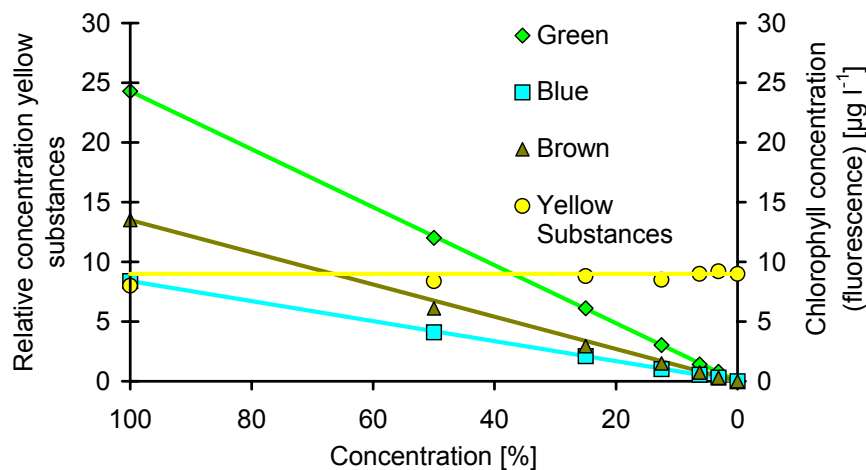


Figure 3.3. Dilution experiments. Fluorescence measurements were made from samples from dilution experiments on algae and YS. Water from river Elbe (sample taken at Hamburg) was filtered through Whatman G/F filters (pore size 0.7 μm) and fluorescence excitation spectra were taken with the set-up shown in Figure 3.1.

In conclusion, the new correction for YS enables measurements in waters with low Chl content or where the share of YS is so large that YS fluorescence becomes significantly to Chl fluorescence. The linear independence of the YS norm spectra from the algal spectra is demonstrated in Figure 3.1 and by the successful dilution experiment of Figure 3.3. In combination with the submersible instrument of *Chapter 2* it facilitates assessment of algal population distribution together with a relative analysis of the amount of YS. For most investigations, the resolution of 3 or 4 algal groups should be sufficient. The accuracy of algal group differentiation is limited by species-dependent variability within an individual algal group and by the influence of environmental factors on the fluorescence yield (e.g., see *Chapter 2*) but also on the variations of the norm spectra of YS (see Figure 3.2). This technique is an important new tool in aquatic ecology and for supervision of aquatic resources. Investigations not feasible because of the high organic contents with other methods may become practicable. Differential assessment of phytoplankton and Chl corrected for yellow substance fluorescence will, henceforth, be much more refined.

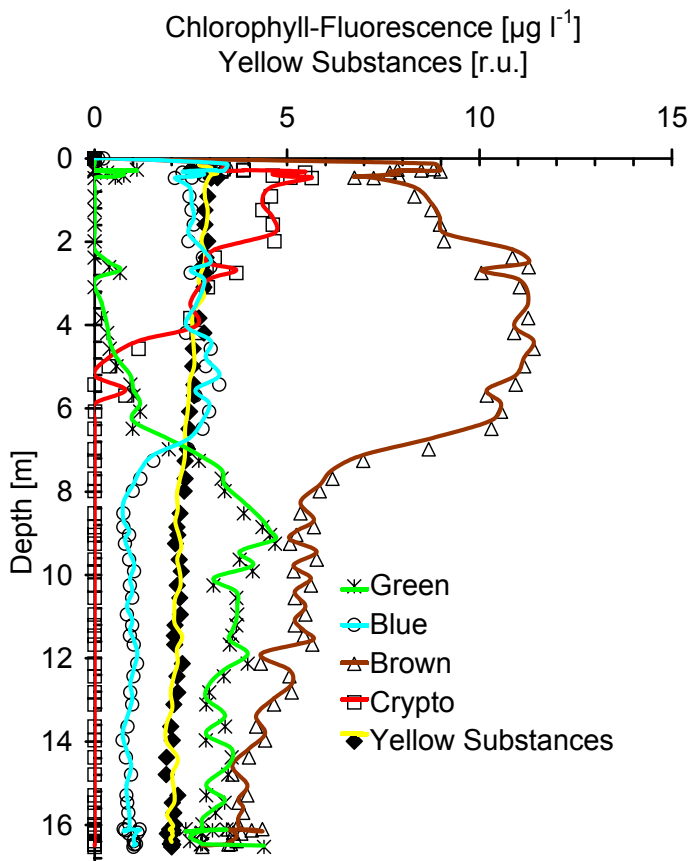


Figure 3.4. Depth profile of deconvoluted fluorescence excitation spectra of the Plußsee taken with the submersible instrument. The fluorescence spectrum of filtered water from 1 m depth was taken as a YS fingerprint. Fingerprints of algae shown in Figure 3.1 were employed as norm spectra for the detection of spectral algal groups.

Chapter 4. A model for correcting the fluorescence signal from a free-falling depth profiler

4.1 Abstract

Measuring chlorophyll fluorescence at five different wavelengths provides the discrimination of four algal groups (*Chapter 2 and 3*). Here the problems associated with a free-falling depth profiler for algal discrimination are considered. When F_0 , F , and F_m are determined sequentially using one measurement cell, then the algae inside the cell have a different light history depending on their different locations in the cell as caused by the induction curve of chlorophyll fluorescence. Mathematical algorithms are developed which enable the evaluation of the integral fluorescence signal (averaged for 1s) for different velocities of the falling probe. This yields a correction factor that allows the use of calibration factors from stationary suspensions for the determination of algal concentrations in flowing suspensions. The predictions of the model are compared with measurements in flowing suspensions containing chlorophyta, cyanobacteria, cryptophyta and diatoms. The comparison shows the reliability of the algorithms. The necessity for correction by the algorithm is proved for dark-adapted cells and is less important for light-adapted cells.

4.2 Introduction

Remark: The findings described in this Chapter are from the Diploma thesis of Jens Schimanski (Schimanski (2002)). The work was carried out under my supervision.

In *Chapter 2* and *3* it was demonstrated that for an intense screening in all three spatial dimensions, Chl fluorescence is the most appropriate parameter since it provides fast and low-cost measurements. As result, many measurement devices have been developed. The first depth profiling of Chl fluorescence has been carried out by Kiefer (1973). Kolber & Falkowski (1993) used the pump and probe technique for profiling the photochemical yield of phytoplankton for primary production *in situ*. It is, however, also useful to measure parameters other than Chl concentrations. Schreiber (1994) assessed photosynthetic activity parameters of algae and cyanobacteria by the PAM-technique *in vivo*. Moldaenke *et al.* (1995) used the 1-Hz technique as a measure of photosynthetic activity. Kolber *et al.* (1998) developed fast repetition rate techniques.

On-line algal discrimination is of special interest. As described in the preceding chapters, it is based on the feature that different algal classes have different activation spectra for Chl fluorescence (Yentsch & Yentsch (1979); Yentsch & Phinney (1985)). However, a measurement of whole spectra requires too much effort for large-scale *in situ* investigations. Kolbowski & Schreiber (1995) overcame this problem by showing that measurements at only four wavelengths emitted by LEDs to be sufficient for the discrimination between three groups of algae. Evaluation was based on a linear regression using so-called norm spectra (Figure 2.4) for each of the algal classes: The work in both groups led to the construction of two instruments, i.e., the Phyto-PAM (pulse amplitude modulation, Walz, Effeltrich, Germany) and the AOA (Algae On-line Analyser, bbe Moldaenke, Kiel, Germany). The measurement with different activation spectra can also be used for F_0 and F_m determination, and thus a species-specific Genty parameter (Genty *et al.* (1989); Schreiber (1994)) can be calculated (Kolbowski & Schreiber (1995); Ruser (2001)).

All these measurements (combination of algal discrimination and the assessment of photochemical yield) were done of non-flowing (stationary) suspensions. However, for large-scale screening, measurements of flowing water are desirable. For the measurement of Chl depth profiles, a diving profiler is the most desirable instrument of ocean (and lake) researchers.

Measurements on a flowing water body or with a moving probe pose special problems as different algae in the measuring system have different light histories. Some of them are already inside the measuring chamber when the light is switched on, others enter during the light period. In order to account for these effects a mathematical model is developed, and its capacity for prediction of the fluorescence signal is tested experimentally. This model provides an algorithm for determination of the algal concentrations and electron transport rates of a flowing suspension using the scaling factors obtained from chlorophyll fluorescence of stationary suspensions.

4.3 Materials and methods

4.3.1 Algal growth

Algae were grown in the laboratory illuminated for 8 h per day by 18 W light bulbs (Osram) providing $20 \mu\text{Em}^{-2}\text{s}^{-1}$. The nutrient solution was renewed every two weeks. *Chlorella vulgaris* (chlorophyta): Growth in modif. K-nutrient solution (Schlösser 1994) in sterile 5 l-Erlenmeyer flasks, aerated by a pump. *Microcystis aeruginosa* (cyanobacteria), *Cyclotella* sp. (diatom), *Cryptomonas* sp. (cryptophyta): growth in sterile 100 ml-Erlenmeyerflasks in WC-nutrient solution (Guillard & Lorenzen (1972)).

4.3.2 Chlorophyll determination

Chl content was measured with a bbe-cuvette fluorometer (*Chapter 2*, bbe-Moldaenke, Kiel, Germany) calibrated by HPLC (Wiltshire *et al.* (1998)).

4.3.3 Fluorometer set-up

A new flow-through fluorometer was built for the following investigations. The set-up is shown in Figure 4.1. The measuring cell consisted of a cylindrical glass cuvette with an inner diameter of 2.83 cm and an illuminated length of 8.3 mm. A rubber piston was used to clean the glass regularly. Six LEDs provided the measuring light with wavelengths of 370 nm (with Balzers B-42-Filter blocking light with wavelength longer than 430 nm), 470 nm (this was used instead of the 450 nm LED of *Chapter 2* and 3 because of a higher light intensity), 525 nm, 570 nm, 590 nm and 610 nm, and four laser diodes were used for F_m light (Hitachi HL6501MG, 658 nm, providing $3000 \mu\text{Em}^{-2}\text{s}^{-1}$ at an area of 227 mm^2 in the cuvette with a diffuser in order to prevent sprinkles). The different lights were bundled together by a dichroitic mirror (Balzers R-65, Liechtenstein), focussed on the measuring cuvette. 5 % of the light was diverted to a photodiode by means of a beam splitter (optical glass, Menzel Gläser, Germany). This signal was used for feed-back control of light intensity. The detector (Photomultiplier, Hamamatsu H6779-01) behind a 685-nm band pass filter (bbe fk-1, bbe Moldaenke, Kiel, Germany) was mounted rectangularly to the light of the LEDs.

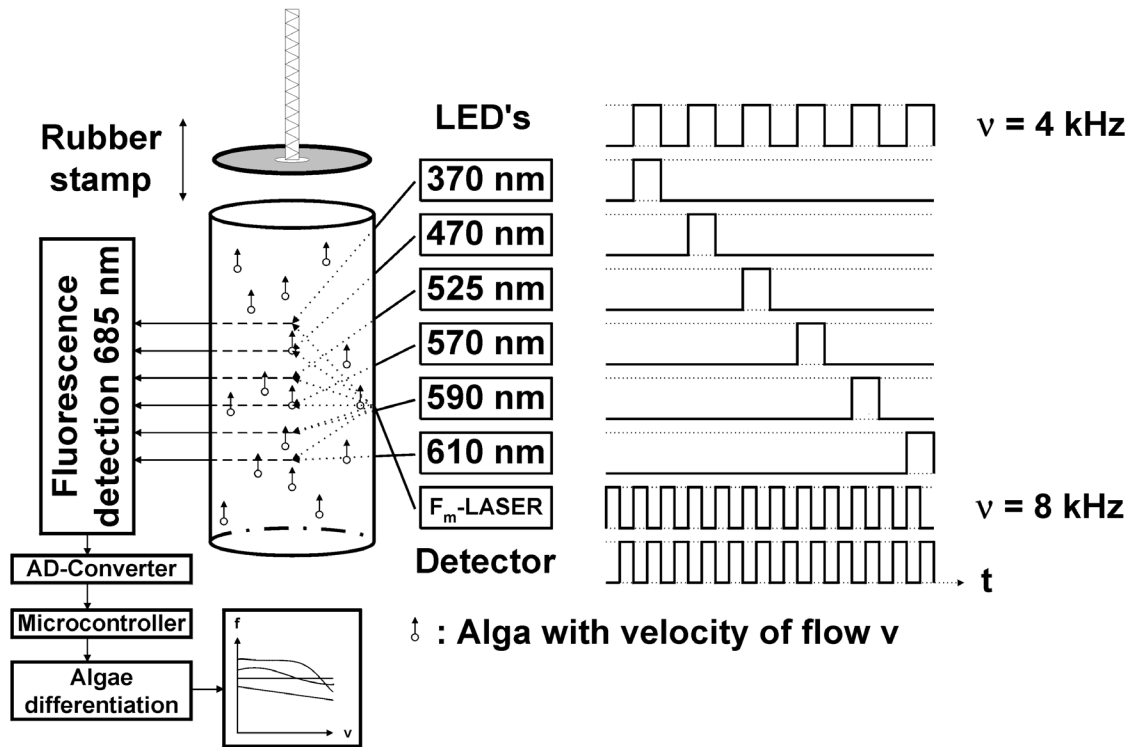


Figure 4.1. Experimental set-up. Timing of the LEDs, the laser and the detector in an F_m measurement.

The timing of the diodes is shown at the right-hand side of Figure 4.1. The diodes for the measuring light were switched on for $125 \mu\text{s}$ in sequential order, with a dark interval of $125 \mu\text{s}$ between two diodes. The detector was switched sensitive for $62.5 \mu\text{s}$ in the second halves of the light-on phase and light-off phases, respectively, of the diodes. For measurements with background light (F_m -determination), the laser diodes were chopped by 8 kHz in such a way that they were on when the detector is off in order to prevent overload of the photomultiplier.

Fluorescence was measured in three different modes: In F -measurements, the measuring light was also used as actinic light for the induction of an induction curve. The average light intensity as caused by the LEDs with the light protocol in Figure 4.1 was $20 \mu\text{Em}^{-2}\text{s}^{-1}$. In an F_m -measurement, the laser was switched on as shown in Figure 4.1. For F_0 -measurements, the gap between the LEDs was increased to $49 \cdot 250 \mu\text{s} + 125 \mu\text{s} = 12.375 \text{ ms}$ in order to reduce the average light intensity of the measuring light by a factor of 50 ($0.4 \mu\text{Em}^{-2}\text{s}^{-1}$). Control experiments showed that there was no dependence on the F_0 signal of light intensity below $2 \mu\text{Em}^{-2}\text{s}^{-1}$ indicating that F_0 conditions were achieved.

4.3.4 Mathematical evaluation

Determination of the concentrations of different algal groups in a mixed suspension is based on a fitting algorithm using so-called norm curves (see *Chapter 2* and *Appendix A*), an approach initially introduced by Kolbowski & Schreiber (1995) and Tabrizi *et al.* (1998) for the evaluation of photoacoustic signals. A so-called norm curve is obtained from a suspension containing only one group of algae of a known concentration (e.g., a suspension of $10 \mu\text{g/l}$ Chl as determined by HPLC) under steady state conditions at a given light intensity. Such a norm curve is defined by the set of fluorescence signals $h_{g,\lambda}$ (Equation (4.1)) from such a standard

suspension measured at different excitation wavelengths λ (six in the set-up of Figure 4.1). The index g indicates the group (green, blue, brown, mixed). In order to reduce noise, the data points of the norm curve ($h_{g,\lambda}$) were the averages obtained from 20 subsequent responses to the measuring pulses with a separation of 1.5 ms.

$$h_{g,\lambda} = \frac{\sum_{t=1}^{20} f_{g,\lambda,t,n}}{20} \quad (4.1)$$

with t being the time index of the sampling pulses. n indicates norm-curve conditions. $h_{g,\lambda}$ has to be determined separately for F_0 , F_m and F .

The signal from a suspension ($f_{g,\lambda}$) containing a_g times more Chl of this group than the calibrating suspension is (analogous to *Chapter 2*)

$$f_{g,\lambda} = a_g h_{g,\lambda} \quad (4.2)$$

Thus, a_g is a measure of algal concentrations in terms of the calibrating suspension. In mixed suspensions (different algal species), the signal f_λ obtained (by averaging over 20 samples as in Equation (4.1)) at a single wavelength λ is a superposition of the contributions of the individual groups

$$f_\lambda = \sum_{g=1}^4 a_g h_{g,\lambda} \quad (4.3)$$

In order to reveal the individual component concentrations (described by a_g) in the mixed suspension, fits were performed automatically every 30 ms (i.e., after each averaging procedure according to Equation (4.1)) by minimising the weighted sums of squares:

$$X^2 = \sum_{\lambda=1}^{N_\lambda} \left(\frac{f_\lambda - \sum_{g=1}^4 a_g h_{g,\lambda}}{\sum_{g=1}^4 a_g w_{g,\lambda}} \right)^2 \quad (4.4)$$

The weighting factors $w_{g,\lambda}$ in the denominator account for different reliabilities of the measured signals. In *Chapter 2* and *Appendix A* the scatter of the data points was used as weighting factor

$$w_{g,\lambda} = \sigma_{g,\lambda} \quad (4.5)$$

As mentioned above, the $h_{g,\lambda}$ (norm curves) were obtained from measurements on suspensions containing a single algal group of known (unit) concentration (Beutler (1998) and *Chapter 2*). However, the a_g only can be used as a measure of algal concentration if the measurement on the unknown suspension is done under the same light regime (e.g., algae are adapted to the same intensity) as prevailed during the determination of the norm curves $h_{g,\lambda}$. This caveat

results from the fact that the calibration factor ($h_{g,\lambda}$ vs. biomass) is influenced by photochemical and non-photochemical quenching factors (Schreiber & Krieger (1996)).

This variability may constitute a serious problem in a depth profiler with varying light regimes for the sequential determination of F , F_0 and F_m . When light intensity changes, an induction curve is initiated that causes temporal variation of photochemical and non-photochemical quenching factors. Now, a model is required that provides a correction factor c_g that enables the calculation of the "real" $a_{stat,g}$ (stationary suspension) from the measured one, $a_{flow,g}$ (flowing suspension).

$$a_{stat,g} = c_g a_{flow,g} \quad (4.6)$$

The correction factor c_g is expected to be time-dependent. For the sake of data reduction (in order to enable an on-line determination of concentrations), the data sets obtained every 30 ms (Equation (4.1)) are not considered, but rather the integral over the whole measuring period t_m , usually $t_m = 930$ ms. Thus, the model below applies to the integral signals of F and F_0 according to

$$F_\lambda = \frac{\sum_{t=1}^{t_m/30ms} f_\lambda}{\frac{t_m}{30ms}} = \frac{\sum_{t=1}^{t_m/30ms} \sum_{g=1}^4 a_g h_{g,\lambda}}{\frac{t_m}{30ms}} \quad (4.7a)$$

with f_λ and $h_{g,\lambda}$ being averaged values of 20 sampling points as defined in Equation (4.1). The group-specific signal $F_{\lambda,g}$ is obtained from Equation (4.7) for all but one a_g being zero.

$$F_{g,\lambda} = \frac{\sum_{t=1}^{t_m/30ms} f_\lambda}{\frac{t_m}{30ms}} = \frac{\sum_{t=1}^{t_m/30ms} a_g h_{g,\lambda}}{\frac{t_m}{30ms}} \quad (4.7b)$$

In the case of F_m measurements, the strong light would saturate the photomultiplier. Thus, the laser diodes were chopped with 8 kHz, and the fluorescence was measured in the dark-periods of the lasers (Figure 4.1). The single laser pulse intensity did not saturate the PS II acceptor Q_A . Consequently, several laser pulses were required to reach the F_m value (see Figure 4.5, below). $F_{\lambda,m}$ is the maximal value of the f_λ (Equations (4.1) to (4.3)) induction curve. (Here, the index d indicates measurement at saturating laser flashes in the off-periods of the laser, Figure 4.1).

$$F_{m,\lambda} = \max(f_{\lambda,d}) \quad (4.8)$$

The group-specific $F_{m,g,\lambda}$ is obtained in a similar manner to $F_{g,\lambda}$ in Equation (4.7 b).

4.3.5 Model for the depth profiler

The problem particular to the depth profiler is that the algae are at different positions inside and outside the cuvette when the modulated light is switched on. Switching on and off is required because F and F_m (Equations (4.2) and (4.3)) are measured sequentially. Thus, a model was necessary that enables the calculation of this effect on the fluorescence recorded by the detector and which provides an algorithm that can eliminate the effect of the moving suspension. Several simplifying assumptions were made, but the experiments below show that they were legitimate.

1. Algal concentrations are low. Thus, there is no self-absorption and the fluorescence signal is proportional to the concentration. This is tested below (as tested in Figure 4.3, below)
2. Illumination of the cuvette is homogeneous. This implies that only the spatial coordinate in the direction of the flow has to be considered.
3. Laminar flow.

In the equations below, the symbols f_a , f_b and f_c (calculated by the model) are assigned to the signals from the flowing suspension, and f_{ind} (induction curves) holds for a single "average" alga in a stationary suspension containing only a single group.

For the mathematical treatment, two cases must be considered.

Case 1: At least one alga is exposed to the full light period t_m of about 1 s. This implies that the velocity v of the suspension is

$$v < \frac{L}{t_m} \quad (4.9a)$$

Case 2: None of the algae sees light for the full time period t_m . This implies

$$v > \frac{L}{t_m} \quad (4.9b)$$

Case 1.

Figure 4.2 shows the sections of the cuvette which should be considered.

Section a comprises all $n_a(0)$ algae that see the switching on of the series of light pulses, but leave the cuvette during the light period. Its length is $x_{a,1} = v t_m$, and $n_a(0) = v t_m \rho$ (ρ being the number of "average" algae per volume). All algae of section a $n_a(0)$ contribute to the first point of the induction curve ($t=0$), but their number $n_a(t)$ decreases linearly to $n_a(t_m) = 0$ at the end of the light period, because they leave the cuvette at a time depending on their position when the light is switched on.

$$f_a(t) = n_a(t)f_{ind}(t) = n_a(0)\left(1 - \frac{t}{t_m}\right)f_{ind}(t) = \rho Av(t_m - t)f_{ind}(t) \quad (4.10)$$

with f_{ind} being the induction curve of a single "average" alga measured in the non-flowing suspension.

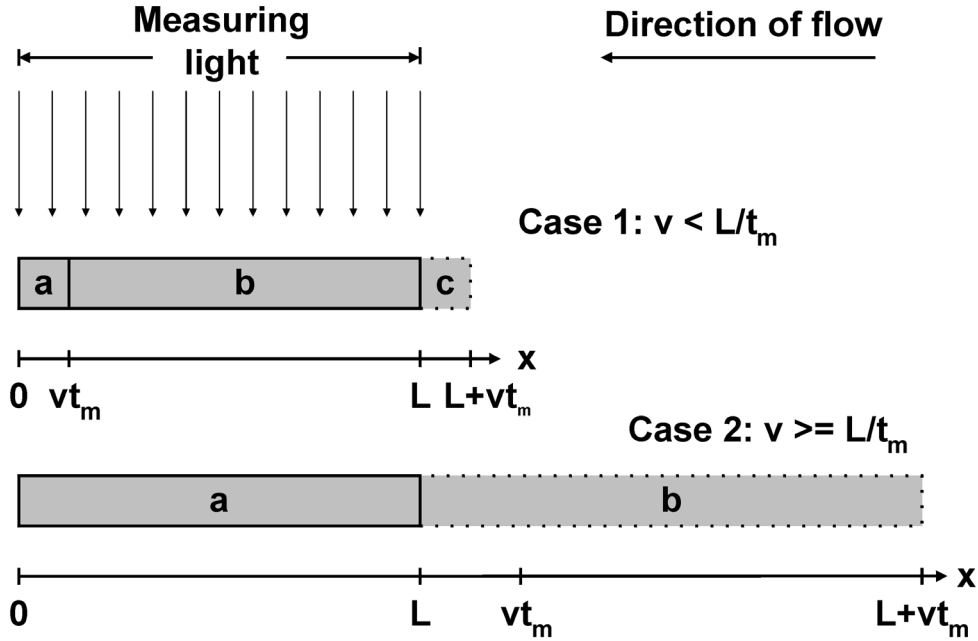


Figure 4.2. Sections dividing the cuvette in regions with algae that are exposed to different light regimes. The density of the algae is ρ , and the diameter of the cuvette is A . (A) Case 1: Low flow velocities. At least one alga sees the whole light period of length t_m . (B) Case 2: The flow rate is so high that none of the algae sees the whole light period.

Section b comprises all n_b algae that see the full light period. Its length is $x_{b,1} = L - v t_m$. Its contribution is quite simple as they all contribute equally to the whole light response.

$$f_b(t) = n_b f_{ind}(t) = \rho A(L - vt_m) f_{ind}(t) \quad (4.11)$$

The algae in section c enter the cuvette after light has been switched on. Its length upstream the cuvette is $x_{c,1} = v t_m$. Whereas all algae in sections a and b have started their induction kinetics at $t=0$, the algae of section c start the kinetics when they enter the cuvette. If section c is divided in K subsections each containing $\Delta N = vt_m \rho A / K$ algae, the algae in the k -th subsection enter the cuvette at $t_k = k t_m / K$. Thus each of them is in a different state:

$$f_c(t) = \sum_{k=0}^K \Delta N f_{ind}\left(t - \frac{k}{K} t_m\right) \quad (4.12)$$

Considering that $f_{ind} = 0$ for $t - t_k < 0$, the upper limit of the sum can be set to

$$f_c(t) = \rho v A \frac{t_m}{K} \sum_{k=0}^{\text{trunc} \frac{tK}{t_m}} f_{ind}(t - \frac{k}{K} t_m) \quad (4.13)$$

with $\text{trunc}(K t/t_m)$ being the truncated integer of $K t/t_m$.

If the density ρ is high enough, the sum can be replaced by an integral

$$f_c(t) = \rho A v \int_0^t f_{ind}(t-s) ds \quad (4.14)$$

Summarising the above sections leads to the overall signal

$$f_{all}(t) = f_a(t) + f_b(t) + f_c(t) = \rho A(L-vt) f_{ind}(t) + \rho A v \int_0^t f_{ind}(t-s) ds \quad (4.15a)$$

with ρ being the number of "average" algae per unit volume. As mentioned above, f_{ind} is the fluorescence induction curve of a single "average" alga. It is often easier to use the data obtained from the suspension used for calibration. In that case

$$f_{all}(t) = r_\rho A(L-vt) f_{ind}^c(t) + r_\rho A v \int_0^t f_{ind}^c(t-s) ds \quad (4.15b)$$

with $r_\rho = \rho/\rho_c$ (number of "average" algae per volume of the measured suspension/ number of average algae per volume of the calibrating suspension = Chl concentration of the measured solution/ Chl concentration of the calibrating suspension). f_{ind}^c is the fluorescence induction curve measured at the calibrating suspension.

For case 2 (None of the algae sees light for the full time period t_m), two sections have to be considered as illustrated in Figure 4.2.

Section a extends over the whole cell $x_{a,2} = L$. The equation is similar to that of section a for case 1:

$$f_a(t) = n_a(0) \left(1 - \frac{t}{L/v}\right) f_{ind}(t) = \rho A(L-vt) f_{ind}(t) \quad \text{for } 0 \leq t \leq \frac{L}{v} \quad (4.16)$$

$$f_a(t) = 0 \quad \text{for } \frac{L}{v} \leq t \leq t_m \quad (4.17)$$

Section b comprises of all algae which enter the cuvette during the light period t_m . All of them start the induction curve when they enter the cuvette. After $t_L = L/v$, a stationary state is reached as each alga leaving the cell is replaced by an incoming one. This leads to

$$f_b(t) = \rho A v \int_0^t f_{ind}(t-s) ds \quad \text{for } 0 \leq t \leq \frac{L}{v} \quad (4.18)$$

$$f_b(t) = f_b\left(\frac{L}{v}\right) = \text{const} \quad \text{for } \frac{L}{v} < t \leq t_m \quad (4.19)$$

Summarising the signals from both segments and using the calibration in terms of the calibrating solution (as in Equations (4.15a) and (4.15b)) leads to:

$$f(t) = r_\rho A(L - vt)f_{ind}^c(t) + r_\rho Av \int_0^t f_{ind}^c(t-s) ds \quad \text{for } 0 \leq t < \frac{L}{v} \quad (4.20a)$$

$$f(t) = r_\rho Av \int_0^{L/v} f_{ind}^c(t-s) ds = \text{const} \quad \text{for } \frac{L}{v} \leq t \leq t_m \quad (4.20b)$$

The final determination of the concentrations of the algal groups can be done as follows:

A. In the case of F and F₀, the simple approach calculates the integral signals according to Equation (4.7) or (4.8):

$$F_\lambda = \frac{\sum_{t=i}^{t_m/30ms} f_{\lambda,i}}{\frac{t_m}{30ms}} \quad (4.21)$$

with $f_{\lambda,i}$ being the averaged values (according to Equation (4.1)) of $f(t)$ as given by Equation (4.15a,b) or Equation (4.20a,b). The index i labels the 30-ms time subintervals of the 930-ms measuring interval. F_m is obtained from $f(t)$ in Equations (4.15a,b) or (4.20a,b) according to Equation (4.8). Then, the four $a_{\text{flow},g}$ are obtained from a fitting routine based on Equation (4.4) with f_λ in Equation (4.4) being replaced by F_λ . A problem is the selection of the norm-curves that have to be used for $h_{g,\lambda}$ in Equation (4.4). In either case (discussed below), the evaluated $a_{\text{flow},g}$ are not the desired group-specific measures of algal concentrations. The correction factor (according to Equation (4.6)) depends on the kind of norm curves available. One possibility is to use the integral (or sum in digital processing system) over the induction curve $f_{\text{ind},g,\lambda}^c$ (e.g., Figure 4.4, below) instead of $h_{g,\lambda}$ in Equation (4.4)

$$X^2 = \sum_{\lambda=1}^{N_\lambda} \left(\frac{F_\lambda - \sum_{g=1}^4 a_{\text{flow},g} \sum_{i=1}^{i_r} f_{\text{ind},g,\lambda,i}^c}{\sum_{g=1}^4 a_g w_{g,\lambda}} \right)^2 \quad (4.22)$$

$f_{\text{ind},g,\lambda,i}^c$ (i = time index) is obtained from an algal group g of known concentration (e.g. Figure 4.4, below) measured under the conditions of the position where the falling probe is to be used. In that case the correction factor (Equation (4.6)) is

$$c_g = \frac{a_{stat,g}}{a_{flow,g}} = \frac{\sum_{\lambda=1}^6 \sum_{i=1}^{i_T} f_{ind,g,\lambda,i}^c}{\sum_{\lambda=1}^6 \sum_{i=1}^{i_T} f_{g,\lambda,i}} \quad (4.23)$$

i_T is the number of data points in one record, i.e., measuring time (here $t_m = 930$ ms) divided by single average time (here 30 ms, see Equation (4.7 a, b)). Summarising over λ implies that the absorption spectrum does not change during the induction curve. The denominator of Equation (4.22) was calculated using Equations (4.15 a, b) or (4.20 a, b) using $f_{ind,g,\lambda}^c$ measured separately for each algal group. The denominator of Equation (4.23) is not a measured, but a theoretical parameter. $a_{stat,g} = c_g a_{flow,g}$ (with $a_{flow,g}$ obtained from the curve fitting evaluation according to Equation (4.4)) yields algal concentrations as multiples of those used for the determination of $f_{ind,g,\lambda}^c$.

The other possibility is to use Equation (4.4) directly, i.e. by employing steady-state fluorescence of each algae group, $h_{g,\lambda}$, as employed in *Chapter 2* and *Appendix A*). $h_{g,\lambda}$ may be stored numerically on the computer for each algal group or has to be determined at an adequate sample from the place where the falling probe is to be used. In that case a second calibration factor (form factor c_f) is required.

$$c_f = \frac{\sum_{i=1}^{i_T} f_{ind,g,\lambda,i}}{f_{ss,g,\lambda} \cdot i_a} \quad (4.24)$$

Then (using the stationary $h_{g,\lambda}$ in Equation (4.4)), the real concentrations

$$a_{stat,g} = c_g \cdot c_f \cdot a_{flow,g} \quad (4.25)$$

are obtained as multiples of the concentrations of the suspension used for the determination of $h_{g,\lambda}$. $f_{ind,g,\lambda}^c$ can be stored on the computer. However, the curve shape of $f_{ind,g,\lambda}^c$ may strongly depend on light conditions. Thus, the factor c_f should be determined from a suspension at the place of the measurement. The concentration need not be determined, as this cancels out in the quotient of Equation (4.24).

B. The most elaborate approach would not employ pre-averaging in the time domain, but base the fit on all individual data points

$$X^2 = \sum_{i=1}^{i_T} \sum_{\lambda=1}^{N_\lambda} \left(\frac{f_{\lambda,i} - \sum_{g=1}^4 a_{flow,g} f_{ind,g,\lambda,i}^c}{\sum_{g=1}^4 a_g w_{g,\lambda}} \right)^2 \quad (4.26)$$

with $f_{\lambda,i}$ being the time-dependent values as given by Equations (4.15 a, b) or (4.20 a, b). In that case, not only the spectral information, but also temporal information contributes to the distinction of the algal groups.

4.4 Results

4.4.1 Fluorometer tests

The assumption that fluorescence is proportional to algal concentration (neglecting self-absorbance) was tested first. A suspension with a Chl *a* concentration of 100 $\mu\text{g/l}$ (*Chlorella vulgaris* measured by a bbe-cuvette fluorometer (*Chapter 2*, bbe-Moldaenke, Kiel, Germany, calibrated by HPLC, Wiltshire *et al.* (1998)) was diluted in steps down to 1 $\mu\text{g/l}$, and the fluorescence signal was taken from the non-flowing suspension in the cuvette. Figure 4.3 A shows the linear relationship between fluorescence signal and concentration.

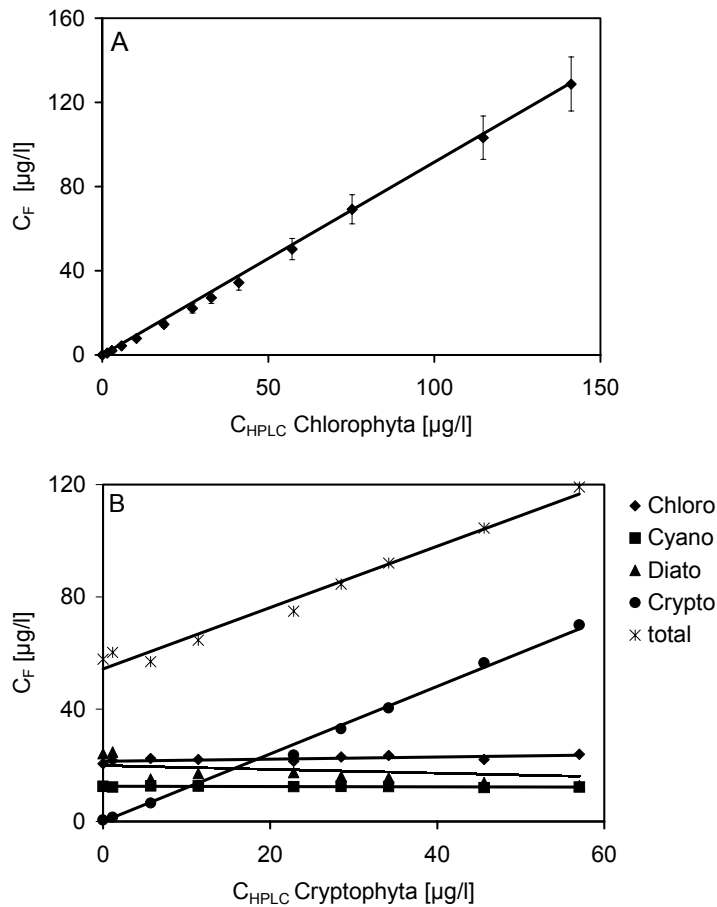


Figure 4.3. (A): Tests of the linear relationship between concentration obtained from HPLC analysis and from the fluorescence signal (C_F , Equation (4.2)) obtained by the set-up in Figure 4.1 (non-flowing solution) from *Chlorella vulgaris* at six different wavelengths of the measuring light. (B): Linearity and superposition in a mixture of *Chlorella vulgaris*, *Microcystis aeruginosa* (cyanobacteria) and *Cyclotella* sp. (diatoms) with a stepwise addition of *Cryptomonas* sp. (cryptophyta).

In another experiment linearity was tested in a mixture of *Chlorella vulgaris* and *Microcystis aeruginosa* (cyanobacteria) with an addition of *Cryptomonas* sp. (cryptophyta) in steps. Figure 4.3 B shows that also in a mixture linearity and the principle of superposition holds.

4.4.2 Fluorescence induction curves

The induction curves which are required for the model of Equations (4.15 a, b) and (4.20 a, b) were obtained for F and F_m measurements from dark- and light-adapted cells in a non-flowing suspension. For F_0 measurements, such induction curves are not required, as F_0 light has no actinic effect. Dark-adapted cells were obtained by holding the algae grown in complete darkness for 24 h before the experiments. Light-adapted cells were exposed to an illumination of $100 \mu\text{Em}^{-2}\text{s}^{-1}$ for 24 h prior to the experiments. Experiments were started 15 min after dilution to the desired concentrations. In the case of dark-adapted cells, the dilution was done in the dark.

Figure 4.4 shows the induction curves of dark-adapted and light-adapted cells. The first fluorescence value obtained from the integral over the first 25 ms after onset of measuring light and saturating laser light is normalised to 1.

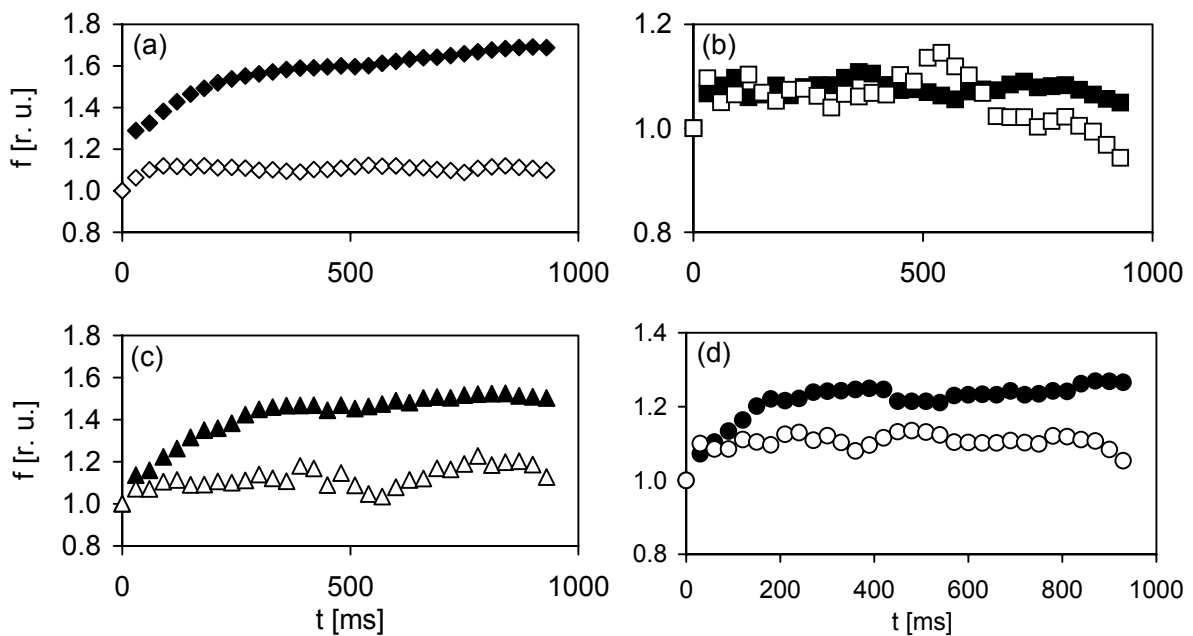


Figure 4.4. F-induction curve (Equation (4.2)) as obtained from the actinic action of the measuring light ($20 \mu\text{E m}^{-2}\text{s}^{-1}$) on non-flowing dark- (dark symbols) and light adapted (light symbols) algae: $f(t)$. “1.0” is the normalised value at $t = 0$. (a) *Chlorella vulgaris* (b) *Microcystis aeruginosa* (c) *Cyclotella* sp. (d) *Cryptomonas* sp..

In the case of the F-measurements, the light-adapted algae do not show a strong time-dependence, whereas most of the dark-adapted algae do. This is not surprising as dark-adapted algae have to adjust to the new light regime whereas light-adapted are already adapted to the measuring conditions. The increase in fluorescence indicates a decrease of photochemical quenching due to the reduction of the ETC. The cyanobacteria, however, do not show any significant change in photochemical quenching. The scatter in the traces may result from inhomogeneous distribution of algae in the flowing medium.

The F_m value is obtained when the light intensity is so high that Q_A is fully reduced. In some instruments this is achieved by a saturating single-turn over flash as lasting for about $10 \mu\text{s}$ e.g., provided by the flash light unit XST103 (Walz, Effeltrich, Germany). In the case of

such a strong light source, no correction for a flowing suspension is necessary because of the short exposure time. However, it is difficult to install such a strong light source in a diving profiler. The laser diodes used in the depth profiler are not strong enough to achieve saturation within an individual 67- μ s pulse. Thus, the cells have to be exposed for some 100 ms to the light, before F_m is reached. This is similar to the conditions prevailing in instruments using a halogen bulb, like the Standard PAM. Figure 4.5 shows the development of Q_A reduction. The peak value is the correct F_m value as has been tested by using laser flashes of different intensity. Behind the maximum value, an increase in non-photochemical quenching led to a decrease of fluorescence at the end of the induction curve, especially in the case of diatoms and dark adapted cyanobacteria .

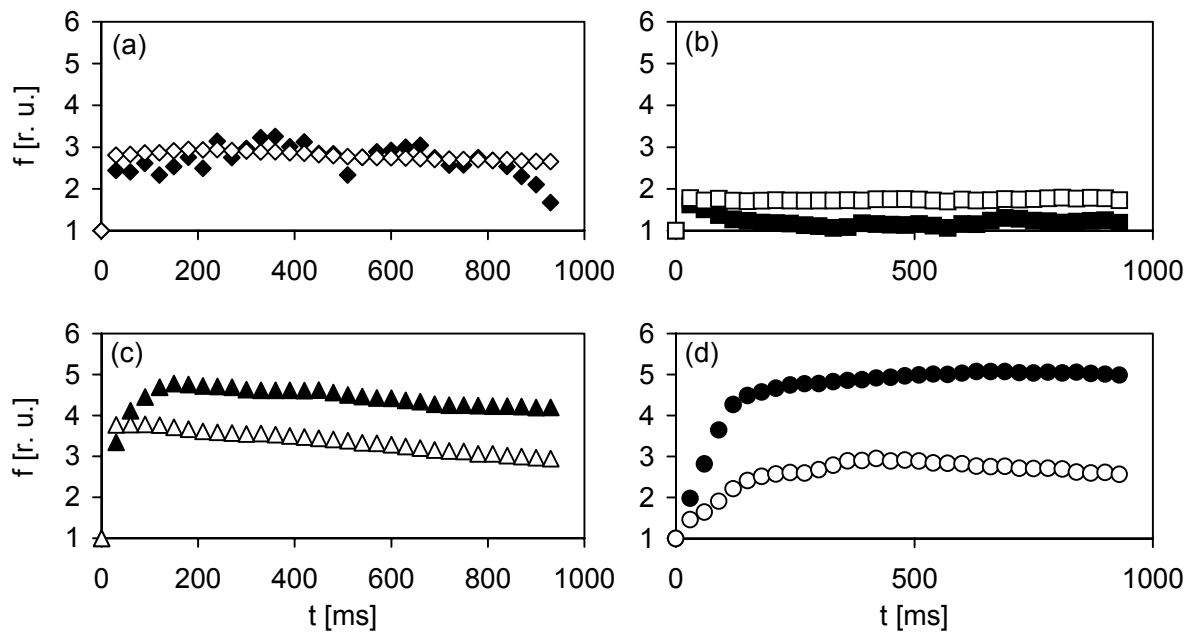


Figure 4.5. Development of the F_m -value during a series of laser light pulses obtained from dark (dark symbols) - and light-adapted (light symbols) algae (Equation (4.2)). “1.0” is the normalised value at $t=0$. The light intensities of pre-illumination were $0 \mu\text{Em}^{-2}\text{s}^{-1}$ for dark-adapted cells and $100 \mu\text{Em}^{-2}\text{s}^{-1}$ for light-adapted cells. (a) *Chlorella vulgaris* (b) *Microcystis aeruginosa* (c) *Cyclotella* sp. (d) *Cryptomonas* sp..

4.4.3 Tests with flowing suspensions

The flow of the measured suspensions was between 0 to 10 cm/s. The range of 0 to 4 cm/s was achieved by gravitational flow out of a storage vessel 2 m above the set-up. At higher velocities, a membrane pump had to be used. The pump, however, damaged the cryptophyta. Chlorophyta and diatoms also suffered, and thus the data above 4 cm/s are less reliable.

On the basis of the equations of the model for the flowing system (Equations (4.15 a, b) and (4.20 a, b)) using the induction curves from the non-flowing system and the measured Chl fluorescence (Equations (4.2) and (4.3)) of the flowing suspension was predicted and compared with the measured ones (Figures 4.6 and 4.7).

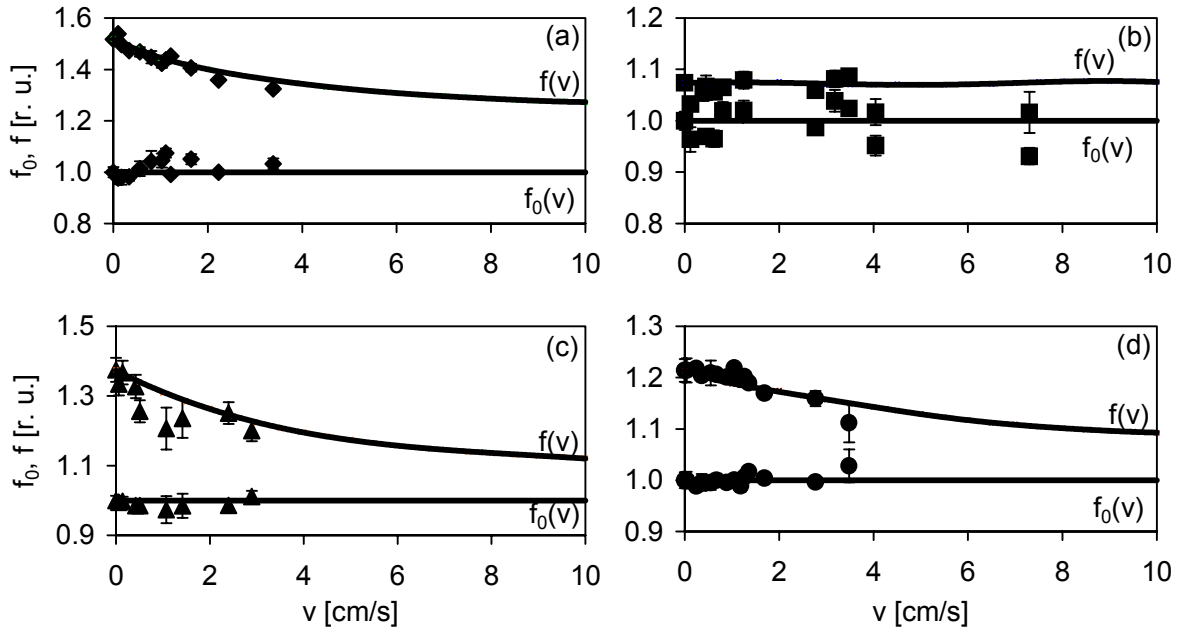


Figure 4.6. Comparison of predicted (smooth lines) and measured F and F_0 signals (Equation (4.3a)) from dark-adapted algae in a solution flowing with velocities on the x-axis. The prediction was done by means of Equations (4.15 a, b) and (4.20 a, b). The light intensities were $0 \mu\text{Em}^{-2}\text{s}^{-1}$ for dark-adapted (d) cells and $100 \mu\text{Em}^{-2}\text{s}^{-1}$ for light-adapted (l) cells. (a) *Chlorella vulgaris* (b) *Microcystis aeruginosa* (c) *Cyclotella* sp. (d) *Cryptomonas* sp..

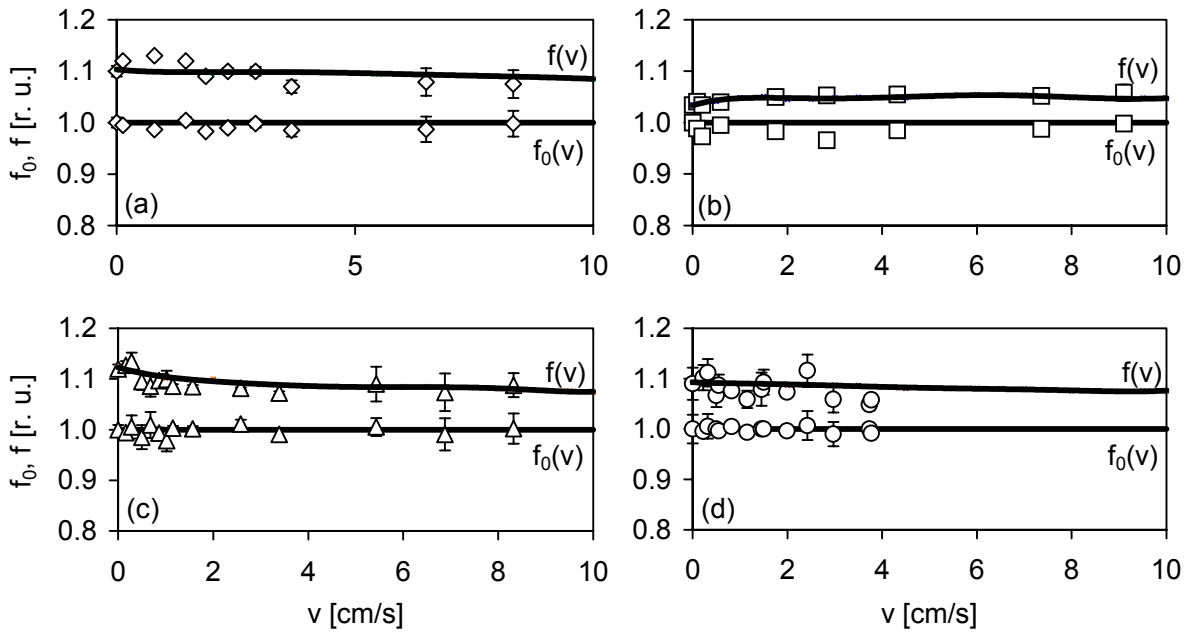


Figure 4.7. Comparison of predicted (smooth lines) and measured F and F_0 signals (Equation (4.3 a)) from light-adapted algae ($100 \mu\text{Em}^{-2}\text{s}^{-1}$) in a solution flowing with the velocity given at the x-axis. The prediction was done by means of Equations (4.15 a, b) and (4.20 a, b). (a) *Chlorella vulgaris* (b) *Microcystis aeruginosa* (c) *Cyclotella* sp. (d) *Cryptomonas* sp..

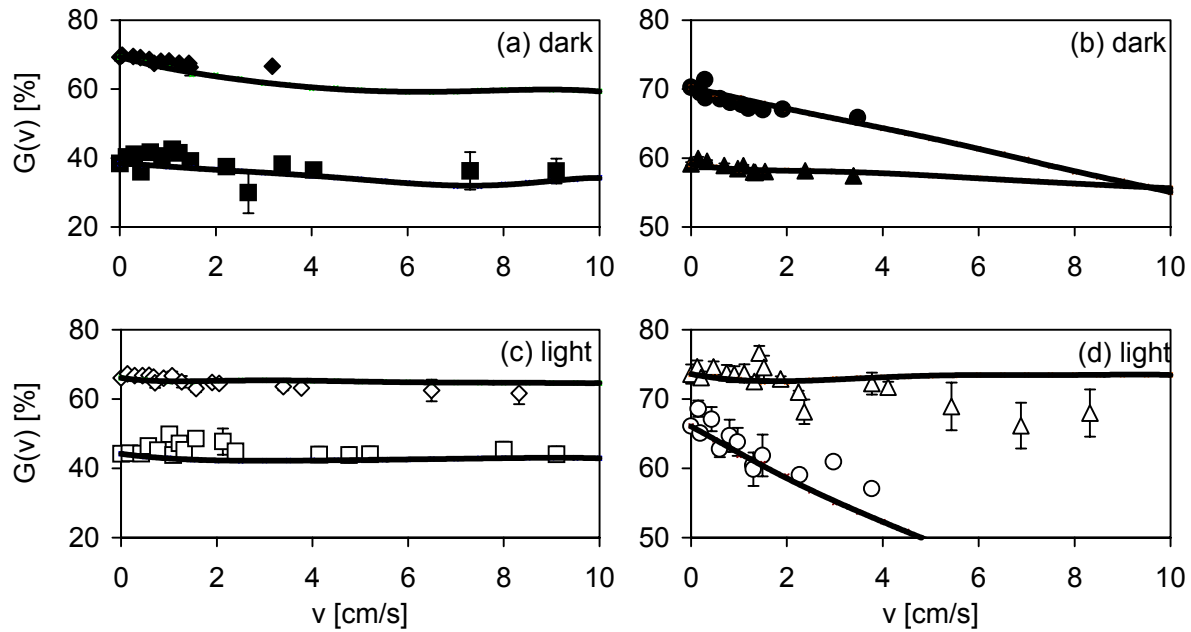


Figure 4.8. Comparison of predicted and measured Genty parameters from dark- (a, c) and light-adapted algae (c, d: pre-illumination $100 \mu\text{Em}^{-2}\text{s}^{-1}$) in a solution flowing with velocities as given on the x-axis. The prediction was done by means of Equations (4.15 a, b) and (4.20 a, b). (a, b) *Chlorella vulgaris* (diamonds), *Microcystis aeruginosa* (squares), (c, d) *Cyclotella* sp. (triangles), *Cryptomonas* sp. (circles).

Figures 4.6 to 4.8 show a very good coincidence between predicted and measured values. F_0 -fluorescence is independent of the velocity (Figures 4.6 and 4.7). This means that the fluorescence of the flowing and the non-flowing system is the same. In that case a correction by the model (Equations (4.15 a, b) and (4.20 a, b)) would not be necessary. This holds, as expected, for all F_0 -measurements of dark- and light-adapted algae. In the case of the F -measurements, the deviation is higher in dark-adapted than in light-adapted algae. The deviation decreases with velocity, and is smallest for the cyanobacteria. The decrease of deviation with velocity results from decreasing integral light exposure with increasing velocity.

4.5 Discussion

The results in Figures 4.6 to 4.8 show that algal concentrations can be measured reliably if the signal from the flowing suspension is corrected by the model described above (Equations (4.15 a, b) and (4.20 a, b)). The application requirements of this model are different for different conditions and for different species. In order to obtain an overview of the results the correction factor (Equation (4.25))

$$\Delta F = \frac{F(v=0) - F(v=5)}{F(v=0)} = 1 - (c_f c_g)^{-1} (v=5) \quad (4.27)$$

for flow rates of 5 cm/s vs. the non-flowing suspension is shown in table 4.1.

Kind of measurement	Dark adaptation	Light adaptation
f(v) Chlorophyta	13	1
f(v) Cyanobacteria	1	0
f(v) Diatoms	15	3
f(v) Cryptophyta	7	1
G(v) Chlorophyta	14	2
G(v) Cyanobacteria	12	4
G(v) Diatoms	3	1
G(v) Cryptophyta	11	25

Table 4.1. Deviation (relative error in %) of the fluorescence value measured at a flow velocity $v = 5$ cm/s from that of the stationary suspension as calculated by means of Equation (4.27).

It is obvious that this factor is highest for dark-adapted cells. Cyanobacteria do not need a correction factor. A remarkable feature of Figure 4.6 is the convergence of the F - and the F_0 -signal, as expected, since the average light intensity decreases with increasing flowing velocity.

The problem with taking depth profiles in lakes or in the ocean is the acquisition of data for the model calculations. The norm curves ($h_{g,\lambda}$ in Equation (4.4) or $f_{\text{ind},g,\lambda}^C$ in Equation (4.26), Figure 4.4) for the expected species have to be determined in either case, i.e., for measurements in flowing as well as in stationary suspensions. Optimum results would be obtained, if the determination of norm curves was done with algae from the location where the depth profiles were taken. This would account for local conditions of nutrition and light history. It could also be recommended to measure the light intensity of the natural environment before the algae enter the measuring cell. This would help to select a set of norm curves most suitable for the actual experiment. It also requires the measurement of norm

curves of algae adapted to different light intensities. The computer should store as many sets of curves that the curves for intermediate intensities can be obtained by interpolation.

The above approach would provide optimum reliability. Experience obtained from many measurements with this protocol will show whether some of these parameters and curves have a predictable behaviour and thus can be replaced by standard curves stored in the computer. We expect that the errors will stay below 20 %, if typical norm curves determined in the laboratory or in the water are used instead of locally determined norm curves.

Furthermore, the induction curves f_{Cind} have to be known for Equations (4.15 a, b) to (4.20 a, b). They have to fulfil the same requirements as the norm-curves. The most reliable procedure is the determination with species isolated at the site of the measurement. However, also here experience will show to what extent stored induction curves measured in the laboratory can be used instead. Another important result of the experiments carried out in this chapter is that the F_0 fluorescence is almost not affected by different flow velocities. This means that determination of Chl and spectral algal by means of *Chapter 2* and *3* can be carried out if the measuring light intensities are low enough (close to F_0 conditions) without a correction. Experience shows that this assumption is valid if the measuring light intensities are below $5 \mu\text{E m}^{-2} \text{s}^{-1}$ (see also *Discussion of Chapter 7*).

Chapter 5. A reduced model of the fluorescence from the cyanobacterial photosynthetic apparatus designed for the *in situ* detection of cyanobacteria

5.1 Abstract

Fluorometric determination of the chlorophyll content of cyanobacteria is impeded by the unique structure of their photosynthetic apparatus, that is, the phycobilisomes in the light-harvesting antennae. The problems are caused by the variations in the ratio of the pigment phycocyanin to chlorophyll a resulting from adaptation to varying environmental conditions. In order to improve in fluorometric analysis of algae (*Chapter 2*) a simplified energy distribution model describing energy pathways in the cyanobacterial photosynthetic apparatus was conceptualised. Two sets of mathematical equations were derived from this model and tested. Fluorescence of cyanobacteria was measured with a new fluorometer at seven excitation wavelength ranges and at three detection channels (650 nm, 685 nm and 720 nm) *in vivo*. By employing a new fit procedure it was possible to correct for variations in the cyanobacterial fluorescence excitation spectra and to account for other phytoplankton signals. The effect of energy state transitions on the phycocyanin fluorescence emission of phycobilisomes were documented. The additional use of the phycocyanin fluorescence signal in combination with our recently developed mathematical approach for phytoplankton analysis based on chlorophyll fluorescence spectroscopy allows a more detailed study of cyanobacteria and other phytoplankton *in vivo* and *in situ*.

5.2 Introduction

Cyanobacteria are potentially the most interesting organisms in ecological and phylogenetic studies. Not only do they belong to the oldest organisms on Planet Earth (Golubic & Lee (1999); Lotter (2001)) but they also are extremely important primary producers (Waterbury *et al.* (1979); Ting *et al.* (2002)). Moreover many of them are toxic and thus are often nuisance organisms as candidates for aquatic algal blooms (Codd *et al.* (1999); Carmichael (2001)). Cyanobacteria are also unique from a bioenergetic point of view, as energy transfer in the antennae is different from that in other photosynthesising cells. In this chapter two aspects of this peculiarity were investigated. Firstly, there is the theoretical question as to which pigments are involved in energy transfer mechanisms and where the energy is transferred. Secondly, solving this question is required for furnishing the mathematical tools for the quantitative determination of cyanobacteria in aquatic systems by means of fluorescence analysis.

In cyanobacteria, light absorption processes of photosynthesis take place in PBSs, PS II and PS I (Glazer (1989); Bryant (1995); van Thor *et al.* (1998)). In contrast to phytoplankton other than cyanobacteria, the outer light-harvesting antennae of cyanobacteria contain no Chl. In blue species not containing PE the PBSs consist PC and in the core regions of APC. Linker polypeptides are present in the phycobilisomes (they are un-pigmented, with the exception of the large core linker L_{CM}). PC and APC contain the ether-linked chromophore phycocyanobilin and can occur in phycobilisomes as trimers or hexamers.

Early investigations of energy transfer in the cyanobacterial photosynthetic apparatus dealt with research on energy flux in PBSs from phycobilins to another and were carried out by fluorescence- and absorption studies in the pico- or nanosecond range (Gantt & Lipschulz (1973a, b); Searle *et al.* (1978); Holzwarth *et al.* (1982); Gillbro *et al.* (1983); Wendler *et al.* (1984); Gillbro *et al.* (1985)). This and further investigations lead to models for energy transfer in PBSs (Yamazaki *et al.* (1984); Mimuro *et al.* (1985)).

In PBSs of *Synechococcus leopoliensis* 6301 with no PE and at photon densities of 10^{11} photons / cm^2 or less, energy is distributed within the PC rods with time constants of ~ 20 ps (Suter & Holzwarth (1987); van Grondelle *et al.* (1994)). In trimers or hexamers of PC or APC the equilibrium of excitation energy is extremely fast by weak excitonic interactions (van Grondelle *et al.* (1994)) as in PC monomers exciton transfer becomes important at donor acceptor distances below 2 nm (Csatorday *et al.* (1984); Sauer & Scheer (1988); Holzwarth *et al.* (1990)).

The main energy transfer process from PC to APC is Förster-transfer with rates of ~ 45 ps and ~ 120 ps. Other investigations focused on the energy transport from PBSs to PS II or PS I (Harnischfeger & Codd (1978); Mimuro & Fujita (1978); Kawamura *et al.* (1979); Redlinger & Gantt (1982); Ley (1984)). This all leads to a downhill energy transfer from PC via APC and core proteins to PS II or PS I in static measurements (μs -range and higher

(Holzwarth *et al.* (1990); van Thor *et al.* (1998))). The energy transfer through the core pigments is very efficient and is thought to exceed 95 % (Glazer (1989)).

The phycobilins within the PBSs are highly fluorescent. PC emits at a maximum emission wavelength between 650 nm and 660 nm *in vivo*. The majority of Chl is associated with PS I (for details on cyanobacterial PS I see Myers *et al.* (1980); Gill & Wittmershaus (1999); Gobets *et al.* (2001)) and contributes significantly to fluorescence emission at room temperature. Chls occur in monomers and trimers in PS I. Up to three different fluorescence emission bands of species-dependent PS I Chl pools have been found at 712 nm, 722 nm and 733 nm (Gobets *et al.* (2001)).

However, the possibility to include these models in algorithms for the determination of the amount of cyanobacteria in natural aquatic systems was not approached until now. Fit algorithms are required that account for changes in the energy fluxes as caused by changes in environmental conditions are practical in use and account for changes in the cyanobacterial excitation spectra. A reduction of the picture of the cyanobacterial photosynthetic apparatus is required to carry out fast measurements.

The reasons for the variability of the cyanobacterial excitation spectra lie in adaptation mechanisms of the cyanobacterial photosynthetic apparatus. This adaptation variability has greater implications on fluorescence than it has in green plants. The adaptation of the photosynthetic apparatus to different environmental conditions (Demarsac & Houmard (1993); Müller *et al.* (1993); Reuter & Müller (1993); Bryant (1995)) as a result of light or nutrient shifts is mediated by changes in the PC content in the PBS and in PS I to PS II ratio. The increase of PC in the PBS enlarges the optical absorption cross-section of the LHC. Additionally, the PS I to PS II ratio depends on light intensities (Kawamura *et al.* (1979)), CO₂ concentrations or on the concentration of NaCl (Schubert & Hagemann (1990); Schubert *et al.* (1993)) in the growth medium. Chl associated with PS II has a different fluorescence quantum yield as compared to that of PS I (Pfündel (1998)). Chl/PS can be species-dependent, or its variability can be induced by stress, e.g. iron deficiency. When cyanobacteria become limited to iron PBSs may be degraded, and a pigment protein complex similar to CP43' is expressed by the *isiA* gene (iron stress induced). Even though the operation of *isiA* is not fully understood it would influence fluorometric analysis as the number of efficient Chl/PS I is increased (Riethman & Sherman (1988); Straus (1994); Falkowski & Raven (1997)), and non-photochemical quenching of PS II fluorescence is enhanced (Boekema *et al.* (2001)). Further short-term variations of the energy coupling between PBS/PS I and PBS/PS II, i.e., so-called state transitions are correlated with the redox state of the ETC. They modulate the transport of energy into PS I and PS II (Williams & Allen (1987); Biggins & Bruce (1989); Campbell *et al.* (1998); van Thor *et al.* (1998)). Consequently, two different states are distinguished: 'state 1' and 'state 2'. In state 1, PS II is supplied with more energy than in state 2. Oxidisation of the plastoquinone pool and/or redox factors in the cytochrome b₆/f complex shift to state 1.

This variability of the cyanobacterial photosynthetic apparatus causes problems in phytoplankton detection and discrimination based on fluorescence (*Chapter 2*). The aim is to evolve a practical model for the cyanobacterial photosynthetic apparatus and a fit algorithm that can cope with these adaptation mechanism.

The apparent constancy of their peripheral antennae (see *Chapter 2*) enables the characterization of these spectral algal groups by a set of very similar fluorescence excitation spectra per group (represented by a so-called norm spectrum). This does not hold for the blue group where PBSs function as peripheral antennae (mainly PC). Their characteristic norm spectra change with environmental conditions. This variability hinders the determination of group-specific biomass. For instance, Lee *et al.* (1994); Lee *et al.* (1995) detected PC by *in vivo* fluorescence using two excitation-emission wavelengths but were not able to correct for other pigments or adaptation mechanism of cyanobacteria. Cowles *et al.* (1993) and Desiderio *et al.* (1997) presenting vertical profiles of phycobilin-containing algae could not present their results in terms of biomass or diversity of algal groups. The problem of variable energy transfer between different pigments can be handled by the new model developed here. The model is used for improving the fit routine and for the fluorometric discrimination of algae.

In order to test the applicability of the model, cyanobacteria were grown under various conditions. *In vivo* fluorescence of cyanobacteria was measured in a novel fluorometer employing seven excitation wavelengths and three detection channels at wavelengths of 650 nm (PC emission), 685 nm (PS II emission) and 720 nm (PS I emission), respectively (Campbell *et al.* (1998); van Thor *et al.* (1998)). It should be verified that the rapid determination of Chl and PC amounts *in vivo* and *in situ* on the basis of the simplified energy distribution model (Figure 5.5, below) is an efficient tool for detecting cyanobacteria. This requires a new algorithm that includes a new mathematical fitting strategy which automatically can cope with the variations of the cyanobacterial fluorescence excitation spectra. The progress in multispectral fluorescence analysis should be demonstrated for different cyanobacterial species also in dilution experiments in the presence of other microalgae.

5.3 Materials and methods

5.3.1 Growth experiments

The experiments were carried out in order to evaluate the fluorescence reaction of cyanobacteria grown under various environmental conditions and for test of the models (see *Appendix B*). Therefore in different growth experiments the cyanobacterium *Synechococcus leopoliensis* was grown in 0.7 litre WC growth media (Guillard & Lorenzen (1972)) at a temperature of 18 °C. The cultures were bubbled with air. A photograph of a typical growth experiment can be seen in Figure 5.1 . The growth light intensity in the empty vessels was 20 $\mu\text{E m}^{-2}\text{s}^{-1}$ or if not as otherwise stated. After an initial growth period of fourteen days, experiments were carried out. The Chl content was determined by HPLC-analyses and the PC content was determined spectrophotometrically. The number of active PS II-centres was measured by evaluating oxygen evolution under flash-light illumination (see below). Diluted cyanobacterial samples were measured in the multi-channel fluorometer (Figure 5.2, below).



Figure 5.1. Typical set-up of a growth experiment. Eight growth vessels were installed in front of a light tube and bubbled with air.

Light intensity. To evaluate the effect of different growth light intensities cyanobacteria were grown under eight different light intensities. This was achieved by covering culture vessels by different grey filter combinations (LEE Standard 209, 210, 211, 298, LEE filters, Great Britain) placed in front of a light tube (L 58W/11-860, Lumilux-Daylight, Osram, Germany). Light intensity was measured with the PhAR sensor Hansatech QRT 1 (Hansatech, U.K.) in the covered glass vessels). The following light intensities were used in the experiment: 3, 6, 9, 13, 18, 25, 35 and 50 $\mu\text{E m}^{-2}\text{s}^{-1}$. The nutrient solution was WC-medium (Guillard & Lorenzen 1972).

The effect of different nitrate, phosphate and total nutrient concentrations on fluorescence was evaluated in the following three experiments.

Growth under different sodium nitrate concentrations. *Synechococcus leopoliensis* was cultivated in WC-medium (Guillard & Lorenzen (1972)). The (sodium) nitrate concentrations were adjusted to 0.1, 0.58, 2.9, 5.9, 8.8, 12, 17.6 or 24 mmol l⁻¹ by addition of different adequate concentrations of sodium nitrate.

Growth under different di-potassium hydrogen phosphate concentrations. *Synechococcus leopoliensis* was grown in WC-medium with the phosphate component replaced by 0.0087, 0.02, 0.05, 0.1, 0.25, 0.5, 1 and 2 mmol l⁻¹ K₂HPO₄.

Effect of total nutrient concentration on fluorescence. To vary total nutrient concentrations algae were grown in mixtures of WC (Guillard & Lorenzen (1972)) and BG11 medium (Rippka & Herdman (1992)). The relative amounts of BG11 medium (Rippka & Herdman (1992)) used in the eight vessels were 0, 12.5, 25, 50, 62.5, 75, 87.5 and 100 %.

Different cyanobacterial species. *Microcystis* spec. (four species), *Synechococcus* spec. (two species), *Anabaena* spec., *Aphanizomenon* spec. (three species) were grown under the conditions described above to test the effect of different species on the reliability of the fluorescence measurement.

Aging cultures. To investigate the effect of the age of the batch cultures on pigment composition and fluorescence algae were grown in a 10-l flask. After a week of initial growth, the culture was sampled on average every three days over a period of 30 days.

5.3.2 Fluorescence measurements

For the determination of norm spectra and for laboratory and *in vivo* experiments, a bench-top fluorometer was constructed. Figure 5.2 illustrates the function of the fluorometer. 25 ml of algal suspension could be filled in a cuvette (dimensions 25 x 25 x 70 mm). Seven LEDs (370 nm, 430 nm, 470 nm, 525 nm, 570 nm, 590 nm, 610 nm) were switched on sequentially at a frequency of 5 kHz. The duration of the measuring pulse was 0.1 ms. The LED light was passed through a short-pass filter (50% transmission at 615 nm DT cyan special, Balzers, Liechtenstein and a focusing lens (additionally the light of five LEDs was passed through following cut of filters: 370 nm – B42, 430 nm - C54, 470 nm – C54, 525 nm – C54, 570 nm G51/56, all Balzers to cut of light with wavelengths higher than 580 nm). Chl fluorescence emitted by the algal suspension was coupled into the common end of a multi-leg fibre bundle (Polytec, US). The signal was detected at the end of the fibre bundle by using three photomultiplier tubes (H6779-01, Hamamatsu, Hamamatsu-City, Japan) behind band pass filter combinations at following peak wavelength/halfwidth (order from detector to sample):

650 nm/ 10 nm: Calflex x, Balzers, Liechtenstein + band pass interference filter (IF), 650nm/ 10 Dr. Anders GmbH, Germany + gelatine filter long pass (GFH) 685, Göttinger Farbfilter, Germany + R61, long pass, dichroitic filter, Balzers + IF 650nm/ 10nm, Dr. Anders GmbH,
685 nm/ 10 nm: Calflex x, Balzers, + IF, 685 nm/ 10 Dr. Anders GmbH, interference filter, Dr. Anders, Germany 685 nm/ 10 nm

720 nm/ 25 nm: Calflex x + RG 9, Schott Glas, Germany.

The photomultiplier signal was digitised by an AD-converter (12-bit AD-converter, conversion rate of 500 kHz) and processed by the same microcontroller (MM-103-5CAQ 18, Phytec, Mainz, Germany) used for control of the LEDs.

Four laser diodes (Hitachi HL6501MG, 658 nm) with a diffuser in order to prevent sprinkles were placed opposite the LEDs. These provided an additional actinic light of $3000 \mu\text{Em}^{-2}\text{s}^{-1}$ at an area of 227 mm^2 in the cuvette.

F_o , F_m , F and F_v were measured according to the definition of van Kooten & Snel (1990) see *Chapter 1*). Prior to the measurement (if not otherwise stated) the algae were dark-adapted for 90 s and F_o fluorescence was determined for 60s at an intensity of the measuring light below $1 \mu\text{Em}^{-2}\text{s}^{-1}$. Then the laser diodes were switched on for 1s and F_m was determined from the recorded kinetics on three detection channels for seven excitation wavelengths. This was followed by the measurement of F for 60s at an intensity of the measuring light below $5 \mu\text{Em}^{-2}\text{s}^{-1}$.

For the detection of state transitions, algal samples were illuminated with the white light of a Xenon lamp (HLX 64640, 24V, 150 W, Xenophot, Osram, Germany) in a slide projector. Grey filters (Lee filters, UK) were used to provide different light intensities. The samples were illuminated 15 minutes prior to the measurement.

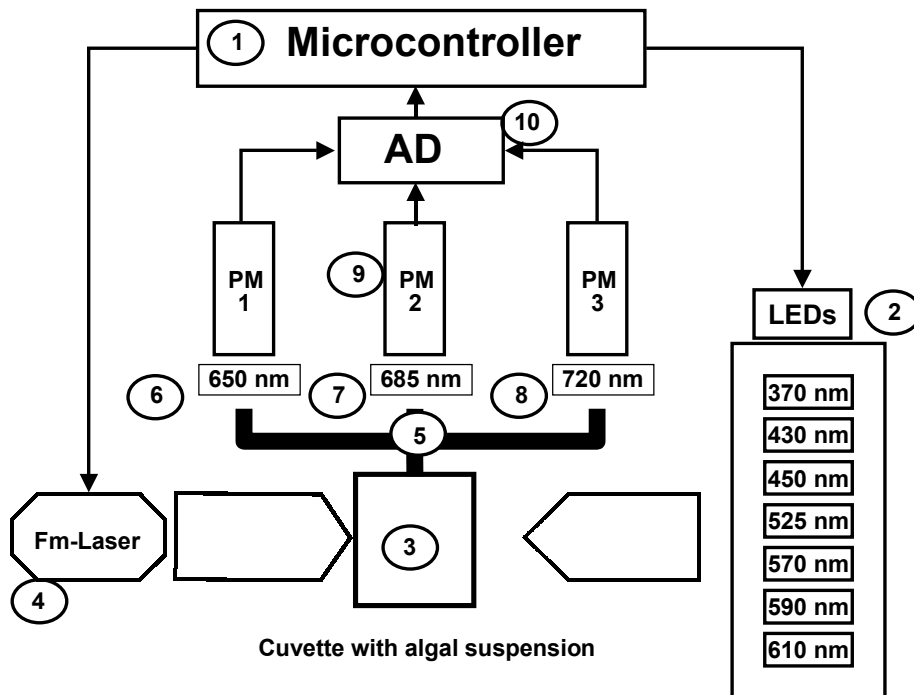


Figure 5.2. Fluorometer set-up: microcontroller, (2) seven LEDs (measuring-light), (3) sample cuvette containing algal suspension, (4) diode laser (Fm-light), (5) multi-leg fibre bundle, (6) band-pass filter (650 nm), (7) band-pass filter (685 nm), (8) band-pass filter (720 nm), (9) three photomultipliers (PM1-3) and (10) 12-bit AD-converter (conversion rate of 500 kHz).

5.3.3 Determination of chlorophyll concentrations

Concentrations of Chl (for calibrating the fluorometer, see norm spectra) were determined according to Wiltshire *et al.* (1998) and *Chapter 2* using HPLC.

5.3.4 Phycobilin determination

The algal suspension was filtered through a Whatman GF/F-filter. The filter was subsequently frozen at - 30 °C for at least 24 hours. After thawing, quartz sand and an extraction solution (0.1 M P-puffer [pH 6.8], 10 mM Na₂EDTA, LYSOZYME [0.1 mg l⁻¹] (Campanella *et al.* (2000))) were added to the filter. The samples were then homogenized using a Teflon stick and stored in the cold at 7°C for 12 hours. Next the samples were ultra-sonificated for 130 minutes at 30°C (not more than 35°C) allowing enzyme degradation of cell walls. They were then centrifuged at 3600 g at 15°C for 15 minutes. Extracts were filtered (Spartan 30/0, 2 RC, Schleicher & Schuell, Germany, 0.2µm pore size) and measured in a spectrophotometer (UV-DU 650, Beckman, USA). The equations for the determination of PC and PE are given in Bennett & Bogorad (1973):

$$C_{PC} = [A_{615} - 0,474 (A_{652})] / 5,34 \quad (5.1)$$

$$C_{APC} = [A_{652} - 0,208 (A_{615})] / 5,09 \quad (5.2)$$

$$C_{PE} = [A_{562} - 2,41 (C_{PC}) - 0,849 * (C_{APC})] / 9,62 \quad (5.3)$$

with A_{λ} : absorbance measured at wavelength λ

C_{PC} , C_{APC} and C_{PE} concentration of PC, APC and PE in mg ml⁻¹

These equations hold for algae containing just PC as well as those containing both pigments.

5.3.5 Number of photosystem II reaction centres

In order to determine the total amount of oxygen evolving from PS II reaction centres algal or cyanobacterial suspensions were illuminated by saturating flash lights (e.g. Myers *et al.* (1980)). For four light flashes one oxygen molecule is evolved per intact PS II reaction centre. The number of evolved oxygen molecules were measured in a Clark-electrode-cuvette unit (S1-electrode, DW2-cuvette-unit, Hansatech, Great Britain). The sample volume was placed in a light absorbing black housing. Illumination and optical measurements could be carried out at four optical ports (inner diameter: 16 mm).

The flash light illumination was provided by a Xenon flash tube (FX 1150, EG&G, USA) connected to one of the optical ports of the measuring chamber by a Perspex guide (length: 25 mm, diameter: 16 mm). In order to block light of wavelengths lower than 430 nm, an optical filter was inserted between the Perspex guide and cuvette (GG435, Balzers, Liechtenstein). This prevented potential damage of the PSs by the light flashes. The measurements were carried out with a flash frequency of between 10 Hz and 20 Hz at 20° C.

The light flashes had to fulfil two requirements: Firstly, they had to saturate the photochemical reactions of the PS II reaction centres and secondly they had to lead to single charge separation (so-called 'single-turnover'-flashes). By variation of flash intensity, frequency and number it was possible to test the saturating effects of the flashes.

5.4 Results

5.4.1 Effect of pigment variability on two different evaluation problems

One task is to determine the concentrations of PC, Chl and PS II from the measured spectra in a suspension that contains no other phytoplankton besides cyanobacteria. In that case, the approach is straight forward, i.e., the variability is a result of the analysis by the model described below and does not require special precautions. The second task, however, the quantitative determination of the amounts of individual spectral phytoplankton groups in a mixed suspension (as occurring in lakes and oceans) has to cope with the problem of variable spectral properties of cyanobacteria. Here we start with the first case in order to get a survey of what effects have to be taken into account when the second problem has to be approached.

5.4.2 Cyanobacteria with different pigmentation for the investigation for variability of spectra and for testing the model

The influence of various growth conditions on pigment ratios in *Synechococcus leopoliensis* is demonstrated in Figure 5.3 A-D. Light intensity and total nutrient content seem to have complementary effects on PS II to Chl ratio and PC to Chl ratio, whereas the effect of P and N nutrition in Figure 5.3 B, C does not show such a complementary behaviour. Species dependence of pigment ratios is shown for ten different cyanobacterial species in Figure 5.4. A changing ratio of PS II/Chl *a* indicates a changed ratio of PS II to PS I but could also mean an accumulation of IsiA or similar proteins which would also influence this ratio by changing PS I/ Chl binding (Boekema *et al.* (2001)). The ratio of PC to Chl *a* changed by a factor twelve in all four growth experiments (compare Figure 5.3A and C) while the number of PS II centres changed five-fold. The different pigmentation types of Figures 5.3 and 5.4 were used for the test of model developed in the next section.

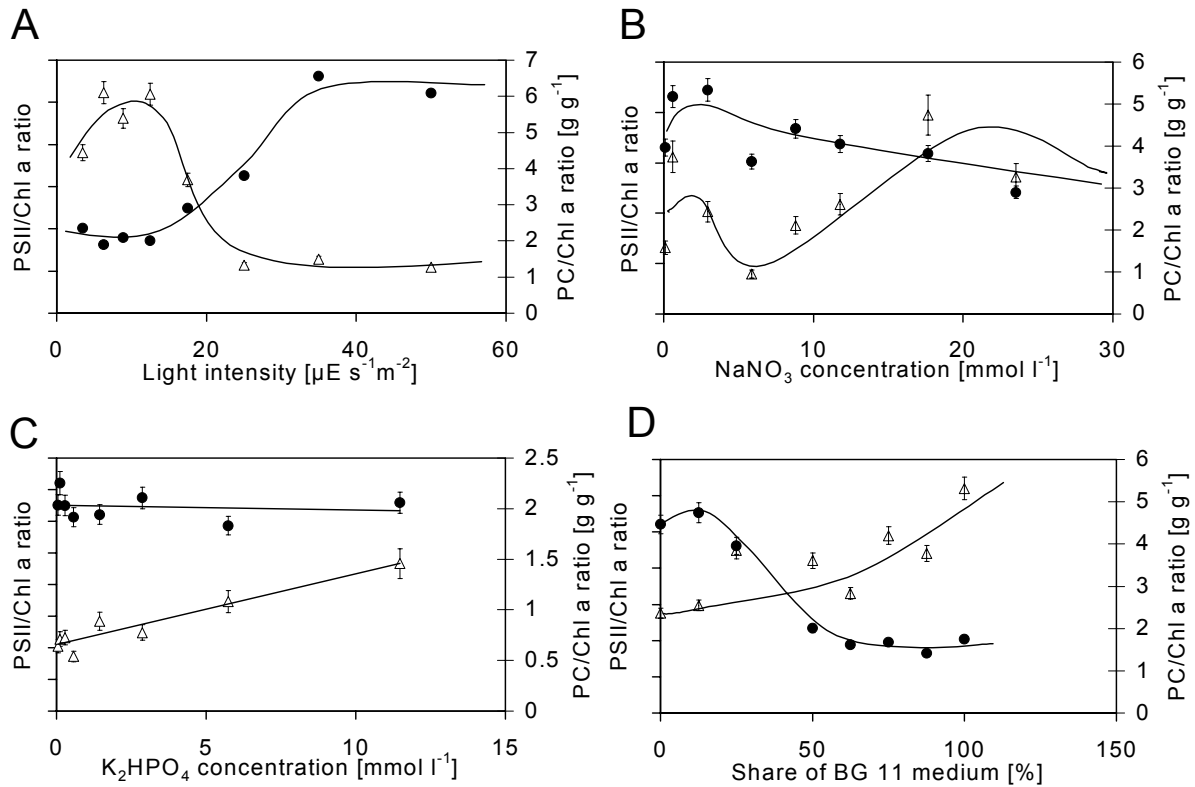


Figure 5.3. Change of the pigment ratios and number of PS II reaction centres under variation of growth conditions (open triangles: ratio of PC to Chl *a*; filled circles ratio of number PS II centres to Chl *a* concentration). Variation of A) growth light intensities; B) NaNO_3 concentration; C) K_2HPO_4 concentration; D) share of BG11 medium in culture.

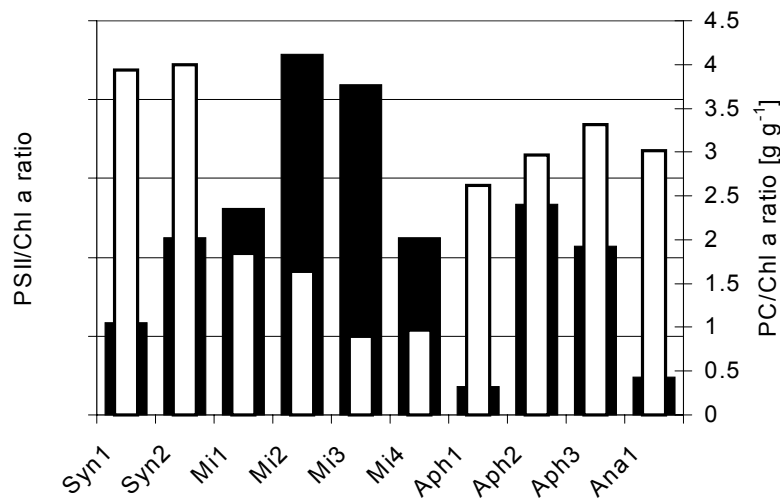


Figure 5.4. Pigment ratios and number of PS II reaction centres of ten different cyanobacterial species (open bars: ratio of PC to Chl *a*; filled bars ratio of number PS II centres to Chl *a* concentration). Mi 1-4: *Microcystis* spec., Syn 1,2: *Synechococcus* spec., Ana: *Anabaena* spec., Aph1-3: *Aphanizomenon* spec.

5.4.3 A simplified model of energy transfer in the antennae of cyanobacteria

Figure 5.5 shows the pigments of the photosynthetic apparatus of cyanobacteria and the flow of energy between them. The mathematical description of this model is presented in Appendix B.

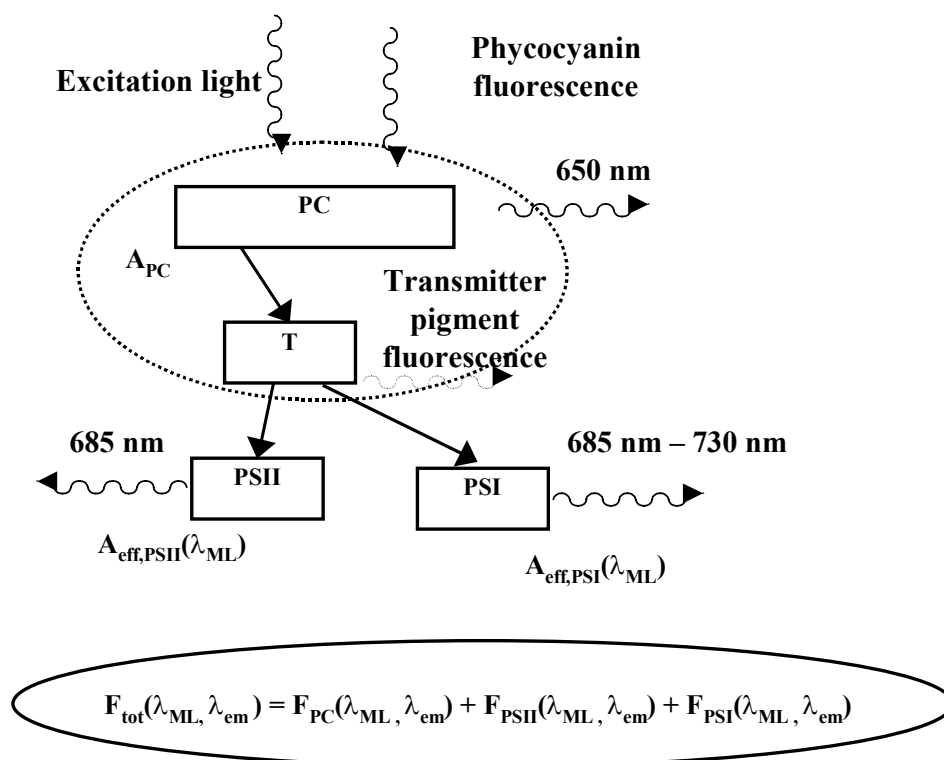


Figure 5.5. Simplified model of absorption and fluorescence emission processes in PBSs and PSs in cyanobacteria (PE-free organisms like *Synechococcus leopoliensis*): $A_{\text{eff, PS II}}(\lambda_{\text{ML}})$, $A_{\text{eff, PS I}}(\lambda_{\text{ML}})$; effective absorption cross-section (in m^2) of PS II and PS I, $A_{\text{PC}}(\lambda_{\text{ML}})$: PC absorption cross-section (in m^2); $F_{\text{PC}}(\lambda_{\text{ML}}, \lambda_{\text{em}})$, $F_{\text{PS II}}(\lambda_{\text{ML}}, \lambda_{\text{em}})$, $F_{\text{PS I}}(\lambda_{\text{ML}}, \lambda_{\text{em}})$: total, PC, PS II and PS I fluorescence intensity; λ_{ML} : wavelength of measuring light; λ_{em} : fluorescence emission wavelength. The core proteins of PBS (e.g. APC) are classified as ‘transmitter pigments’. The absorption and fluorescence properties of the ‘transmitter pigments’ were neglected in the latter consideration and reduced to the function as energy transmitters. Fluorescence model adapted and simplified from Suter & Holzwarth (1987) and van Thor *et al.* (1998).

5.4.4 Test of the first assumption with cyanobacteria of different pigmentation types (Equation (B8) in the Appendix A)

The first assumption (Equation (B8)) is verified by Figure 5.6 A showing that the same linear relationship holds between $F_{610,650}$ (fluorescence intensity measured at 610 nm excitation and 650 nm emission) and PC content for all growth conditions employed in Figure 5.3. Further, the correlation coefficient for $F_{610,650}$ to the PC content for the ten different species in Figure 5.4 having pigment ratios was $R^2 = 0.9186$ (Figure 5.6 B). Thus, Equation (B8) can be used in Equations (B9) to (B17).

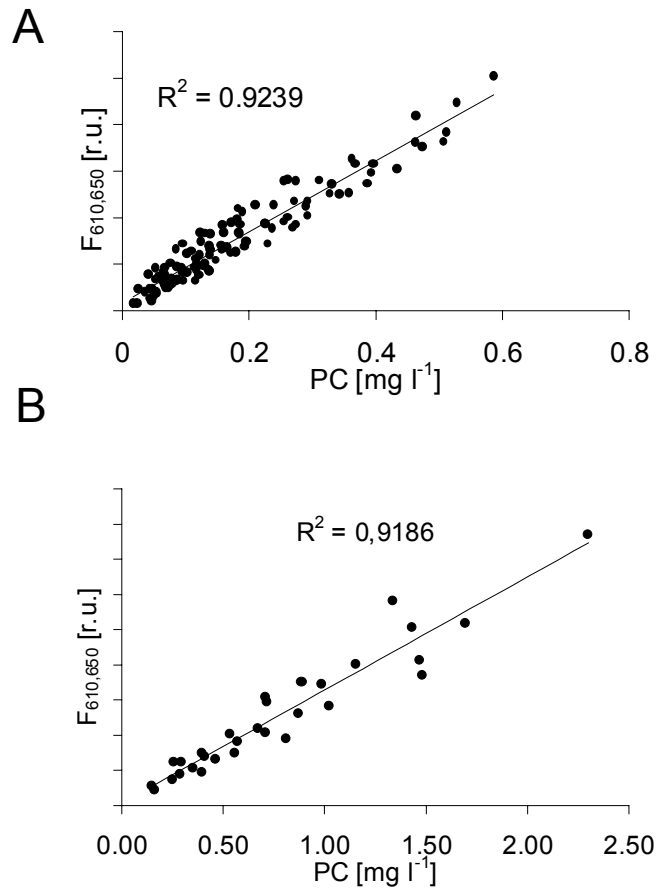


Figure 5.6. Dependence of the spectrophotometrically estimated PC content on the fluorescence signal $F_{610,650}$ measured at the cyanobacteria with the pigment ratios shown in: A) Figure 5.3 A-D and B) Figure 5.4.

5.4.5 Estimation of chlorophyll and photosystem II by fluorescence in cyanobacteria

To verify Equation (B9b) the second assumption represented by Equation (B16) was tested for the cultures with pigment ratios shown in Figure 5.3. The model in Figure 5.5 suggests that scenarios of excitation and emission lights should be adequate for cyanobacteria to find the best estimates of the concentrations of Chl *a* and the concentration of PS II reaction centres.

We therefore define: **scenario 1:** $\lambda_{1ML} = 470 \text{ nm}$, $\lambda_{1em} = 685 \text{ nm}$
 $\lambda_{2ML} = 610 \text{ nm}$, $\lambda_{2em} = 685 \text{ nm}$

and **scenario 2:** $\lambda_{1ML} = 610 \text{ nm}$, $\lambda_{1em} = 720 \text{ nm}$
 $\lambda_{2ML} = 610 \text{ nm}$, $\lambda_{2em} = 685 \text{ nm}$

Thus, two different sets of $F_{\text{tot}}(\lambda_{1\text{ML}}, \lambda_{1\text{em}})$ and $F_{\text{tot}}(\lambda_{2\text{ML}}, \lambda_{2\text{em}})$ were used in Equations (B9b) and (B16) and their efficiency was compared. In scenario 1 it is assumed that fluorescence described by the pair $\lambda_{1\text{ML}} = 470 \text{ nm}$ and $\lambda_{1\text{em}} = 685 \text{ nm}$ originates mainly from direct Chl excitation and thus mainly from PS I. Fluorescence related to $\lambda_{2\text{ML}} = 610 \text{ nm}$ and $\lambda_{2\text{em}} = 685 \text{ nm}$ is thought to be light that was absorbed by the PBS and emitted by PS II. If fluorescence is assigned to $\lambda_{1\text{ML}}$ and $\lambda_{1\text{em}}$. In scenario 2 it is predominately light emitted from PS I (720 nm) excited by 610 nm which was originally absorbed by the PB. The second wavelength is the same as in scenario 1.

Linear regressions were calculated on PS II centres and Chl concentrations from Equations (B9b) and (B16) on the reference estimates. The results are shown in Figures 5.7 A-D.

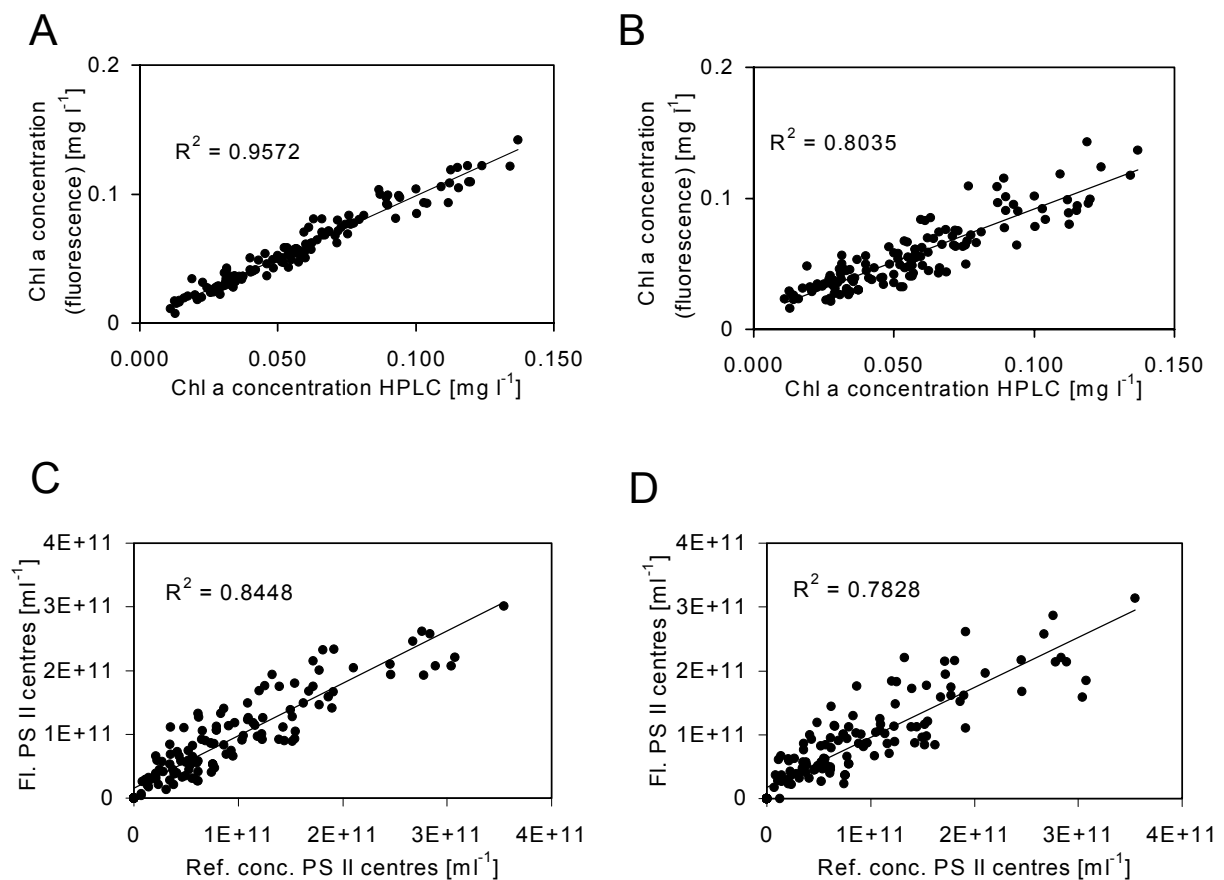


Figure 5.7. Linear regressions of the calculated PS II centres and Chl concentrations from Equations (B9b) and (B16) on the reference estimates shown in Figure 5.3 A-D: A) Chl *a* estimated by scenario 1 B) Chl *a* estimated by scenario 2 C) PS II reaction centres estimated by scenario 1 D) PS II reaction centres estimated by scenario 2.

For both the estimation of Chl *a* and PS II centre concentrations a better correlation was found for scenario 1. Scenarios 1 and 2 were tested for different cyanobacterial species in a same manner as above. The calculated correlation for PS II centres and Chl concentrations from Equations (B9b) and (B16) on the reference estimates are shown in Figure 5.8 A-D. Again scenario 1 was found to be superior to scenario 2 for determination of PS II centres and Chl concentrations. Because of these results the following considerations are based on scenario 1.

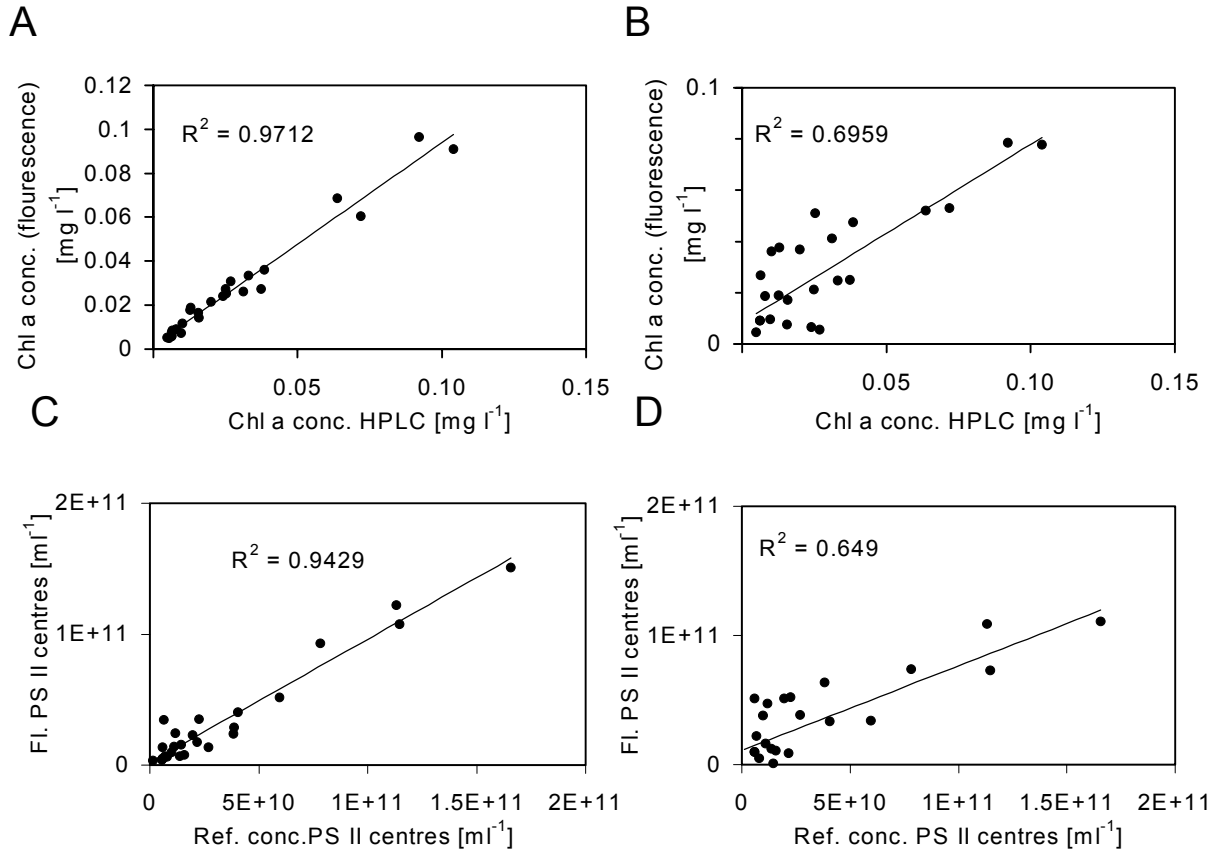


Figure 5.8. Linear regressions of the calculated PS II centres and Chl concentrations from Equations (B9b) and (B16) on the reference estimates of different cyanobacterial species shown in Figure 5.4: A) Chl *a* estimated by scenario 1 B) Chl *a* estimated by scenario 2 C) PS II reaction centres estimated by scenario 1 D) PS II reaction centres estimated by scenario 2.

5.4.6 Variation of cyanobacterial fluorescence excitation spectra

The fluorescence excitation spectra of cyanobacteria are variable due to different pigment contents. In order to incorporate these variable spectra a parametric description of this variability is necessary. Figure 5.9 shows the norm spectra used for the evaluation of cyanobacteria spectra for the 650 nm and 685 nm channels. They are positioned between two measured extreme excitation spectra of fluorescence (defined as vectors $\underline{c}_{hi\lambda_{em}}$ and $\underline{c}_{low\lambda_{em}}$ shown as bold lines with circles). They were selected from the spectra of the pigmentation types (shown in Figure 5.3 and 5.4). The spectra were normalised to the fluorescence intensity excited by 470 nm.

40 lines between these two extreme curves were calculated by linear interpolation as follows

$$\underline{c}_{l_{\lambda_{em}}} = (l_{\lambda_{em}}/40) \underline{c}_{low\lambda_{em}} + (40-l_{\lambda_{em}})/40 \underline{c}_{hi\lambda_{em}} \quad \text{for } l_{\lambda_{em}} = 1 \text{ to } 40 \quad (5.4)$$

with: $l_{\lambda_{em}}$: number of spectra between the extreme curves in Figure 5.9. The assumptions of Equation (5.4) were verified by the test described below.

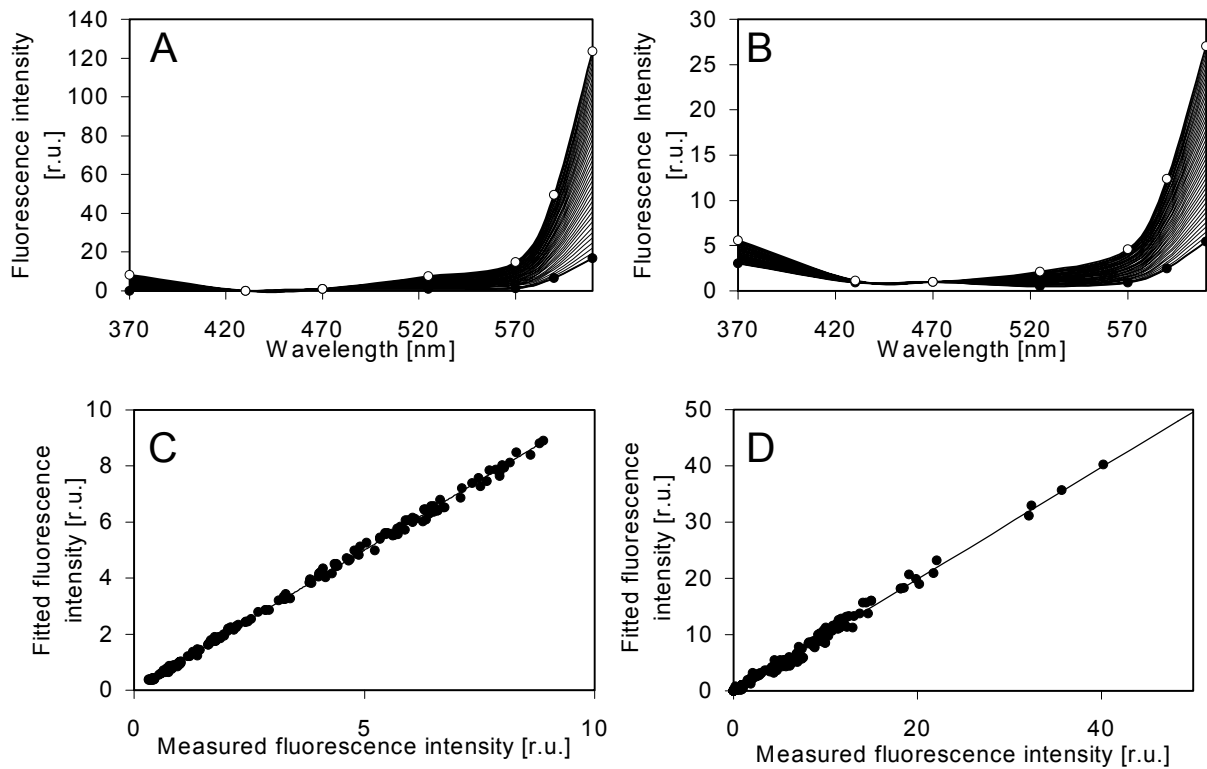


Figure 5.9. Variation of cyanobacterial fluorescence excitation spectra and estimation by an artificial norm spectra matrix:

A) and B) Bold lines: two extremes (defined as $\underline{c}_{hi\lambda_{em}}$ and $\underline{c}_{low\lambda_{em}}$) of fluorescence excitation spectra of the cyanobacteria with the pigment ratios given in Figures 5.3 and 5.4. The spectra are normalised to the fluorescence intensity under excitation with 470 nm. Thin lines: artificial norm spectra matrices $\underline{C}_{\lambda_{em}}$. (A) $\lambda_{em} = 650$ nm; B) $\lambda_{em} = 685$ nm; C) (650 nm) and D) (685 nm). The correlation of measured fluorescence intensity for all excitation wavelengths at a single detection wavelength to the fitted fluorescence data by estimation of Equation (5.4).

In order to find out whether $\underline{c}_{l,em}$ (Equation (5.4)) describes the excitation spectra of natural samples with sufficient precision (i.e. deviation less than 5 %) $\underline{c}_{l,em}$ was fitted to the measured spectra of the cyanobacteria in Figures 5.3 and 5.4 by the following procedure. For each of the 40 $\underline{c}_{l,em}$ ($1 < l < 40$) the deviation of the measured spectrum $c_{m,\lambda_{ex},\lambda_{em}}$ and adequate multiple of $\underline{c}_{l,\lambda_{ex},\lambda_{em}}$ was described by the error

$$e_{lex,l}^2 = \sum_{\lambda_{ex}} \left(c_{m,\lambda_{ex},\lambda_{em}} - s_l \underline{c}_{l,\lambda_{ex},\lambda_{em}} \right)^2 \quad (5.5)$$

This resulted in a minimum value of $e_{lex,l}^2$ for one l (the number of the norm vector describing this particular spectrum of cyanobacteria). This is illustrated in Figure 5.9 C and D. The fitted fluorescence is obtained from the components of the vector $s_l \underline{c}_{l,em}$. Thus each $\underline{c}_{l,em}$ results in seven points for the seven wavelengths in Figure 5.9 A and B. The measured fluorescence presents the components of the vector of the measured spectrum. The different wavelengths are not indicated as only the location on the x=y-line is of interest. The average deviation from the fitted to the measured data was lower than 3 %. A higher number of $l_{\lambda,em}$ than 40 did not increase the precision.

For fitting measured spectra of unknown samples, a matrix $\underline{C}_{\lambda,em}$ of artificial cyanobacterial norm spectra was used ($\underline{C}_{\lambda,em} \in \mathfrak{R}^n \times \mathfrak{R}^n$). The rows $\underline{c}_{l,em}$ of $\underline{C}_{\lambda,em}$ are the thin lines in Figure 5.9 A and B as calculated by Equation (5.4). With the use of a discrete matrix $\underline{C}_{\lambda,em}$ for the cyanobacterial norm spectra saved calculation time was saved in a fit procedure for the estimation of algal groups (described in *Appendix C*).

5.4.7 Norm spectra of other spectral algal groups

To determine pigments of cyanobacteria in a mixture of different algal species it is necessary to account for the presence of other phytoplankton therein. This can be achieved by the use of norm spectra for other phytoplankton in a mathematical fit. Norm spectra were recorded on the 650 nm and 685 nm detection channel. The spectra are shown in Figure 5.10 for four different species. These norm spectra were used as elements of matrix $\underline{N}_{\lambda,em,l_{\lambda,em}}$ in the fit described in the *Appendix C*.

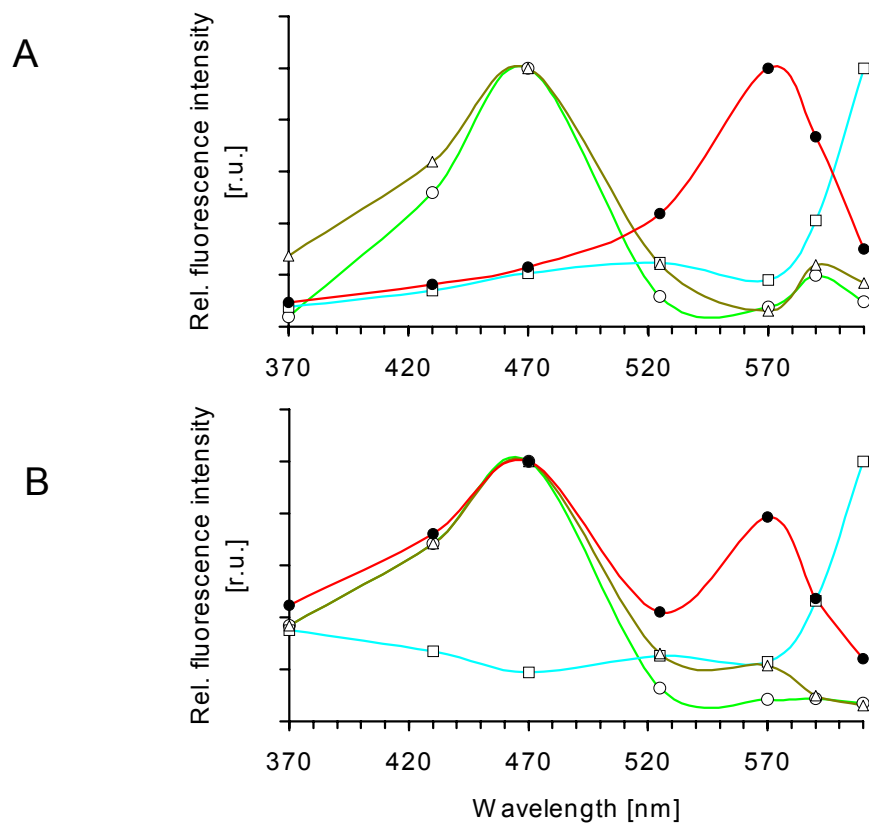


Figure 5.10. Fluorescence excitation spectra of four spectral algal groups obtained with the fluorometer set-up of Figure 5.2 normalised to maximum. A) spectrum at 650 nm detection wavelength, B) spectrum at 685 nm detection wavelength. Green spectral group (open circles): *Chlorella vulgaris*, blue spectral group (open squares), *Synechococcus leopoliensis*, brown spectral group (open triangles): *Cyclotella* sp., mixed spectral group: *Cryptomonas* sp. (closed circles). The spectra differ significantly and can be used as norm spectra in spectral analysis.

5.4.8 Tests using dilution experiments

By the use of the norm spectra given in Figures 5.9 and 5.10, the mathematical fit in the Appendix C as well as scenario 1 it should be possible to determine the amount of cyanobacterial PC and Chl. In a dilution experiment (Figure 5.11 A), a culture of *Synechococcus leopoliensis* was diluted from PC concentration of $750 \mu\text{g l}^{-1}$ down to $1 \mu\text{g l}^{-1}$. It was possible to determine PC concentrations and Chl *a* concentrations at a PC concentration of $1 \mu\text{g l}^{-1}$ with an average error lower than 5%.

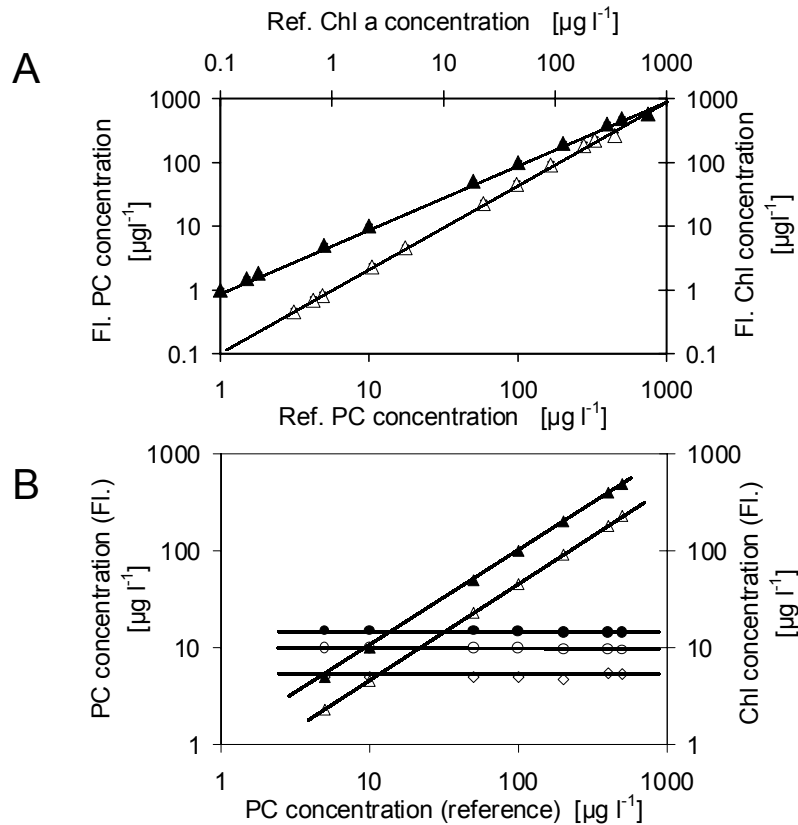


Figure 5.11. A) Dilution of *Synechococcus leopoliensis* culture measured in the fluorometer. The fluorometrically determined PC content (closed triangles) is shown versus the spectrochemically determined PC content. The fluorometric estimate of the Chl content (open triangles) is shown relative to reference Chl contents. B) Variation of contribution of blue algal group in the presence of other phytoplankton. The fluorometrical estimate of the Chl (green: open circles, blue: open triangles, brown: open diamonds, mixed: closed circles) content and the fluorometrically determined PC content (closed triangles) is shown versus the spectrochemically determined PC content of the blue group.

In another test (Figure 5.11 B) the contribution of the blue algal group (*Synechococcus leopoliensis*) was changed relative to the presence of other phytoplankton. Algal suspensions with a constant Chl content of the green spectral group (*Chlorella vulgaris*), brown spectral group (*Cyclotella* sp.), mixed spectral group (*Cryptomonas* sp.) and a varying PC and Chl content of the blue group were used. The Chl *a* concentrations of the spectral algal groups were kept constant as follows: green ($10 \mu\text{g l}^{-1}$), brown ($5 \mu\text{g l}^{-1}$) and mixed ($15 \mu\text{g l}^{-1}$).

5.4.9 Aging cultures

Cyanobacteria in batch culture evince exponential growth at the beginning of the culture period. This is *de facto* analogous to the situation of a cyanobacterial bloom *in situ*. They show a decrease in total Chl in later stages of the growth period due to nutrient limitation. In order to test the scenario 1 and the mathematical fit procedure given in the *Appendix C*, spectra of the samples were determined in the fluorometer. In Figure 5.12 A the PC and Chl concentrations during an aging experiment of a batch culture are shown. The fluorometrically determined PC and Chl values are in good agreement with the reference data obtained from HPLC, photometry and oxygen electrode over the total growth experiment. The number of PS II

reaction centres determined by fluorescence and the reference method are shown in Figure 5.12 B. It also depicts the reference ratio of PC to APC amounts and the energetic coupling of PBSs to PS II in terms of the ratio $F_{v\ 610,685}$ to $F_{v\ 470,685}$. The overall estimation of PS II reaction centres by fluorescence corresponded with the reference estimation of PS II reaction centres by the flash light method. Although the ratio of PC to APC decreased with the culture age, the estimation of PS II reaction centres was not affected. The energetic coupling of PBSs to PS II centres increased with a lower PC to APC ratio. This was probably due to the fact that a higher contribution of light was absorbed by APC than by PC, and energetic coupling of APC to PS II is of course higher than from PC via APC to PS II. The energetic coupling (in Figure 5.12 B) decreased between days 30 and 32, presumably as result of degradation processes within the core region of the PBSs. The fluorometrical determination of PS II leads to a higher result than the reference method on days 30 to 32.

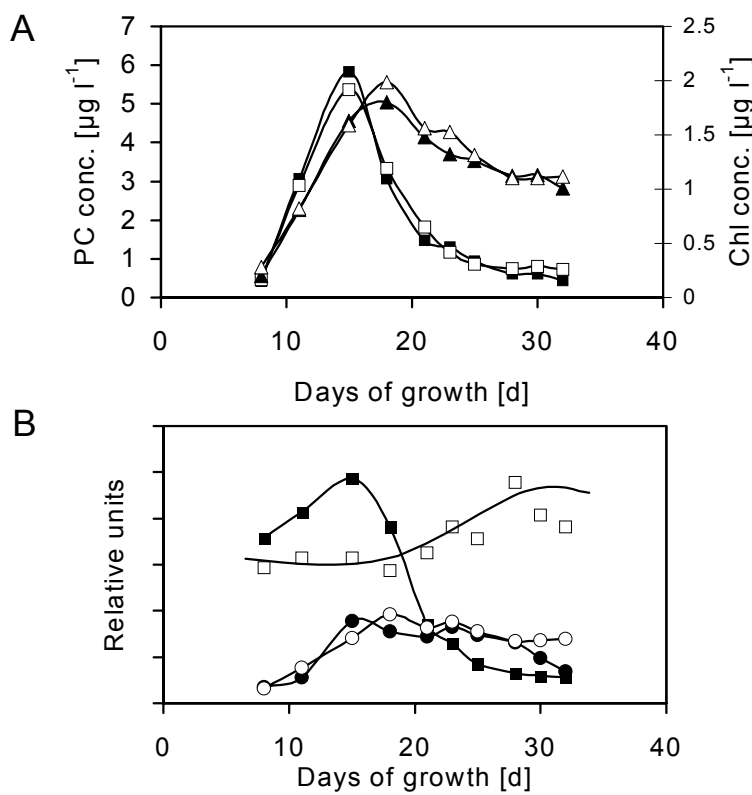


Figure 5.12. Pigment concentrations measured at different ages (in days) of a cyanobacterial batch culture. A) PC and Chl concentrations: open triangles - fluorometrically determined PC concentration, closed triangles: reference PC concentration, open circles - fluorometrically determined Chl concentration, closed circles: reference Chl concentration. B) open circles: fluorometrically determined PS II reaction centres, closed circles reference PS II reaction centres, closed squares: reference ratio PC to APC amount, open squares: energetic coupling of PBSs to PS II in terms of the ratio $F_{v\ 610,685}$ to $F_{v\ 470,685}$.

5.4.10 Sensitivity to changed light intensity

In another experiment, the influence of energy state transitions and photoinhibitory effects induced by changed light intensity on the fluorometric pigment and PS II centre concentration estimates (Figure 5.13) was investigated. The fluorometric estimates of PC, Chl and PS II were measured and calculated in dependence on the light intensities. The ratio of

$F_{v610,685} / F_{v470,685}$ is a relative measure of energy reaching PS II by light absorption and transfer from the PBS to PS II ($F_{v610,685}$) and energy reaching PS II by light absorption of PS II directly ($F_{v470,685}$). The energetic coupling of PBSs was highest when the samples were adapted with light intensity in the range of the growth light (between $10 \mu\text{E m}^{-2} \text{s}^{-1}$ – $100 \mu\text{E m}^{-2} \text{s}^{-1}$). This is in correspondence with results of the investigations by Campbell & Öquist (1996). Low coupling to PS II was found in dark adapted and high light adapted cells. The change of the fluorometric estimate of PC changes less than 5 % while the change of Chl and PS II is less than 10 %.

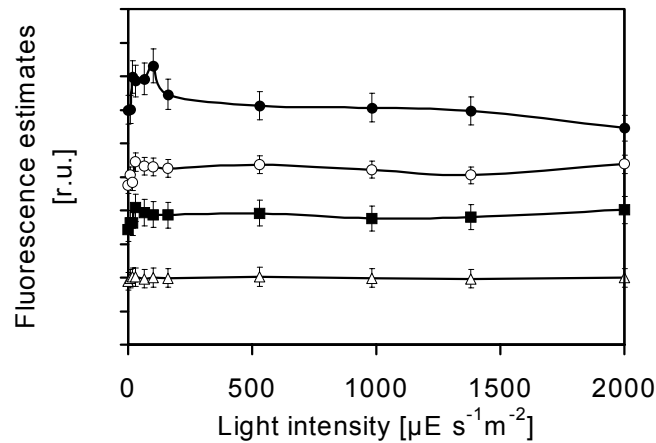


Figure 5.13. Fluorometric pigment and PS II reaction centre estimates under light adaptation with different light intensities: closed circles: energetic coupling of PBSs to PS II in terms of the ratio $F_{v 610,685}$ to $F_{v 470,685}$, open triangles: fluorometrically determined PC concentration, open circles: fluorometrically determined Chl concentration, closed squares: fluorometrically determined PS II reaction centres. Dark-adaptation time prior to measurement was 1 s and adaptation time to light intensity 15 min. Three samples were averaged per data set. Measuring duration of F_o and F_m was 1s.

5.5 Discussion

5.5.1 Variation of cyanobacterial pigments

The necessity of taking the high spectral variability of blue cyanobacteria into account is demonstrated by the great variation of the photosynthetic apparatus structure under different growth conditions (Figure 5.3) and for different species (Figure 5.4). This variability originates from large changes in the ratios of PC to Chl and PS II to Chl. The values of these ratios were similar to those reported in the literature (Kawamura *et al.* (1979); Schubert & Hagemann (1990); Demarsac & Houmard (1993); Müller *et al.* (1993); Reuter & Müller (1993); Schubert *et al.* (1993); Bryant (1995)). This may be due to an increase of PC within the PBSs and/or to changes in size and number of PS I reaction centres (Kawamura *et al.* (1979); Schubert & Hagemann (1990); Demarsac & Houmard (1993); Müller *et al.* (1993); Reuter & Müller (1993); Schubert *et al.* (1993); Bryant (1995)), with the ratio of PBSs to PS II being accepted as constant (Myers *et al.* (1980)). This variability effects the spectral fluorescence emission of the cyanobacterial photosynthetic apparatus (Equations (B1)). The resulting instable norm spectra can cause problems in the fluorometric spectral phytoplankton analysis (*Chapter 2*) and can lead to false Chl estimations and algal group identification. Figures 5.6 to 5.8 demonstrate that these problems can be overcome by the model described in *Appendix B*, and that sufficient precision (deviations below 15 %) of specific biomass detection can be achieved.

5.5.2 Applicability of the model in Figure 5.5 for the estimation of cyanobacterial pigments

The comparison of chemically determined amounts of PC, Chl and PS II with the values obtained from fluorescence (Figures 5.3, 5.4 and 5.6 to 5.8) verifies that the model in Figure 5.5 is a suitable basis of the fluorometric analysis of cyanobacteria. This also implies that the assumption 1 (PC can be evaluated from the $F_{610,650}$ signal) and that the assumption 2 (amount of Chl per PS II and PS I is constant) hold under the investigated conditions. The variability of the cyanobacterial antennae (as provided by the conditions in Figures 5.3 and 5.4) does not corrupt the fluorometric analysis when this variability is restricted to the number of pigments. It must be analysed whether the reliability of fluorometric determination suffers if fluorometric properties and coupling ratios are changed.

Thus, the reliability of the analysis depends on whether the gross rate constants $k_{1,\lambda_{ML},\lambda_{em}}$ to $k_{5,\lambda_{ML},\lambda_{em}}$ from Equations (B7a) to (B7e) in *Appendix B* are constant or, if they are not constant, have only minor influence on the coefficients in Equations (B9a,b) and (A16). The only source of variability in $k_{1,\lambda_{ML},\lambda_{em}}$ to $k_{5,\lambda_{ML},\lambda_{em}}$ is in the fluorescence yields $\Phi_{F,PC}$, $\Phi_{F,PS II}$ and $\Phi_{F,PS I}$ and in the energy transfer yields $\Phi_{T,PS I}$ and $\Phi_{T,PS II}$. Several workers (Dau (1994b, a); Govindjee *et al.* (1996); Campbell *et al.* (1998); van Thor *et al.* (1998)) have shown that the fluorescence quantum yields $\Phi_{F,PC}$, $\Phi_{F,PS II}$, $\Phi_{F,PS I}$ are approximately constant under the

experimental conditions employed here, i.e., when the cyanobacteria are given enough time to adapt to the prevailing light intensities.

Experiments have not been done under conditions of iron-deficiency as the incentive to develop the approach described here originally came from limnological projects. Especially, in oceans, iron-deficiency may cause a strong reduction of PBS and the expression of the *isiA*-gene leads to increased deactivation in PS II (decreasing O₂ evolution and fluorescence yield, i.e. $\Phi_{F,PS II}$, Park *et al.* (1999); Sandstrom *et al.* (2001)) and to an increase of the effective antenna size of PS I by 60 % (Boekema *et al.* (2001)) to 100% (Andrizhiyevskaya *et al.* (2002)) thus changing $\Phi_{F,PS I}$. The change in the number of PBS can be handled by our approach as PBS determination requires only Equation (B8). In the case of PS I, at least Chl content associated to PS I may be estimated correctly. However, the underestimation of PS II is caused by *isiA*-induced high fluorescence quenching (Boekema *et al.* (2001); Andrizhiyevskaya *et al.* (2002)), remains to be investigated.

In the two scenarios defined in the Results section, $F_{610,685}$ is used. The main part of this fluorescence emission originates from light energy absorbed by PC, transferred to PS II ($\Phi_{T,PS II}$) and emitted as fluorescence. The range of the reported values of $\Phi_{T,PS II}$ is between 1 and 0.9 (Campbell *et al.* (1998); van Thor *et al.* (1998)). This maximum change of about 10% causes an even smaller change in the calibration coefficients $c_{2,PS I}$ and $c_{2,PS II}$ (Equation (B9)) as the related $k_{4,\lambda_{ML},\lambda_{em}}$ (Equation (B7d)) is part of a sum including other gross rate-constants. If an increase in $\Phi_{T,PS II}$ occurs concomitantly with a decrease in $\Phi_{T,PS I}$ (state transitions, Campbell *et al.* (1998); van Thor *et al.* (1998)), then the effect is even smaller (Equations (B10) and (B13)). In contrast, the reported range of $\Phi_{T,PS I}$ 0 to 0.1 (Campbell *et al.* (1998); van Thor *et al.* (1998)) seems to imply major changes. Fortunately, $\Phi_{T,PS I}$ does not play a major role in scenario 1 ($F_{470,685}$ and $F_{610,685}$), and thus its variability can be ignored.

Scenario 2 makes use of $F_{610,720}$ that is strongly influenced by light energy absorbed by PC and transferred to PS I. Figures 5.7 D and 5.8 D show that the resulting influence on $k_{4,\lambda_{ML},\lambda_{em}}$ (Equation (B7d)) corrupts the calibration factor $c_{2,PS I}$ in Equation (B9a) via Equation (B10). Thus, PS I determination should be based on the $F_{470,685}$ signal of scenario 1.

However, it should be mentioned that scenario 1 (using $F_{470,685}$ and $F_{610,685}$) yields more reliable results regarding PS II centres and total Chl concentration as compared to scenario 2 ($F_{610,720}$ and $F_{610,685}$).

Regardless of the above caveats application to a wide range of species under different conditions (Figures 5.3 and 5.4) has shown that the model-based evaluation of cyanobacterial pigments is quite reliable.

5.5.3 Variation of cyanobacterial pigments

For the separation of cyanobacteria pigment amount from that of other phytoplankton, the above biophysical problems of antennae organisation play a minor role, because Figures 5.11 to 5.13 show that the concept of parameter-dependent norm spectra (*Appendix B*) can handle all variations that have occurred in our investigations. Selecting 40 norm curves out of the two-dimensional field of the weighted sum of the two extreme curves $c_{hi\lambda_{em}}$ and

$c_{low\lambda_{em}}$ (Figures 5.9 A and B) reduces the parameters from two to one, providing the benefit that the fit-procedure has only one non-linear parameter l (Equation (C1)). Figures 5.9 C and D demonstrate the success of this strategy for the different excitation spectra shown in Figure 5.9 A and B.

The most important feature is that all 40 norm spectra $c_{l,\lambda_{em}}$ (Figure 5.9) are linear-independent from the norm spectra of the other phytoplankton. This has the consequence that an error in the determination of one group of phytoplankton cannot be compensated by errors in the other groups. The reliability is verified by the dilution experiments of Figures 5.11 A and B where the cyanobacterial norm spectra and the pigment concentrations of diverse algal groups were correctly estimated. This parametric description (Equation (5.1)) is the key to overcome the fit problems originating from the great variability of the fluorescence excitation spectra.

The application of the non-linear fit procedure to selected samples includes some important situations. Figures 5.12 A and B show that a correct assessment of pigments during aging of a batch culture was achieved. This is a situation which might occur during a natural phytoplankton bloom. It demonstrates that scenario 1 and the fit procedure also hold for degrading pigment systems. Changing light illumination over a time scale of minutes can induce photoinhibition and energy state transitions (PBS coupling). We found that the highest deviation for pigment estimation caused by state transitions and photoinhibition together was less than 10 % (Figure 5.13). The small variation of $F_{610,650}$ is not surprising as the fluorescence emission originates from PC and not from regions of the PBS where the change in energy transfer and photoinhibition takes place.

The employment of only two detection wavelengths (650 nm, Equation (B8) and 685 nm, scenario 1) as implied by the usage of scenario 1 enables the construction of a simpler instrument. The use of only three adequate signals out of 28 in scenario 1 or 2 is important for on-line analysis as it saves computer time. The employment of only two detection wavelengths as implied by the use of scenario 1 saves computation time in the fit procedure. This property is also important for on-line analysis.

The approach of *Appendix B* and scenario 1 can also solve the problem of the estimation of true photochemical yield in cyanobacteria (van Thor *et al.* (1998)) as caused by the interference with the PC fluorescence emission. Basing the calculation of the relative contributions of PS II fluorescence on the parametric fit procedure provides a better estimation of the photochemical yield of cyanobacterial PS II. The estimation of photochemical yield does not even suffer from inconstant parameters $k_{1,\lambda_{ML},\lambda_{em}}$ to $k_{5,\lambda_{ML},\lambda_{em}}$ from Equations (B7a to e) in *Appendix B* discussed above because the relationship between fluxes and relative changes in fluorescence is not influenced by changes in $\Phi_{F,PC}$, $\Phi_{F,PS II}$, $\Phi_{F,PS I}$, $\Phi_{T,PS I}$ or $\Phi_{T,PS II}$.

The principle of parameter-dependent norm spectra can be transferred to other algal groups like red cyanobacteria ($\lambda_{em} = 570 - 580$ nm) or cryptophytes (see *Chapter 6*). This can be achieved by an extension of the set-up in Figure 5.2 with further detection wavelengths between 590 nm and 630 nm for the measurement of other phycobilin emissions such as PE of red cyanobacteria ($\lambda_{em} = 570 - 580$ nm) or cryptophytes ($\lambda_{em} = 590 - 620$ nm) (MacColl &

Guard-Friar (1987)). Such an extension would solve adaptation problems that might occur in red cyanobacteria and would enable the differentiation between cryptophytes and red cyanobacteria.

Chapter 6. An algorithm and practical fluorescence models from red cyanobacteria and cryptophyta designed for the *in situ* detection of phytoplankton

6.1 Summary

In fluorometric phytoplankton analysis the detection of red cyanobacteria is hindered by adaptation processes of the cyanobacterial photosynthetic apparatus and spectral interferences with cryptophyta. In order to overcome these problems a simplified energy distribution model accounting for energy pathways in the red cyanobacterial photosynthetic apparatus and the apparatus of cryptophyta was designed. Mathematical equations were derived that enabled the calculation of the pigment content in both organisms at the same time: cryptophyta and red cyanobacteria. This resulted in a new fluorometer for phytoplankton with seven excitation wavelengths and at four detection channels (600 nm, 620 nm, 650 nm and 685 nm) *in vivo*. An extension of the fit procedure of *Chapter 5* and *Appendix C* allowed corrections for variations in the fluorescence excitation spectra of red cyanobacteria and cryptophyta in the presence of other phytoplankton signals. The new approach provided correct fluorometric pigment estimation in the presence of energy state transitions. The combination of fluorescence emission excitation matrices, the fluorescence models and the fit-enhanced algorithm will provide better information for phytoplankton analysis.

6.2 Introduction

In pelagic systems Chl maxima of red cyanobacteria are often found at depth: in the so-called deep chlorophyll maxima (DCMs). In these DCMs red cyanobacteria containing PE are very abundant due to their ability to survive in this chromatic niche (e.g. van den Hoek *et al.* (1995), Lampert & Sommer (1997)). They are important primary producers and they can cause toxic blooms which may be fatal in reservoir drinking water (Leboulanger *et al.* (2002)). Due to the fact that DCMs are not usually visible at the surface, their occurrence is often overlooked. Optical probe technology (spectral fluorescence analysis) can aid detection and quantification of these red cyanobacteria DCMs because they enable easy depth profiling (*Chapter 2* and Leboulanger *et al.* (2002)). Adaptation processes in the photosynthetic apparatus of phytoplankton due to environmental changes can affect fluorometric analysis (*Chapter 6*). In addition, the cryptophyta are common companions of the cyanobacteria (Becker *et al.* (2002)) which also can contain PE. This can lead to mistakes in the identification of red cyanobacteria. To solve these problems it is imperative to obtain a quantitative description of the optical and energy transfer processes in cyanobacteria and cryptophyta.

In cyanobacterial species containing PE, the PBSs consist of the PBs, PE, PC and in the core regions of PBS APC. Linker polypeptides are present in the PBSs (they are non-pigmented, with the exception of the large core linker L_{CM}).

Energy transfer processes in PBSs containing PE are analogous to those in PBSs containing no PE (see *Chapter 5* and *Appendix B*) and the main energy transfer process from PE via PC to APC is downhill Förster-transfer. PE from cyanobacteria emits at a maximum emission wavelength between 580 nm and 600 nm *in vivo* in addition to the PC, APC, PS II and PS I (*Chapter 5*). Cryptophyta use PBs as a light harvesting antenna in addition to a Chl c_2 Chl a antenna. Seven different phycobilins are known (Lichtle *et al.* (1992); McKay *et al.* (1992)). The phycobilins and the Chl c_2 Chl a antenna are associated with PS II (McKay *et al.* (1992)). This also implies that most Chl is associated with PS II. Ecologically important freshwater species like some *Rhodomonas spec.* and *Cryptomonas ovata* contain PE₅₆₆ with an absorption maximum of 566 nm and a fluorescence emission maximum of 617 nm (MacColl & Guard-Friar (1987); Rowan (1989); Becker *et al.* (2002)). Much less is known about the energy transfer in cryptophyta than in cyanobacteria but it can be assumed that energy is transferred down-hill from PE to the Chl antennae (Maccoll & Berns (1978); Lichtle *et al.* (1980); Harnischfeger & Herold (1981)) under moderate illumination.

Red cyanobacteria and cryptophyta possess the ability to adapt their photosynthetic apparatus to environmental conditions similar to blue cyanobacteria. The adaptation in red cyanobacteria (Demarsac & Houmard (1993); Müller *et al.* (1993); Reuter & Müller (1993); Bryant (1995)) as a result of shifts in light or nutrient conditions is mediated by changes in the PE and PC content in the PBS and in PS I to PS II ratio this analogue to blue cyanobacteria as given in *Chapter 5*. In cryptophyta, the size of the PE and Chl c_2 Chl a antennae relative to PS

II can change due to light or nutrient shifts (Sciandra *et al.* (2000)). Similar to blue cyanobacteria, short term 'energy state transitions' are known in red cyanobacteria and cryptophyta (see *Chapter 5* and Harnischfeger & Herold (1981); Williams & Allen (1987); Biggins & Bruce (1989); Campbell *et al.* (1998); van Thor *et al.* (1998)).

This variability of the cryptophyta and red cyanobacterial photosynthetic apparatus can cause problems in phytoplankton detection and discrimination based on fluorescence (*Chapter 2*).

For blue cyanobacteria, these problems were overcome by the approach described in *Chapter 5*. In spite of the variations in the ratio of the pigment PC to Chl *a* as caused by adaptation to varying environmental conditions, it became possible to determine PC, Chl *a* and PS II centre concentrations by the measurement of fluorescence excitation spectra with just two emission channels (650 nm and 685 nm). This was achieved by the development of a new fit procedure based on a simplified energy distribution model of the cyanobacterial photosynthetic apparatus.

Here, the problem of spectral fluorometric analysis in red cyanobacteria is approached. Special consideration of cryptophyta containing PE₅₆₆ was achieved by developing simple fluorescence models for both organisms by means of a new fluorometer with four emission channels (600 nm, 620 nm, 650 nm and 685 nm). This required the extension of the fit procedure of *Chapter 5* and *Appendix C*.

6.3 Materials and methods

6.3.1 Growth experiments

Different growth conditions similar to those in *Chapter 5* were employed in order to provide a great variety of fluorescence phenotypes for testing the models developed in *Appendix D* and *E*. In all growth experiments, the cyanobacterium *Synechococcus rubescens* and the cryptophyta *Cryptomonas ovata* were grown in 0.7 litre WC growth media (Guillard & Lorenzen (1972)) at a temperature of 18 °C. The cultures were bubbled with air. The growth light intensity in the empty vessels was 20 $\mu\text{E m}^{-2}\text{s}^{-1}$ unless otherwise stated. For *Cryptomonas ovata* all parameters were kept constant apart from the growth light intensities.

After an initial growth period of fourteen days, experiments were carried out. The Chl content was determined by HPLC-analyses, and the PE, PC content was determined spectrophotometrically. The number of active PS II-centres was measured by evaluating oxygen evolution under flash-light illumination (see *Chapter 5*) in cultures of red cyanobacteria. Dilute phytoplankton samples were measured in the multi-channel fluorometer (Figure 6.1, below).

Light intensity. Growth of cyanobacteria under eight different light intensities was achieved by covering culture vessels by different grey filter combinations (LEE Standard 209, 210, 211, 298, LEE filters, Great Britain) placed in front of a light tube (L 58W/11-860, Lumilux-Daylight, Osram, Germany). Intensity was measured with the PhAR sensor Hansatech QRT 1 (Hansatech, U.K.) in the covered glass vessels). In the experiments, the following light intensities were used: 3, 6, 9, 13, 18, 25, 35 and 50 $\mu\text{E m}^{-2}\text{s}^{-1}$. The nutrient solution was WC-medium (Guillard & Lorenzen (1972)).

The effect of different nitrate, phosphate and total nutrient concentrations on fluorescence was evaluated in the following three experiments.

Growth under different sodium nitrate concentrations. *Synechococcus rubescens* was cultivated in WC-medium (Guillard & Lorenzen (1972)). The (sodium) nitrate concentrations were adjusted to 0.1, 0.58, 2.9, 5.9, 8.8, 12, 17.6 or 24 mmol l^{-1} by addition of different concentrations of sodium nitrate.

Growth under different di-potassium hydrogen phosphate concentrations. *Synechococcus rubescens* was grown in WC-medium with the original phosphate component replaced by 0.0087, 0.02, 0.05, 0.1, 0.25, 0.5, 1 and 2 mmol l^{-1} K_2HPO_4 .

Different cyanobacterial and cryptophyta species. *Lyngbya maior*, *Planktothrix rubescens*, *Oscillatoria redekii*, *Planktothrix redekii*, *Synechococcus rubescens* (all cyanobacteria) and *Cryptomonas* (3 different species) were obtained from SAG collection in Göttingen, Germany.

Effect of total nutrient concentration on fluorescence. Variation of total nutrient concentrations was achieved by growing algae in mixtures of WC (Guillard & Lorenzen (1972)) and BG11 medium (Rippka & Herdman (1992)). The relative amounts of BG11

medium (Rippka & Herdman (1992)) in the eight vessels were 0, 12.5, 25, 50, 62.5, 75, 87.5 and 100 %.

Aging cultures. To investigate the effect of the age of the batch cultures on pigment composition and fluorescence *Synechococcus rubescens* were grown in a 10-l flask. After a week of initial growth, fluorescence measurements were carried out.

6.3.2 Fluorescence measurements

Figure 6.1 shows the set-up for the determination of norm spectra, for laboratory and *in vivo* experiments. Basically, the set-up is similar to the bench-top fluorometer described in *Chapter 5* supplemented by a fourth detection channel. The measuring times and evaluation procedures were also identical to those of *Chapter 5*. The set-up in Figure 6.1 enabled the measurement of F_o , F_m , F and F_v according to the definition of van Kooten & Snel (1990) at seven fluorescence excitation wavelengths (370 nm, 430 nm, 470 nm, 525 nm, 570 nm, 590 nm, 610 nm). LED light was passed through the same optics as described in *Chapter 5*. The peak detection wavelengths of the four detector channels were defined by band pass filter combinations with the following peak wavelength/halfwidth: (listed from detector to sample):

600 nm/ 10 nm: Calflex x, Balzers, Liechtenstein + band pass IF, 600nm/ 10 Dr. Anders GmbH, Germany, GFH 681, Göttinger Farbfilter, Germany + OG 590, long pass dye filter, Schott Glas, Germany + band pass IF 600nm/ 10nm, Dr. Anders GmbH

620 nm/ 10 nm: Calflex x, + band pass IF, 620nm/10 Dr. Anders GmbH + long pass GFH 681, Göttinger Farbfilter, + OG 590, long pass, dye filter, Schott Glas + IF 620nm/10nm, Dr. Anders GmbH,

650 nm/ 10 nm: see *Chapter 5* for details

685 nm/ 10 nm: see *Chapter 5* for details

Four laser diodes (Hitachi HL6501MG, 658 nm) with a diffuser in order to prevent sprinkles were placed opposite the LEDs. They provided an additional actinic light of $3000 \mu\text{Em}^{-2}\text{s}^{-1}$ over an area of 227 mm^2 in the cuvette. They were also used for the detection of state transitions. The light intensity of the laser diodes was voltage controlled. In that case the samples were illuminated 15 minutes prior to the measurement.

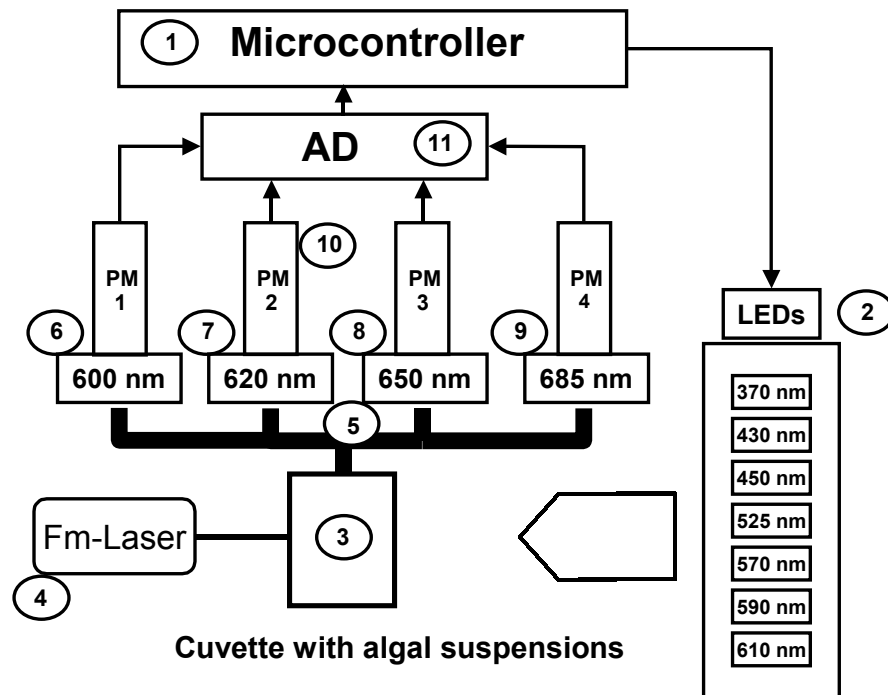


Figure 6.1. Fluorometer set-up: microcontroller, (2) Seven LEDs (measuring-light), (3) Sample cuvette containing algal suspension, (4) Diode laser (Fm-light), (5) Multi-leg fibre bundle, (6) Band-pass filter (600 nm), (7) Band-pass filter (620 nm), (8) Band-pass filter (650 nm), (9) Band-pass filter (685 nm), (10) Four photomultipliers (PM1-4), (11) 12-bit AD-converter (conversion rate of 500 kHz).

6.3.3 Pigment determination

Determination of Chl concentrations. Concentrations of Chl *a* and Chl *c*₂ (required for calibrating the fluorometer, see norm spectra) were determined according to Wiltshire *et al.* (1998) using HPLC.

Phycobilin determination. The amount of phycobilins in algal suspensions was determined in a wet chemical spectrophotometric analysis as described in *Chapter 5*. The equations for the determination of PC and PE are given in Bennett & Bogorad (1973). These equations hold for PE₅₆₆ of cryptophyta as well. The concentration of cryptophyta PE₅₆₆ is given in red cyanobacterial PE equivalents.

6.4 Results

6.4.1 Red cyanobacteria grown with different pigmentation

Synechococcus rubescens was subject to various growth conditions (see above) in order to obtain an estimate of the range of variations in pigmentation and to obtain cyanobacteria with different excitation spectra for the test of the model given in *Appendix D*. The influence of light intensity during growth is shown in Figure 6.2 A PE/Chl *a* ratio increased with light intensity while PS II/Chl *a* ratio and PE/PC ratio decreased with higher light intensities. A variable ratio of PS II/Chl *a* indicate a changed ratio of PS II to PS I. Sodium nitrate (Figure 6.2B) had little influence over a wide range of starting concentrations. Above 10 mM, PE/PC and the PS II/Chl *a* ratio increased strongly. Di-potassium hydrogen phosphate (Figure 6.2C) led to a maximum in PE/Chl ratio at starting concentrations of around 6 mmol l⁻¹. PE/PC ratio and PS II/Chl *a* ratio obtained maximum values at lower concentrations and showed a moderate decrease at higher concentrations. The effect of total nutrient concentration in the starting medium is depicted in Figure 6.2 D.

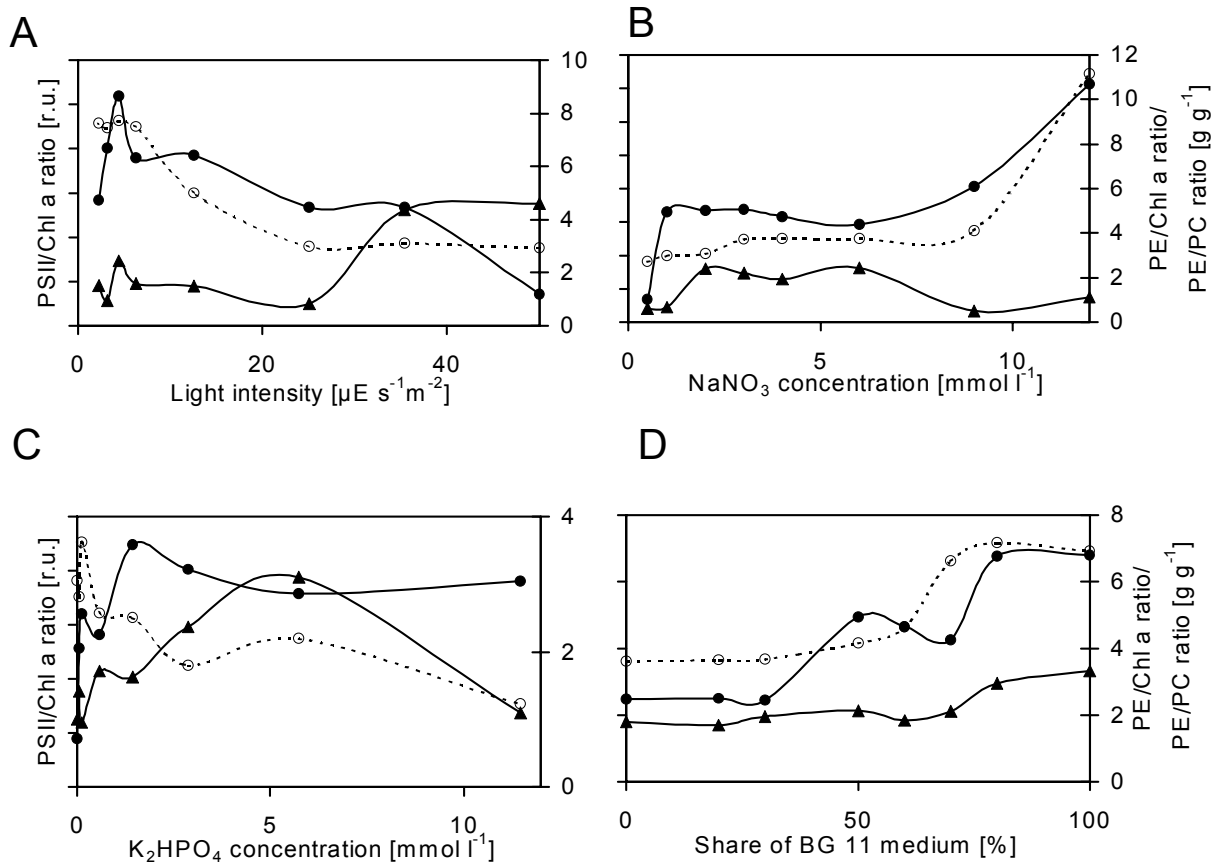


Figure 6.2. Change of the pigment ratios and number of PS II reaction centres under variation of growth conditions in *Synechococcus rubescens* as caused by variation of A) growth light intensities; B) NaNO₃ concentration; C) K₂HPO₄ concentration; D) share of BG11 medium in culture. (filled triangles with solid line: ratio of PE to Chl *a*; filled circles with solid line: ratio of number PS II centres to Chl *a* concentration; open circles with dashed line: ratio of PE to PC). Chl was determined by HPLC, PE, PC by chemical analysis and PS II centres by oxygen flash yield measurement.

All three pigment ratios go up with higher total nutrient concentrations. In the growth experiments shown in Figure 6.2, the PE/PC and PS II/Chl *a* ratios were closely correlated. Species dependence of pigment ratios of PE, PC PS II and Chl under the same growth conditions is shown for five cyanobacterial species in Figure 6.3. Due to very low pigment concentrations in four cultures it was not possible to determine the number of PS II reaction centres with sufficient accuracy.

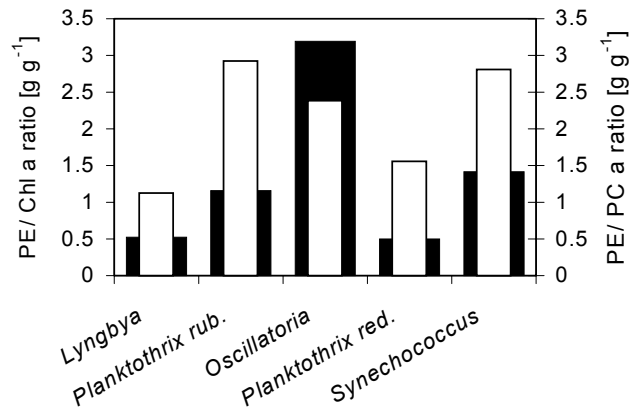


Figure 6.3. Pigment ratios of five different cyanobacterial species (open bars: PE/PC; filled bars PE centres/Chl *a* concentration). *Lyngbya*: *Lyngbya maior*, *Planktothrix rub.*: *Planktothrix rubescens*, *Oscillatoria*: *Oscillatoria redekii*, *Planktothrix red.*: *Planktothrix redekii*, *Synechococcus*: *Synechococcus rubescens*. Chl was determined by HPLC, PE, PC by chemical analysis and PS II centres by oxygen flash yield measurement.

The variations of the pigment ratios shown in Figures 6.2 and 6.3 were in the following ranges: ratio of PE/Chl between 0.7 g g⁻¹ and 6 g g⁻¹, PE/PC ratio between 1 and 11 g g⁻¹, and PS II/Chl changed four fold in Figure 6.2.

6.4.2 Growth of cryptophyta under different light intensities and growth of different species

In order to test the fluorescence model given in *Appendix E* for cryptophyta and to evaluate the variability of their fluorescence spectra, cryptophyta were grown under different light intensities (Figure 6.4). Due to the simpler nature of the model for cryptophyta (*Appendix E*) than for red cyanobacteria (*Appendix D*) a smaller number of cultures was necessary. Furthermore, testing the model did not require the determination of PS II reaction centre concentrations. It was not possible to grow the organisms at light intensities higher than 50 μE m² s⁻¹ as those cultures did not grow. Figure 6.4 shows that the Chl *c*₂/Chl *a* ratio obtains a low plateau between 6.3 μE m² s⁻¹ and 25 μE m² s⁻¹, and the ratio of PE/Chl *a* decreased strongly after a peak at 6.3 μE m² s⁻¹.

Species dependence of PE/Chl *a* ratios and Chl *c*₂/Chl *a* ratios is shown for three different PE-containing cryptophyta grown under the same conditions as in Figure 6.3. In Figures 6.4 and 6.5, the PE/Chl *a* ratio varied from 0.25 gg⁻¹ to 1.5 gg⁻¹ and the ratio of Chl *c*₂/Chl *a* changed between 0.4 gg⁻¹ and 1.2 gg⁻¹. The different types of pigmentation provided by the growth conditions described in this section were used in the following investigations.

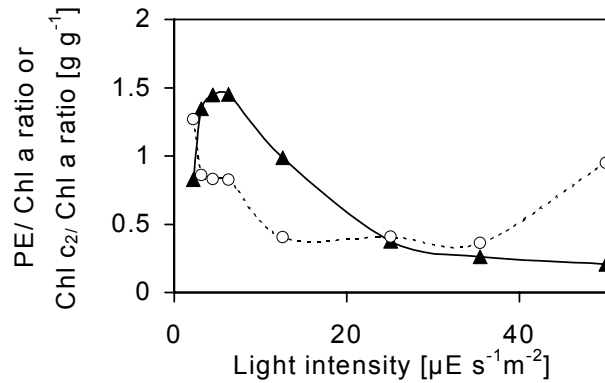


Figure 6.4. Change of the PE Chl *a* ratio (filled triangles, solid line) and the Chl c_2 / Chl *a* ratio (open circles, dashed line) in cryptophyta under variation of growth light intensities. Chl was determined by HPLC; PE, PC by chemical analysis and PS II centres by oxygen flash yield measurement.

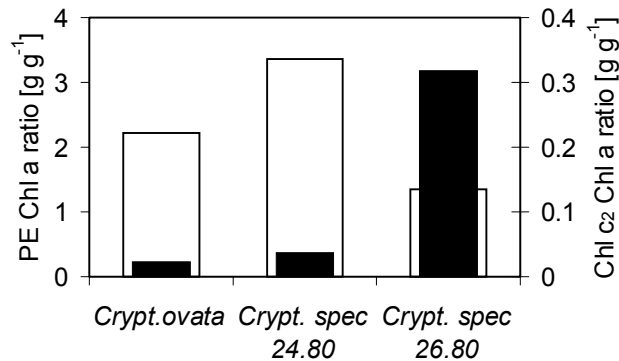


Figure 6.5. PE/Chl *a* ratios and the Chl c_2 /Chl *a* ratio of three different cryptophyta (open bars: PE/PC; filled bars PE centres/ Chl *a* concentration) Chl was determined by HPLC, PE, PC by chemical analysis and PS II centres by oxygen flash yield measurement.

6.4.3 Simplified models of energy transfer in the antennae of red cyanobacteria and cryptophyta

Figures 6.6 and 6.7 show the pigments of the photosynthetic apparatus of cyanobacteria and cryptophyta and the flow of energy between them. The mathematical description of these models is presented in *Appendix D* for red cyanobacteria and in *Appendix E* for cryptophyta.

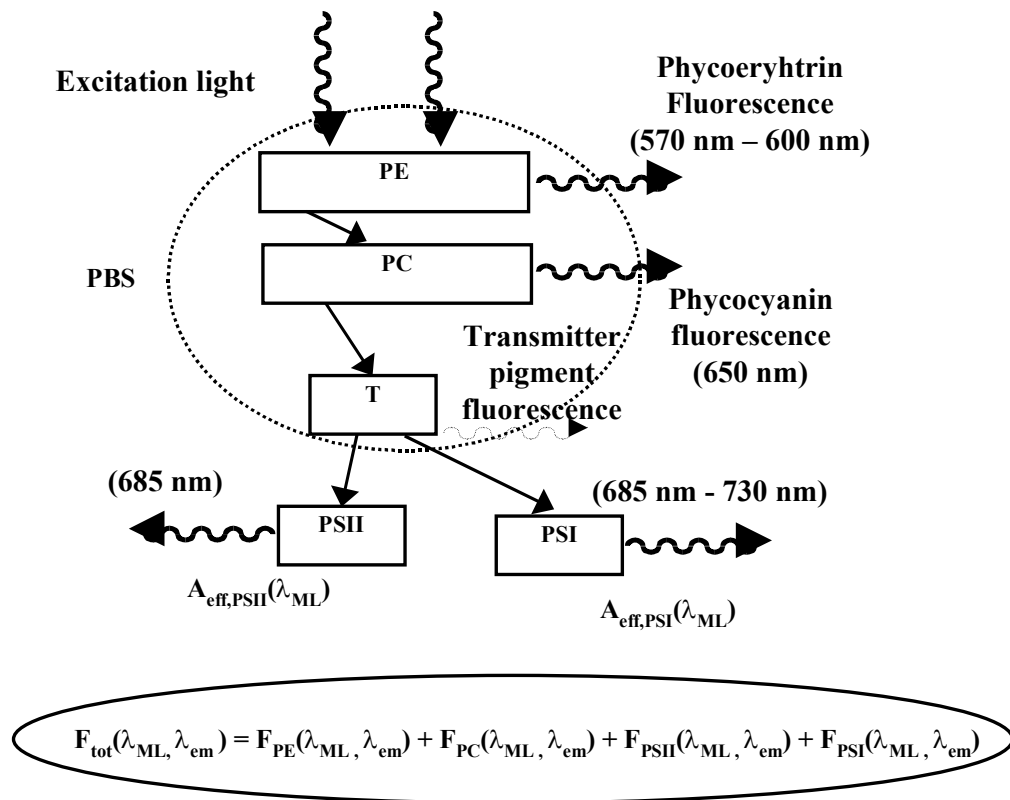


Figure 6.6. Simplified model of absorption and fluorescence emission processes in PBSs and PSs in cyanobacteria (PE-containing organisms like *Synechococcus rubescens*): $A_{\text{eff,PSII}}(\lambda_{\text{ML}})$, $A_{\text{eff,PSI}}(\lambda_{\text{ML}})$; effective absorption cross-section (in m^2) of PS II and PS I, $A_{\text{PE}}(\lambda_{\text{ML}})$, $A_{\text{PC}}(\lambda_{\text{ML}})$: PE and PC absorption cross-section (in m^2); $F_{\text{PE}}(\lambda_{\text{ML}}, \lambda_{\text{em}})$, $F_{\text{PC}}(\lambda_{\text{ML}}, \lambda_{\text{em}})$, $F_{\text{PSII}}(\lambda_{\text{ML}}, \lambda_{\text{em}})$, $F_{\text{PSI}}(\lambda_{\text{ML}}, \lambda_{\text{em}})$: total PE, PC, PS II and PS I fluorescence intensity; λ_{ML} : wavelength of measuring light; λ_{em} : fluorescence emission wavelength. The core proteins of PBS (e.g. APC) are classified as ‘transmitter pigments’ analogous to *Chapter 5*. The absorption and fluorescence properties of the ‘transmitter pigments’ (T) were neglected in the latter consideration and reduced to the function of energy transmitters. Fluorescence model adapted and simplified from Zhou *et al.* (1992).

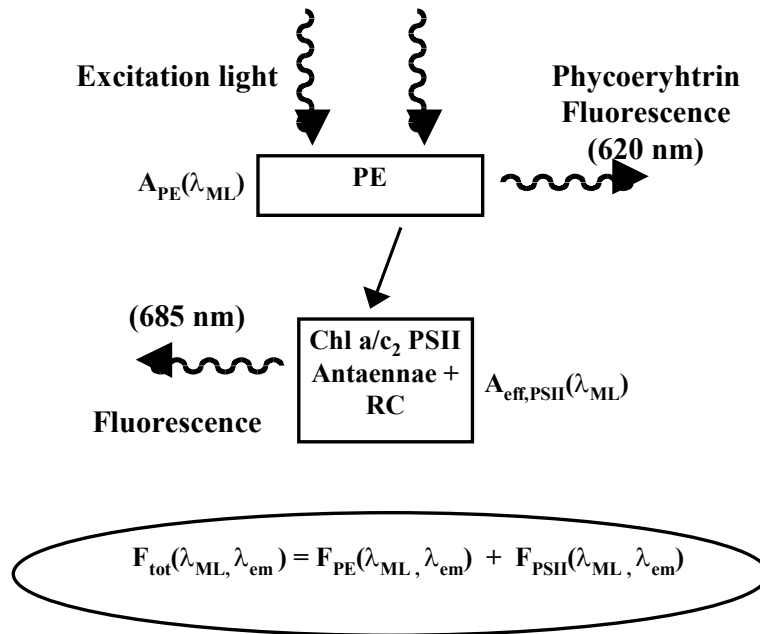


Figure 6.7. Simplified model of absorption and fluorescence emission processes in PSs of cryptophyta containing PE (like *Cryptomonas ovata*) PBSs : $A_{\text{eff, PS II}}(\lambda_{\text{ML}})$, effective absorption cross-section (in m^2) of PS II, $A_{\text{PE}}(\lambda_{\text{ML}})$ PE absorption cross-section (in m^2); $F_{\text{PE}}(\lambda_{\text{ML}}, \lambda_{\text{em}})$, $F_{\text{PS II}}(\lambda_{\text{ML}}, \lambda_{\text{em}})$: total PE, PS II fluorescence intensity; λ_{ML} : wavelength of measuring light; λ_{em} : fluorescence emission wavelength. PS I fluorescence between 600 nm and 685 nm emission is assumed to be neglected (for details see Holzwarth (1991); van Grondelle *et al.* (1994)).

6.4.4 Validation of fluorescence model of the red cyanobacterial apparatus

In order to test fluorescence model for the red cyanobacterial apparatus and the parametrical description of *Appendix D* comparison of the concentrations of PE, PC and Chl and PS II centres of red cyanobacteria calculated from fluorescence data with those obtained from HPLC analysis and chemical analysis were made. The values at the x-axis of Figure 6.8 (concentrations of PE, PC, Chl and PS II centre red cyanobacteria) were determined by HPLC and chemical analysis (“ref.” in Figure 6.8) those at the y-axis by fluorometric analysis on the basis of the fluorescence model in *Appendix D* (PE by Equation (D8), PC by Equation (D10), PS II reaction centre by Equation (D12a), and Chl-estimates by Equation (D24). Linear regression of the data obtained from the pigmentation types of Figure 6.2 A- D and Figure 6.3 at three different concentration levels resulted in a ratio very close to one with a high correlation coefficient. The mean standard error for pigment estimation in Figure 6.8 was 12 % for PE, 15 % for PC, 10 % for Chl and 18 % for PS II. These are in the range of the errors of the reference estimates. Calculations were made under the simplifying assumption that c_{chl} is equal to zero. This only decreased the precision by 1% and enabled use of a simpler and

faster fit in *Appendix F*. This also demonstrates the validity of the three assumptions in *Appendix D* by means of Equations (D8), (D10), (D12a) and (D24).

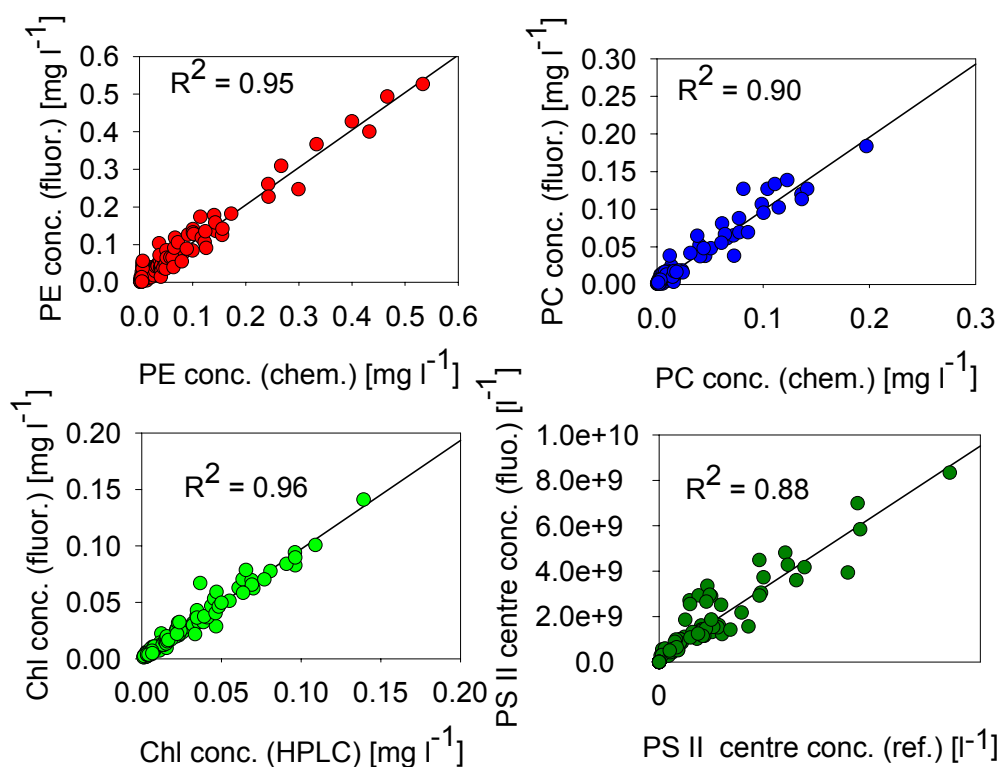


Figure 6.8. Linear regressions of the calculated PE, PC and Chl and PS II centre concentrations of red cyanobacteria from Equations (D8), (D10), (D12a) and (D24) on the reference estimates shown in Figures 6.3 and 6.4 (except D, D uses references estimates of Figure 6.3 only): A) PE B) PC C) Chl *a* and D) PS II reaction centres.

6.4.5 Comparison of the calculated and measured phycoerythrin, chlorophyll and photosystem II centre concentrations in cryptophyta

Analogous to red cyanobacteria (Figure 6.8) the model for cryptophyta given in *Appendix E* was verified by calculating linear regressions for fluorometrically determined PE- (with Equation (E13)), and Chl-estimates (with Equation (E14)) versus chemically determined concentrations of the samples in Figures 6.5 and 6.6. Figure 6.9 shows that the estimation of pigments by fluorescence coincided with the reference estimates. The standard error was determined to be 12 % for PE- and 11 % for Chl-estimation.

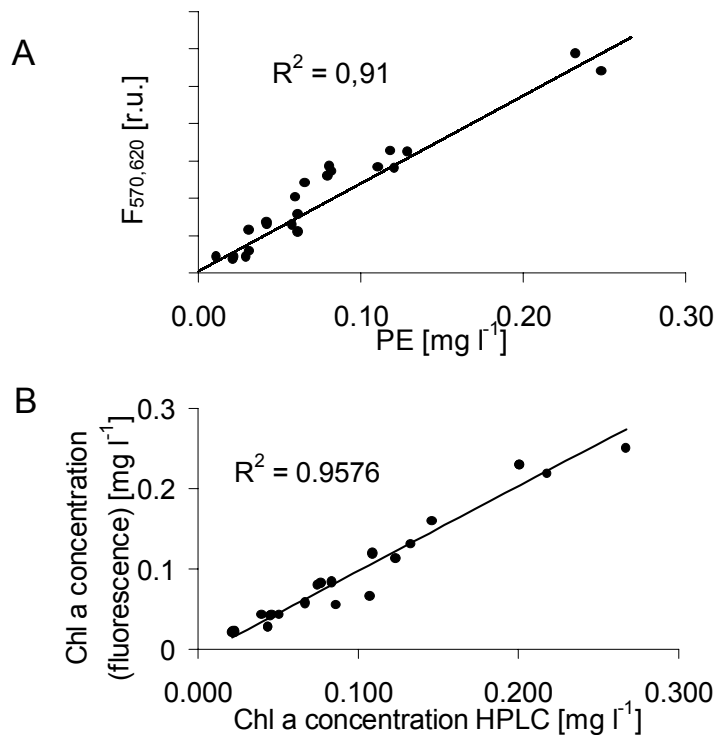


Figure 6.9. Linear regressions of the calculated PE and Chl *a* concentrations in cryptophyta from Equations (E13) and (E14) on the reference estimates shown in Figures 6.5 and 6.6: A) PE B) Chl *a* new fit procedure was developed in *Appendix F* in order to provide a means of determining the concentrations of groups by means of the new emission channels 600 nm and 620 nm. The mathematical fit is an extension of that given in *Chapter 5* and *Appendix C*.

The norm spectra and the fit procedure had to fulfil all requirements as requested in the fit procedure described in *Chapter 5* and *Appendix C*, i.e., constancy of the norm spectra or, if not constant, the variances induced by environmental conditions could be described by a single parameter. The new approach in *Appendix F* demanded the extension of these requirements to the norm spectra at the four emission wavelengths 600 nm, 620 nm, 650 nm and 685 nm. The mean excitation spectra of the algae with pigmentation of Figures 6.2 – 6.5 are shown in Figure 6.10. The spectra were normalised to excitation with 570 nm. The highest standard deviation (10%) of the mean spectra had the spectra of cryptophyta with an emission wavelength of 685 nm at excitation with 470 nm light. This is sufficiently small enough for the algal estimation.

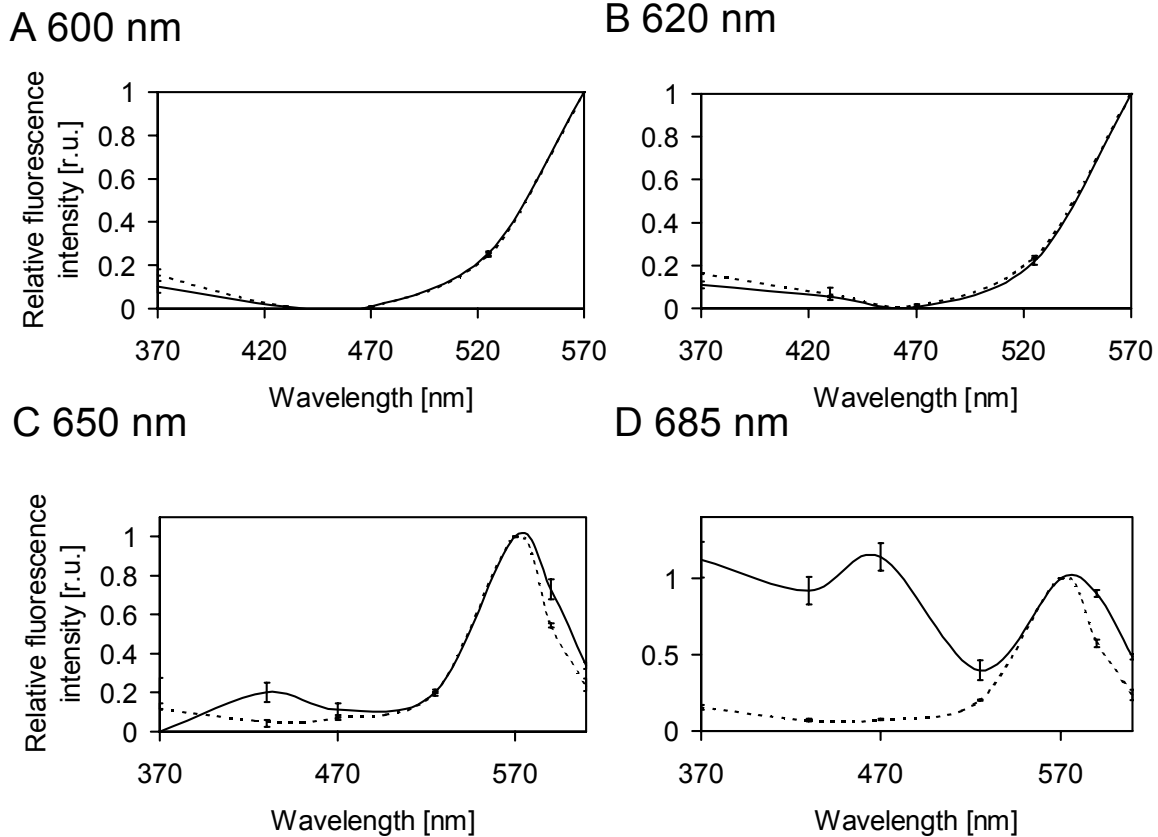


Figure 6.10. Fluorescence excitation spectra of red cyanobacteria (dashed line) and cryptophyta (solid line) obtained with the fluorometer set-up of Figure 6.1 normalised to fluorescence intensity at 570 nm excitation. The spectra represent the mean spectra of the organism with the pigment ratios shown Figures 6.2–6.5. A) spectrum at 600 nm detection wavelength, B) spectrum at 620 nm detection wavelength, C) spectrum at 650 nm detection wavelength, D) spectrum at 685 nm detection wavelength. Error bars represent the standard deviation of the mean. Lines are interpolated manually between the data points.

Another property of the mathematical fit procedure was that it used fixed fluorescence emission spectra at emission wavelengths of 600 nm and 620 nm for cryptophyta and red cyanobacteria (see $N_{600nm,620nm}(\lambda_{ex}, g)$ in *Appendix F*). The emission spectra are shown in Figure 6.11. They are the mean of the spectra obtained from the pigmentation types depicted in Figures 6.2 to 6.5. The spectra were normalised to the fluorescence intensity emission at 600 nm. The different treatments (Figures 6.2 - 6.5) resulted in a standard deviation of the mean spectra at emission with 620 nm less than 3 % (as indicated by the error bars in Figure 6.11). This implies that invariable emission spectra can be assumed at emission wavelengths of 600 nm and 620 nm. At emission wavelength of 685 nm, the highest standard deviations (ca. 25 %) were found at 685 nm for both groups of algae. This variation can be handled by the fit procedure in *Appendix F*.

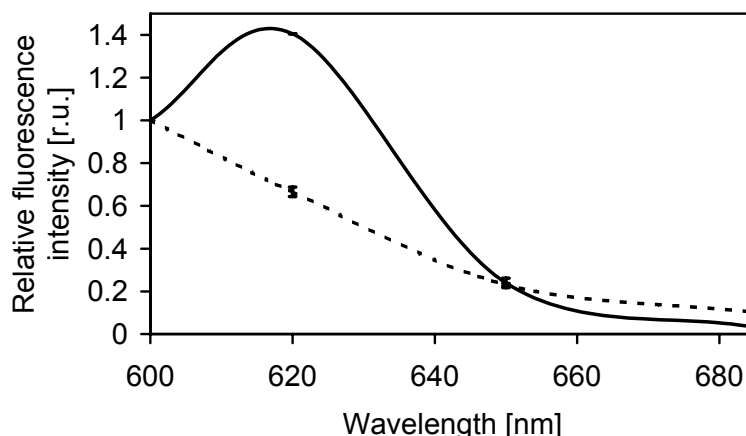


Figure 6.11. Fluorescence emission spectra of red cyanobacteria and cryptophyta obtained with the fluorometer set-up of Figure 6.1 at an excitation wavelength of 570 nm normalised to 1 at 600 nm emission. The spectra represent the mean spectra of the organism with the pigment ratios shown Figures 6.3 – 6.5. Red cyanobacteria: Dashed line, cryptophyta: Solid line. Error bars represent the standard deviation of the mean resulting from different treatments.

6.4.6 Identification in the presence of other phytoplankton

By the use of the fit procedure given in *Appendix F* and the equations of the models in *Appendices A* and *B* it was possible to determine the amount of red cyanobacterial PE, PC and Chl in the presence of other phytoplankton. In a dilution experiment, the contribution of the red algal group (*Synechococcus rubescens*) was changed while other phytoplankton remained constant abundant. Algal suspensions with constant Chl contents of the green spectral group (*Chlorella vulgaris*), blue spectral group (*Synechococcus leopoliensis*), brown spectral group (*Cyclotella* sp.), mixed spectral group (*Cryptomonas* sp.) and a varying PE, PC and Chl content of the red group were used. The Chl *a* concentrations of the spectral algal groups were kept constant as follows: green $15 \mu\text{g l}^{-1}$, blue $8 \mu\text{g l}^{-1}$, brown $10 \mu\text{g l}^{-1}$ and mixed $4 \mu\text{g l}^{-1}$.

Figure 6.12 A shows that a linear increase of cyanobacterial Chl *a* concentration was found correctly even in the presence of higher Chl *a* concentrations of other phytoplankton. The same was found for the cyanobacterial concentrations of phycobilins (Figure 6.12 B). The lowest total resolution of the system in terms total Chl *a* concentration was $0.5 \mu\text{g l}^{-1}$ (with a standard deviation of 10 % in 10 measurements; data not shown).

With higher concentrations of the red group the estimation of the groups with smaller Chl (Figure 6.12 A) and phycobilins content was slightly influenced (drop at the right-hand side of the horizontal lines in Figure 6.12)

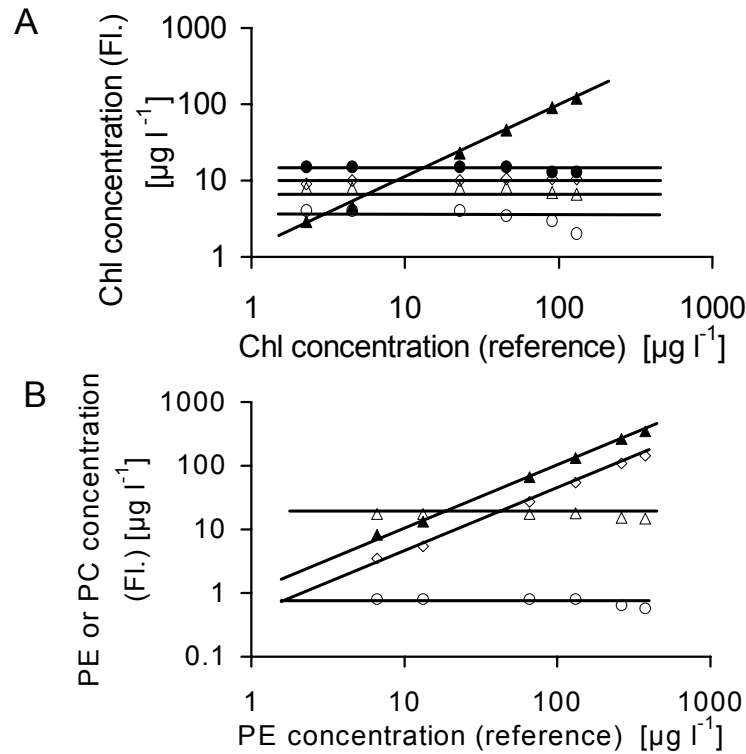


Figure 6.12. Variation of contribution of red algal group in the presence of other phytoplankton. A) The fluorometrical estimate of the Chl (green: closed circles, blue: open triangles, brown: open diamonds, mixed: open circles, red: closed triangles) content is shown versus the Chl content measured with reference (HPLC) B) The fluorometrical estimate of the PE and PC concentration red, blue, mixed group is shown versus the spectrochemically determined PE content of the red group. Red-PE: closed triangles; red-PC: open diamonds; blue-PC: open triangles; Cr-PE: open-circles

6.4.7 Aging of red cyanobacterial cultures

Cyanobacteria in batch culture grow exponentially at the beginning of the culture period. This is comparable to the situation of a cyanobacterial bloom *in situ*. In the later stages of the growth period, they show a decrease in total Chl due to nutrient limitation. The resulting changes in pigment concentrations were used for testing the fit procedure given in *Appendix F* and the validity of the equations of the model in *Appendix D*. Spectra of the samples from the aging batch culture were determined in the fluorometer. In Figure 6.13 A, the evaluated PE and PC concentrations are shown. The pigment concentrations reached a maximum after 30 days of growth. The overall estimation of PE and PC was in good agreement with the reference results. The measurement of PE had a smaller error than the estimation of PC (Figure 6.13 A). Figure 6.13 B depicts the measured Chl and PS II reaction centre concentration during the aging experiment. The decline of Chl and PS II reaction centre concentration was slower than the decline of the phycobilins. Again the overall estimations by fluorescence were highly correlated to the reference estimates. The determination of Chl and PS II centres showed an underestimation in the beginning and an overestimation in the end of the growth period (Figure 6.13 B).

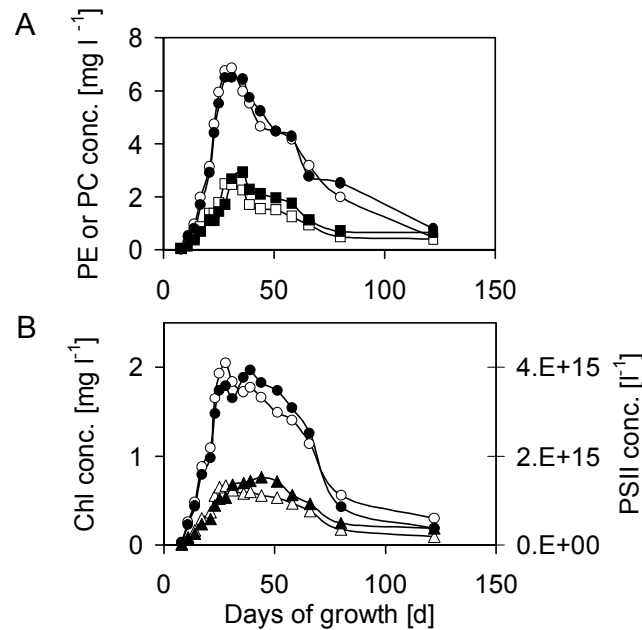


Figure 6.13. Pigment concentrations measured at different ages (in days) of a red cyanobacterial batch culture. A) PE and PC concentrations: open circles - fluorometrically determined PE concentration, closed circles: reference PE concentration, open squares - fluorometrically determined PC concentration, closed circles: reference PC concentration, B) open triangles: fluorometrically determined PS II reaction centres, closed triangles: reference PS II reaction centres, open circles - fluorometrically determined Chl concentration, closed circles: reference Chl concentration.

6.4.8 Sensitivity to state transitions (coupling of phycobilisome to photosystem II)

State transitions in green algae described the variable coupling of LHC antennae to PS II and presumably also to PS I. Red light moves LHC antennae to PS II, however also light intensity has an influence on the association of LHC antennae and photosystems. In the case of PE and PC containing algae, also the coupling of PBS to PS II is variable.

Here, the influence of energy state transitions induced by changes in light intensity on the estimates of fluorometric pigment concentration was investigated in red cyanobacteria (Figure 6.14 A) and in cryptophyta (Figure 6.14 B). The fluorometric estimates of PE, PC, Chl and PS II in red cyanobacteria and PE and Chl in cryptophyta were measured in dependence on the light intensities. $F_{v570,685} / F_{v470,685}$ is a measure of the ratio of the energy reaching PS II via direct light absorption and via transfer from the PE to PS II ($F_{v570,685}$) to the energy reaching PS II by light absorption of PS II directly ($F_{v470,685}$). The energetic coupling of PBSs was highest (Figure 6.14 A) when the samples were adapted with light intensities in the range of the growth light (between $10 \mu\text{E m}^{-2} \text{s}^{-1}$ – $100 \mu\text{E m}^{-2} \text{s}^{-1}$). This is in remarkable correspondence with results of the investigations on blue cyanobacteria by Campbell & Öquist (1996) and *Chapter 5*. Low coupling to PS II (Figure 6.14 B) was found in dark-adapted and high-light-adapted cells. The variation in Figure 6.14 of all fluorometric estimates in both organisms was less than 10 %. However, the dependence on light intensity was not very strong.

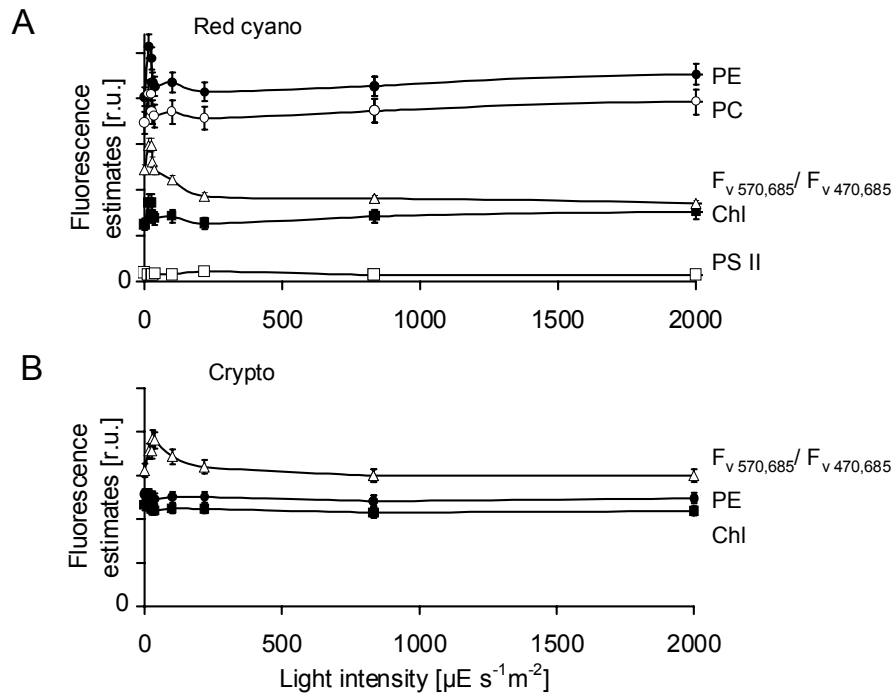


Figure 6.14. A) Fluorometric pigment and PS II reaction centre estimates under light adaptation with different light intensities in *Synechococcus rubescens*: open triangles: energetic coupling of PBSs to PS II in terms of the ratio $F_{v570,685}$ to $F_{v470,685}$, closed circles: fluorometrically determined PE concentration, open circles: fluorometrically determined PC concentration, closed squares: fluorometrically determined Chl concentration, open squares fluorometrically determined PS II reaction centres. Dark-adaptation time prior to measurement was 1 s and adaptation time to light intensity 15 min. Three samples were averaged per data set. Measuring duration of F_0 and F_m was 1s.

B) Fluorometric pigment centre estimates under light adaptation with different light intensities in *Cryptomonas ovata*: open triangles: energetic coupling of PBSs to PS II in terms of the ratio $F_{v570,685}$ to $F_{v470,685}$, closed circles: fluorometrically determined PE concentration, closed squares: fluorometrically determined Chl concentration. Dark adaptation time prior to measurement was 1 s and adaptation time to light intensity 15 min. Three samples were averaged per data set. Measuring duration of F_0 and F_m was 1s.

6.5 Discussion

6.5.1 Variation of cyanobacterial pigments and cryptophytal pigments

The necessity for a special evaluation algorithm for red cyanobacteria and cryptophyta becomes obvious from the great variation of the photosynthetic apparatus resulting from different growth conditions and in different species as shown in Figures 6.2 and 6.3. Red cyanobacteria and cryptophyta like other phytoplankton possess the ability to balance the photosynthetic apparatus to achieve a finely tuned overall photosynthetic process.

In red cyanobacteria, this variability became apparent in large changes of the ratios of PE /Chl, PE/PC and PS II/Chl (Figures 6.2 and 6.3). The values of these ratios were similar to those reported in the literature (Kawamura *et al.* (1979); Schubert & Hagemann (1990); Demarsac & Houmard (1993); Müller *et al.* (1993); Reuter & Müller (1993); Schubert *et al.* (1993); Bryant (1995)). Probably, an increase of PE, PC within the PBSs and/or changes in size and number of PS I reaction centres may be the origin of this variability (Kawamura *et al.* (1979); Schubert & Hagemann (1990); Demarsac & Houmard (1993); Müller *et al.* (1993); Reuter & Müller (1993); Schubert *et al.* (1993); Bryant (1995)), the ratio PBS/PS II being accepted as constant (Myers *et al.* (1980)).

The variability of pigment composition affects the spectral characteristics of fluorescence emission of the red cyanobacterial photosynthetic apparatus (*Appendix D*). The resulting status-dependent norm spectra can cause problems in the fluorometric spectral phytoplankton analysis (see *Chapters 2 and 5*) and can lead to false Chl estimations and algal group identification. Figures 6.8 to 6.9 demonstrate that these problems can be overcome by the model described in *Appendix D*, and that sufficient precision (deviations below 15 %) of specific biomass detection can be achieved.

In the cryptophyta *Cryptomonas ovata*, the light-induced adaptation processes and the species-specific variability lead to differences in PE/Chl *a* and Chl *c*₂/Chl *a* ratio (Figures 6.4 to 6.5). These changes in pigmentation stand for a change in the absorption cross section of the PE and Chl *c*₂ Chl *a* antennae. Their effect on fluorometric analysis (also reported by Sciandra *et al.* (2000)) can be accounted for by the model in *Appendix E*.

6.5.2 Reliability of prediction of pigment contents in red cyanobacteria by the model in *Appendix D*

The assumption given in Equations (D6) is that the fluorescence yields and energy transfer rates among pigments in the red cyanobacterial photosynthetic apparatus are constant (analogue to blue cyanobacteria in *Chapter 5* and *Appendix B*). This simplifying assumption yields good pigment estimates in Figure 6.8 and results in only small deviations in pigment estimation as shown Figure 6.14 A. Even though this is an example of changes in $\Phi_{T,PS II}(\lambda_{ML})$ (and thus, an offence against the assumption of Equation (D6d)), the effect on Chl estimation

is not serious. This seems to result from the fact that the apparent minor changes in the pigment estimation of PS II centres and Chl in this figure might be compensated by changes in other pigment-to-pigment coupling sites.

Another interesting simplification of the real world by the model can be seen in the first two assumptions for phycobilin fluorescence represented by Equations (D8) and (D10). This means that the fluorescence emissions in the channels 600 nm, 620 nm and 650 nm result exclusively from phycobilin fluorescence emission. On the first sight, this seems to be in contradiction to the results of Wyman (1992). This author explained deviations between PE content determined at 570 nm and chemically by means of variable coupling between PE and PC. Support for this hypothesis came from the observation that decoupling by glycerol caused a good coincidence between fluorometrically and chemically determined PE contents. The new approach, however, based on norm curves can distinguish between fluorescence coming from PE and PC. The results show that the assumption of constant coupling between PE and PC can be maintained. As an alternative explanation in line with results obtained here, the deviations observed by Wyman (1992) seem to result from fluorescence from PC, which led to additional components in the measured fluorescence with varying magnitude.

Assumption three of the model in *Appendix D* is basically in accordance with the model for blue cyanobacteria in *Chapter 5* and *Appendix B*. This involves information about the energy distribution to PS II and PS I and their architecture. It is not surprising that total Chl content in red cyanobacteria could also be estimated by three fit coefficients in Equation (D24) (with the assumption that $c_{1,Chl}$ is equal to naught) as the emission spectra at 685 nm show very low variation (below 5 %) in Figure 6.11 This is probably due to the fact that the contribution of PS II reaction centres to the total Chl content can be neglected.

6.5.3 Prediction of pigment contents in cryptophyta by the model in

Appendix E

The distinguishing features of the model described in *Appendix F* for cryptophyta in comparison with the model of red cyanobacteria in *Appendix E* is that PC is lacking as an intermediate to PS II (Figure 6.7), and most Chl is associated with PS II in *Cryptomonas* spp.. This rendered the model for pigment estimation in *Appendix F* much simpler than that for the cyanobacterial model. The model for cryptophyta also assumes constant fluorescence yields and energy transfer rates (Equation (E 9) – (E11)). The validity of the two assumptions given by Equations (E13) and (E14) holds within in the error ranges in Figure 6.9. It is remarkable that Equation (E14) is valid although the Chl c_2 /Chl a ratio changes by a factor of three in Figures 6.4 and 6.5. This might be explained by a minor role of Chl c_2 in light-harvesting complex as compared to that of PE.

To estimate the pigments of red cyanobacteria and cryptophyta in the presence of other phytoplankton the fit procedure of *Appendix F* was established. The fit procedure includes the results of the growth experiments (stable norm spectra; Figure 6.10) and of norm spectra of the blue cyanobacteria and of other phytoplankton (see *Chapter 5* and *Appendix C*). The mathematical fit procedure can utilize information from excitation and emission spectra for the determination of the pigments of five spectral algal groups by the use of the fluorescence

models of *Appendix D* and *E* and the model for blue cyanobacteria of *Chapter 5* and *Appendix B*.

The fit procedure also takes spectral changes in the emission spectra (Figure 6.11) into account. The additional use of the 600 nm and 620 nm channels provide another characteristic feature for the differentiation of cryptophytes like *Cryptomonas ovata* containing PE₅₆₆ and red cyanobacteria by virtue of the spectral differences in this region (Figure 6.11). This distinguishing feature is necessary as the difference in the 685 nm excitation spectra (Figure 6.10 D) is not powerful as there are spectral interferences with Chl of the chlorophyta and chromophyta (data not published).

The mathematical linear independence of the spectra and the correct operation of the fit are demonstrated in the dilution experiments of Figure 6.12. Figure 6.11 demonstrates the correct assessment of pigments by the mathematical fit during aging of a batch culture. This is a simulation of a situation that might occur during a natural phytoplankton bloom. It demonstrates that the model of *Appendix F* and the fit procedure also hold for degrading pigment systems.

Changing light illumination over a time scale of minutes can induce photoinhibition and energy state transitions of algal PSs. While effects of photoinhibitory illumination on norm spectra were discussed in *Chapter 2* under 685 nm emission, the effect of light intensities that induce state transitions and photoinhibitory effects on the models in *Appendix D* and *E*, and the mathematical fit procedure can be seen in Figure 6.14. It was found that the highest deviation for pigment estimation caused by state transitions and photoinhibition together was less than 15 % in both organisms. Both organisms in Figure 6.14 show highest coupling to PS II in the range of growth light intensities. This is similar to the results of Campbell & Öquist (1996) and was found *Chapter 5* with blue cyanobacteria.

The approach presented here should be adequate for most aquatic systems. In the case of cryptophytes or cyanobacteria containing different types of phycobilins, the detection channel can be adapted to the emission wavelength. The fluorescence models can be used analogously for different organisms of the same group as only the spectral characteristic might change and not the energy transfer and structural characteristics. A problem in natural waters might be the interference with yellow substances. This problem can be solved by a special norm spectrum for yellow substances for all four detection channels in the same way this was carried out for the single detection channel in *Chapter 3*.

Another prospect for this methods would be the application of this method to picoplankton in the worlds oceans. They often have a mixed LHC system consisting of Chls and PBs. A further improvement of the fluorometer system will become feasible if more sensitive CCD detectors become available at all wavelengths for the measurements of more emission wavelengths for an enhanced spectral analysis of other PBs.

Chapter 7. In situ analysis of phytoplankton by deconvolution of fluorescence excitation and emission matrices

7.1 Abstract

The previous chapters show that phytoplankton can be distinguished *in situ* and *in vivo* by fluorometric excitation and emission analysis. This is due to differences within the peripheral antennae of photosystem II in different spectral groups of phytoplankton. In this chapter the approach of *Chapter 6* was tested with natural samples. The approach enabled the determination of Chl of five spectral groups of phytoplankton and phycobilins of three spectral types. A correction for YS was included using norm spectra from filtered natural samples. The pigment estimation of this method was compared to reference estimates obtained by high performance liquid chromatography and by wet chemical analysis from. Reference and fluorometric methods showed similar results. The measuring principle was installed in a submersible instrument that enabled the measurement of fluorescence depth-profiles with pigment estimation in a few minutes *in situ*. Profiles obtained with the instrument were compared to those obtained with the bench-top instrument. The correlation between both methods was very high.

7.2 Introduction

In *Chapter 2* it was shown that it is possible to distinguish between four algal groups within *in situ* fluorescence profiles and to correlate the biomass concentrations of different spectral groups of algae. The method of distinguishing five main spectral groups of phytoplankton (green, blue, brown mixed and red) is based on the pigment composition of the peripheral antennae which contribute most to the fluorescence excitation spectra (*Chapter 2*).

Leboulanger *et al.* (2002) introduced a norm spectrum from the red algal group to estimate toxic red cyanobacteria blooms in the absence of cryptophyta. However, the variations in the ratio of the pigment PC to Chl *a* as caused by adaptation to varying environmental lead to changes in the curve shape of the norm curves and render unreliable the original curve fitting approach with fixed norm curves. In *Chapter 5* these problems originating from the special architecture of the blue cyanobacterial photosynthetic apparatus were overcome by using parameter-dependent variable norm curves and by increasing the spectral information by measuring fluorescence excitation spectra at two emission channels (650 nm and 685 nm). The new fit algorithm that was capable of determining PC, Chl *a* and PS II centres was based on a simplified energy distribution model of the cyanobacterial photosynthetic apparatus.

The extension of this approach to spectral fluorometric analysis in red cyanobacteria under special consideration of cryptophyta containing PE₅₆₆ was achieved by developing simple fluorescence models for both organisms (*Chapter 6*, *Appendices D* and *E*). This required the employment of a new fluorometer with four emission channels (600 nm, 620 nm, 650 nm and 685 nm) and enabled the discrimination of red cyanobacteria and cryptophyta in one sample. Both approaches of *Chapter 5* and *6* were tested in the laboratory but not in natural samples.

In natural waters, fluorescence of phytoplankton interferes with fluorescence emission from YS. In *Chapter 3* it was possible to correct the fluorometric algal group estimation of *Chapter 2* for the influence on YS by additional UV-excitation. The determination of the distribution of the spectral algal groups and YS is based on the premise that the measured excitation spectrum at a fixed emission wavelength is a superposition of the signals from the individual cells (see Equation (3.1) in *Chapter 3*).

Pigment concentrations of Chl and phycobilins can be calculated by means of the mathematical fit procedure described in *Chapter 6* and *Appendix F* that achieves the deconvolution of the measured fluorescence spectra $F(\lambda_{ML}, \lambda_{em})$ in order to evaluate the individual spectra of involved spectral algal groups. The analysis of natural freshwater samples resulted in the differentiation between red cyanobacteria and cryptophyta and in the estimation of three types of phycobilins. The YS correction was based on the fluorescence spectra of filtered natural samples (analogous to *Chapter 3*). The reliability of the approach

was tested by comparing the fluorometric pigment estimates from natural samples with HPLC and spectrophotometric analysis.

In one set of experiments, water samples were taken at different depths and analysed in a stationary fluorometer. In another set, a new submersible fluorometer with four fluorescence emission channels and six excitation wavelengths was tested. To verify that the fluorometric approaches work in a large variety of ecological situations six different lakes were chosen. These lakes differed in their phytoplankton community structure and the content of YS. They also contained different amounts of one or two different phycobilins-containing phytoplankton groups.

7.3 Materials and methods

Water samples were taken from different lakes in Northern Germany at different depths with a 2 l Ruttner water sampler. The Chl and phycobilin content were analysed by HPLC and chemically as given below. Fluorescence measurements were carried out in a lab-based fluorometer as shown below. For the determination of YS, other subsamples were filtered through a Whatman GF/F-filter (pore-size 0.7 μ m). Then, the filtered samples were measured in the bench-top fluorometer as described below, and amounts of YS were determined as reference to the YS estimates by fluorescence of the unfiltered samples.

In lakes Krummsee and Schmarksee, the submersible instrument (see below) was used parallel to the measuring procedure described above. Temperature profiles of lakes were obtained with a submersible PT 100 temperature sensor (Lab facility Ltd, US).

7.3.1 Fluorescence measurements

Subsamples of the water samplers were measured in the bench-top instrument as described in detail in Figure 6.1 of *Chapter 6*. The calculation of the fluorometric estimates of Chl and phycobilins was done by the fit procedure given in *Chapter 6* and *Appendix F*. This resulted in separate Chl estimates for five spectral algal groups (green, blue, brown, mixed (cryptophyta) and red). The total Chl concentration was calculated as the sum over all Chl group estimates. The phycobilin estimations from fit calculation gave two separate estimates for PC (blue and red) and to separate estimates for PE (red and mixed (cryptophyta)). The sum of the individual PCs and PEs gave the total amount of PE and PC. A sixth norm spectrum for YS (see Figure 7.1) was introduced in the mathematical fit of *Chapter 6* and *Appendix F*. This enabled the calculation of a relative amount of YS. The norm curve of YS was determined by measuring six surface samples in the bench-top fluorometer.

The samples were collected at the same sites as those in Figures 7.3 to 7.7, 7.9. Prior to the measurement, the samples were filtered through a Whatman GF/F filter as described above in order to obtain samples without phytoplankton. The mean value of the spectra is given in Figure 7.1.

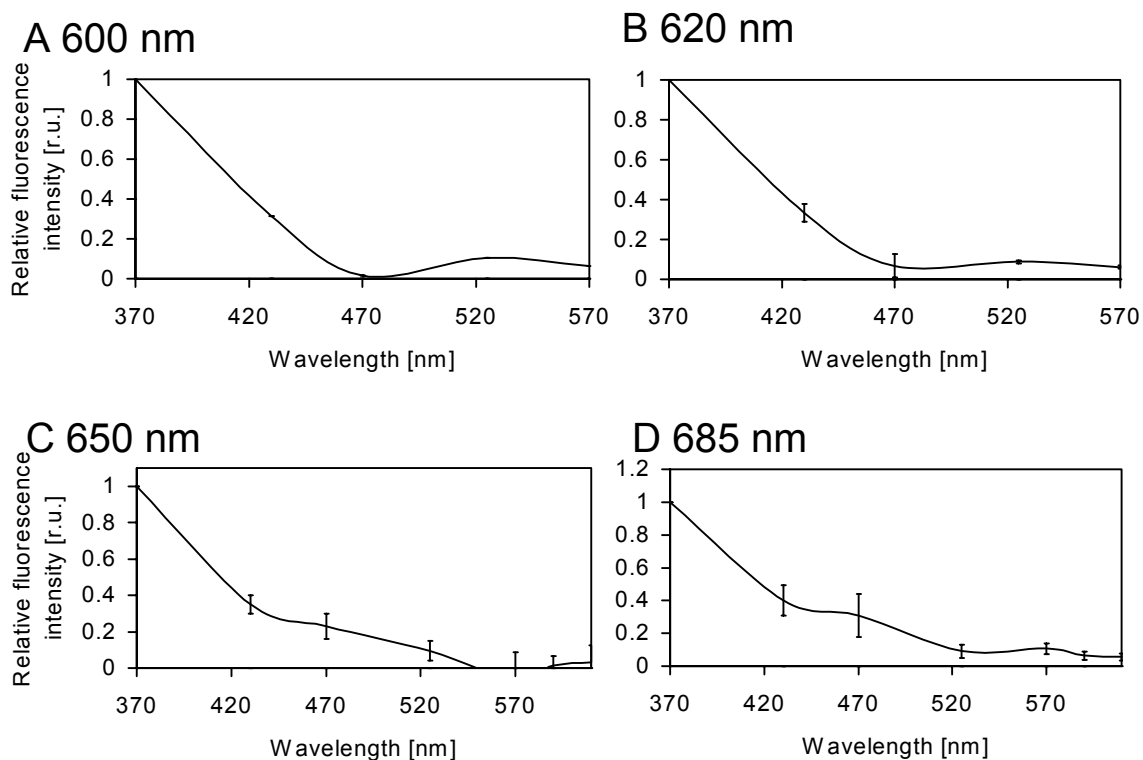


Figure 7.1. Mean fluorescence excitation spectra of filtered water samples taken from different lakes measured at different emission wavelengths: A) 600 nm, B) 620 nm, C) 650 nm D) 685 nm. The error bars indicate the standard deviation of the mean. The spectra were normalised to fluorescence intensity at an excitation with 370 nm light. Those spectra were used as norm curves for YS.

7.3.2 Fluorescence profiler

Depth profiles obtained from *in situ* experiments were recorded with the submersible instrument shown in Figure 7.2. Briefly, the optical set-up of the bench-top instrument (see above and *Chapter 6*, Figure 6.1) was installed inside two tubes acting as separate probes (each probe was similar to that described in *Chapter 2*). A single tube contained two detectors, one LED array (with six excitation LEDs) and one microcontroller. In one of the tubes, the 600 nm and 620 nm detector and in the other one the 650 nm and 685 nm detector were installed. The LEDs and filters used in both tubes were the same as those in *Chapters 5* and *6*. The seventh LED used in *Chapters 5* and *6* at 430 nm emission was not used because the light intensity of this LED was so low that its contribution in the fit procedure *Chapter 6* and *Appendix F* was negligible. The 610 nm and 590 nm LEDs were not used in the tube with the 600 nm and 620 nm detector. The measurement-light intensities induced by the LEDs in both measuring chambers were $5 \mu\text{E m}^{-2}\text{s}^{-1}$. The LEDs were switched sequentially with 5 kHz repetition rate. This enabled the determination of F spectra according to van Kooten & Snel (1990), see also *Chapter 1*. An external computer started synchronous data acquisition from the four detectors.

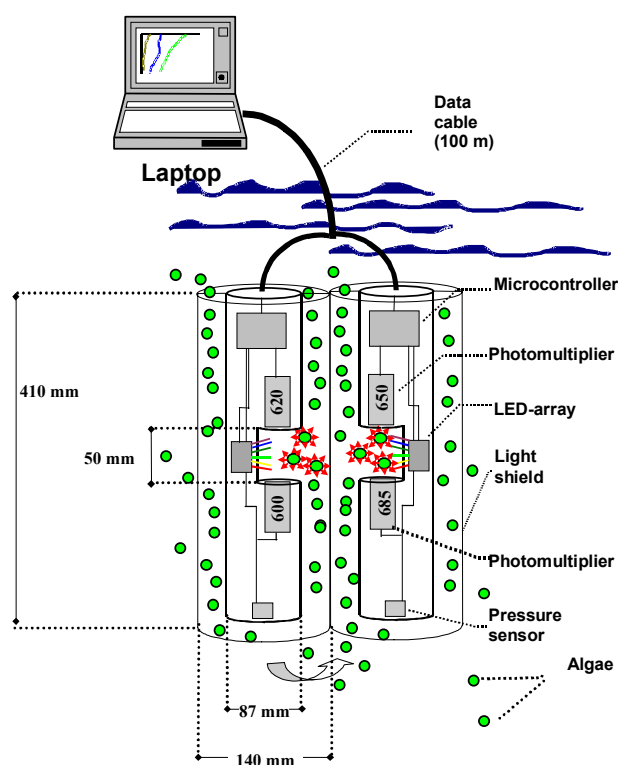


Figure 7.2. The submersible probe. All electronic and optical components were enclosed in two stainless steel housings with an open measuring cavity (50 mm height) as indicated. The stainless steel housing is encased in a black polyethylene cylinder (diameter of 140 mm), open at the bottom and top, serving as a light shield. Two photomultipliers were installed in each probe equipped with one LED excitation array per two detectors. Data was transferred on-line via a RS 485 interface and a cable to a personal computer, on board a research vessel. The measured pressure (piezo-sensor) was used to calculate the actual water depth; deconvolution of the data was done with the connected computer.

Light shields in the form of two outer tubes prevented the incidence of direct sunlight. Measurement of water pressure by piezo-sensor enabled the calculation of the submersion depth. Data could be stored in the probe or could be transferred on-line to a PC. In the latter case, the probe measured continuously and sent a set of data (water depth and fluorescence data) every second to a PC or laptop. Sample water flowed across both measuring cavities when the instrument was lowered into the water. The algal distribution was assumed to be the same in both measuring cavities. The calibration and the fit procedure for pigment estimation was the same as for the bench-top fluorometer.

7.3.3 Pigment determination

Determination of Chl concentrations. Concentrations of Chl *a* were determined according to Wiltshire *et al.* (1998) using HPLC (see Chapter 2).

Phycobilin determination. The amount of phycobilins in algal suspensions was determined in a wet chemical spectrophotometric analysis as described in Chapter 5.

7.4 Results

The test of the applicability to natural waters of the measuring and fit procedure of *Chapter 6* and *Appendix F* with samples containing phycobilins, the fluorometric determination of Chl, phycobilin and YS estimates was compared with the references estimates (see Materials and methods).

Different lakes were selected in order to check the performance in different scenarios regarding depth-dependence, algal composition and alga/YS ratio. For example: in the Schmarksee, all groups were present with the green group dominating near the surface, whereas in deeper layers red cyanobacteria were in the majority. The Schmarksee is known for the occurrence of toxic blooms of red cyanobacteria leading to the death of horses drinking the water. The Krummsee is an example for a very simple scenario with a peak consisting nearly exclusively of red cyanobacteria. Cryptophyta were the strongest group in the Schöhsee. In the Plußsee regions with dominance of the brown group or the blue cyanobacteria could be found.

Measurements in the Schmarksee and the Plußsee provided analysis with a low background of YS. The Krummsee and the Schöhsee had considerable amounts of YS with complementary depth-dependencies of concentrations of algae and YS. Measurements in the Plußsee at two different times of the year showed the capability of the approach to monitor changes in depth-dependence and in algae/YS concentrations.

Details of the fluorescence analysis are presented in Figures 7.3 to 7.7 below. Figures 7.8 and 7.10 show the correlation between the values obtained from fluorescence analysis and from chemical analysis.

Figure 7.3 shows the depth profiles measured in the Schmarksee. The total Chl concentration exhibits a maximum at 3 m in Figure 7.3 A with a high concentration of the brown spectral group. The depth profile shows peaks resulting from different organisms: green group at 1m, brown group at 3m and red cyanobacteria at 3.5 m. The red cyanobacteria peak could also be found in the estimates of phycobilins due to a high peak in red cyanobacterial phycobilins (Figure 7.3 B). The YS concentration showed only very small changes with depth (Figure 7.3 B). The temperature change with depth is small (inset of Figure 7.3)

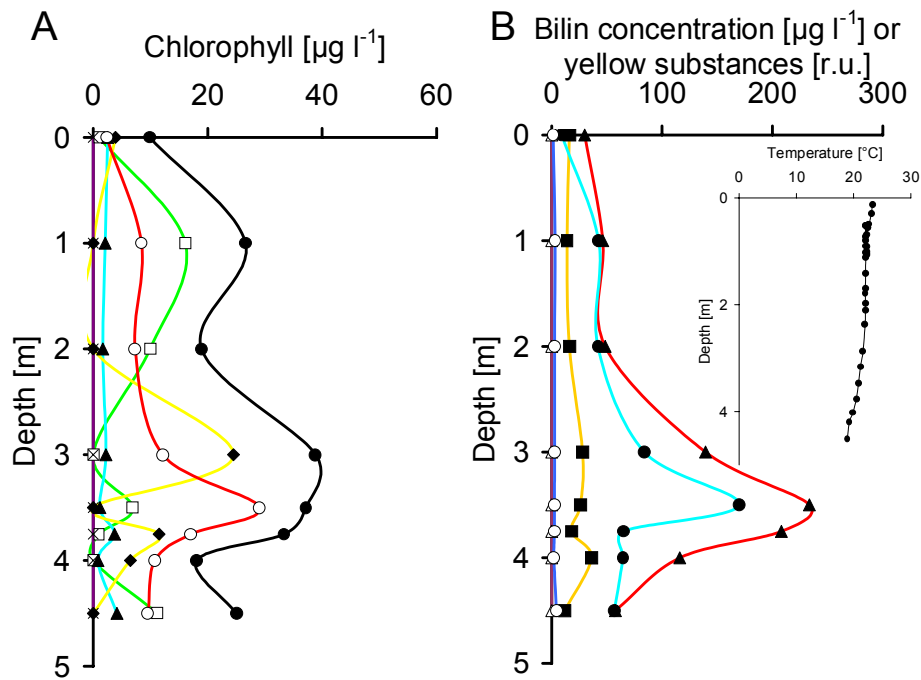


Figure 7.3. Fluorescence depth profile taken in the Schmarksee (August 15th). Fluorescence was determined from water samples in the laboratory. The inset shows the temperature profile. A) Chl contents estimated by fluorescence: closed circles, total Chl; open squares, green group; closed triangles, blue group; closed diamonds, brown group; crosses mixed (cryptophyta) group; open circles, red group. B) Phycobilin contents estimated by fluorescence, open circles, PC (blue), open triangles; PE (cryptophyta), closed triangles PE (red), closed circles PC (red), closed squares, YS.

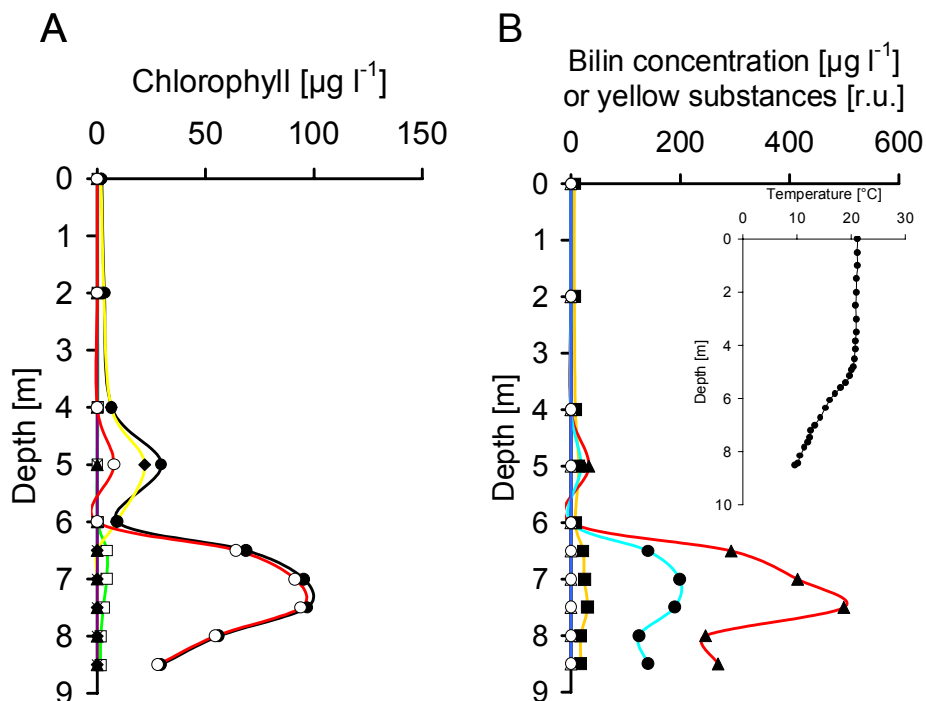


Figure 7.4. Fluorescence depth profile taken in the Krummsee (September 11th). Fluorescence was determined from water samples in the laboratory. The inset shows the temperature profile. A) Chl contents estimated by fluorescence: closed circles, total Chl; open squares, green group; closed triangles, blue group; closed diamonds, brown group; crosses mixed (cryptophyta) group; open circles, red group. B) Phycobilin contents estimated by fluorescence, open circles, PC (blue), open triangles; PE (cryptophyta), closed triangles PE (red), closed circles PC (red), closed squares, YS

The water of Krummsee was very clear in the upper four meters. The data showed a stratified situation on September 11th. Consequently, low Chl and phycobilin concentration were detected in the surface layers (0 m – 4 m). At five metre, there was a peak in Chl concentration dominated by the brown spectral group (Figure 7.4 A). At a depth of 7.5 m fluorescence estimates had a maximum of red cyanobacterial Chl, PE and PC (Figure 7.4 A and B). The estimates of YS had also a maximum at this depth. The temperature profile (see inset Figure 7.4) of the lake indicated a zone with strong heat exchange in the first four metres.

The profile taken in the Schöhsee on July 25th showed high populations of cryptophyta and brown algae between 0 m and 8 m members. Cyanobacteria were absent. (Figure 7.5 A and B). Below 8 m only cryptophyta were detected. The total Chl concentration decreased almost linearly with depth in Figure 7.5 A. The detection of YS concentration increased by a factor 2 at a depth of 9 m (Figure 7.5 B). A pronounced Chl maximum was missing here.

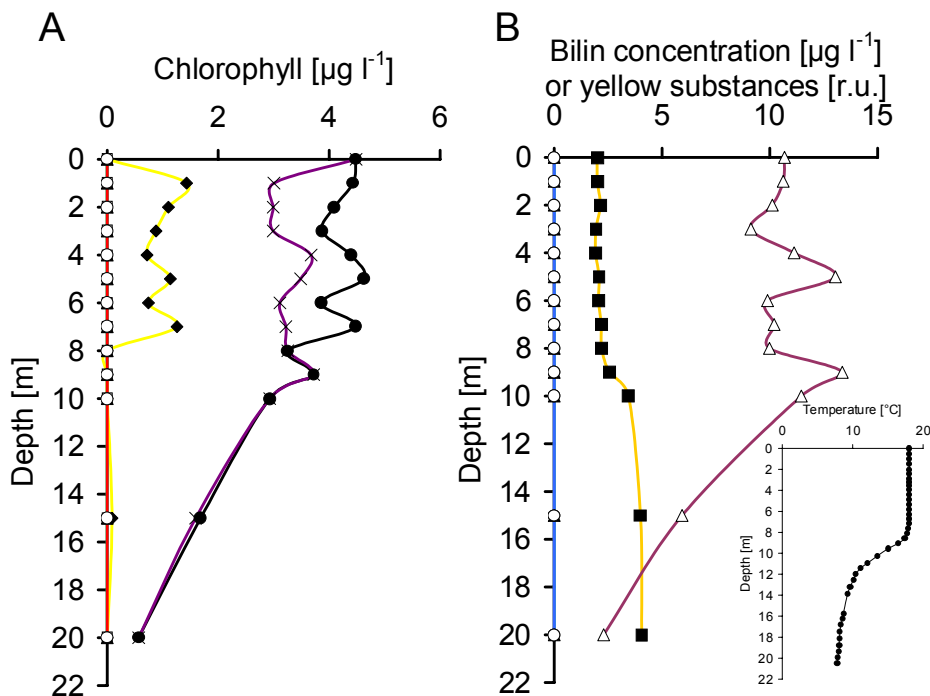


Figure 7.5. Fluorescence depth profile taken in the Schöhsee (July 25th). Fluorescence was determined from water samples in the laboratory. The inset shows the temperature profile. A) Chl contents estimated by fluorescence: closed circles, total Chl; open squares, green group; closed triangles, blue group; closed diamonds, brown group; crosses, mixed (cryptophyta) group; open circles, red group. B) Phycobilin contents estimated by fluorescence, open circles, PC (blue), open triangles; PE (cryptophyta), closed triangles PE (red), closed circles PC (red), closed squares, YS.

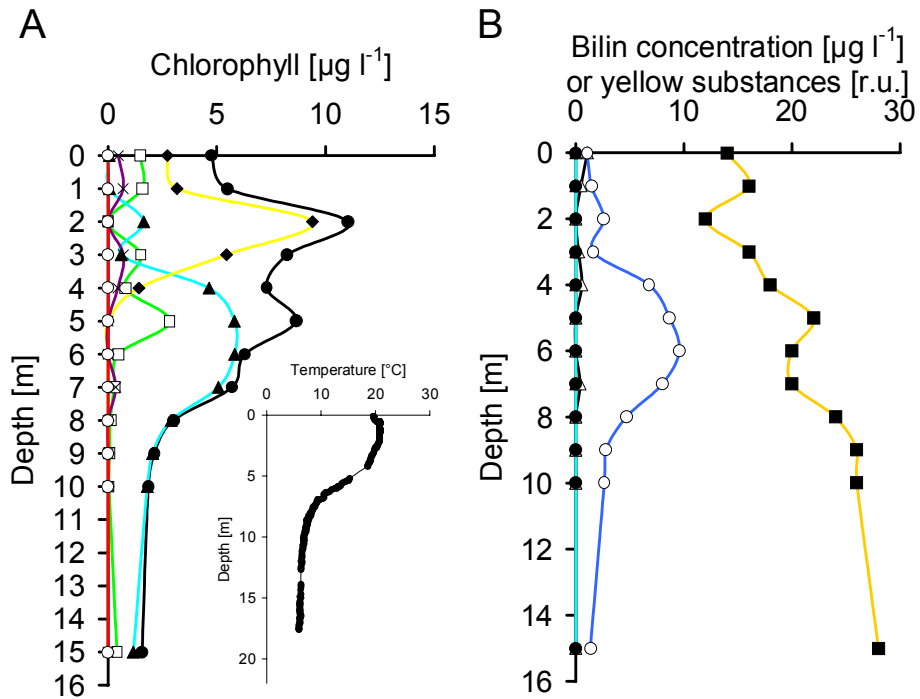


Figure 7.6. Fluorescence depth profile taken in the Plußsee (July 11th). Fluorescence was determined from water samples in the laboratory. The inset shows the temperature profile. A) Chl contents estimated by fluorescence: closed circles, total Chl; open squares, green group; closed triangles, blue group; closed diamonds, brown group; crosses, mixed (cryptophyta) group; open circles, red group. B) Phycobilin contents estimated by fluorescence, open circles, PC (blue), open triangles; PE (cryptophyta), closed triangles PE (red), closed circles PC (red), closed squares, YS.

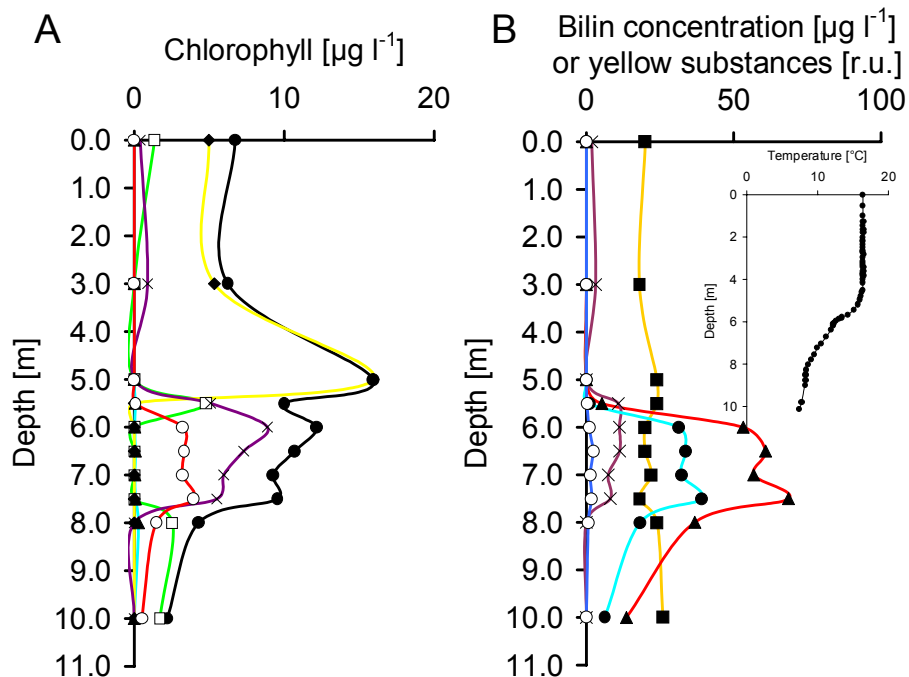


Figure 7.7. Fluorescence depth profile taken in the Plußsee (September 25th). Fluorescence was determined from water samples in the laboratory. The inset shows the temperature profile. A) Chl contents estimated by fluorescence: closed circles, total Chl; open squares, green group; closed triangles, blue group; closed diamonds, brown group; crosses, mixed (cryptophyta) group; open circles, red group. B) Phycobilin contents estimated by fluorescence, open circles, PC (blue), open triangles; PE (cryptophyta), closed triangles PE (red), closed circles PC (red), closed squares, YS.

In Figures 7.6 and 7.7 profiles from the eutrophic Plußsee taken at different dates (July 11th and September 25th) are depicted. The fluorescence profile measured in July showed a stratified situation with two Chl maxima at 4 m and 6 m depths (Figure 7.6 A). The 2 m maximum was assigned to the presence of the brown spectral group whereas the maximum at 6 m was due to blue cyanobacteria. This corresponds to the maximum in blue cyanobacterial PC estimation in Figure 7.6 B at 6m. Interestingly, the YS estimate increased with deeper depths (Figure 7.6 B). A quite different picture was found in September (Figure 7.7). The maximum in total Chl concentration induced by the brown spectral group was located at five metre. Between 6 m and 8 m, a peak of phycobilins carrying red cyanobacteria and cryptophyta were found. The YS concentration showed a slight increase with depth.

The fluorometric estimates of Figures 7.3 to 7.7 were compared with reference estimates measured from subsamples of the water taken from the lakes. The correlation of the fluorometric Chl estimates to the Chl concentration HPLC had a high correlation coefficient and were in good agreement (Figure 7.8 A). The correlation of the sum of cryptophytal and red cyanobacterial PE measured fluorometrical shows small deviations from the chemical results of the PE concentration from the profiles shown in Figures 7.3, 7.4 and 7.7. In the measurements shown in Figures 7.5 and 7.6 the phycobilin content was too low as to be determined chemically.

The agreement of the PC estimation has a slightly smaller correlation coefficient than the PE estimation. The comparison of YS estimates of filtered and unfiltered samples correspond to each other. In samples from Krummsee and Plußsee at depths with a high PE concentration up to ten percent of the total PE concentration was found in the filtered subsamples by fluorometric analysis in addition to YS content. This might be due to free dissolved PE in the samples or cells which burst during the filtration. The precision of pigment estimation (in Figure 7.8 A-D; indicated by different symbols for different depth profiles) was similar in all five depth profiles, with one exception. This was the determination of YS in lake Krummsee (Figure 7.8 B). In this case the slope calculated in the correlation to the reference estimates was lower than one. This might indicate that large undissolved (diameter > 0.7 µm) detritus particles were present in the unfiltered samples but not in the filtered reference. Those particles are high likely to have a similar spectrum than YS. In the case that the amount of detritus particles is correlated with YS concentration the slope of the correlation for the Krummsee could be reduced and the correlation coefficient high Figure 7.8 A. The measured fluorescence intensity for each spectral group 7.3 to 7.7 was significantly correlated to the biovolume (from counts of parallel taken water samples; see *Chapter 2* for method) of associated algae found at different depths for these groups.

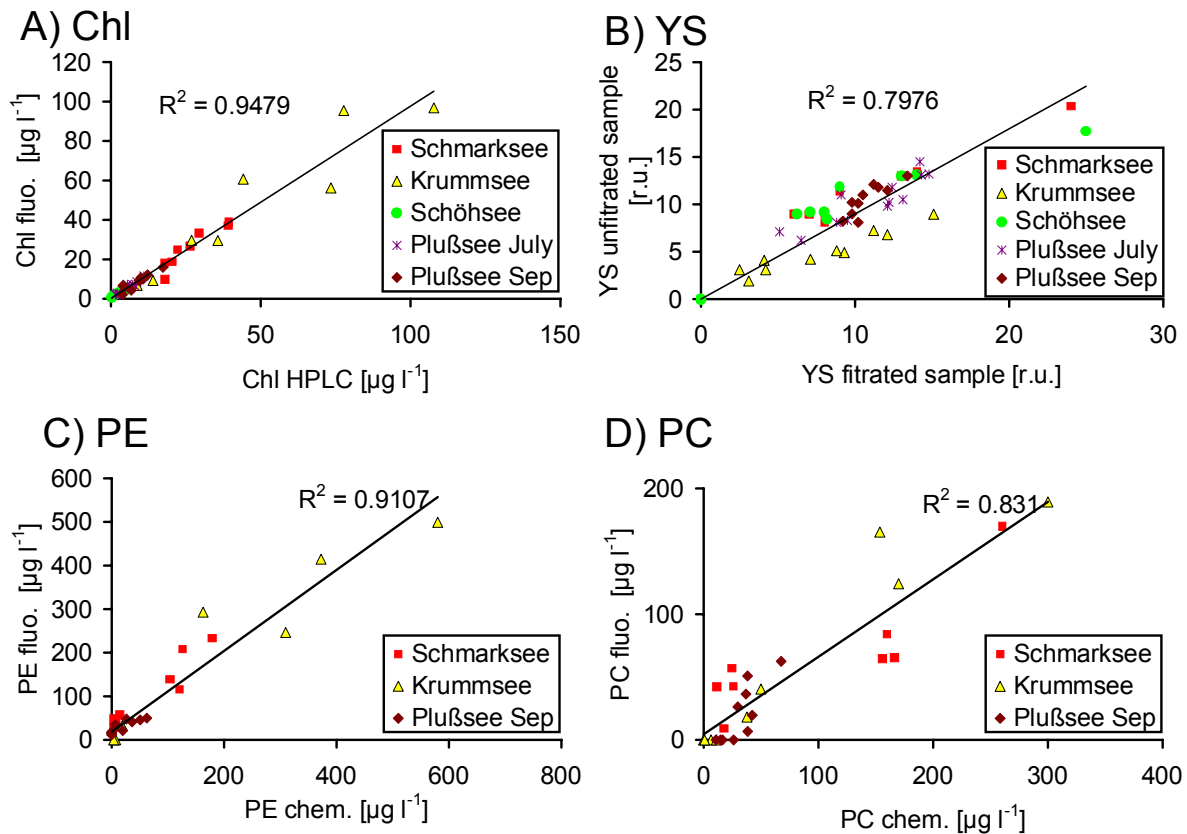


Figure 7.8. Linear regressions of fluorometrically determined Chl, YS, PE, PC and Chl of Figures 7.3 to 7.7 (for PE and PC of Figures 7.3, 7.4 and 7.7) on the reference estimates: A) Chl B) YS C) PE and D) PC reaction centres.

The measurements in the Heidensee represent a time series of fluorometric Chl and phycobilin analysis (Figure 7.9). Here, a sample was taken from the same site from the lake's surface every three days in average for a month (September – October 2002). Two maxima were found due to cyanobacterial blooms in Chl and PC concentration on September 23rd and October 1st. After this date the PC and the Chl concentration of the blue spectral group showed a sharp decline and the pigment estimates of the cryptophyta increased. The fluorometrically determined YS concentration increased slightly from the 26th of September. The Heidensee showed the highest, relative amount, of YS of all of the investigated lakes.

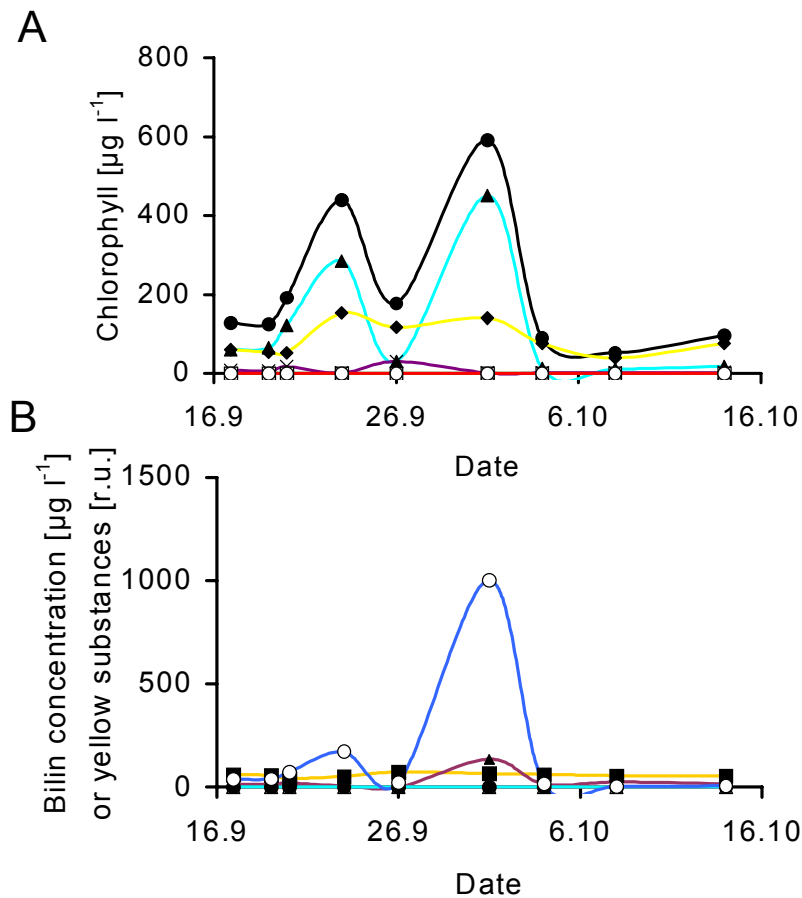


Figure 7.9. Time series of fluorescence estimates taken in the Heidensee (from September 25th). Fluorescence was determined from water samples in the laboratory. A) Chl contents estimated by fluorescence: closed circles, total Chl; open squares, green group; closed triangles, blue group; closed diamonds, brown group; crosses, mixed (cryptophyta) group; open circles, red group.

B) Phycobilin contents estimated by fluorescence, open circles, PC (blue), open triangles; PE (cryptophyta), closed triangles PE (red), closed circles PC (red), closed squares, YS.

A comparison of the pigment estimates obtained by fluorescence and by the reference methods for Chl, phycobilins and YS is given in Figure 7.10. The overall estimation of Chl compared to HPLC analysis is very good. The determination of PE has a higher estimation error than in the example of the depth profiles shown in Figure 7.7. The determination of PC is better than the estimation of PE in the example of the Heidensee. The comparison of the estimates of YS in filtered and unfiltered samples were also in good agreement. In the case of the Heidensee no phycobilins were detected in the filtered samples due to the absence of red cyanobacteria in Figure 7.9 A. No difference in the precisions of pigment estimations was observed from samples obtained before or after the Chl maximum of October 1st in Figure 7.10.

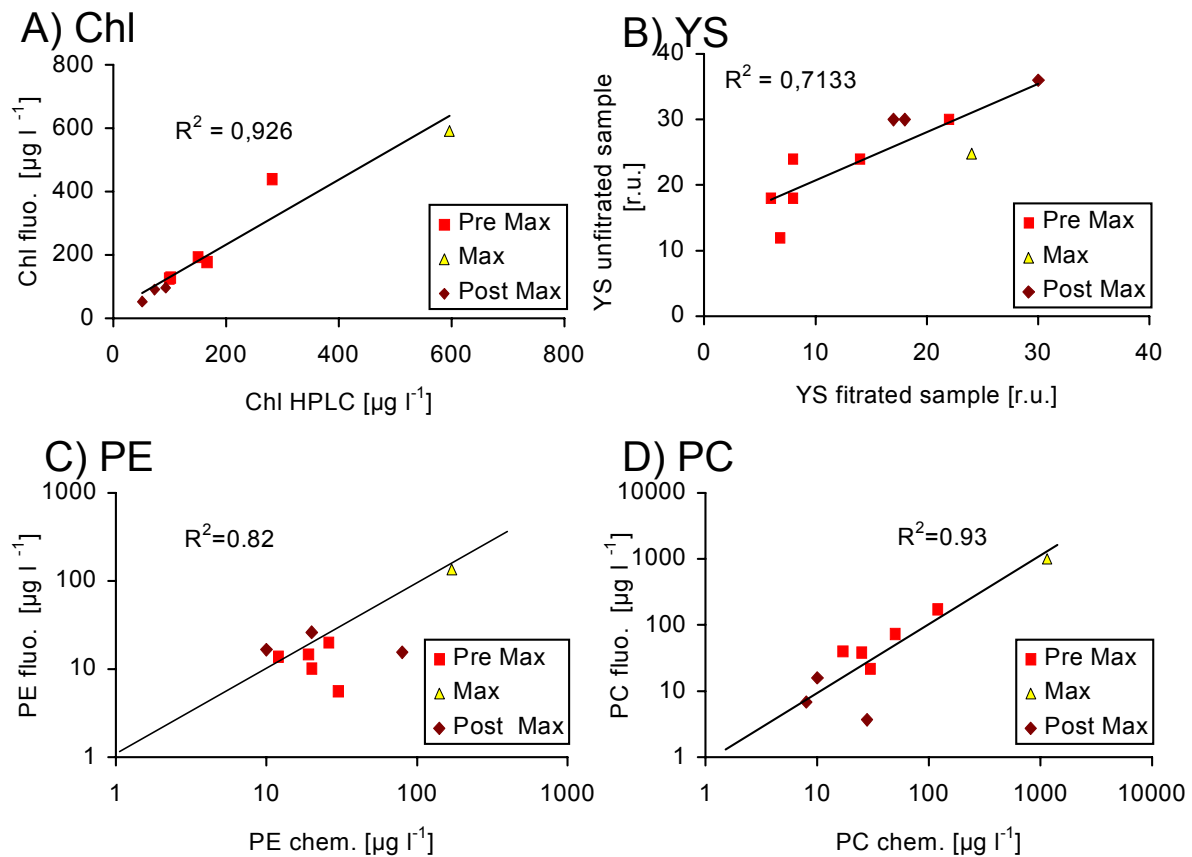


Figure 7.10. Linear regressions of fluorometrically determined Chl, YS, PE, PC and Chl of Figure 7.9 on the reference estimates: A) Chl B) YS C) PE and D) PC

Figure 7.11 and Figure 7.12 show example fluorescence profiles recorded with the submersible instrument depicted in Figure 7.1 in Krummsee and Plußsee at the same times and sites as the profiles obtained with the bench-top fluorometer (Figure 7.4 and Figure 7.7). In both profiles the detected algal Chl and phycobilins concentration were in very good agreement with those obtained by the stationary bench-top instrument. Table 7.1 shows the correlation coefficients of the algal group estimates obtained with the bench-top fluorometer to those obtained with the depth profiler (interpolated graphically from Figures 7.11 and 7.12 for even depths of Figures 7.4 and 7.7).

	R^2	Slope
Chl	0.97	0.97
YS	0.81	1.02
PE	0.98	0.96
PC	0.98	0.96

Table 7.1. Correlation coefficients and slopes of the algal group estimates obtained with the bench-top fluorometer to those obtained with the depth profiler calculated for a linear regression (data from Figures 7.4, 7.7, 7.11 and 7.12).

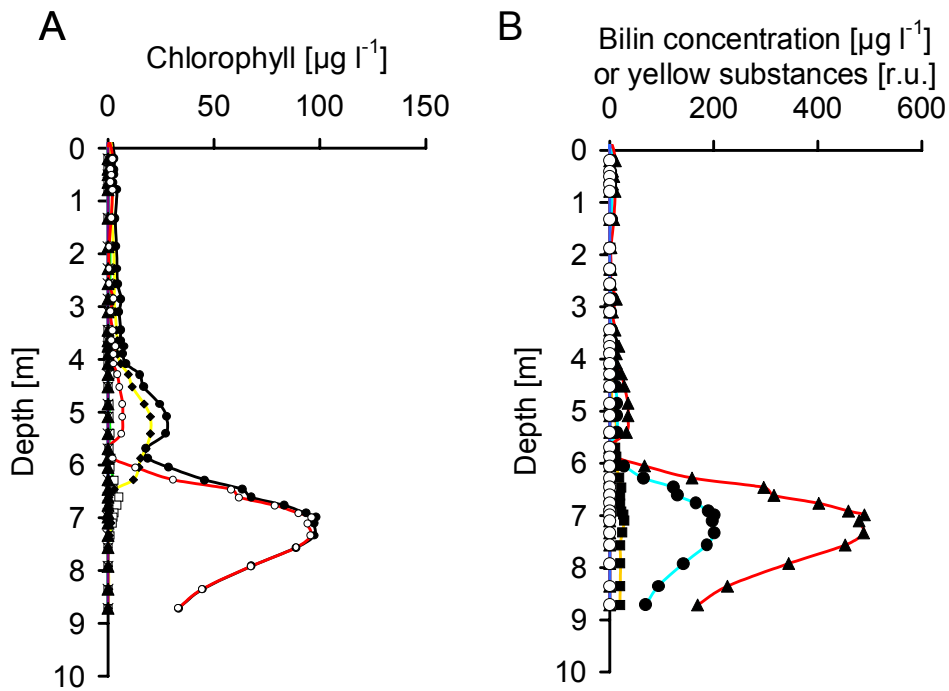


Figure 7.11. Fluorescence depth profile taken in lake Krummsee (September 11th) with the submersible instrument shown in Figure 7.2. This profile was taken at the same site and time as shown in Figure 7.4. A) Chl contents estimated by fluorescence: closed circles, total Chl; open squares, green group; closed triangles, blue group; closed diamonds, brown group; crosses, mixed (cryptophyta) group; open circles, red group. B) Phycobilin contents estimated by fluorescence, open circles, PC (blue), open triangles; PE (cryptophyta), closed triangles PE (red), closed circles PC (red), closed squares, YS.

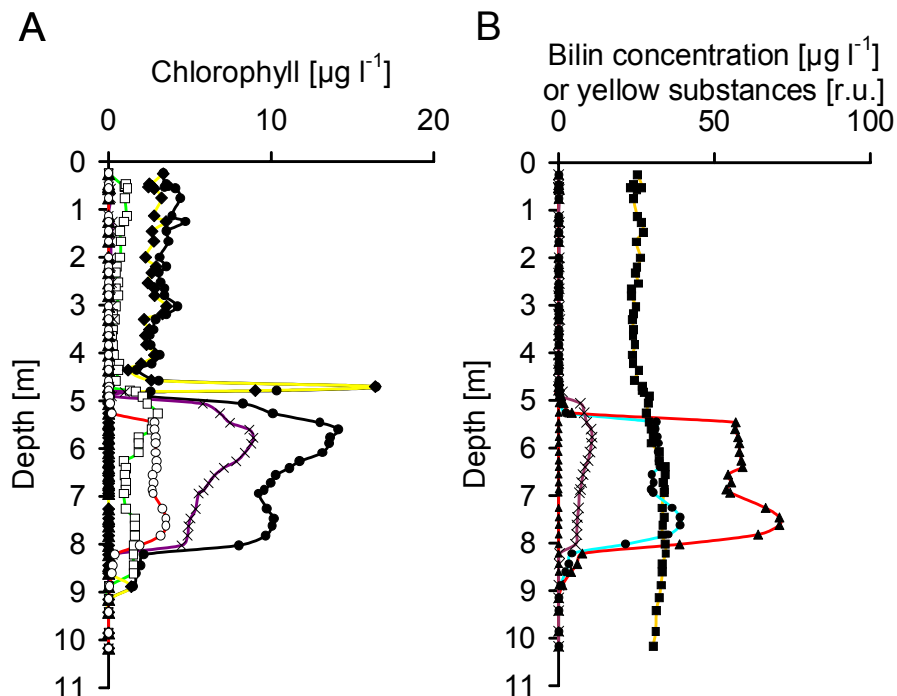


Figure 7.12. Fluorescence depth profile taken in lake Plußsee (September 25th) with the submersible instrument shown in Figure 7.2. The profile was taken at the same site and time as shown in Figure 7.7. A) Chl contents estimated by fluorescence: closed circles, total Chl; open squares, green group; closed triangles, blue group; closed diamonds, brown group; crosses, mixed (cryptophyta) group; open circles, red group. B) Phycobilin contents estimated by fluorescence, open circles, PC (blue), open triangles; PE (cryptophyta), closed triangles PE (red), closed circles PC (red), closed squares, YS.

7.5 Discussion

The fluorometric method for the determination of phytoplankton employed here was tested in various situations (Figures 7.3 to 7.7 and Figure 7.9). In all samples, phycobilins were detected by the fluorometric approach. The experiments represent typical algal distributions of phycobilin-containing phytoplankton in freshwater with one or two phycobilin-containing phytoplankton being present.

The results obtained with the bench-top fluorometer were in good agreement with the Chl, phycobilin and YS estimate of the reference methods. The best correlation of all estimates to its reference estimate was found for Chl (Figure 7.8 A). This demonstrates the reliability of the fluorometric estimation method for Chl determination in natural samples. One reason for the good Chl estimation is the low standard error of the employed reference method (HPLC analysis; standard error below 3 %). The correlation coefficients for the determination of PE and PC were slightly weaker. A possible reason could be that PE and PC estimation is not good when large amounts of other phycobilins or YS are present. This was the case in Figure 7.8 (correlation of pigments of all recorded depth profiles) for the determination of PC. This was probably due to the dominance of the PE containing phytoplankton. The predictability of all pigments (Figure 7.8) was similar in all five profiles for all pigments with the exception of the deviation of the slope for YS estimation (Figure 7.8 B and discussion below). In Figure 7.10 the determination of PE has a lower correlation coefficient. In this measurement the blue cyanobacteria dominated and caused errors in the PE determination. One of the main causes for the deviation of chemical and fluorometrical phycobilin determination methods was potentially that the chemical reference method itself could be corrupted by YS and had a high standard deviation (up to 30 % for natural samples). The low resolution of the chemical method (see Plußsee (July) and lake Schöhsee) might be explained by a high contribution of non-phycobilin carrying algae and detritus. This resulted in glass fibre filters becoming dogged during filtration with the result that only small amounts of samples could be filtered.

Problems with free PBs were small. As mentioned in the results section above only small amounts of phycobilins in samples with a high concentration of PE were estimated in filtered samples for the reference determination. Free PBs were not found in filtered samples in the lab-cultures of *Chapter 5* and *6*.

It is also possible that the fluorescence offsets were induced by the filtration process by burst cells as it was unlikely that free phycobilins were stable for a long time in natural systems.

The fluorometric detected YS concentrations (in Figures 7.3 to 7.7 and Figure 7.9) corresponded to the estimation of YS although the fluorescence signal of YS is very small compared to the total fluorescence of the samples (1 %- 5 %). The good estimation of YS was probably due to the unique fluorescence characteristics with high fluorescence intensity at 370 nm excitation. The results show that the correction for YS was a good method to improve the fluorometric analysis especially when the Chl concentration was very low and the contribution

of YS fluorescence was relatively high. The deviation of the slope for YS estimation in the Krummsee (Figure 7.8 B) from the overall estimation of YS in Figure 7.8 B, has probably no consequence for the precision of the estimation methods. The observed deviation is likely to be caused by real differences of the unfiltered and filtered reference samples and probably caused by a lack of detritus particles in the filtered samples (see also results section above).

Figures 7.11 and 7.12 demonstrate that it is possible to apply the measuring protocol to a submersible fluorometer and to obtain depth profiles of fluorescence excitation spectra measured at four emission wavelengths. In combination with the fit procedure of *Chapter 6* and *Appendix F* it can determine the phytoplankton distribution of five spectral algal groups in a few minutes. Figures 7.11, 7.12 and Table 7.1 demonstrate that the results obtained with the submersible instrument of Figure 7.1 were equivalent to the estimates measured with the bench-top instrument.

The two main differences between the measuring set-up of the bench-top instrument and the submersible were, firstly, that the submersible instrument measures fluorescence at a flowing suspension (effects of flow velocity on fluorescence measurements at flowing suspension were discussed in detail in *Chapter 4*). The second difference is the installation of the four photomultiplier in two different measuring chambers of the submersible instrument.

The first point would reduce the fluorescence signal measured with the submersible instrument compared to that measured with the stationary instrument (*Chapter 4*). The slopes calculated by the regressions (Table 7.1) from stationary on submersible instrument profiles were close to one. This means that the fluorescence signals were not strongly reduced due to the movement of the instrument. Probably, the flow velocities and the excitation light intensities employed in the submersible probe were low enough to exclude such effects. This would be in accordance with *Chapter 4*. The second difference of the two measuring systems did not exert a detectable effect on the results obtained with the submersible probe, the correlation coefficients given in Table 7.1 were very high. Probably the horizontal distribution of the phytoplankton was constant enough in the dimension of the measuring chambers of the submersible probe (Figure 7.1).

In conclusion, the test of the approach over a wide range of fresh water lakes in different situations resulted in a good agreement with the reference results.

Conclusion

Since Yentsch & Yentsch (1979) discovered the potential of spectral differences of phytoplankton fluorescence as a tool for *in situ* analysis of phytoplankton communities, it has been highly desirable to establish methods, algorithms and mathematical models to move this powerful approach from a laboratory based method to a fast and flexible *in situ* method. This thesis shows that now even more is possible. Originating from the lab-based approach of Beutler (1998), where it was possible to differentiate phytoplankton fluorescence of four groups by the use of Chl excitation spectra, the concept was adapted to probe technology and tested (*Chapter 2*). This enabled the rapid *in situ* differentiation of four algal groups by using a submersible instrument in the time range of a few minutes.

Although this approach is affected by fluorescence of yellow substances and can only differentiate between four spectral algal groups this approach delivers good results if cyanobacteria are a minority within the plankton community. The usefulness of this approach has also been demonstrated by Leboulanger *et al.* (2002) who introduced an extra norm spectrum for the red cyanobacteria. Here, good results were achieved in the absence of cryptophyta in freshwater lakes. The influence of scattering particles and pre-illumination effects was shown to be small (*Chapter 2*). Deviations might occur if blue cyanobacteria are present in the sample. In this case the estimation method would inaccurate Chl estimates in the range of a factor two due to adaptation processes.

Another unknown parameter with regard to the *in situ* estimation of Chl fluorescence was the velocity of the probe during measurement. Further, two constraints of the method were shown to be the influence of YS fluorescence and the presence of the fifth spectral algal group (the red cyanobacteria) in some ecologically important situations.

The problem of YS fluorescence was overcome in *Chapter 3*. Typically, the presence of YS fluorescence would lead to higher Chl estimates with the method described in Beutler (1998) and *Chapter 2*. This problem was solved by the use of a sixth excitation LED with 370 nm emission and the introduction of a YS norm spectrum. Firstly, the norm spectrum of YS had to fulfil two requirements, i.e., the linear independence of the phytoplankton norm spectra. Secondly, different spectra of YS had to be similar and a mean norm spectrum for YS could be used that is valid in many different water types. Both was shown to be possible in *Chapter 3*. The norm spectra were linearly independent of the algal norm spectra and the norm spectra of YS showed such a small deviation in different water types, that it was applicable as a mean spectrum.

The effect on F_0 , F_M and F by the movement of the probe was investigated in *Chapter 4*. This was achieved by evolving the mathematical model for correction of the fluorescence parameters for the probes movement described in *Chapter 4*. The mathematical

model was tested by experiments carried out in a new flow-through fluorometer with samples measured at different flow velocities. The two main results were, firstly, that the influence of the probe's movement on the measured Chl fluorescence in the case of F_0 and F at measuring light intensities below $5 \mu\text{E m}^{-2} \text{s}^{-1}$, (*Chapter 2*) can be neglected. Secondly, the application of a model for correcting fluorescence parameters enabled the measurement of photosynthetic parameter with a submersible fluorometer. This also means that higher measuring light-intensities for the determination of Chl could be employed in the measuring procedure of *Chapter 2* and *3* if the correction of the model presented in *Chapter 4* was used. This would enhance the Chl resolution of the measuring system.

A major breakthrough for the spectral analysis of phytoplankton was the addition of detection wavelengths in *Chapter 5* allowing the detailed analysis of the photosystems of blue cyanobacteria in the presence of other algal groups. This was also achieved by combining a parametrical description of the fluorescence characteristics of the photosynthetic apparatus of cyanobacteria (mathematical model of *Appendix B*) and a new fit algorithm shown in (*Appendix C*). This approach did not only solve the problems with blue cyanobacteria raised from variable norm spectra and interferences with changes in phycobilin fluorescence emission caused by species and physiological state dependent variations of the photosynthetic apparatus. But this approach also provided the means for transferring this principle to other phycobilins-carrying organism such as red cyanobacteria and cryptophyta. It made possible the differentiation of five spectral algal groups and the elimination of the influence of adaptation processes originating from these organisms.

One assumption had always to be taken into account for the investigations presented in this thesis. That was the time a fit procedure needs to estimate the desired parameters. For online-analysis the time required by the fit procedure had to be low. Different weighting factors at different excitation LEDs and algal groups made the estimation method in the approach of *Chapter 2* non-linear and time-consuming. However, it was possible by the approximation as carried out in the fit procedure of *Appendix A* to linearise this fitting problem by the use of an iterative Gaussian fit. In *Chapters 5* and *6* it was possible to save calculation time by minimisation of a Gauss-based core fit with a simplex algorithm. This led to a robust and fast solution of the fitting problem.

Finally in *Chapter 7* it was demonstrated that the investigated topics in *Chapters 2 – 6* can be directly transferred to *in situ* plankton analysis. The theory on fluorescence in photosynthetic systems evolved in the previous chapters, fluorescence of YS, fit procedures and behaviour of norm spectra were shown to be very useful in combination with probe technology in phytoplankton analysis. Potentially the estimation of phycobilins by fluorescence opens new investigation potential *in situ*. It is now possible to estimate phycobilin to Chl ratios *in situ* for a spectral algal group. This will provide valuable information of the status of the photosynthetic apparatus of these organisms *in situ*.

Future investigations will show if the fluorometric models for the phycobilin containing organisms of *Appendix B*, *D* and *E* can be transferred to picoplankton like prochlorophyta. Many of these organisms have a peripheral antenna composed of Chl *a/b* and

a PB. These organisms are important in the open ocean and play an essential role in primary production.

Another useful approach would be to install more detection wavelengths in the infrared region. At wavelengths such as 880 nm it would be possible to detect bacteriochlorophyll as applied by Kolber *et al.* (2001) As those organism have many different antennae-types with different bacteriochlorophyll types emitting at several wavelengths in the infrared region it should be possible to differentiate between different photosynthetic bacteria *in situ* with analogous approach.

Abstract

Fingerprints of excitation and emission spectra of chlorophyll and phycobilin fluorescence can be used to differentiate 'spectral groups' of microalgae *in vivo* and *in situ*, e. g. vertical profiles can be taken within a few minutes. The investigated spectral groups of algae (green group - chlorophyta; blue - blue cyanobacteria; brown - heterokontophyta, haptophyta, dinophyta; red - red cyanobacteria and mixed - cryptophyta) are each characterised by a specific composition of photosynthetic antennae pigments and, consequently, by a specific excitation and emission spectrum of the chlorophyll and phycobilin fluorescence. Particularly relevant are chlorophyll *a*, chlorophyll *c*, phycocyanin, phycoerythrin, fucoxanthin and peridinin.

In a first approach, a laboratory based instrument and a submersible instrument were constructed containing light-emitting diodes to excite chlorophyll fluorescence in five distinct wavelength ranges to facilitate the differentiation of four spectral algal groups (green, blue, brown, mixed). They were measured under a fixed emission wavelength. Norm spectra were determined for the four spectral algal groups (several species per group). Using these norm spectra and the actual five-point excitation spectrum of a water sample, an estimate of the group-specific chlorophyll concentration is rapidly obtained for each algal group. This was accomplished by the development of a fast mathematical fit procedure. *In vivo* and *in situ* measurements based on calibration experiments were compared with results obtained by high performance liquid chromatography and biovolume estimations from the light microscope. Depth profiles of the distribution of spectral algal groups taken over a time period of few minutes were shown. The described method for algal differentiation opens new research areas and monitoring and supervision facilities related to photosynthetic primary production in aquatic environments.

Yellow substances (coloured dissolved organic matter) may interfere with the measurement because of an overlap of the excitation spectra with those of phytoplankton. The use of an ultra-violet excitation source (370 nm light-emitting diode) enabled differentiation between algal fluorescence and fluorescence by yellow substances. The resulting six-point excitation spectra were deconvoluted on the basis of norm spectra. A mean norm spectrum for yellow substances was obtained from natural samples. In a new submersible instrument the correction of chlorophyll fluorescence measurements for the influence of yellow substances was tested in *in vivo* and *in situ* experiments.

Specific problems associated with the principle of a free-falling depth profiler for algae discrimination were also considered. When F_0 , F and F_m are determined sequentially with one measuring cell, then phytoplankton inside the cell experiences a different light history according to different locations in the cell. This leads to a superposition of different induction curves of chlorophyll fluorescence. Mathematical algorithms were developed that enable the

evaluation of the integral fluorescence signal (averaged for 1s) for different velocities of the falling probe. This yields a correction factor which allows the usage of calibration factors obtained from stationary suspensions for the determination of algal concentrations in flowing suspensions. The predictions of the model were compared with measurements in flowing suspensions containing chlorophyta, cyanobacteria, cryptophyta and diatoms. The comparison showed the reliability of the algorithms. The requirement of corrections by the algorithm was high for dark-adapted cells and less important for light-adapted cells.

Fluorometric determination of the chlorophyll content of cyanobacteria is impeded by the unique structure of their photosynthetic apparatus, that is, the phycobilisomes in the light-harvesting antennae. The problems are caused by the variations in the ratio of the pigment phycocyanin to chlorophyll *a* resulting from adaptation to varying environmental conditions. In order to improve fluorometric analysis of algae a simplified energy distribution model describing energy pathways in the cyanobacterial photosynthetic apparatus was conceptualised. Two sets of mathematical equations were derived from this model and tested. Fluorescence of cyanobacteria was measured with a new fluorometer at seven excitation wavelength ranges and at three detection channels (650 nm, 685 nm and 720 nm) *in vivo*. By employing a new fit procedure it became possible to correct for variations in the cyanobacterial fluorescence excitation spectra and to account for other phytoplankton signals. The effect of energy state transitions on the phycocyanin fluorescence emission of phycobilisomes were documented. The additional use of the phycocyanin fluorescence signal at 650 nm in combination with the previously developed mathematical approach for phytoplankton analysis based on chlorophyll fluorescence spectroscopy allows a more detailed study of cyanobacteria and other phytoplankton *in vivo* and *in situ*.

The detection of red cyanobacteria with these newly developed methods is not possible because of adaptation processes of the cyanobacterial photosynthetic apparatus and spectral interferences with cryptophyta. To overcome these problems a simplified energy distribution model accounting for energy pathways in the red cyanobacterial photosynthetic apparatus and the apparatus of cryptophyta was designed. Mathematical equations were derived that enabled the calculation of the pigment content in both organisms: cryptophyta and red cyanobacteria. This resulted in the extension of a fluorometer previously developed for phytoplankton, with seven excitation wavelengths and four detection channels (600 nm, 620 nm, 650 nm and 685 nm). An extension of the fit procedure allowed corrections for variations in the fluorescence excitation spectra of red cyanobacteria and cryptophyta in the presence of other phytoplankton signals. The new approach provided correct fluorometric pigment estimation also in the presence of energy state transitions. The combination of fluorescence emission excitation matrices, the fluorescence models and the enhanced fit algorithm provides valuable information for phytoplankton analysis.

Finally, the set-up was tested successfully with natural samples. It enabled the determination of chlorophyll in five spectral groups of phytoplankton and of the phycobilins in three spectral types. A correction for yellow substances was included using mean fluorescence spectra of filtered natural samples. The pigment estimation of this method was compared to reference estimates obtained by high performance liquid chromatography and wet chemical

analysis of natural freshwater samples. Reference and fluorometric methods showed similar results. This measuring principle was installed as a submersible instrument which makes possible the measurement of fluorescence depth-profiles via pigment estimation *in situ* in a time scale of a few minutes. Profiles obtained with the instrument were compared to those obtained with the stationary instrument. The correlation between both methods was very high. This demonstrates the success and the large step forward in phytoplankton analysis achieved by this method.

Zusammenfassung

Fluoreszenzanregungs- und Emissionsspektren können ähnlich einem Fingerabdruck benutzt werden, um „spektrale Algengruppen“ des Phytoplanktons *in vivo* und *in situ* zu unterscheiden. Das ermöglicht z. B. die Aufnahme von Tiefenprofilen ihrer Pigmentverteilung in wenigen Minuten. Die spektralen Algengruppen (Grün – Chlorophyta, Blau – blaue Cyanobakterien, Bräunlich – Heterokontophyta, Dinophyta, Haptophyta, Rot – rote Cyanobakterien und Gemischt – Cryptophyta) lassen sich durch einen für die Gruppe spezifischen Aufbau der Photosyntheseantennenpigmente und damit mit einem spezifischen Fluoreszenzanregungs- und Emissionsspektrum der Chlorophyll- und Phycobilinfluoreszenz kennzeichnen

In einem ersten Ansatz wurden ein Laborgerät sowie eine Tauchsonde entwickelt. Leuchtdioden in diesen Geräten regten die Chlorophyllfluoreszenz in fünf verschiedenen Wellenlängenbereichen an. Gemessen wurde unter einer festen Emissionswellenlänge. Dieses ermöglichte die Unterscheidung von vier spektralen Algengruppen. Von diesen Gruppen wurden Normspektren (verschiedene Spezies pro Gruppe) aufgenommen. Diese Normspektren dienten in einem hier entwickelten mathematischen Anpassungsverfahren zur Online-Analyse dazu, aus einem Fünf-Punkt-Wasserprobenspektrum die Chlorophyllkonzentrationen der vier spektralen Algengruppen zu bestimmen.

In vivo und *in situ* Messungen wurden mit Ergebnissen aus der Hochdruck-Flüssigkeits-Chromatographie und Biovolumenbestimmungen mit Hilfe des Lichtmikroskops verglichen. Die beschriebene Methode eröffnet mannigfache Anwendungsmöglichkeiten in verschiedenen Forschungsgebieten und in unterschiedlichen Überwachungsaufgaben in aquatischen Gebieten.

Durch eine Überlappung von Gelbstoffspektren mit denen des Phytoplanktons können Gelbstoffe mit der Messung interferieren. Die Verwendung einer Ultraviolett-Lichtquelle (370 nm Leuchtdiode) ermöglichte die Differenzierung von Phytoplankton- und Gelbstofffluoreszenz. Das resultierende „Sechs-Punkt-Wasserprobenspektrum“ konnte mit Hilfe eines Dekonvolutionsverfahrens auf der Basis von Normkurvenspektren zerlegt werden. Hierbei gelang es, ein mittleres Normkurvenspektrum auch für Gelbstoffe zu definieren. In einer weiteren Tauchsonde konnte die neuentwickelte Gelbstoffkorrektur der Chlorophyllfluoreszenz durch *in vivo* und *in situ* Experimente getestet werden.

Als nächstes wurden Probleme betrachtet, die bei einer freifallenden Tauchsonde auftreten können. Wenn F_0 , F , und F_m sequentiell innerhalb einer Messzelle bestimmt werden, besitzt das darin befindliche Phytoplankton verschiedene Lichtvorgeschichten. Dieses führt zur Überlagerung von verschiedenen Induktionskurven der Chlorophyllfluoreszenz. Die Entwicklung mathematischer Algorithmen ermöglichte die Bestimmung der

Fluoreszenzsignale bei verschiedenen Fallgeschwindigkeiten. Daraus ergaben sich Faktoren, die eine Korrektur der Kalibrierfaktoren der stationären Messungen für Durchflussmessungen ermöglichten. Die Vorhersage des Modells wurde in Durchflussmessungen mit Phytoplankton suspensionen getestet (mit Chlorophyta, Cyanobakterien, Diatomeen und Cryptophyta). Bei helladaptierten Algen war die Korrektur durch das Modell wichtiger als bei dunkeladaptierten Algen.

Die fluorometrische Bestimmung des Chlorophyllgehaltes von Cyanobakterien wird durch die einzigartige Struktur ihres Photosyntheseapparates behindert. Hierbei sind die äußeren Antennen - die Phycobilisomen – besonders wichtig. Die Probleme bei der Chlorophyllbestimmung werden durch Veränderung des Phycocyanin zu Chlorophyllverhältnisses verursacht. Um die fluorometrische Chlorophyllbestimmung zu verbessern, wurde ein vereinfachtes Energieverteilungsmodell des Photosyntheseapparates von Cyanobakterien erstellt. Zwei verschiedene Gleichungssysteme, die sich aus dem Modell ergaben, wurden getestet und verglichen. Die Entwicklung eines neuen Fluorometer erlaubte die *in vivo* Messung der Fluoreszenz von Cyanobakterien bei sieben Anregungs- und drei Emissionswellenlängen.

Unter Verwendung eines neuen mathematischen Anpassungsverfahrens wurde es möglich, den Veränderungen in den Anregungsspektren von Cyanobakterien Rechnung zu tragen. Der Einfluss von Lichtkurzzeitadaptation auf die Fluoreszenzemission von Phycobilisomen wurde untersucht. Die zusätzliche Verwendung des Phycocyaninfluoreszenzsignals (gemessen bei einer Emissionswellenlänge von 650 nm) in Kombination mit dem vorher entwickelten mathematischen Ansatz zur Phytoplanktonanalyse erlaubte eine detailliertere Bestimmung von Cyanobakterien und anderem Phytoplankton *in vivo* und *in situ*.

Die Detektion von roten (phycoerythrinhaltigen) Cyanobakterien ist mit den hier zuvor entwickelten Methoden nicht möglich. Dieses liegt an Adaptationsprozessen des Photosyntheseapparates sowie an spektralen Überlagerungen mit Cryptophyta. Die Beseitigung dieser Probleme gelang mit vereinfachten Energieverteilungsmodellen der Photosyntheseapparate von roten Cyanobakterien und Cryptophyta. Die mathematische Beschreibung lieferte Gleichungen zur Pigmentbestimmung in beiden Organismen. Zur messtechnischen Umsetzung wurde das vorher entwickelte Fluorometer auf vier Detektionskanäle erweitert (600 nm, 620 nm, 650 nm und 685 nm). Eine Weiterentwicklung des mathematischen Anpassungsalgorithmus ermöglichte die fluorometrische Pigmentbestimmung in roten Cyanobakterien und Cryptophyta in der Anwesenheit von anderen spektralen Algengruppen. Der Einfluss von Kurzzeitlichtadaptation auf die Pigmentbestimmung wurde untersucht. Die Kombination der Fluoreszenzanregungs- und -emissionmatrizen, der Fluoreszenzmodelle und des verbesserten Anpassungsalgorithmus sorgt für eine weiter differenzierende Phytoplanktonanalyse.

Abschließend folgte der Test der Entwicklungen mit natürlichen Proben. Das Gerät und die neuen Algorithmen ermöglichten die Bestimmung der Chlorophyllkonzentrationen von fünf spektralen Algengruppen und von drei spektral verschiedenen Phycobilinen. Eine Gelbstoffkorrektur konnte auch hierfür mithilfe eines mittleren Spektrums von filtrierten

Wasserproben durchgeführt werden. Die Pigmentbestimmung dieser Methode wurde mit der von Referenzmessungen aus der Hochdruck-Flüssigkeits-Chromatographie und einer nasschemischen Bestimmung von natürlichen Wasserproben verglichen. Die Installation des Messprinzips in eine Tauchsonde ermöglichte die Messung von Fluoreszenztiefenprofilen innerhalb weniger Minuten. Der Vergleich der mit der Tauchsonde gemessenen Profile mit denen der stationären Messung des Laborgerätes machte deutlich, dass die Korrelation zwischen beiden Methoden sehr hoch war. Dieses demonstriert den Erfolg und den Fortschritt, die durch die Entwicklung dieser Methode erreicht wurden.

Appendix

Appendix A. Fitting by norm spectra

This fit procedure was employed in *Chapter 1*.
The measurement of a sample yields a vector

$$\underline{M} = (F_1, F_2, F_3, F_4, F_5) \quad (\text{A1})$$

with F_i being the Chl fluorescence measured at the wavelength no. i .

The norm curves are vectors

$$\underline{n}_k = (f_{k,1}, f_{k,2}, f_{k,3}, f_{k,4}, f_{k,5}) \quad (\text{A2})$$

with $f_{k,i}$ being the Chl fluorescence of the k -th norm spectrum measured at wavelength no. i .

Usually the contribution a_k of each group can be obtained by solving the linear regression problem (Tabrizi *et al.* (1998)) for

$$\underline{M} = \sum a_k \underline{n}_k \quad (\text{A3})$$

However, to account for different reliabilities from the $f_{i,k}$ of the norm curves depending on wavelength (index i) and on species (index k), the weighting factors $\sigma_{k,i}$ are introduced into the error sum

$$\chi^2(a_1, a_2, \dots) = \sum_{i=1}^{n_i} \left(\frac{F_i - \sum_{k=1}^{n_k} a_k f_{ki}}{\sum_{k=1}^{n_k} a_k \sigma_{ki}} \right)^2 \quad (\text{A4})$$

with: n_i = number of vector components, n_k = number of norm curves

Because of the a_k in the denominator, χ^2 is a non-linear function of the a_k . Non-linear minimisation algorithms for the solution of the problem are available (Press (1989); Tabrizi *et al.* (1998)). An iteration procedure turned out to converge faster. This is an advantage for on-line measurements. It begins with a guess for the a_k ($a_k = 1$) in the dominator and a fit using a linear regression for the a_k in the numerator. In the next step, the new a_k are used for the

denominator, etc. After two to three iteration steps the procedure converges, i.e. the a_k in the denominator and in the numerator became equal.

In detail, after the guess of the a_k the following parameters were calculated

$$\sigma_{i,j} = \sum_{k=1}^{n_k} a_{k,j} \sigma_{ki} \quad (\text{A5})$$

$$f_{i,k} = f_i / \sigma_{i,k} \quad (\text{A6})$$

$$N_{k,i,j} = N_{k,i} / \sigma_{i,j} \quad (\text{A7})$$

Then, a semi-linear fitting problem was obtained:

$$\chi_j^2 = \sum_{i=1}^{n_i} \left(f_{i,j} - \sum_{k=1}^{n_k} a_{k(j+1)} N_{k,i,j} \right)^2 \quad (\text{A8})$$

The absolute minimum of χ_j^2 is obtained for the Chl concentrations which are represented by the components of $\underline{a}_{(j+1)}$ (Gaussian normal method) with

$$\underline{a}_{(j+1)} = \left(\underline{\underline{N}}_j^T \underline{\underline{N}}_j \right)^{-1} \underline{\underline{N}}_j^T \underline{f}_j \quad (\text{A9})$$

When the Chl concentration of an algal group is zero or close to zero, the minimisation algorithm described above may result in negative values for the respective $C_{CHLa,k}$. Negative concentration values can occur due to the inaccuracy of the norm spectra or the noise in the fluorescence data. To overcome this problem, the following approach was useful: Whenever an iteration delivered a negative component of $\underline{a}_{(j)}$, the next iteration was done under the assumption that the respective $C_{CHLa,k}$ is zero. This means that the n_k -value and the dimension of the corresponding vectors and matrices are reduced in the subsequent iterations.

Applying the algorithm for determination of the individual Chl concentration showed that two iterations were sufficient.

Appendix B. Energy distribution model (blue cyanobacteria)

In phycobilisome containing organisms (like blue cyanobacteria) unlike the chlorophyta the assumption of REE involving all antenna pigments is not valid. For PBS-containing organisms, the excited state equilibration within the PS II core antenna is still under scrutiny, but it is highly likely that the assumption of REE for the PS II core antenna is sufficiently good. The REE domain, however, is unlikely to include the peripheral PS II antenna (meaning the PBS). Any absorption event occurring in the PBS system is followed by rapid transfer of excited state energy to the core antenna which competes with loss processes (fluorescence and non-radiative decays).

A simplified mathematical model that describes energy transfer and fluorescence processes within the cyanobacterial photosynthetic apparatus and which is useful for fluorometric *in situ* detection of cyanobacteria was set up as shown in Figure 5.5. This leads to the following mathematical description.

Fluorescence of PC in PBS containing algae. The following equations are only valid for algal suspensions which are sufficiently optically thin. Additional terms which correct for mutual shading of algae and for fluorescence reabsorption would otherwise be required. Thus, the fluorescence intensity of the pigments are

$$F_P(\lambda_{ML}, \lambda_{em}) = c_{instr, P} I_{ML}(\lambda_{ML}) N_P A_{eff,k}(\lambda_{ML}) \Phi_{F,P} \quad (B1)$$

with

P= 1: PC, P= 2 : PS II, P = 3: PS I

and $c_{instr, P}$ being the calibrating constant of the instrument obtained from the comparison of fluorescence data and spectrochemical determination (Figure 5.6 to 5.8), $I_{ML}(\lambda_{ML})$ the light intensity of the measuring light of wavelength λ_{ML} (in $\mu E m^{-2} s^{-1}$); N_P the number of pigment molecules in the sample volume; $\Phi_{F,P}$ the fluorescence yield of pigment P. $\Phi_{F, PS II}$ and its variability are discussed by Dau (1994b), Dau (1994a), Govindjee *et al.* (1996) and others.

The effective absorption cross-section (in m^2) per molecule $A_{eff,P}(\lambda_{ML})$ can be more complex due to energy transfer between pigments. $A_{eff,PC}$ depends only on PC, thus,

$$A_{eff,PC}(\lambda_{ML}) = A_{PC}(\lambda_{ML}) \quad (B2a)$$

In the case of the other ones, two pigments are always involved.

$$A_{\text{eff,PS II}}(\lambda_{\text{ML}}) = \Phi_{\text{T,PS II}}(\lambda_{\text{ML}}) A_{\text{peri,PS II}}(\lambda_{\text{ML}}) + A_{\text{core,PS II}}(\lambda_{\text{ML}}) \quad (\text{B2b})$$

$$A_{\text{eff,PS I}}(\lambda_{\text{ML}}) = \Phi_{\text{T,PS I}}(\lambda_{\text{ML}}) A_{\text{peri,PS I}}(\lambda_{\text{ML}}) + A_{\text{core,PS I}}(\lambda_{\text{ML}}) \quad (\text{B2c})$$

$\Phi_{\text{P,Q}}$: describes the energy transfer yield from pigment P to pigment Q.

In PBS containing algae, the peripheral antenna of PS I and PS II is PBS. Thus, the peripheral antenna of PS II and PS I is the same in cyanobacteria and is given as:

$$A_{\text{peri,PS I}}(\lambda_{\text{ML}}) = A_{\text{peri,PS II}}(\lambda_{\text{ML}}) = A_{\text{PCeff}}(\lambda_{\text{ML}}) = A_{\text{PC}}(\lambda_{\text{ML}}) \quad (\text{B3})$$

In PBS containing algae the absorption cross-section of the peripheral antenna of PS I and PS II is equal to the absorption cross section of the PBS in phycoerythrin-lacking cyanobacteria, and thus proportional to the PC content in the PBS (APC content is neglected). This leads to:

$$A_{\text{peri,PS II}}(\lambda_{\text{ML}}) = N_{\text{PC}}(\lambda_{\text{ML}})/N_{\text{PS II}} c_1(\lambda_{\text{ML}}) \text{ with } c_1(\lambda_{\text{ML}}) = \text{constant} \quad (\text{B4a})$$

and

$$A_{\text{peri,PS I}}(\lambda_{\text{ML}}) = N_{\text{PC}}(\lambda_{\text{ML}})/N_{\text{PS I}} c_2(\lambda_{\text{ML}}) \text{ with } c_2(\lambda_{\text{ML}}) = \text{constant} \quad (\text{B4b})$$

Overall fluorescence in PBS containing algae. The overall fluorescence for a single excitation and emission wavelength is given as a sum of the fluorescence of PC, PS II and PS I:

$$F_{\text{tot}}(\lambda_{\text{ML}}, \lambda_{\text{em}}) = F_{\text{PC}}(\lambda_{\text{ML}}, \lambda_{\text{em}}) + F_{\text{PS II}}(\lambda_{\text{ML}}, \lambda_{\text{em}}) + F_{\text{PS I}}(\lambda_{\text{ML}}, \lambda_{\text{em}}) \quad (\text{B5})$$

In the instrument of Figure 5.2, there are 7 excitation wavelengths (λ_{ML}) and 3 emission wavelengths (λ_{em}). Thus, Equation (B6) represents a set of 21 equations. Introducing Equations (B1) to (B4) converts Equation (B5) to:

$$F_{\text{tot}}(\lambda_{\text{ML}}, \lambda_{\text{em}}) = (N_{\text{PC}} (k_{1,\lambda_{\text{ML}},\lambda_{\text{em}}} + k_{2,\lambda_{\text{ML}},\lambda_{\text{em}}} + k_{4,\lambda_{\text{ML}},\lambda_{\text{em}}}) + (N_{\text{PS II}} k_{3,\lambda_{\text{ML}},\lambda_{\text{em}}}) + (N_{\text{PS I}} k_{5,\lambda_{\text{ML}},\lambda_{\text{em}}}) \quad (\text{B6})$$

with the gross rate constants (rate constants because they are fluorescence flux per pigment number)

$$k_{1,\lambda_{\text{ML}},\lambda_{\text{em}}} = I_{\text{ML}}(\lambda_{\text{ML}}) c_{\text{instr,PC}} A_{\text{PC}}(\lambda_{\text{ML}}) \Phi_{\text{F,PC}} \quad (\text{B7a})$$

$$k_{2,\lambda_{\text{ML}},\lambda_{\text{em}}} = I_{\text{ML}}(\lambda_{\text{ML}}) c_{\text{instr,PS II}} A_{\text{PC}}(\lambda_{\text{ML}}) c_1(\lambda_{\text{ML}}) \Phi_{\text{T,PS II}}(\lambda_{\text{ML}}) \quad (\text{B7b})$$

$$k_{3,\lambda_{\text{ML}},\lambda_{\text{em}}} = I_{\text{ML}}(\lambda_{\text{ML}}) c_{\text{instr,PS II}} A_{\text{core,PS II}}(\lambda_{\text{ML}}) \Phi_{\text{F,PS II}} \quad (\text{B7c})$$

$$k_{4,\lambda_{\text{ML}},\lambda_{\text{em}}} = I_{\text{ML}}(\lambda_{\text{ML}}) c_{\text{instr,PS I}} A_{\text{PC}}(\lambda_{\text{ML}}) \Phi_{\text{T,PS I}}(\lambda_{\text{ML}}) c_2(\lambda_{\text{ML}}) \quad (\text{B7d})$$

$$k_{5,\lambda_{\text{ML}},\lambda_{\text{em}}} = I_{\text{ML}}(\lambda_{\text{ML}}) c_{\text{instr,PS I}} A_{\text{core,PS I}}(\lambda_{\text{ML}}) \Phi_{\text{F,PS I}} \quad (\text{B7e})$$

In the Discussion of *Chapter 5* it is shown that under most circumstances these rate constants can be assumed to be constant (independent of species and growth conditions).

The determination of the pigment numbers N_P and of the 5 gross rate constants from the 14 Equations (B6) requires a lot of computer time that may not be available in on-line applications. As 8 unknown parameters need only 8 equations, the number of equations is reduced by the following assumptions:

First assumption. The number of PC molecules is proportional to the fluorescence intensity at an excitation wavelength of 610 nm and emission at the 650 nm channel. This means that $c_{instr,PC} I_{ML}(\lambda_{ML}) A_{PC}(\lambda_{ML}) \Phi_{F,PC}$ is set as constant in Equation (B1). No interference with PS II and PS I fluorescence is expected.

$$N_{PC} = c_{1,PC} F_{610,650} \quad (B8)$$

Since N_{PC} can be replaced by $F_{610,650}$ in Equation (B6), only two unknown variables remain in Equation (B6). Thus, two adequate equations (i.e, $F(\lambda_{1ML}, \lambda_{1em})$ and $F(\lambda_{2ML}, \lambda_{2em})$) out of the A6-set have to be selected to calculate $N_{PS II}$ and $N_{PS I}$.

This leads to the following solutions:

$$N_{PS I} = c_{1,PS I} F_{tot}(\lambda_{1ML}, \lambda_{1em}) - c_{2,PS I} F_{610,650} - c_{3,PS I} F_{tot}(\lambda_{2ML}, \lambda_{2em}) \quad (B9a)$$

$$N_{PS II} = c_{1,PS II} F_{tot}(\lambda_{1ML}, \lambda_{1em}) - c_{2,PS II} F_{610,650} - c_{3,PS II} F_{tot}(\lambda_{2ML}, \lambda_{2em}) \quad (B9b)$$

The coefficients $c_{1,PC}$, $c_{1,PS I}$, $c_{2,PS I}$, $c_{3,PS I}$ and $c_{1,PS II}$, $c_{2,PS II}$, $c_{3,PS II}$ have to be determined from calibration measurements like those in Figures 5.6 to 5.8, where the N_{PC} , $N_{PS I}$ and $N_{PS II}$ are known from (physico)chemical determinations.

Their relationships with the biophysical gross rate constants are:

for PS I

$$c_{1,PS I} = k_{3,\lambda_{1ML},\lambda_{1em}} [(k_{5,\lambda_{1ML},\lambda_{1em}} k_{3,\lambda_{2ML},\lambda_{2em}}) - (k_{5,\lambda_{2ML},\lambda_{2em}} k_{3,\lambda_{1ML},\lambda_{1em}})]^{-1} \quad (B10)$$

$$c_{2,PS I} = c_{1,PC} [(k_{1,\lambda_{1ML},\lambda_{1em}} + k_{2,\lambda_{1ML},\lambda_{1em}} + k_{4,\lambda_{1ML},\lambda_{1em}}) k_{3,\lambda_{2ML},\lambda_{2em}} - (k_{1,\lambda_{2ML},\lambda_{2em}} + k_{2,\lambda_{2ML},\lambda_{2em}} + k_{4,\lambda_{2ML},\lambda_{2em}}) k_{3,\lambda_{1ML},\lambda_{1em}}] [(k_{5,\lambda_{1ML},\lambda_{1em}} k_{3,\lambda_{2ML},\lambda_{2em}}) - (k_{5,\lambda_{2ML},\lambda_{2em}} k_{3,\lambda_{1ML},\lambda_{1em}})]^{-1} \quad (B11)$$

$$c_{3,PS I} = k_{3,\lambda_{2ML},\lambda_{2em}} [(k_{5,\lambda_{1ML},\lambda_{1em}} k_{3,\lambda_{2ML},\lambda_{2em}}) - (k_{5,\lambda_{2ML},\lambda_{2em}} k_{3,\lambda_{1ML},\lambda_{1em}})]^{-1} \quad (B12)$$

for PS II

$$c_{1,PS II} = k_{5,\lambda_{1ML},\lambda_{1em}} (k_{5,\lambda_{2ML},\lambda_{2em}} k_{3,\lambda_{1ML},\lambda_{1em}} - k_{5,\lambda_{1ML},\lambda_{1em}} k_{3,\lambda_{2ML},\lambda_{2em}})^{-1} \quad (B13)$$

$$c_{2,PS II} = c_{1,PC} [k_{5,\lambda_{1ML},\lambda_{1em}} (k_{1,\lambda_{2ML},\lambda_{2em}} + k_{2,\lambda_{2ML},\lambda_{2em}} + k_{4,\lambda_{2ML},\lambda_{2em}}) + (k_{1,\lambda_{1ML},\lambda_{1em}} + k_{2,\lambda_{2ML},\lambda_{2em}} + k_{4,\lambda_{2ML},\lambda_{2em}}) k_{5,\lambda_{2ML},\lambda_{2em}}] [(k_{5,\lambda_{2ML},\lambda_{2em}} k_{3,\lambda_{1ML},\lambda_{1em}} - k_{5,\lambda_{1ML},\lambda_{1em}} k_{3,\lambda_{2ML},\lambda_{2em}})]^{-1} \quad (B14)$$

$$c_{3,PS II} = (k_{5,\lambda_{2ML},\lambda_{2em}} k_{3,\lambda_{1ML},\lambda_{1em}} - k_{5,\lambda_{1ML},\lambda_{1em}} k_{3,\lambda_{2ML},\lambda_{2em}})^{-1} k_{5,\lambda_{2ML},\lambda_{2em}} \quad (B15)$$

Second assumption. The amount of Chl per PS II and PS I reaction centre ($p_{1,\text{Chl}}$, and $p_{2,\text{Chl}}$, respectively) is supposed to be constant. Under this assumption (whose validity is implied by Figures 5.7 and 5.8), the parameters $c_{1,\text{Chl}}$ to $c_{3,\text{Chl}}$ can be obtained from a fit of the conc_{Chl} (measured by HPLC) to a weighted sum of three fluorescence signals.

$$\text{conc}_{\text{Chl}} = c_{1,\text{Chl}} F_{\text{tot}}(\lambda_{1\text{ML}}, \lambda_{1\text{em}}) + c_{2,\text{Chl}} F_{610,650} + c_{3,\text{Chl}} F_{\text{tot}}(\lambda_{2\text{ML}}, \lambda_{2\text{em}}) \quad (\text{B16})$$

with the coefficients given by the parameters of Equations (B10) and (B15)

$$c_{1,\text{Chl}} = (c_{1,\text{PS II}} + c_{1,\text{PS I}}), c_{2,\text{Chl}} = -(c_{2,\text{PS II}} + c_{2,\text{PS I}}), c_{3,\text{Chl}} = -(c_{3,\text{PS II}} + c_{3,\text{PS I}}) \quad (\text{B17a,b,c})$$

During the calibration experiments, Equations (B17) can be used to control the calibration factors of Equations (B9), or Equation (B16) used to calculate Chl concentration in *in situ* experiments.

In order to determine cyanobacterial fluorescence in the presence of phytoplankton from other spectral algal groups it is necessary to deconvolute the measured fluorescence spectra into individual spectra that are designed for one group only. This is done by extending the fitting routine of *Chapter 2* and *Appendix A*.

Appendix C. Mathematical fit for several excitations wavelengths and detection wavelengths with variable cyanobacterial norm spectra

In order to calculate the fluorescence parameters ($F_{610,650}$, $F_{470,685}$, $F_{610,685}$) for scenario 1 (*Chapter 5*) and by Equations (B8), (B9b) and (B16), a fit procedure was developed that

- accounts for fluorescence emission from other spectral algal groups in the sample
- corrects for variations of the cyanobacterial norm spectra
- evaluates the fit for two emission channels
- is fast enough for implementation in on-line analysis.

Therefore the following matrices and vectors were defined:

$\underline{N}_{\lambda_{em},lem}$: (4 x 7) matrix of algal norm spectra at a single emission wavelength
(Figure 5.10)

$\underline{C}_{\lambda_{em}}$: (7 x 40) matrix of cyanobacterial norm spectra at a single emission wavelength
(Figure 5.9 A and B)

$\underline{a}_{\lambda_{em},lem}$: (1x4) solution vector of phytoplankton concentrations for four phytoplankton groups.

$\underline{f}_{\lambda_{em}}$: (1 x 7) vector, measured F-spectrum at a single detection wavelength
(7 excitation wavelengths)

λ_{em} : detection wavelength (650 nm, 685 nm in scenario 1).

The variability of the norm spectra of the blue cyanobacteria requires a non-linear fit routine. Thus, the fit routine was split into two parts, the core fit and the main fit. The core fit was a subroutine of the main fit. The main fit selected two spectra, one out of the set of 40 norm spectra of the 650 nm detector and one of the 685 nm detector (Figure 5.9). These two norm spectra were handed over to the core fit. The core fit used these individual blue norm spectra and calculated the error sums by linear regression of the two measured spectra at 650 nm and 685 nm. Under the guidance of a simplex algorithm (Nelder & Mead (1965)), this procedure was repeated. Finally, the main fit took that pair of norm spectra and the resulting weighting factors which delivered the minimum error sum as the true fit.

Core fit. The core fit calculated two linear regressions to approximate the measured spectra at 650 nm and at 685 nm using the three norm spectra from the three algal groups plus the 650 nm or 685 nm norm spectrum of the cyanobacteria as proposed by the main fit, if scenario 1 was used.

This yielded two sets of $a_{\lambda_{em},\lambda_{em}}$ (concentrations) of the individual groups

$$a_{\lambda_{em},\lambda_{em}} = \left(N_{\lambda_{em},\lambda_{em}}^T N_{\lambda_{em},\lambda_{em}} \right)^{-1} N_{\lambda_{em},\lambda_{em}}^T f_{\lambda_{em}} \quad (C1)$$

for $\lambda_{em} = 650$ nm and 685 nm, separately, with the error sum

$$\chi_{\lambda_{em},\lambda_{em}}^2 = \sum_{i=1}^{n_i} \left(f_{i,\lambda_{em}} - \sum_{k=1}^{n_k} a_{k,\lambda_{em}} N_{k,i,\lambda_{em},\lambda_{em}} \right)^2 \quad (C2)$$

with n_i (number of LEDs) = 7, n_k (number of groups) = 4.

In order to prevent negative elements of the solution vectors $a_{\lambda_{em},\lambda_{em}}$ all permutations with one to four algal groups being excluded were tested. The combination of algal groups which had a solution vector $a_{\lambda_{em},\lambda_{em}}$ without negative elements and yielded the smallest $\chi_{\lambda_{em},\lambda_{em}}^2$ was handed over to the main fit.

Main fit. This algorithm minimised

$$\chi_{I_{650},I_{685}}^2 = \chi_{650,I_{650}}^2 + \chi_{685,I_{685}}^2 \quad (C3)$$

by suggesting different pairs of norm spectra with the indices $I_{650\text{ nm}}$ $I_{685\text{ nm}}$ to the core fit under the guidance of a simplex algorithm (Nelder & Mead (1965)). The first three components of the final solution vector $a_{685,I_{685}}$ provided the concentrations of the three algal groups. The fourth components of $a_{685,I_{685}}$ and $a_{650,I_{650}}$ were taken to calculate the real spectra of the cyanobacteria at 685 nm and 650 nm. These spectra were used for the analysis described in *Appendix B*.

Appendix D. Fluorescence model of phycoerythrin-containing cyanobacteria

The flux of energy between the pigment systems of red cyanobacteria and the resulting generation of fluorescence are illustrated in Figure 6.6. The implications for fluorometric Chl determination of PE as an additional pigment in cyanobacteria are described in mathematical terms below. The derivations are done under the assumption that the algal suspensions are optically sufficiently thin, otherwise additional terms would be required to correct for mutual shading of algae and for fluorescence reabsorption. The mathematical description is similar to that for cyanobacteria containing only PC and APC in *Chapter 5* and *Appendix B*.

Fluorescence of pigments. The fluorescence intensity of the pigments are

$$F_P(\lambda_{ML}, \lambda_{em}) = c_{instr, P} I_{ML}(\lambda_{ML}) N_P A_{eff,k}(\lambda_{ML}) \Phi_{F,P} \quad (D1)$$

with

$$P=1 : PE; P= 2: PC, P= 3 : PS II, P = 4: PS I$$

and $c_{instr, P}$ being the calibrating constant of the instrument, $I_{ML}(\lambda_{ML})$ the light intensity of the measuring light of wavelength λ_{ML} (in $\mu E m^{-2} s^{-1}$); N_P the number of pigment molecules in the sample volume; $\Phi_{F,P}$ the fluorescence yield of pigment P. $\Phi_{F, PS II}$ and its variability are discussed by Dau (1994b), Dau (1994a), Govindjee *et al.* (1996) and others.

The effective absorption cross-section (in m^2) per molecule $A_{eff,P}(\lambda_{ML})$ can be more complex due to energy transfer between pigments. Only $A_{eff,PE}$ depends only on PE, thus,

$$A_{eff,PE}(\lambda_{ML}) = A_{PE}(\lambda_{ML}) \quad (D2a)$$

In the case of the other ones always two pigments are involved

$$A_{eff,PC}(\lambda_{ML}) = \Phi_{T,PC}(\lambda_{ML}) N_{PE} A_{PE}(\lambda_{ML}) + N_{PC} A_{PC}(\lambda_{ML}) \quad (D2b)$$

$$A_{eff,PS II}(\lambda_{ML}) = \Phi_{T,PS II}(\lambda_{ML}) A_{peri,PS II}(\lambda_{ML}) + A_{core,PS II}(\lambda_{ML}) \quad (D2c)$$

$$A_{eff,PS I}(\lambda_{ML}) = \Phi_{T,PS I}(\lambda_{ML}) A_{peri,PS I}(\lambda_{ML}) + A_{core,PS I}(\lambda_{ML}) \quad (D2d)$$

$\Phi_{P,Q}$: describes the energy transfer yield from pigment P to pigment Q.

In PBS containing algae the peripheral antenna of PS I and PS II is the PBS. Thus, the peripheral antenna of PS II and PS I is the same in cyanobacteria and are given as.

$$A_{peri,PS I}(\lambda_{ML}) = A_{peri,PS II}(\lambda_{ML}) = A_{PCeff}(\lambda_{ML}) = \Phi_{T,PC}(\lambda_{ML}) N_{PE} A_{PE}(\lambda_{ML}) + A_{PC}(\lambda_{ML}) \quad (D3)$$

Total fluorescence in PBS containing algae. The total fluorescence (F without pigment index) is given as a sum of the fluorescence intensities given above.

$$F(\lambda_{ML}, \lambda_{em}) = F_{PE}(\lambda_{ML}, \lambda_{em}) + F_{PC}(\lambda_{ML}, \lambda_{em}) + F_{PS II}(\lambda_{ML}, \lambda_{em}) + F_{PS I}(\lambda_{ML}, \lambda_{em}) \quad (D4)$$

The instrument has 7 excitation wavelengths (λ_{ML}) and 4 emission wavelengths (λ_{em}). Thus Equation (D4) represents a set of 28 equations. Introducing Equations (D1) to (D3) converts Equation (D4) to

$$F(\lambda_{ML}, \lambda_{em}) = [k_{1,\lambda_{ML},\lambda_{em}} N_{PE}] + [k_{2,\lambda_{ML},\lambda_{em}} N_{PE} + k_{3,\lambda_{ML},\lambda_{em}} N_{PC}] + [k_{4,\lambda_{ML},\lambda_{em}} N_{PE} + k_{5,\lambda_{ML},\lambda_{em}} N_{PC} + k_{6,\lambda_{ML},\lambda_{em}} N_{PS II}] + [k_{7,\lambda_{ML},\lambda_{em}} N_{PE} + k_{8,\lambda_{ML},\lambda_{em}} N_{PC} + k_{9,\lambda_{ML},\lambda_{em}} N_{PS I}] \quad (D5)$$

with the gross rate constants (rate constants because they are fluorescence flux per pigment number).

$$k_{1,\lambda_{ML},\lambda_{em}} = I_{ML}(\lambda_{ML}) c_{instr,PE} A_{PE}(\lambda_{ML}) \Phi_{F,PE} \quad (D6a)$$

$$k_{2,\lambda_{ML},\lambda_{em}} = I_{ML}(\lambda_{ML}) c_{instr,PC} \Phi_{T,PC}(\lambda_{ML}) A_{eff,PE}(\lambda_{ML}) \Phi_{F,PC} \quad (D6b)$$

$$k_{3,\lambda_{ML},\lambda_{em}} = I_{ML}(\lambda_{ML}) c_{instr,PC} A_{PC}(\lambda_{ML}) \Phi_{F,PC} \quad (D6c)$$

$$k_{4,\lambda_{ML},\lambda_{em}} = I_{ML}(\lambda_{ML}) c_{instr,PS II} \Phi_{T,PS II}(\lambda_{ML}) \Phi_{F,PS II} \Phi_{T,PC}(\lambda_{ML}) N_{PE} A_{eff,PE}(\lambda_{ML}) \quad (D6d)$$

$$k_{5,\lambda_{ML},\lambda_{em}} = I_{ML}(\lambda_{ML}) c_{instr,PS II} \Phi_{T,PS II}(\lambda_{ML}) \Phi_{F,PS II} N_{PC} A_{PC}(\lambda_{ML}) \quad (D6e)$$

$$k_{6,\lambda_{ML},\lambda_{em}} = I_{ML}(\lambda_{ML}) c_{instr,PS II} A_{core,PS II}(\lambda_{ML}) \Phi_{F,PS II} \quad (D6f)$$

$$k_{7,\lambda_{ML},\lambda_{em}} = I_{ML}(\lambda_{ML}) c_{instr,PS I} \Phi_{T,PS I}(\lambda_{ML}) \Phi_{T,PC}(\lambda_{ML}) A_{eff,PE}(\lambda_{ML}) \Phi_{F,PS I} \quad (D6g)$$

$$k_{8,\lambda_{ML},\lambda_{em}} = I_{ML}(\lambda_{ML}) c_{instr,PS I} \Phi_{T,PS I}(\lambda_{ML}) A_{PC}(\lambda_{ML}) \Phi_{F,PS I} \quad (D6h)$$

$$k_{9,\lambda_{ML},\lambda_{em}} = I_{ML}(\lambda_{ML}) c_{instr,PS I} A_{core,PS I}(\lambda_{ML}) \Phi_{F,PS I} \quad (D6i)$$

In order to solve the set of Equations (D4) it is necessary that the gross rate constants of Equation (D6) are constant, i.e., independent of light intensity and growth conditions. This leads to the first assumption.

First assumption. The gross rate constants $k_{i,\lambda_{ML},\lambda_{em}}$ remain constant. This assumption needs comments, and in the Discussion of *Chapter 6* its validity is considered with the result that it is verified by reported results from other workers and by the experimental findings (compare Appendix B).

The determination of the pigment numbers N_P and of the 9 gross rate constants from the 28 equations (D4) needs a lot of computer time that may be not available in on-line applications. As 13 unknown parameters need only 13 equations, the number of equations is reduced by the following assumptions:

Second assumption. A simple solution of Equation (D4) is obtained under the assumption that fluorescence emission at 600 nm and 650 nm induced by excitation with 570 nm light originates mainly from PE and PC molecules. Representing this assumption separately for emission at 600 nm and 650 nm leads to the

$$F_{570,600} = F_{PE,570,600} + F_{PC,570,600} \quad \text{and} \quad F_{PS II,570,600} \approx F_{PS I,570,600} \approx 0 \quad (\text{D7a,b,c})$$

$$F_{570,650} = F_{PE,570,650} + F_{PC,570,650} \quad \text{and} \quad \text{with } F_{PS II,570,650} \approx F_{PS I,570,650} \approx 0 \quad (\text{D7d,e,f})$$

Equations (D7a-f) lead to the omission of $N_{PS II}$ and $N_{PS I}$ in the equations for $F_{570,600}$ and $F_{570,650}$ in the D4-set. The solution of the resulting system of two equations leads a simple relationship between N_{PE} and N_{PC} to the two signals $F_{570,650}$ and $F_{570,600}$.

$$N_{PE} = c_{1,PE} F_{570,650} + c_{2,PE} F_{570,600} \quad (\text{D8})$$

The $c_{i,PE}$ have to be determined by calibration experiments (Figure 6.8A and B). Their relationship to the gross rate constants (Equations (D6)) is obtained from the solution of Equations (D7):

$$c_{1,PE} = -k_{3,570,600} k_{3,570,650}^{-1} (k_{1,570,600} + k_{2,570,600} - k_{1,570,650} k_{3,570,650}^{-1} k_{3,570,600} - k_{2,570,650} k_{3,570,600} k_{3,570,650}^{-1}) \quad (\text{D9a})$$

$$c_{2,PE} = (k_{1,570,600} + k_{2,570,600} - k_{1,570,650} k_{3,570,650}^{-1} k_{3,570,600} - k_{2,570,650} k_{3,570,600} k_{3,570,650}^{-1})^{-1} \quad (\text{D9b})$$

and

$$N_{PC} = c_{1,PC} F_{570,650} + c_{2,PC} F_{570,600} \quad (\text{D10})$$

$$\text{with } c_{1,PC} = (k_{1,570,600} + k_{2,570,600}) (-k_{3,570,650} (k_{1,570,650} + k_{2,570,650})^{-1} - k_{3,570,600} (k_{1,570,600} + k_{2,570,600})^{-1})^{-1} \quad (\text{D11a})$$

$$c_{2,PC} = (k_{1,570,650} + k_{2,570,650}) (-k_{3,570,650} (k_{1,570,650} + k_{2,570,650})^{-1} - k_{3,570,600} (k_{1,570,600} + k_{2,570,600})^{-1})^{-1} \quad (\text{D11b})$$

Since N_{PE} and N_{PC} can be replaced by $F_{570,650}$ and $F_{570,600}$ in Equation (D5), only two unknown variables remain in Equation (D5). Thus, two adequate equations (i.e, $F(\lambda_{1ML}, \lambda_{1em})$ and $F(\lambda_{2ML}, \lambda_{2em})$) out of the D5-set have to be selected to calculate $N_{PS II}$ and $N_{PS I}$.

This leads to the following solutions

$$N_{PS II} = c_{1,PS II} F(\lambda_{1ML}, \lambda_{1em}) + c_{2,PS II} F(\lambda_{2ML}, \lambda_{2em}) + c_{3,PS II} F_{570,650} + c_{4,PS II} F_{570,600} \quad (\text{D12a})$$

and

$$N_{PS\ I} = c_{1,PS\ I} F(\lambda_{1ML}, \lambda_{1em}) + c_{2,PS\ I} F(\lambda_{2ML}, \lambda_{2em}) + c_{3,PS\ I} F_{570,650} + c_{4,PS\ I} F_{570,600} \quad (D12b)$$

$F(\lambda_{1ML}, \lambda_{1em})$ and $F(\lambda_{2ML}, \lambda_{2em})$ were selected using the findings of *Chapter 5* where it was found that PS II fluorescence was mainly represented at a wavelength of maximal phycobilin absorption (570 nm in case of PE) and 685 nm emission. PS I gives the strongest signal under Chl absorption (470 nm) and 685 nm emission. This leads to the selection of

$$F(\lambda_{1ML}, \lambda_{1em}) = F_{570,685} \quad (D13)$$

and

$$F(\lambda_{2ML}, \lambda_{2em}) = F_{470,685} \quad (D14)$$

The parameters $c_{i,PS\ II}$ and $c_{i,PS\ I}$ of Equation (D12) have to be determined by calibration experiments like those in Figure 6.8. Their relationship to the gross rate constants (Equations (D6)) are obtained from a solution of the two selected Equations (D18) with N_{PC} and N_{PE} being substituted by Equations (D8) and (D10).

For PS II:

$$c_{1,PS\ II} = k_{9,570,685}^{-1} [k_{9,470,685}^{-1} k_{6,470,685} - k_{9,570,685}^{-1} k_{6,570,685}]^{-1} \quad (D15)$$

$$c_{2,PS\ II} = k_{9,470,685}^{-1} [k_{9,470,685}^{-1} k_{6,470,685} - k_{9,570,685}^{-1} k_{6,570,685}]^{-1} \quad (D16)$$

$$\begin{aligned} c_{3,PS\ II} = & ([k_{1,470,685} + k_{2,470,685} + k_{4,470,685} + k_{7,470,685}] k_{9,470,685}^{-1} - \\ & [k_{1,570,685} + k_{2,570,685} + k_{4,570,685} + k_{7,570,685}] k_{9,570,685}^{-1} \\ & [k_{9,470,685}^{-1} k_{6,470,685} - k_{9,570,685}^{-1} k_{6,570,685}]^{-1} \\ & [- k_{3,570,600} k_{3,570,650}^{-1} \\ & (k_{1,570,600} + k_{2,570,600} - k_{1,570,650} k_{3,570,650}^{-1} k_{3,570,600} - k_{2,570,650} k_{3,570,600} k_{3,570,650}^{-1})) + \\ & ([k_{3,470,685} + k_{5,470,685} + k_{8,470,685}] k_{9,470,685}^{-1} + \\ & [k_{3,570,685} + k_{5,570,685} + k_{8,570,685}] k_{9,570,685}^{-1}) \\ & [k_{9,470,685}^{-1} k_{6,470,685} - k_{9,570,685}^{-1} k_{6,570,685}]^{-1} \\ & [(k_{1,570,600} + k_{2,570,600}) (- k_{3,570,650} (k_{1,570,650} + k_{2,570,650})^{-1} - \\ & k_{3,570,600} (k_{1,570,600} + k_{2,570,600})^{-1})^{-1}] \end{aligned} \quad (D17)$$

$$\begin{aligned}
c_{4,PS II} = & \quad ([k_{1,470,685} + k_{2,470,685} + k_{4,470,685} + k_{7,470,685}] k_{9,470,685}^{-1} - & \quad (D18) \\
& [k_{1,570,685} + k_{2,570,685} + k_{4,570,685} + k_{7,570,685}] k_{9,570,685}^{-1} \\
& [k_{9,470,685}^{-1} k_{6,470,685} - k_{9,570,685}^{-1} k_{6,570,685}]^{-1} \\
& [(k_{1,570,600} + k_{2,570,600} - k_{1,570,650} k_{3,570,650}^{-1} k_{3,570,600} - \\
& k_{2,570,650} k_{3,570,600} k_{3,570,650}^{-1})^{-1}] - \\
& ([k_{3,470,685} + k_{5,470,685} + k_{8,470,685}] k_{9,470,685}^{-1} + \\
& [k_{3,570,685} + k_{5,570,685} + k_{8,570,685}] k_{9,570,685}^{-1}) \\
& [k_{9,470,685}^{-1} k_{6,470,685} - k_{9,570,685}^{-1} k_{6,570,685}]^{-1} \\
& [(k_{1,570,650} + k_{2,570,650}) (- k_{3,570,650} (k_{1,570,650} + k_{2,570,650})^{-1} - \\
& k_{3,570,600} (k_{1,570,600} + k_{2,570,600})^{-1})^{-1}]
\end{aligned}$$

For PS I:

$$c_{1,PS I} = k_{6,570,685}^{-1} [k_{6,470,685}^{-1} k_{9,470,685} - k_{6,570,685}^{-1} k_{9,570,685}]^{-1} \quad (D19)$$

$$c_{2,PS I} = k_{6,470,685}^{-1} [k_{6,470,685}^{-1} k_{9,470,685} - k_{6,570,685}^{-1} k_{9,570,685}]^{-1} \quad (D20)$$

$$\begin{aligned}
c_{3,PS I} = & \quad ([k_{1,470,685} + k_{2,470,685} + k_{7,470,685} + k_{4,470,685}] k_{6,470,685}^{-1} - & \quad (D21) \\
& [k_{1,570,685} + k_{2,570,685} + k_{7,570,685} + k_{4,570,685}] k_{6,570,685}^{-1} \\
& [k_{6,470,685}^{-1} k_{9,470,685} - k_{6,570,685}^{-1} k_{9,570,685}]^{-1} \\
& [- k_{3,570,600} k_{3,570,650}^{-1} \\
& (k_{1,570,600} + k_{2,570,600} - k_{1,570,650} k_{3,570,650}^{-1} k_{3,570,600} - k_{2,570,650} k_{3,570,600} k_{3,570,650}^{-1})] + \\
& ([k_{3,470,685} + k_{8,470,685} + k_{5,470,685}] k_{6,470,685}^{-1} + \\
& [k_{3,570,685} + k_{8,570,685} + k_{5,570,685}] k_{6,570,685}^{-1}) \\
& [k_{6,470,685}^{-1} k_{9,470,685} - k_{6,570,685}^{-1} k_{9,570,685}]^{-1} \\
& [(k_{1,570,600} + k_{2,570,600}) (- k_{3,570,650} (k_{1,570,650} + k_{2,570,650})^{-1} - \\
& k_{3,570,600} (k_{1,570,600} + k_{2,570,600})^{-1})^{-1}]
\end{aligned}$$

$$\begin{aligned}
c_{4,PS I} = & \left([k_{1,470,685} + k_{2,470,685} + k_{7,470,685} + k_{4,470,685}] k_{6,470,685}^{-1} - \right. & (D22) \\
& [k_{1,570,685} + k_{2,570,685} + k_{7,570,685} + k_{4,570,685}] k_{6,570,685}^{-1} \\
& [k_{6,470,685}^{-1} k_{9,470,685} - k_{6,570,685}^{-1} k_{9,570,685}]^{-1} \\
& [(k_{1,570,600} + k_{2,570,600} - k_{1,570,650} k_{3,570,650}^{-1} k_{3,570,600} - \\
& k_{2,570,650} k_{3,570,600} k_{3,570,650}^{-1})^{-1}] - \\
& ([k_{3,470,685} + k_{8,470,685} + k_{5,470,685}] k_{6,470,685}^{-1} + \\
& [k_{3,570,685} + k_{8,570,685} + k_{5,570,685}] k_{6,570,685}^{-1}) \\
& [k_{6,470,685}^{-1} k_{9,470,685} - k_{6,570,685}^{-1} k_{9,570,685}]^{-1} \\
& [(k_{1,570,650} + k_{2,570,650}) (- k_{3,570,650} (k_{1,570,650} + k_{2,570,650})^{-1} - \\
& k_{3,570,600} (k_{1,570,600} + k_{2,570,600})^{-1})^{-1}]
\end{aligned}$$

Third assumption. The amount of Chl per PS II or PS I reaction centre is constant, i.e., independent of environmental conditions. Or if some of the reactions centres have a variable amount of associated Chl (e.g. during a repair cycle, (Baroli & Melis (1996)), then the analysis presents an average amount of Chl per PS II or PS I reaction centre.

In other words, in the sum

$$conc_{CHL} = p_{1,Chl} N_{PS I} + p_{2,Chl} N_{PS II} \quad (D23)$$

$p_{1,Chl}$, $p_{2,Chl}$ are assumed to be constant.

Introducing this assumption into Equations (D12) yields the Chl concentration

$$conc_{Chl} = c_{1,Chl} F_{570685} - c_{2,Chl} F_{470685} - c_{3,Chl} F_{570,650} - c_{4,Chl} F_{570,600} \quad (D24)$$

with the coefficients given by the parameters of Equations (D12a) and (D12b):

$$c_{1,Chl} = (c_{1,PS II} + c_{1,PS I}), \quad c_{2,Chl} = -(c_{2,PS II} + c_{2,PS I}), \quad (D25)$$

$$c_{3,Chl} = -(c_{3,PS II} + c_{3,PS I}), \quad c_{4,Chl} = -(c_{4,PS II} + c_{4,PS I}) \quad (D26)$$

Appendix E. Energy distribution model of cryptophytes

The flux of energy between the pigment systems of cryptophytes and the generation of fluorescence is illustrated in Figure 6.7. The derivations were done under the assumption that the algal suspensions are optically sufficiently thin. In cryptophytes the assumption of REE involving all antenna pigments is not valid like in chlorophyta. This is similar to the situation in cyanobacteria. Phycobilins in cryptophytes are localised in the thylakoid lumen. They can serve energy to the Chl c_2 -Chl a antenna. There is only downhill flux from PE to the Chl c_2 -Chl a antenna, thus REE does not hold. Within Chl c_2 -Chl a antenna, REE can be assumed.

The simple model of energy transfer processes in Figure 6.7 leads to a mathematical description that can be used as a basis for a mathematical fit procedure for the estimation of the pigments PE and Chl in cryptophytes.

Fluorescence of PE in cryptophyta. The fluorescence intensity of PE is:

$$F_{PE}(\lambda_{ML}, \lambda_{em}) = c_{instr,PE} N_{PE} I_{ML}(\lambda_{ML}) A_{PE}(\lambda_{ML}) \Phi_{F,PE} \quad (E1)$$

with $c_{instr,PE}$ = a calibration factor of the set-up, N_{PE} = number of PE molecules in the sample volume; $A_{PE}(\lambda_{ML})$ = PE molecule absorption cross-section (in m^2); I_{ML} = intensity of the measuring light (in $\mu E m^{-2} s^{-1}$); λ_{em} , fluorescence emission wavelength, λ_{ML} = wavelength of measuring light; $\Phi_{F,PE}$ = fluorescence yield of PE.

Fluorescence of PS II in cryptophytes. For the fluorescence emission of PS II this results in:

$$F_{PS II}(\lambda_{ML}, \lambda_{em}) = c_{instr,PS II} N_{PS II} I_{ML}(\lambda_{ML}) A_{eff,PS II}(\lambda_{ML}) \Phi_{F,PS II} \quad (E2)$$

$$\text{with} \quad A_{eff,PS II}(\lambda_{ML}) = \Phi_{T,PS II}(\lambda_{ML}) A_{peri,PS II}(\lambda_{ML}) + A_{corePS II}(\lambda_{ML}) \quad (E3)$$

with $c_{instr,PS II}$, $N_{PS II}$, $A_{PS II}(\lambda_{ML})$, I_{ML} defined similarly as in Equation (E1). $A_{peri,PS II}(\lambda_{ML})$ and $A_{core}(\lambda_{ML})$ are the individual absorption cross-sections of the peripheral (PE) and the core antenna (core antenna denotes in case of cryptophyta Chl c_2 -Chl a antenna + reaction centre, the ratio Chl c_2 /Chl a is assumed to be constant). The parameter $A_{eff,PS II}(\lambda_{ML})$ represents an effective absorption cross-section of the PS II (core complex & peripheral antenna); $\Phi_{F,PS II}$ and its variability are discussed in (e.g., Dau (1994b), Dau (1994a), Govindjee *et al.* (1996)). This denotes the wavelength-independent fluorescence yield measurable for direct (absorption by a pigment of the core antenna) or indirect excitation (energy transfer from the peripheral antenna to the core antenna) of the PS II-core antenna. $\Phi_{T,PS II}$: energy transfer yield from the peripheral antenna (PE) to the PS I-core antenna.

In order to allow the estimation of the number of PE molecules, the number of reaction centres and the total amount of Chl *a* in a sample volume from measured fluorescence spectra, two assumptions were made (tested and checked in the results section (*Chapter 6*) above.

Fluorescence of PS I in cryptophytes.

First assumption: As most Chl in cryptophyta resides within the peripheral antenna of PS II Chl fluorescence emission around 685 nm from PS I is assumed to be negligible.

Overall fluorescence in cryptophytes. The overall fluorescence for a single excitation and emission wavelength (in a wavelength range between 600 and 685 nm) is given as a sum of the fluorescence of PE and PS II:

$$F_{\text{tot}}(\lambda_{\text{ML}}, \lambda_{\text{em}}) = F_{\text{PE}}(\lambda_{\text{ML}}, \lambda_{\text{em}}) + F_{\text{PS II}}(\lambda_{\text{ML}}, \lambda_{\text{em}}) \quad (\text{E4})$$

By substituting $F_{\text{PE}}(\lambda_{\text{ML}}, \lambda_{\text{em}})$, $F_{\text{PS II}}(\lambda_{\text{ML}}, \lambda_{\text{em}})$ as given in Equation (E1) to (E3) it can be obtained:

$$F_{\text{tot}}(\lambda_{\text{ML}}, \lambda_{\text{em}}) = [(N_{\text{PE}} c_{\text{instr,PE}} I_{\text{ML}}(\lambda_{\text{ML}}) A_{\text{PE}}(\lambda_{\text{ML}}) \Phi_{\text{F,PE}})] + [(N_{\text{PS II}} c_{\text{instr,PS II}} I_{\text{ML}}(\lambda_{\text{ML}}) ((\Phi_{\text{T,PS II}}(\lambda_{\text{ML}}) A_{\text{peri,PS II}}(\lambda_{\text{ML}})) + A_{\text{core,PS II}}(\lambda_{\text{ML}})) \Phi_{\text{F,PS II}})] \quad (\text{E5})$$

In cryptophytes, the absorption cross-section of the peripheral antenna of PS II is equal to the absorption cross section of the PE. The absorption cross-section is proportional to the PE content in the antenna. Assuming that

$$A_{\text{peri,PS II}}(\lambda_{\text{ML}}) = c_1(\lambda_{\text{ML}}) N_{\text{PE}}/N_{\text{PS II}} \quad (\text{E6})$$

$$\text{with } c_1(\lambda_{\text{ML}}) = \text{constant and } c_2(\lambda_{\text{ML}}) = \text{constant leads to:} \quad (\text{E7})$$

$$F_{\text{tot}}(\lambda_{\text{ML}}, \lambda_{\text{em}}) = I_{\text{ML}}(\lambda_{\text{ML}}) [(N_{\text{PE}} c_{\text{instr,PE}} A_{\text{PE}}(\lambda_{\text{ML}}) \Phi_{\text{F,PE}})] + [c_{\text{instr,PS II}} ((c_1(\lambda_{\text{ML}}) \Phi_{\text{T,PS II}}(\lambda_{\text{ML}}) N_{\text{PE}} A_{\text{PE}}(\lambda_{\text{ML}})) + N_{\text{PS II}} A_{\text{core,PS II}}(\lambda_{\text{ML}})) \Phi_{\text{F,PS II}}] \quad (\text{E8})$$

Introducing the gross rate constants $k_{i,\lambda_{\text{ML}},\lambda_{\text{em}}}$

$$I_{\text{ML}}(\lambda_{\text{ML}}) c_{\text{instr,PE}} A_{\text{PE}}(\lambda_{\text{ML}}) \Phi_{\text{F,PE}} = k_{1,\lambda_{\text{ML}},\lambda_{\text{em}}} \quad (\text{E9})$$

$$I_{\text{ML}}(\lambda_{\text{ML}}) c_{\text{instr,PS II}} c_1(\lambda_{\text{ML}}) \Phi_{\text{T,PS II}}(\lambda_{\text{ML}}) A_{\text{PE}}(\lambda_{\text{ML}}) = k_{2,\lambda_{\text{ML}},\lambda_{\text{em}}} \quad (\text{E10})$$

$$I_{\text{ML}}(\lambda_{\text{ML}}) c_{\text{instr,PS II}} A_{\text{core,PS II}}(\lambda_{\text{ML}}) \Phi_{\text{F,PS II}} = k_{3,\lambda_{\text{ML}},\lambda_{\text{em}}} \quad (\text{E11})$$

into Equation (E8) leads to Equation (E12) for the overall fluorescence:

$$F_{\text{tot}}(\lambda_{\text{ML}}, \lambda_{\text{em}}) = [N_{\text{PE}} (k_{1,\lambda_{\text{ML}},\lambda_{\text{em}}} + k_{2,\lambda_{\text{ML}},\lambda_{\text{em}}}) + (N_{\text{PS II}} k_{3,\lambda_{\text{ML}},\lambda_{\text{em}}})] \quad (\text{E12})$$

Second assumption. The number of PE molecules is proportional to the fluorescence intensity at an excitation wavelength of the 570 nm LED and emission at the 620 nm channel. This means that $c_{\text{instr,PE}} I_{\text{ML}}(\lambda_{\text{ML}}) A_{\text{PE}}(\lambda_{\text{ML}}) \Phi_{\text{F,PE}}$ is set as constant in Equation (E1). No interference with PS II and PS I fluorescence is expected.

$$F_{570,620} k_{1,620}^{-1} = N_{\text{PE}} \quad (\text{E13})$$

According to the *First assumption* it is assumed that Chl *a* amounts associated with PS I can be neglected in the total Chl estimation by fluorescence.

$$\text{Chl} \sim N_{\text{PS II}} = c_{1,\text{PS II}} F_{\text{tot}}(\lambda_{1\text{ML}}, \lambda_{1\text{em}}) - c_{2,\text{PS II}} F_{570,620} \quad (\text{E14})$$

$$F_{\text{tot}}(\lambda_{1\text{ML}}, \lambda_{1\text{em}}) = F_{570,685} \quad (\text{E15})$$

with:

$$c_{1,\text{PS II}} = k_{3,\lambda_{\text{ML}},\lambda_{\text{em}}}^{-1} \quad (\text{E16})$$

$$c_{2,\text{PS II}} = k_{1,620} (k_{1,\lambda_{\text{ML}},\lambda_{\text{em}}} + k_{2,\lambda_{\text{ML}},\lambda_{\text{em}}}) k_{3,\lambda_{\text{ML}},\lambda_{\text{em}}}^{-1} \quad (\text{E17})$$

Appendix F. Mathematical fit for cyanobacterial spectra with several excitations wavelengths and detection wavelengths using variable cyanobacterial norm spectra

In order to calculate the fluorescence parameters for the models in *Appendix D* and *E*, a fit procedure was developed that is capable of:

- accounting for fluorescence emission of other spectral algal groups,
- correcting for variations of the cyanobacterial norm spectra,
- evaluating the fit for four emission channels and
- providing rapid convergence for implementation in on-line analysis.

This was achieved by extending the fit routine of *Chapter 5* and *Appendix C* to four emission wavelengths under the use of the experiments of the result section of *Chapter 6*.

Therefore it was defined:

$N_{\lambda_{em}, \lambda_{em}}(\lambda_{ex}, g)$: (5 x 7) matrix of algal norm spectra at a single emission wavelength. The first index gives the emission wavelength used for the measurement of the norm spectrum. The second index is required because blue cyanobacteria are described by a set of norm spectra (as given in $C_{\lambda_{em}}$). One of these is selected for this N-Matrix. The number in parenthesis are λ_{ex} for the excitation wavelengths at the abscissa of a norm spectrum and g the number of the algal group). The values in the matrix are the fluorescence signals excited with wavelength λ_{ex} for algal group g and measured at emission wavelengths λ_{em} .

$N_{600nm, 620nm}(\lambda_{ex}, g)$: (2 x 14) matrix similar to $N_{600nm, 620nm}(\lambda_{ex}, g)$, but restricted to cryptophyta and red cyanobacteria ($g_{max}=2$). The rows contain two norm spectra measured at the two emission wavelengths 600 nm and 620 nm. The spectra can be seen in Figure 6.10 A and B.

$C_{\lambda_{em}}$: (7 x 40) matrix of blue cyanobacterial norm spectra at a single emission wavelength (Figure 5.9) obtained as described in *Chapter 5*. As mentioned above, the norm spectra of cyanobacteria change with environmental conditions and thus a set of 40 norm spectra are given in matrix C.

$\underline{C}_{600nm,620nm}(\mathbf{n})$	(40 x 14) matrix of blue cyanobacterial norm spectra similar to $C_{\lambda_{em}}$ at emission wavelengths of 600 nm and 620 nm obtained analogous to the description in <i>Chapter 5</i> .
$l_{\lambda_{em}}(\mathbf{n})$:	rows of $\underline{C}_{\lambda_{em}}$ at index n,
$l_{600nm,620nm}(\mathbf{n})$:	rows of $\underline{C}_{600nm,620nm}$ at index n,
$\underline{a}_{\lambda_{em},l_{\lambda_{em}}}$	solution vector of algal concentrations. This implies that the estimated alga concentration may depend on the emission wavelength and the actual norm curve of cyanobacteria.
$\underline{a}_{600nm,620nm}$:	solution vector of algal concentrations at 600 nm and 620 nm detection wavelength,
$\underline{f}_{\lambda_{em}}$:	measured F-spectrum at a single detection wavelength,
$\underline{f}_{600nm,620nm}$:	(1 x 14) vector measured F-spectrum at 600 nm and 620 nm detection wavelength,
λ_{em} :	detection wavelength (600 nm, 620 nm, 650 nm, 685 nm).

The variability of the norm spectra of the blue cyanobacteria requires a non-linear fit routine. Thus, the fit routine was split into two parts, the core fit and the main fit. The core was a subroutine of the main fit. The main fit selected one spectrum out of the set of 40 norm spectra of the blue cyanobacteria and handed it over to the core fit. The core fit always believed that this special blue norm spectrum was the true one and calculated the pigment concentrations by linear regression. However, the core fit was run under supervision of the main fit. The main fit gave to the core fit a sequence of different norm spectra of the blue cyanobacteria, selected by means of a simplex algorithms. During these repetitive runs of the core fit, the main fit inspected the error sums delivered by the core fit. Finally, the main fit took that one with the minimum error as the true fit.

Core fit. Considering all excitation and emission wavelengths, a linear regression for five algal groups had to be carried out with four (7x5) matrices. In order to save computer time, the observation that fluorescence at 600 nm and 620 nm mainly results from red cyanobacteria and cryptophyta was utilised to solve the problems in two steps. Thus, in a first step, the algal concentrations $a_{g,\lambda_{em}}$ were calculated from the signals obtained from the 650 nm and 685 nm detectors by minimising $\chi_{\lambda_{em},l_{\lambda_{em}}}^2$.

$$\chi_{\lambda_{em},l_{\lambda_{em}}}^2 = \sum_{\lambda_{ex}=1}^7 \left(f_{\lambda_{ex},\lambda_{em}} - \sum_{g=1}^5 a_{g,\lambda_{em}} N_{\lambda_{em},l_{\lambda_{em}}}(g,i) \right)^2 \quad \text{with } \lambda_{em} = 650 \text{ nm or } 685 \text{ nm} \quad (\text{F1})$$

The $a_{g,\lambda_{em}}$ are determined by linear regression

$$\underline{a}_{\lambda_{em},l_{\lambda_{em}}} = \left(\underline{N}_{\lambda_{em},l_{\lambda_{em}}}^T \underline{N}_{\lambda_{em},l_{\lambda_{em}}} \right)^{-1} \underline{N}_{\lambda_{em},l_{\lambda_{em}}}^T \underline{f}_{\lambda_{em}} \quad (\text{F2})$$

This enabled the calculation of the fluorescence signal expected at 600 and 620 nm

$$\underline{f_{3,600,620}(\lambda_{ex})} = \sum_{k=1}^3 \underline{a_{k,650nm}} N_{600nm,620nm,l_{650nm}}(\underline{g}, \lambda_{ex}) \quad (F3)$$

resulting from three groups, namely the green, blue and brown one. These fluorescence signals were subtracted from the measured signals at 600 nm or 620 nm, respectively. This led to a simplified version of Equation (F1) for 600nm and 620 nm that was free of the green, blue and brown group.

$$\chi_{600nm,620nm,l_{600nm},l_{620nm}}^2 = \sum_{i=1}^{n_i} \left(f_{i,600nm,620nm}^* - \sum_{k=1}^2 \underline{a_{k,600nm,620nm}} N_{k,i,600nm,620nm,l_{600nm},l_{620nm}} \right)^2 \quad (F4)$$

with f^* being the vector of the reduced values of measured fluorescence

$$f_{i,600nm,620nm}^* = f_{i,600nm,620nm} - \sum_{k=1}^3 \underline{a_{k,650nm}} N_{k,i,600nm,620nm,l_{600nm},l_{620nm}} \quad (F6)$$

for $\lambda_{em} = 600 \text{ nm}, 620 \text{ nm}$:

Linear regression led to

$$\underline{a_{600nm,620nm,l_{600nm},l_{620nm}}} = \left(\underline{N_{600nm,620nm,l_{600nm},l_{620nm}}}^T \underline{N_{600nm,620nm,l_{600nm},l_{620nm}}} \right)^{-1} \underline{N_{600nm,620nm,l_{600nm},l_{620nm}}}^T \underline{f_{\lambda_{em}}^*} \quad (F7)$$

The $\underline{a_{g,\lambda_{em}}}$ for the green, blue and brown group (Equation (F2)) and the $\underline{a_{g,\lambda_{em}}}$ for the red cyanobacteria and the cryptophyta (Equation (F7)) may include unlikely solutions. Such an unlikely solution could be negative values of the $\underline{a_{g,\lambda_{em}}}$. Unlikely solutions were therefore eliminated before the results of the core fit were handed over to the main fit

To prevent negative elements of the solution vectors $\underline{a_{685nm,1685nm}}$, $\underline{a_{650nm,1650nm}}$ and $\underline{a_{600nm,620nm,l_{600nm},l_{620nm}}}$ of Equations (F4) and (F5) it was tested whether one or more phytoplankton groups could be omitted. For this purpose, all permutations with one to four algal groups being excluded were tested. The combination of algal groups which had solution vectors $\underline{a_{685nm,1685nm}}$, $\underline{a_{650nm,1650nm}}$ and $\underline{a_{600nm,620nm,l_{600nm},l_{620nm}}}$ without negative elements and which supplied the smallest $\chi_{1685nm,1650nm}^2$ was stored and compared with the results of the following runs of the core with a different set of $l_{685nm}(k)$, $l_{650nm}(n)$ and $l_{600nm,620nm}(n)$.

Another constraint on the solution vectors results from the expectation that there has to be a limited range of allowed values (Figure 5.9 and 6.4).

$$\frac{\underline{a_{685nm,1685nm}}}{\underline{a_{650nm,1650nm}}} \text{ and } \frac{\underline{a_{600nm,620nm,l_{600nm},l_{620nm}}}}{\underline{a_{650nm,1650nm}}}$$

If these ratios were < 0.5 or > 1.5 the solution was rejected.

Main fit. To find the final solution for $\underline{a}_{685nm,1685nm}$, $\underline{a}_{650nm,1650nm}$ and $\underline{a}_{600nm,620nm,1600nm,620nm}$ $\chi_{1685nm,1650nm}^2$ was defined as follows

$$\chi_{1685nm,1650nm}^2 = \chi_{685nm,1685nm}^2 + \chi_{650nm,1650nm}^2 + \chi_{600nm,620nm,1600nm,620nm}^2 \quad (F8)$$

A simplex-algorithm (Nelder & Mead (1965)) was used to minimise $\chi_{1685nm,1650nm}^2$ of Equation (F8) by variation of the blue cyanobacterial norm curves. It selected one norm spectrum l_{685nm} from \underline{C}_{685nm} and one norm spectrum l_{650nm} from \underline{C}_{650nm} . Further one norm spectrum of $\underline{C}_{600nm,620nm}$ that had the same number as l_{650nm} (because both belong to PC-emission). The set of not unlikely $a_{g,\lambda em}$ obtained with that norm curve that gave the minimum $\chi_{1685nm,1650nm}^2$ was accepted as the final solution.

References

- Anderson D.M. (1997) Turning back the harmful red tide - commentary. *Nature*, 388, 513-514
- Andrizhiyevskaya E.G., Schwabe T.M.E., Germano M., D'Haene S., Kruip J., van Grondelle R. & Dekker J.P. (2002) Spectroscopic properties of psI-*psII* supercomplexes from the cyanobacterium *Synechococcus* PCC 7942. *Biochimica et Biophysica Acta-Bioenergetics*, 1556, 265-272
- Baker N.R. & Webber A.N. (1987) Interactions between photosystems. *Advances in Botanical Research Incorporating Advances in Plant Pathology*, 13, 1-66
- Barlow R.G., Cummings D.G. & Gibb S.W. (1997) Improved resolution of mono- and divinyl chlorophylls a and b and zeaxanthin and lutein in phytoplankton extracts using reverse phase C-8 hplc. *Marine Ecology-Progress Series*, 161, 303-307
- Baroli I. & Melis A. (1996) Photoinhibition and repair in *Dunaliella salina* acclimated to different growth irradiances. *Planta*, 198, 640-646
- Becker A., Meister A. & Wilhelm C. (2002) Flow cytometric discrimination of various phycobilin-containing phytoplankton groups in a hypertrophic reservoir. *Cytometry*, 48, 45-57
- Bennett A. & Bogorad L. (1973) Complementary chromatic adaptation in a filamentous blue-green- alga. *Journal of Cell Biology*, 58, 419-435
- Beutler M. (1998) *Entwicklung eines Verfahrens zur quantitativen Bestimmung von Algengruppen mit Hilfe computergestützter Auswertung spektralaufgelöster Fluoreszenzanregungsspektren*. Diplomarbeit. Univ. Kiel, Kiel
- Biggins J. & Bruce D. (1989) Regulation of excitation-energy transfer in organisms containing phycobilins. *Photosynthesis Research*, 20, 1-34
- Blankenship R.E. (1992) Origin and early evolution of photosynthesis. *Photosynthesis Research*, 33, 91-111
- Boekema E.J., Hifney A., Yakushevskaya A.E., Piotrowski M., Keegstra W., Berry S., Michel K.P., Pistorius E.K. & Kruip J. (2001) A giant chlorophyll-protein complex induced by iron deficiency in cyanobacteria. *Nature*, 412, 745-748
- Briantais J.M., Vernotte C., Krause G.H. & Weis E. (1986) Chlorophyll a fluorescence of higher plants: Chloroplasts and leaves. In: *Light emission by plants and bacteria*. (eds. Govindjee J & Ames D), pp. 539 - 586. Academic Press, Orlando
- Bryant D.A. (1995) *The molecular biology of cyanobacteria*. Kluwer Academic Publisher, Dordrecht.

- Campanella L., Crescentini G., Avino P. & Angiello L. (2000) Simple and rapid procedure for analyzing two phycocyanins (c-pc and apc) from *Spirulina platensis* algae using lplc and hplc methods. *Annali di Chimica*, 90, 153-161
- Campbell D., Hurry V., Clarke A.K., Gustafsson P. & Öquist G. (1998) Chlorophyll fluorescence analysis of cyanobacterial photosynthesis and acclimation. *Microbiology and Molecular Biology Reviews*, 62, 667-683
- Campbell D. & Öquist G. (1996) Predicting light acclimation in cyanobacteria from nonphotochemical quenching of photosystem II fluorescence, which reflects state transitions in these organisms. *Plant Physiology*, 111, 1293-1298
- Carmichael W.W. (2001) Health effects of toxin-producing cyanobacteria: "the cyanohabs". *Human and Ecological Risk Assessment*, 7, 1393-1407
- Carrick H.J. & Schelske C.L. (1997) Have we overlooked the importance of small phytoplankton in productive waters? *Limnology and Oceanography*, 42, 1613-1621
- Codd G.A., Bell S.G., Kaya K., Ward C.J., Beattie K.A. & Metcalf J.S. (1999) Cyanobacterial toxins, exposure routes and human health. *European Journal of Phycology*, 34, 405-415
- Colijn F., Petersen W., Petschatnikov M. & Schroeder F. (2002) A new system for automatic measurements of biological-chemical parameters from ferry boats. *Fishery and Environmental Management*, 08, 1-11
- Cowles T.J., Desiderio R.A. & Neuer S. (1993) In situ characterization of phytoplankton from vertical profiles of fluorescence emission-spectra. *Marine Biology*, 115, 217-222
- Csatorday K., Maccoll R., Csizmadia V., Grabowski J. & Bagyinka C. (1984) Exciton interaction in allophycocyanin. *Biochemistry*, 23, 6466-6470
- Dau H. (1994a) Molecular mechanisms and quantitative models of variable photosystem-II fluorescence. *Photochemistry and Photobiology*, 60, 1-23
- Dau H. (1994b) Short-term adaptation of plants to changing light intensities and its relation to photosystem-II photochemistry and fluorescence emission. *Journal of Photochemistry and Photobiology B-Biology*, 26, 3-27
- Dau H. (1996) On the relation between absorption and fluorescence emission spectra of photosystems: Derivation of a Stepanov relation for pigment clusters. *Photosynthesis Research*, 48, 139-145
- Dau H. & Sauer K. (1996) Exciton equilibration and photosystem II exciton dynamics - a fluorescence study on photosystem II membrane particles of spinach. *Biochimica et Biophysica Acta-Bioenergetics*, 1273, 175-190
- Demarsac N.T. & Houmard J. (1993) Adaptation of cyanobacteria to environmental stimuli - new steps towards molecular mechanisms. *Fems Microbiology Reviews*, 104, 119-189
- Desiderio R.A., Moore C., Lantz C. & Cowles T.J. (1997) Multiple excitation fluorometer for in situ oceanographic applications. *Applied Optics*, 36, 1289-1296
- Doerffer R. (1988) Remote sensing of sunlight induced phytoplankton fluorescence. In: *Application of chlorophyll fluorescence* (ed. Lichtenthaler K), pp. 269-274. Kluwer Academic Publishers, Dordrecht
- Edgar R.K. & Laird K. (1993) Computer-simulation of error rates of Poisson-based interval estimates of plankton abundance. *Hydrobiologia*, 264, 65-77

- Falkowski P.G. & Raven J.A. (1997) *Aquatic photosynthesis*. Blackwell Science, Oxford.
- Gantt E. (1986) Phycobilisomes. In: *Photosynthesis III. Encyclopedia of plant physiology. New ser., V.* (eds. Staehelin LA & Arntzen CJ), pp. 260-268. Springer-Verlag, Berlin
- Gantt E. & Lipschulz C. (1973a) Energy-transfer in phycobilisomes from phycoerythrin to allophycocyanin. *Journal of Phycology*, 9, 19-20
- Gantt E. & Lipschulz C. (1973b) Energy-transfer in phycobilisomes from phycoerythrin to allophycocyanin. *Biochimica et Biophysica Acta*, 292, 858-861
- Genty B., Briantais J.M. & Baker N.R. (1989) The relationship between the quantum yield of photosynthetic electron-transport and quenching of chlorophyll fluorescence. *Biochimica et Biophysica Acta*, 990, 87-92
- Gerhardt V. & Bodemer U. (1998) Delayed fluorescence excitation spectroscopy: A method for automatic determination of phytoplankton composition of freshwaters and sediments interstitial and of algal composition of benthos. *Limnologica*, 28, 313-323
- Gieskes W.W.C. & Kraay G.W. (1984) Phytoplankton, its pigments, and primary production at a central North-sea station in May, July and September 1981. *Netherlands Journal of Sea Research*, 18, 51-70
- Gilbert M., Wilhelm C. & Richter M. (2000) Bio-optical modelling of oxygen evolution using in vivo fluorescence: Comparison of measured and calculated photosynthesis/irradiance (P-I) curves in four representative phytoplankton species. *Journal of Plant Physiology*, 157, 307-314
- Gill E.M. & Wittmershaus B.P. (1999) Spectral resolution of low-energy chlorophylls in photosystem I of *Synechocystis* sp PCC 6803 through direct excitation. *Photosynthesis Research*, 61, 53-64
- Gillbro T., Sandstrom A., Sundstrom V. & Holzwarth A.R. (1983) Polarized absorption picosecond kinetics as a probe of energy-transfer in phycobilisomes of *Synechococcus* 6301. *Febs Letters*, 162, 64-68
- Gillbro T., Sandstrom A., Sundstrom V., Wendler J. & Holzwarth A.R. (1985) Picosecond study of energy-transfer kinetics in phycobilisomes of *Synechococcus* 6301 and the mutant an 112. *Biochimica et Biophysica Acta*, 808, 52-65
- Glazer A.N. (1989) Light guides - directional energy-transfer in a photosynthetic antenna. *Journal of Biological Chemistry*, 264, 1-4
- Gobets B., van Stokkum I.H.M., Rogner M., Kruij J., Schlodder E., Karapetyan N.V., Dekker J.P. & van Grondelle R. (2001) Time-resolved fluorescence emission measurements of photosystem I particles of various cyanobacteria: A unified compartmental model. *Biophysical Journal*, 81, 407-424
- Golubic S. & Lee S.J. (1999) Early cyanobacterial fossil record: Preservation, palaeoenvironments and identification. *European Journal of Phycology*, 34, 339-348
- Govindjee, Knox R.S. & Ames J. (1996) Photosynthetic unit: Antenna and reaction centers. *Photosynthesis Research*, 48, 1-2
- Gower J.e. & Borstad G. (1983) Use of in vivo fluorescence line at 685 nm for remote sensing survey of chlorophyll-a. In: *Oceanography from space*, pp. 329-338. Plenum Press, New York

- Guillard R.R.L. & Lorenzen C.J. (1972) Yellow-green algae with chlorophyllide c. *Journal of Phycology*, 8, 10-14
- Häder D. (1999) *Photosynthese*. Thieme, Stuttgart.
- Haeckel E. (1890) *Plankton-studien*. G. Fischer.
- Hallegraeff G.M. (1993) A review of harmful algal blooms and their apparent global increase. *Phycologia*, 32, 79-99
- Hansen U.P., Dau H., Bruning B., Fritsch T. & Moldaenke C. (1991) Linear-analysis applied to the comparative-study of the I-D-P phase of chlorophyll fluorescence as induced by actinic PS-II light, PS-I light and changes in CO₂-concentration. *Photosynthesis Research*, 28, 119-130
- Harnischfeger G. & Codd G.A. (1978) Factors affecting energy-transfer from phycobilisomes to thylakoids in *Anacystis-nidulans*. *Biochimica et Biophysica Acta*, 502, 507-513
- Harnischfeger G. & Herold B. (1981) Aspects of energy-transfer between phycobilins and chlorophyll in *Chroomonas spec* (cryptophyceae). *Berichte der Deutschen Botanischen Gesellschaft*, 94, 65-73
- Heber U., Egneus H., Hanck U., Jensen M. & Koster S. (1978) Regulation of photosynthetic electron-transport and photophosphorylation in intact chloroplasts and leaves of *spinacia-oleracea* l. *Planta*, 143, 41-49
- Holm-Hansen O. (1965) Fluorometric determination of chl. *Journal du conseil. Conseil Permanent International pour l'Exploration de la Mer*, 30, 3-15
- Holzwarth A.R. (1991) Structure-function-relationships and energy-transfer in phycobiliprotein antennae. *Physiologia Plantarum*, 83, 518-528
- Holzwarth A.R., Bittersmann E., Reuter W. & Wehrmeyer W. (1990) Studies on chromophore coupling in isolated phycobiliproteins. 3. Picosecond excited-state kinetics and time-resolved fluorescence-spectra of different allophycocyanins from *Mastigocladus-laminosus*. *Biophysical Journal*, 57, 133-145
- Holzwarth A.R., Wendler J. & Wehrmeyer W. (1982) Picosecond time resolved energy-transfer in isolated phycobilisomes from *Rhodella-violacea* (rhodophyceae). *Photochemistry and Photobiology*, 36, 479-487
- Hormann H., Neubauer C., Asada K. & Schreiber U. (1993) Intact chloroplasts display ph-5 optimum of O₂-reduction in the absence of methyl viologen - indirect evidence for a regulatory role of superoxide protonation. *Photosynthesis Research*, 37, 69-80
- Jeffrey S.W. & Hallegraeff G.M. (1980) Studies of phytoplankton species and photosynthetic pigments in a warm core eddy of the east Australian current. 1. Summer populations. *Marine Ecology-Progress Series*, 3, 285-294
- Junge W., Lill H. & Engelbrecht S. (1997) ATP synthase: An electrochemical transducer with rotatory mechanics. *Trends in Biochemical Sciences*, 22, 420-423
- Kalle K. (1961) The problem of the Gelbstoff in the sea. *Marine Biological Annual Review*, 4, 91-104
- Karukstis K.K. (1992) Chlorophyll fluorescence analyses of photosystem-II reaction center heterogeneity. *Journal of Photochemistry and Photobiology B-Biology*, 15, 63-74

- Katona E., Neimanis S., Schonknecht G. & Heber U. (1992) Photosystem I-dependent cyclic electron-transport is important in controlling photosystem-II activity in leaves under conditions of water-stress. *Photosynthesis Research*, 34, 449-464
- Kautsky H. & Hirsch A. (1931) Neue Versuche zur Kohlensäureassimilation. *Naturwissenschaften*, 19, 964-975
- Kawamura M., Mimuro M. & Fujita Y. (1979) Quantitative relationship between 2 reaction centers in the photosynthetic system of blue-green-algae. *Plant and Cell Physiology*, 20, 697-705
- Kazakevich Y. & McNair H. (2002) *Basic liquid chromatography*. Online Textbook: <http://hplc.chem.shu.edu/HPLC/index.html>.
- Kiefer D.A. (1973) Fluorescence properties of natural phytoplankton populations. *Marine Biology*, 22, 263-269
- Kolber Z. & Falkowski P.G. (1993) Use of active fluorescence to estimate phytoplankton photosynthesis in-situ. *Limnology and Oceanography*, 38, 1646-1665
- Kolber Z.S., Plumley F.G., Lang A.S., Beatty J.T., Blankenship R.E., VanDover C.L., Vetriani C., Koblizek M., Rathgeber C. & Falkowski P.G. (2001) Contribution of aerobic photoheterotrophic bacteria to the carbon cycle in the ocean. *Science*, 292, 2492-2495
- Kolber Z.S., Prasil O. & Falkowski P.G. (1998) Measurements of variable chlorophyll fluorescence using fast repetition rate techniques: Defining methodology and experimental protocols. *Biochimica et Biophysica Acta-Bioenergetics*, 1367, 88-106
- Kolbowski J. & Schreiber U. (1995) Computer-controlled phytoplankton analyzer based on a 4-wavelength PAM chl fluorometer. In: (ed. P M), pp. 825-828. Kluwer Academic Publishers, Dordrecht.
- Lampert W. & Sommer U. (1997) *Limnoecology: The ecology of lakes and streams*. Oxford University Press, New York; Oxford.
- Leboulanger C., Dorigo U., Jacquet S., Le Berre B., Paolini G. & Humbert J. (2002) Application of a submersible spectrofluorometer for rapid monitoring of freshwater cyanobacterial blooms: A case study. *Aquatic Microbial Ecology*, 30
- Lee T., Tsuzuki M., Takeuchi T., Yokoyama K. & Karube I. (1994) In-vivo fluorometric method for early detection of cyanobacterial waterblooms. *Journal of Applied Phycology*, 6, 489-495
- Lee T.Y., Tsuzuki M., Takeuchi T., Yokoyama K. & Karube I. (1995) Quantitative-determination of cyanobacteria in mixed phytoplankton assemblages by an in-vivo fluorometric method. *Analytica Chimica Acta*, 302, 81-87
- Ley A.C. (1984) Effective absorption cross-sections in *Porphyridium-cruentum* - implications for energy-transfer between phycobilisomes and photosystem-II reaction centers. *Plant Physiology*, 74, 451-454
- Lichtle C., Jupin H. & Duval J.C. (1980) Energy transfers from photosystem-2 to photosystem-1 in cryptomonas-rufescens (cryptophyceae). *Biochimica et Biophysica Acta*, 591, 104-112

- Lichtle C., McKay R.M.L. & Gibbs S.P. (1992) Immunogold localization of photosystem-I and photosystem-II light-harvesting complexes in cryptomonad thylakoids. *Biology of the Cell*, 74, 187-194
- Lotter A.F. (2001) The palaeolimnology of Soppensee (central Switzerland), as evidenced by diatom, pollen, and fossil-pigment analyses. *Journal of Paleolimnology*, 25, 65-79
- Maccoll R. & Berns D.S. (1978) Energy-transfer studies on cryptomonad biliproteins. *Photochemistry and Photobiology*, 27, 343-349
- MacColl R. & Guard-Friar D. (1987) *Phycobiliproteins*. CRC Press, Inc, Boca Raton, Florida.
- Mackey M.D., Mackey D.J., Higgins H.W. & Wright S.W. (1996) Chemtax - a program for estimating class abundances from chemical markers: Application to hplc measurements of phytoplankton. *Marine Ecology-Progress Series*, 144, 265-283
- Mantoura R.F.C. & Llewellyn C.A. (1983) The rapid-determination of algal chlorophyll and carotenoid- pigments and their breakdown products in natural-waters by reverse-phase high-performance liquid-chromatography. *Analytica Chimica Acta*, 151, 297-314
- Matthews B.J.H., Jones A.C., Theodorou N.K. & Tudhope A.W. (1996) Excitation-emission-matrix fluorescence spectroscopy applied to humic acid bands in coral reefs. *Marine Chemistry*, 55, 317-332
- McKay R.M.L., Lichtle C. & Gibbs S.P. (1992) Immunocytochemical characterization of the intrapyrenoid thylakoids of cryptomonads. *Journal of Phycology*, 28, 64-68
- Millie D.F., Dionigi C.P., Schofield O., Kirkpatrick G. & Tester P.A. (1999) The importance of understanding the molecular, cellular, and ecophysiological bases of harmful algal blooms. *Journal of Phycology*, 35, 1353-1355
- Millie D.F., Schofield O.M.E., Kirkpatrick G.J., Johnsen G. & Evens T.J. (2002) Using absorbance and fluorescence spectra to discriminate microalgae. *European Journal of Phycology*, 37, 313-322
- Mimuro M. & Fujita Y. (1978) Excitation-energy transfer between pigment system-2 units in blue-green-algae. *Biochimica et Biophysica Acta*, 504, 406-412
- Mimuro M., Yamazaki I., Yamazaki T. & Fujita Y. (1985) Excitation-energy transfer in the chromatically adapted phycobilin systems of blue-green-algae - difference in the energy-transfer kinetics at phycocyanin level. *Photochemistry and Photobiology*, 41, 597-603
- Mitchell P. (1977) Vectorial chemiosmotic processes. *Annual Review of Biochemistry*, 46, 996-1005
- Mittenzwey K.H., Sinn G., Roof N. & Harsdorf S. (1997) An improved lidar method for monitoring surface waters: Experiments in the laboratory. *International Journal of Remote Sensing*, 18, 2271-2276
- Moldaenke C., Vanselow K.H. & Hansen U.P. (1995) The 1-Hz fluorometer - a new approach to fast and sensitive long-term studies of active chlorophyll and environmental-influences. *Helgolander Meeresuntersuchungen*, 49, 785-796
- Müller C., Reuter W., Wehrmeyer W., Dau H. & Senger H. (1993) Adaptation of the photosynthetic apparatus of *Anacystis- nidulans* to irradiance and CO₂-concentration. *Botanica Acta*, 106, 480-487

- Myers J., Graham J.R. & Wang R.T. (1980) Spontaneous pigment mutants of *Anacystis-nidulans* selected by growth under far-red light. *Archives of Microbiology*, 124, 143-148
- Nelder J.A. & Mead R. (1965) A simplex-method for function minimization. *Computer Journal*, 7, 308-313
- Nusch E. (1980) Comparison of different methods for chlorophyll and phaeopigment determination. *Archiv für Hydrobiologie Beiheft, Ergebnisse der Limnologie*, 14, 14-36
- Ort D. (1994) Photosynthesis. In: *Encyclopedia of agricultural sciences* (eds. Arntzen C & Ritter E). Academic Press, San Diego
- Ort D. & Whitmarsh J. (1996) Specific features of excitation migration in photosynthesis. In: *Light as an energy source and information carrier in plant physiology* (ed. Jennings Rea). Plenum Press, New York
- Park Y.I., Sandstrom S., Gustafsson P. & Öquist G. (1999) Expression of the isia gene is essential for the survival of the cyanobacterium *Synechococcus* sp PCC 7942 by protecting photosystem II from excess light under iron limitation. *Molecular Microbiology*, 32, 123-129
- Pfündel E. (1998) Estimating the contribution of photosystem I to total leaf chlorophyll fluorescence. *Photosynthesis Research*, 56, 185-195
- Press W. (1989) *Numerical recipes*. University Press, Cambridge.
- Redlinger T. & Gantt E. (1982) A Mr 95,000 polypeptide in *Porphyridium-cruentum* phycobilisomes and thylakoids - possible function in linkage of phycobilisomes to thylakoids and in energy-transfer. *Proceedings of the National Academy of Sciences of the United States of America-Biological Sciences*, 79, 5542-5546
- Reuter W. & Müller C. (1993) Adaptation of the photosynthetic apparatus of cyanobacteria to light and CO₂. *Journal of Photochemistry and Photobiology B-Biology*, 21, 3-27
- Riethman H.C. & Sherman L.A. (1988) Purification and characterization of an iron stress-induced chlorophyll-protein from the cyanobacterium *Anacystis-nidulans* r2. *Biochimica et Biophysica Acta*, 935, 141-151
- Rippka R. & Herdman M. (1992) *Pasteur culture collection of cyanobacterial strains in axenic culture. Catalogue of strains*. Institut Pasteur, Paris, France.
- Rowan K.S. (1989) *Photosynthetic pigments of algae*. Cambridge University Press: New York; Cambridge.
- Ruser A. (2001) *Untersuchungen zur Erkennung von Algengruppen und deren photosynthetischer Aktivität im marinen Bereich*. Dissertation. Univ. Kiel, Kiel.
- Sandstrom S., Park Y.I., Öquist G. & Gustafsson P. (2001) Cp43', the isia gene product, functions as an excitation energy dissipator in the cyanobacterium *Synechococcus* sp PCC 7942. *Photochemistry and Photobiology*, 74, 431-437
- Sauer K. & Scheer H. (1988) Excitation transfer in c-phycocyanin - forster transfer rate and exciton calculations based on new crystal-structure data for c-phycocyanins from *Agmenellum-quadruplicatum* and *Mastigocladus-laminosus*. *Biochimica et Biophysica Acta*, 936, 157-170

- Schimanski J. (2002) *Entwicklung und Erprobung eines Durchflußsensors zur Algenklassenbestimmung durch Chlorophyll-Fluoreszenz*. Diplomarbeit. Univ. Kiel, Kiel.
- Schreiber U. (1994) New emitter-detector-cuvette assembly for measuring modulated chlorophyll fluorescence of highly diluted suspensions in conjunction with the standard PAM fluorometer. *Zeitschrift für Naturforschung C - a Journal of Biosciences*, 49, 646-656
- Schreiber U. & Bilger W. (1993) III. Progress in chlorophyll fluorescence research: Major developments during the past years in retrospect. *Progress in Botany*, 54, 151-173
- Schreiber U. & Krieger A. (1996) Two fundamentally different types of variable chlorophyll fluorescence in vivo. *Febs Letters*, 397, 131-135
- Schreiber U., Schliwa U. & Bilger W. (1986) Continuous recording of photochemical and nonphotochemical chlorophyll fluorescence quenching with a new type of modulation fluorometer. *Photosynthesis Research*, 10, 51-62
- Schubert H., Fulda S. & Hagemann M. (1993) Effects of adaptation to different salt concentrations on photosynthesis and pigmentation of the cyanobacterium *Synechocystis* sp PCC-6803. *Journal of Plant Physiology*, 142, 291-295
- Schubert H. & Hagemann M. (1990) Salt effects on 77k fluorescence and photosynthesis in the cyanobacterium *Synechocystis* sp PCC-6803. *Fems Microbiology Letters*, 71, 169-172
- Sciandra A., Lazzara L., Claustre H. & Babin M. (2000) Responses of growth rate, pigment composition and optical properties of *Cryptomonas* sp to light and nitrogen stresses. *Marine Ecology-Progress Series*, 201, 107-120
- Searle G.F.W., Barber J., Porter G. & Tredwell C.J. (1978) Picosecond time-resolved energy-transfer in *Porphyridium-cruentum* .2. Isolated light harvesting complex (phycobilisomes). *Biochimica et Biophysica Acta*, 501, 246-256
- Seppala J. & Balode M. (1998) The use of spectral fluorescence methods to detect changes in the phytoplankton community. *Hydrobiologia*, 363, 207-217
- Shoaf W.T. (1978) Rapid method for separation of chlorophylls-a and chlorophylls- b by high-pressure liquid-chromatography. *Journal of Chromatography*, 152, 247-249
- Stransky H. (1978) Method for the quantitative estimation of chloroplast pigments in the picomole-range by use of a isocratic hplc-system. *Zeitschrift für Naturforschung C - a Journal of Biosciences*, 33, 836-840
- Straus N. (1994) Iron deprivation: Physiology and gene regulation. In: *The molecular biology of cyanobacteria* (ed. Bryant D), pp. 731-750. Kluwer Academic Press, Dordrecht
- Suter G.W. & Holzwarth A.R. (1987) A kinetic-model for the energy-transfer in phycobilisomes. *Biophysical Journal*, 52, 673-683
- Tabrizi H., Schinner K., Spors J. & Hansen U.P. (1998) Deconvolution of the three components of the photoacoustic signal by curve fitting and the relationship of CO₂ uptake to proton fluxes. *Photosynthesis Research*, 57, 101-115

- Ting C.S., Rocap G., King J. & Chisholm S.W. (2002) Cyanobacterial photosynthesis in the oceans: The origins and significance of divergent light-harvesting strategies. *Trends in Microbiology*, 10, 134-142
- Utermöhl H. (1958) Zur Vervollkommnung der Quantitativen Phytoplankton Methodik. *Mitteilungen der Internationalen Vereinigung für Theoretische und Angewandte Limnologie*, 9, 1-38
- van den Hoek C., Mann D. & Jahns H. (1995) *Algae: An introduction to phycology*. Cambridge University Press, Cambridge; New York.
- van Grondelle R., Dekker J.P., Gillbro T. & Sundstrom V. (1994) Energy-transfer and trapping in photosynthesis. *Biochimica et Biophysica Acta-Bioenergetics*, 1187, 1-65
- van Kooten O. & Snel J.F.H. (1990) The use of chlorophyll fluorescence nomenclature in plant stress physiology. *Photosynthesis Research*, 25, 147-150
- van Thor J.J., Mullineaux C.W., Matthijs H.C.P. & Hellingwerf K.J. (1998) Light harvesting and state transitions in cyanobacteria. *Botanica Acta*, 111, 430-443
- Waterbury J.B., Watson S.W., Guillard R.R.L. & Brand L.E. (1979) Widespread occurrence of a unicellular, marine, planktonic, cyanobacterium. *Nature*, 277, 293-294
- Wendler J., Holzwarth A.R. & Wehrmeyer W. (1984) Picosecond time-resolved energy-transfer in phycobilisomes isolated from the red alga *Porphyridium-cruentum*. *Biochimica et Biophysica Acta*, 765, 58-67
- Whitmarsh J. & Govindjee (1995) Photosynthesis. In: *Encyclopedia of applied physics* (ed. Immergut E), pp. 513-532. VCH Publishers, Inc, New York
- Williams W.P. & Allen J.F. (1987) State-1/state-2 changes in higher-plants and algae. *Photosynthesis Research*, 13, 19-45
- Wiltshire K.H., Harsdorf S., Smidt B., Blocker G., Reuter R. & Schroeder F. (1998) The determination of algal biomass (as chlorophyll) in suspended matter from the Elbe estuary and the German bight: A comparison of high-performance liquid chromatography, delayed fluorescence and prompt fluorescence methods. *Journal of Experimental Marine Biology and Ecology*, 222, 113-131
- Witt H.T. (1979) Energy-conversion in the functional membrane of photosynthesis - analysis by light-pulse and electric pulse methods - central role of the electric-field. *Biochimica et Biophysica Acta*, 505, 355-427
- Wyman M. (1992) An in vivo method for the estimation of phycoerythrin concentrations in marine cyanobacteria (*Synechococcus* spp). *Limnology and Oceanography*, 37, 1300-1306
- Yamazaki I., Mimuro M., Murao T., Yamazaki T., Yoshihara K. & Fujita Y. (1984) Excitation-energy transfer in the light harvesting antenna system of the red alga *Porphyridium-cruentum* and the blue-green-alga *Anacystis-nidulans* - analysis of time-resolved fluorescence-spectra. *Photochemistry and Photobiology*, 39, 233-240
- Yentsch C.S. & Menzel D.W. (1963) A method for the determination of phytoplankton chlorophyll and phaeophytin by fluorescence. *Deep-Sea Research*, 10, 221-231
- Yentsch C.S. & Phinney D.A. (1985) Spectral fluorescence - an ataxonomic tool for studying the structure of phytoplankton populations. *Journal of Plankton Research*, 7, 617-632

- Yentsch C.S. & Yentsch C.M. (1979) Fluorescence spectral signatures - characterization of phytoplankton populations by the use of excitation and emission-spectra. *Journal of Marine Research*, 37, 471-483
- Zhou J.H., Gasparich G.E., Stirewalt V.L., Delorimier R. & Bryant D.A. (1992) The cpce and cpcf genes of *Synechococcus* sp PCC-7002 - construction and phenotypic characterization of interposon mutants. *Journal of Biological Chemistry*, 267, 16138-16145

Danksagung

Ein herzlicher Dank geht zunächst an Prof. Ulf-Peter Hansen für die Betreuung und die zahlreichen, fruchtbaren Diskussionen. Mein nächster Dank gilt Karen Wiltshire für die unermüdliche Unterstützung und die konstruktive Kritik an meiner Arbeit.

Ein weiterer Dank geht an Prof. Winfried Lampert, der mir die Möglichkeit gab meine Arbeiten am MPI für Limnologie in Plön durchzuführen.

Ein besonderer Dank für die tolle Zusammenarbeit und ihr sonniges Gemüt geht an Conny Reineke. Außerdem wünsche ich weiterhin gute Besserung: Bleib so optimistisch.

Weiterhin möchte ich mich bei Jan Kruse für die Tage und Nächte über dem Fluorometer, bei Martina Arp für ihre tolle Pionierarbeit zu Beginn des Projektes und Tanja Sonntag und Wolfgang Arp für das Einspringen in letzter Minute bedanken.

Danke an Nicole Aberle für das Mitstreiten in Plön und an alle anderen Plöner.

Danke auch an Jens Schimanski für seine Diplomarbeit, Diskussionen und den sonntäglichen Datentransfer.

Mein nächster Dank geht an alle eifrigen Helfer der bbe Moldaenke GmbH sowie an Christian für die Erstellung zahlloser Fluorometer, die Durchführung des Projektes und die hilfreichen Diskussionen sowie die langjährige Zusammenarbeit.

Ein vorletzter Dank an Prof. Holger Dau und Barbara Meyer für die zahllosen Diskussionen und Hilfestellungen und an Fiete, der mir zeigte wie groß ein Flowcytometer sein kann.

Ein letztes Dankeschön geht an Kirsten, Ursula, Stephan und Christoph für die Unterstützung während der gesamten Zeit.

Curriculum vitae

Name: Martin Beutler
Date of birth.: 03.05.1972 in Schleswig (Germany)

Nationality: German

Education

University: 1991-1995 Physics
Christian-Albrechts Universität Kiel, Germany

1996-1998 Physics
Christian-Albrechts Universität Kiel, Germany

Diploma: 26.06.1998 Diplom-Physiker

Graduate studies: 3/2000 –
to date Doctoral student, Biophysics
*Zentrum für Biochemie und Molekular Biologie
Christian-Albrechts Universität, Kiel, Germany
and
Abteilung Ökophysiologie
Max-Planck Institut für Limnologie, Plön,
Germany*

Working: 7/1998-3/2000 *Company bbe Moldaenke GmbH, Kiel, Germany*
Research physicist

Study abroad: 1995-1996 *Department of Physics
Heriot-Watt University Edinburgh, UK*

Project work: 2/1996-6/1996 *Fibre optics group
Heriot-Watt University Edinburgh, UK*

9/1996-4/1997 *Company bbe Moldaenke GmbH, Kiel, Germany*
Construction and production of fluorometer

Hiermit erkläre ich an Eides statt, dass ich die vorliegende Dissertation selbstständig verfasst habe und keine anderen als die angegebenen Quellen und Hilfsmittel von mir eingesetzt worden sind.

Des weiteren versichere ich, dass die vorliegende Dissertation weder ganz noch zum Teil bei einer anderen Stelle im Rahmen eines Prüfungsverfahrens vorgelegen hat.

Kiel, den